Development and control of pharmaceutical solids using extrusion and granulation

by

Laura Martinez Marcos

A thesis in fulfilment of the requirements for the degree of

Doctor of Philosophy

Strathclyde Institute of Pharmacy and Biomedical Sciences

Glasgow, United Kingdom

2017

Declaration of Authenticity and Author's Rights

This thesis is the result of the author's original research. It has been composed by the author and has not been previously submitted for examination which has led to the award of a degree.

Signed:

Date:

Acknowledgements

I would like to thank my supervisor Professor Gavin Halbert on his continued support, encouragement and invaluable guidance during the course of my studies. I would also like to thank my second supervisor Dr Dimitrios Lamprou for his continued advice and support during my PhD.

Also would like to express my gratitude to the Centre for Innovative Manufacturing in Continuous Manufacturing and Crystallisation (CMAC) for giving me the opportunity to participate in this project and allow me at the same time to become an independent researcher. I would also like to thank Dr Elke Prasad and Dr John Robertson for their support and advice as well as their trust and unconditional help.

Thanks to all my colleagues from CMAC and SIPBS that have shared this journey with me, to the ones that started on the first year and also the recent ones.

I would like to send my thanks to the Engineering and Physical Sciences Research Council (EPSRC) for their financial support and to GlaxoSmithKline (GSK) for the opportunity to perform an industrial placement during my PhD. I also acknowledge BASF and Croda for the kind supply of polymeric materials.

To my parents and Ulf, thank you for being always there for me even through the distance. I would have not been able to complete this thesis without your unconditional support.

Abstract

Nowadays, the pharmaceutical industry is seeking manufacturing processes that enable the delivery of high quality medicines with less cost and delivery time. The introduction of flexible manufacturing equipment such as twin-screw equipment can be used for these purposes and be part of a continuous manufacturing platform. Hot-Melt Extrusion (HME) and Twin-Screw Granulation (TSG) are two applications that can be used with the same processing equipment and reduce the number of stages involved in the manufacturing process. In this thesis the use of HME to produce amorphous solid dispersions of the poorly water soluble drug albendazole is investigated. HME enabled the transformation of the drug solid state from crystalline to amorphous by optimised processing parameters and the use of two suitable hydrophilic polymers as carriers. Amorphous solid dispersions showed an increase of albendazole dissolution properties. Differences in drug release rate indicated possible molecular interactions between the drug molecule and one of the polymers studied. Further studies are required to investigate the type of possible interactions. Computed tomography was used to determine the density differences and the internal structure properties of the extruded materials. This thesis studied the impact of screw element design, processing parameters and mechanism behind granule formation in twin-screw wet granulation. The use of conveying elements only achieved a poor liquid distribution due to the low shear applied. Combined screw configurations of mixing and conveying elements resulted in better liquid distribution properties. Excess of fines production was attributed to a breakage mechanism caused by the use of the distributive feed screw. These results can contribute towards the design of space of TSG processes. Overall, this thesis

showed that the optimisation of processing parameters in HME and TSG can lead to the enhancement of product properties which would be beneficial for continuous manufacturing platforms.

Contents

Nomenclature

δ	Solubility parameter
λ_{max}	Maximum wavelength
Ψ	Spray flux
ABZ	Albendazole
API	Active Pharmaceutical Ingredient
BCS	Biopharmaceutics Classification System
CE	Conveying Element
CQA	Critical Quality Attributes
DCS	Developability Classification System
DFS	Distributive Feed Screw
DME	Distributive Mixing Element
DoE	Design of Experiments
DSC	Differential Scanning Calorimetry
E_h	Group contributions to hydrogen bonds energy
EC	Ethyl cellulose
EVA	Ethylene vinyl-acetate
F_d	Group contributions to dispersive forces

F_p	Group contributions to polar forces
FaSSIF	Fasted Intestinal Fluid
FDC	Fixed-dose Drug Combination
FTIR	Fourier Transformed Infrared spectroscopy
GSD	Granule Size Distribution
HME	Hot-Melt Extrusion
HPC	Hydroxy-propyl cellulose
HPLC	High-Performance Liquid Chromatography
HPMC	Hydroxy-propyl methylcellulose
HPMC-AS	Hydroxy-propyl methylcellulose acetate succinate
HPMC-P	Hydroxy-propyl methylcellulose phthalate
HSM	Hot-Stage Microscopy
HU	Hounsfield Unit
IR	Immediate Release
KE	Kneading Element
KF	Karl-Fischer
L/S	Liquid to solid ratio
LH	Long Hold

LOD	Loss on Drying
M_p	Melting point
MEC	Molar Extinction Coefficient
Micro-CT	Micro-Computed Tomography
NIR	Near-infrared spectroscopy
NMR	Nuclear Magnetic Resonance
ODT	Oral Disintegrating Tablet
OPC	Optical Particle Counting
PAT	Process Analytical Technology
PCS	Photon Correlation Spectroscopy
PEG	Poly (ethylene glycol)
PEO	Poly (ethylene oxide)
PIV	Particle Image Velocimetry
PM	Physical Mixture
PVA	Poly (vinyl alcohol)
PVP	Poly (vinyl pyrrolidone)
PSD	Particle Size Distribution
QbD	Quality by Design

RCF	Relative Centrifugal Force
RH	Relative Humidity
ROI	Region of Interest
SEM	Scanning Electron Microscopy
SH	Short Hold
SLAD	Solubility Limited Absorbable Dose
SPCE	Short Pitch Conveying Element
SR	Sustained Release
T_g	Glass Transition Temperature
T_m	Melting Temperature
TSG	Twin-Screw Granulation
USP	United States Pharmacopeia
Vi	Group contributions to molar volume
VA	Vinyl acetate
VOI	Volume of Interest
Xi	Upper limit of size interval i
XRPD	X-Ray Powder Diffraction
Yi	Mass fraction in size interval i

List of figures

List of tables

1. Introduction

1.1. Introduction

Traditional manufacturing processes of pharmaceuticals are performed following a batch system where each operation or process is initiated and finalised in separate streams. Current pharmaceutical batch manufacturing processes involve high costs and production times with long lead times in between the different stages involved (e.g. days or weeks). The implementation of continuous manufacturing processes would allow the production of high quality medicines in a shorter period of time and in a flexible manner (Teżyk et al., 2016). In order to produce high quality medicines it is necessary to properly establish and monitor all the steps that are part of the manufacturing process. This can be achieved by the implementation of a Quality by Design (QbD) approach using tools such as Design of Experiments (DoE) and Process Analytical Technologies (PAT) (ICH, 2009). Some other advantages of continuous manufacturing processes are the possibility to integrate analytical monitoring tools to provide real-time information on the product being manufactured as well as ease of scale-up or scale-down when required (Allison et al., 2015). Hot-Melt Extrusion (HME) and Twin-Screw Granulation (TSG) represent two manufacturing processes of intermediate stages that can be transferred into a continuous platform by modifying the basic equipment set-up. Production of solid oral dosage forms such as tablets or capsules can be obtained after HME or TSG processes by introducing further post-processing techniques. The equipment used either as an extruder or as a granulator can provide a great flexibility as well as the ability to produce homogeneous products with specific properties in a relatively short period of time. For example, the processing parts such as screw element configuration can be easily changed in few minutes and the resulting product just

takes 10 to 20 minutes to be produced (throughputs ≥ 0.2 kg/h). Previous to processing, steady state is achieved after 10 minutes when constant conditions such as barrel temperatures and screw speed are achieved. When compared to the actual batch process, the respective times for the tasks mentioned greatly decreases. This capability of twin-screw equipment is due to the main processing element, a rotating twin-screw that is composed of diverse screw elements to transport and mix the materials. Both manufacturing techniques are included in this thesis as two different applications that could be later implemented as part of a continuous manufacturing platform.

1.2. Background / Literature review

1.2.1. Poorly water soluble drugs

Low water solubility of Active Pharmaceutical Ingredients (APIs) for oral administration, is a current major issue that can compromise drug absorption and efficacy in the patient leading to low bioavailability properties. It is expected that around 60 % of the drug candidates selected during early development phases are poorly water soluble (O'Donnell, 2012). To overcome this issue, novel approaches such as particle engineering and formulation approaches are frequently used (Karashima et al., 2016; Kawabata et al., 2011; Kawakami, 2012; Taupitz et al., 2013). Some of the factors influencing solubility are the composition of the aqueous media, temperature, pH, solid state (amorphous, crystalline), polymorph type, counter ions (salt formation) and ionic strength. The solubility profile of the drug gives information about its features and drug precipitation trend in vivo. In addition, pH changes of the gastrointestinal media may highly influence the solubility and/or absorption of weakly basic or weakly acid drugs. The United States Pharmacopeia

(USP) classified drug compounds regarding its solubility, from very soluble compounds to practically insoluble compounds (Table 1.1).

Table 1.1. USP® solubility classified according to Dahan et al., (Dahan et al., 2014)

Solubility definition	**Parts of solvent required for one part of solute**	**Solubility range (mg/mL)**	**Solubility assigned (mg/mL)**
Very soluble	<1	≥1,000	1,000
Freely soluble	From 1 to 10	100-1,000	100
Soluble	From 10 to 30	33-100	33
Sparingly soluble	From 30 to 100	10-33	10
Slightly soluble	From 100 to 1,000	1-10	1
Very slightly soluble	From 1,000 to 10,000	0.1-1	0.1
Practically insoluble	≥10,000	<0.1	0.01

Poorly water soluble drugs can also be administered intravenously as parenteral formulations. In this case, the drug must be previously solubilised using different methods such as micronisation, nano-sizing, complexation, pH adjustment and the use of co-solvents or surfactants.

1.2.1.1. Classification of poorly water soluble drugs

There are different systems established to classify drug substances for oral administration according to their physicochemical properties such as solubility, intestinal permeability and more recently, metabolism characteristics. The current international system of reference is the Biopharmaceutics Classification System (BCS) as shown in Figure 1.1. This system was established in 1995 and classifies drugs into different groups (I, II, III and IV) regarding their solubility and permeability properties (Stegemann, 2007).

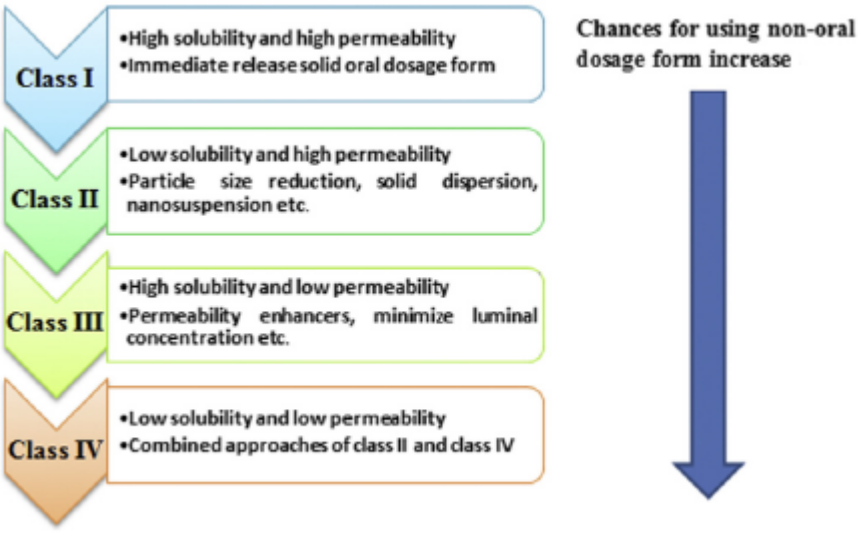

Figure 1.1. BCS classification of drug compounds. Reproduced from (Amidon, 1995; Baghel et al., 2016)

The Developability Classification System (DCS) arose recently as an improved system based on the BCS (Butler, 2010). Some of the modifications implemented by the DCS include the estimation of drug solubility in simulated human fasted intestinal fluid (FaSSIF), solubility limited absorbable dose (SLAD) and the expression of the dissolution rate taking into account the particle size of the drug. In the DCS, drugs are classified following the BCS (Class I, II, III and IV) due to the compound solubility and permeability properties. Moreover, the DCS expands class II into two sub-classes, IIa and IIb. This sub-classification differentiates between drug compounds that are dissolution rate limited (IIa) and drug compounds that are solubility limited (IIb). Therefore, solubility properties of the drug do not compromise drug absorption in the case of drug compounds classified as IIa due to their high permeability. However, drug solubility plays a main role to obtain a successful absorption in the case of IIb compounds.

With respect to the BCS, drug compounds classified as Class II and IV can be highly influenced by polymorphism changes and therefore these compounds should be considered for polymorph screening specially in early development phases (Sherry Ku, 2008). Some examples of poorly soluble drugs that can be classified within BCS Class II are carbamazepine (antiepileptic), dapsone (antirheumatic/leprosy), griseofulvin (antifungal), nitrofurantoin (antibacterial), phenytoin (antiepileptic), trimethoprim (antibiotic) and valproic acid (antiepileptic).

1.2.1.2. Methods to enhance solubility

The possible modifications that can be applied in order to increase the solubility and dissolution properties of an API are based on possible chemical changes such as the formation of a salt complex or pro-drugs. Salt formation is defined as a two-step process in which proton transfer in solution takes place followed by a crystallisation step (Stegemann, 2007).

Polymorphs of drug substances can be classified as non-mixed polymorphs (free base or acid) and as mixed polymorphs like salts, co-crystals, hydrates or solvates. Some thermodynamic conditions used during storage of the final dosage form can induce drug polymorphic changes. Therefore, conditions such as pressure, temperature, solvent and storage time should be controlled. The final selection of the drug molecule is based on factors such as molecular weight, functional groups, conformation, lipophilicity, stereochemistry, solubility, polymorphism, salt formation and crystallinity, among others (Stegemann, 2007). Polymorph screening provides useful information on the lattice energy of crystals that can be used to improve the solubility and dissolution properties of the compound and therefore oral bioavailability properties. However, it is recommended to perform polymorph

screening in the early stages of drug development (Stegemann, 2007). Currently there are different approaches available in the formulation and development stages of poorly soluble drugs:

- Particle size reduction by the application of milling or spray drying techniques
- Solid-state engineering approaches such as the formation of polymorphs, hydrates or solvates
- Formulation techniques such as hot-melt extrusion as a solid dispersion method
- Formation of micro-emulsions and other systems like liposomes
- Complexation method with compounds such as cyclodextrins
- Addition of micellar or surfactant systems such as poloxamers

From all the approaches mentioned above, particle size reduction and the formation of amorphous solid dispersions are the most promising and successful techniques that can be used to increase the solubility properties of poorly soluble drugs (Williams, 2010). Amorphous materials possess a disordered structure with no long-range order, opposite to the organised structure of crystalline materials. The internal disordered structure of amorphous materials provides high mobility properties to the molecules which can lead to increased solubility properties but also to low physical and chemical stability.

1.2.2. Amorphous solid dispersions

Amorphous materials:

As mentioned above, amorphous materials have a disordered structure and increased surface area, volume and free energy which provide increased solubility and faster

dissolution properties. The possible pharmaceutical implications and advantages of amorphous solid dispersions such as bioavailability enhancement of poorly water soluble drugs will be covered later in this literature review. Transformation from a crystalline to an amorphous form implies various physical changes and thermodynamic transitions (Figure 1.2). First, the crystalline material is heated up to a melting temperature (T_m) where the material experiences a physical change from an organised to a disorganised structure, which involves heat transfer (1^{st} order transition). Then the material is suddenly cooled down at a fast rate being then in a super-cooled liquid state. At this point, there is an equilibrium between the cooling temperature that is below the T_m and the molten material. One of the main characteristic parameters that determine the conversion of a molten material from a rubbery state to a solid glassy state is defined as the glass transition temperature (T_g) (2^{nd} order transition), which forms at further cooling and does not involve a physical change or heat transfer (Baird and Taylor, 2012). After T_g is reached, the system is at a non-equilibrium phase known as glassy state.

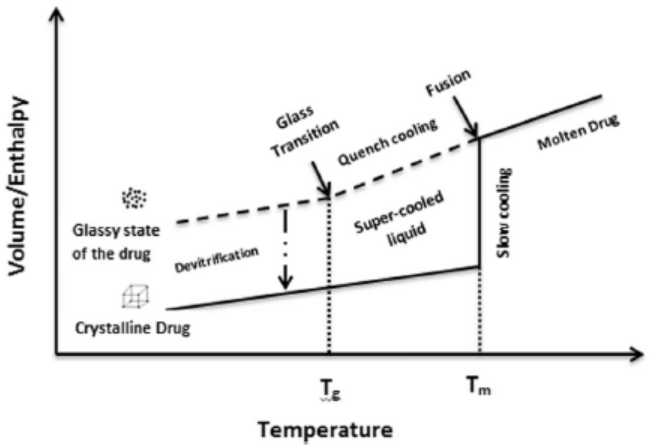

Figure 1.2. Thermodynamic changes experienced by a crystalline drug when transformed to a molten state (T_m) by temperature increase and rapidly cooled to form a glassy state. Reproduced from (Baghel et al., 2016)

It is well known that the apparent water solubility of the amorphous form is highly increased compared to the crystalline form. The main difference resides on the hygroscopic tendency of the amorphous form. Amorphous materials have no crystal lattice which provides a higher free energy resulting in increased solubility properties and can lead to supersaturation of the drug in solution. However, an increase in molecules movement can promote physical changes into crystal polymorphs and therefore affect product stability (Zhang et al., 2004).

Amorphous drug-polymer systems:

Some of the key factors involved in assuring stability of amorphous drug-polymer systems are the T_g of the system and the storage temperature (Lakshman, 2008). The solid state forms of the product can be determined based on the initial forms of the components as well as the conditions applied. Newman et.al., (Newman et al., 2012) demonstrated that amorphous solid dispersions constitute the most suitable solid form due to an increase in the powders surface area and also provide higher solubility and supersaturation properties. The conditions required to achieve an amorphous solid dispersion comprise an adequate rate of cooling as well as a processing temperature that is below the melting point (T_m) of the API. These considerations were taken into account during the selection of processing parameters of chapters 2 and 3 of this thesis.

Amorphous solid dispersions can be prepared using different methods. The most common methods for the production of amorphous solid dispersions are the solvent evaporation method, spray drying, freeze drying and hot-melt extrusion (HME). Some of these methods have been used to produce current commercially available

products (Table 1.2). In this literature review the preparation of amorphous solid dispersions by HME technique is reviewed in detail (section 1.2.2.2).

Table 1.2. Commercialised amorphous solid dispersions for oral administration according to Newman (Newman, 2015)

Product	**Compound**	**Dispersion polymer**	**Dispersion process**	**Dosage form**	**Approval**
Rezulin®	Troglitazone	PVP	HME	Tablet	1997 (withdrawn in 2000)
Kaletra®	Lopinavir, ritonavir	PVP-VA	HME	Tablet	2007
Intelence®	Etravirine	HPMC	Spray drying	Tablet	2008
Isoptin®	Verapamil	HPC/ HPMC	HME	Tablet	2009
Zortress®	Everolimus	HPMC	Spray drying	Tablet	2010
Onmel®	Itraconazole	HPMC	HME	Tablet	2010
Norvir®	Ritonavir	PVP-VA	HME	Tablet	2010
Incivek®	Telaprevir	HPMC-AS	Spray drying	Tablet	2011
Zelboraf®	Vemurafenib	HPMC-AS	Solvent/antisolvent precipitation	Tablet	2011
Kalydeco®	Ivacaftor	HPMC-AS	Spray drying	Tablet	2012

1.2.2.1. Types of amorphous solid dispersions

There are different types of amorphous solid dispersions that can be classified depending on the physical state of its components, drug and polymer. Factors such as the components physicochemical properties as well as the preparation method or any possible interactions between both components can determine the physical state and therefore, the type of amorphous solid dispersion. The physical state of each component, drug and polymer, can be classified as crystalline, amorphous or molecularly dispersed. The most common types of amorphous solid dispersions according to this physical state classification are solid solutions, crystalline glass suspensions, amorphous glass suspensions and solid glass solutions (Dhirendra,

2009) (Figure 1.3). The last three types are considered the most common amorphous solid dispersions obtained when processing techniques such as HME or spray drying are used. A compilation of all types of amorphous solid dispersions is provided in Table 1.3. In this thesis, the design intent is driven by the properties of the polymers selected (amorphous or crystalline) and the formation of molecularly dispersed drug throughout the polymeric matrix. According to this classification, extruded materials (chapters 2 and 3) would correspond to glass solutions (VI) and continuous solid solutions (III).

Table 1.3. Classification of amorphous solid dispersions based on the components physical state according to Dhirendra et al., (Dhirendra, 2009)

Solid dispersion type		**Matrix ***	**Drug ****	**No. phases**
I	Eutectics	C	C	2
II	Amorphous precipitations in crystalline matrix	C	A	2
III	Continuous solid solutions	C	M	1
	Discontinuous solid solutions	C	M	2
	Substitutional solid solutions	C	M	1 or 2
	Interstitial solid solutions	C	M	2
IV	Glass suspension	A	C	2
V	Glass suspension	A	A	2
VI	Glass solution	A	M	1

*A: matrix in the amorphous state, C: matrix in the crystalline state

**A: drug dispersed as amorphous clusters in the matrix, C: drug dispersed as crystalline particles in the matrix, M: drug molecularly dispersed throughout the matrix

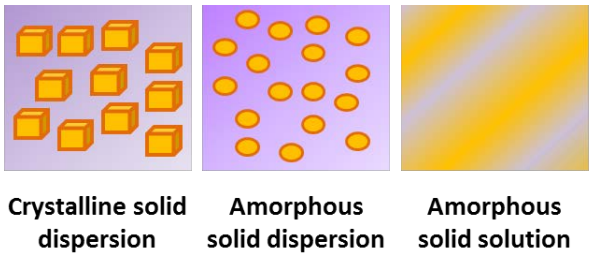

States of solid dispersion	Crystalline solid suspension	Amorphous solid dispersion	Amorphous solid solution
Polymer phase	A	A	A
Drug phase	C	A	A
Appearance	Opaque	Transparent	Transparent
A DSC will find	T_g+M_p	2 x T_g	1 x T_g

A: amorphous, C: crystalline, T_g: glass transition temperature, M_p: melting point

Figure 1.3. Solid states of amorphous solid dispersions produced by HME. Figure and table according to Shah et al., (Shah et al., 2013)

1.2.2.2. Amorphous solid dispersions by HME

HME technique has been extensively used for decades within the plastic (Michaeli et al., 1993) and food industries (Cheng and Friis, 2010). More recently, it has gained interest for its potential application in the field of pharmaceuticals (Crowley et al., 2007). In this field, HME technique is used with the purpose of producing a solid dispersion of a drug into a polymeric matrix at a molecular level. The application of this technique aims to enhance the dissolution rate as well as the absorption of poorly soluble drugs. In order to produce an amorphous solid dispersion, a twin-screw extruder is used as main processing equipment together with other auxiliary and downstream processing equipment. The elements of the extruder comprise the

feeding zone or hopper where the product is introduced, the twin-screws and the barrel to transport and homogeneously mix the materials and a die located at the end of the barrel that produces a uniformly shaped strand. As part of the auxiliary equipment, there are heating and cooling devices provided to control the barrel zones. Another important element of twin-screw extruders is the ports where Process Analytical Technology (PAT) tools can be attached. Some of the most common PAT tools used to monitor HME processes are Raman and NIR probes. The inclusion of these analytical techniques provides in-line measurements of the process. HME process and the different parts of the equipment are depicted in Figure 1.4 (Maniruzzaman, 2012).

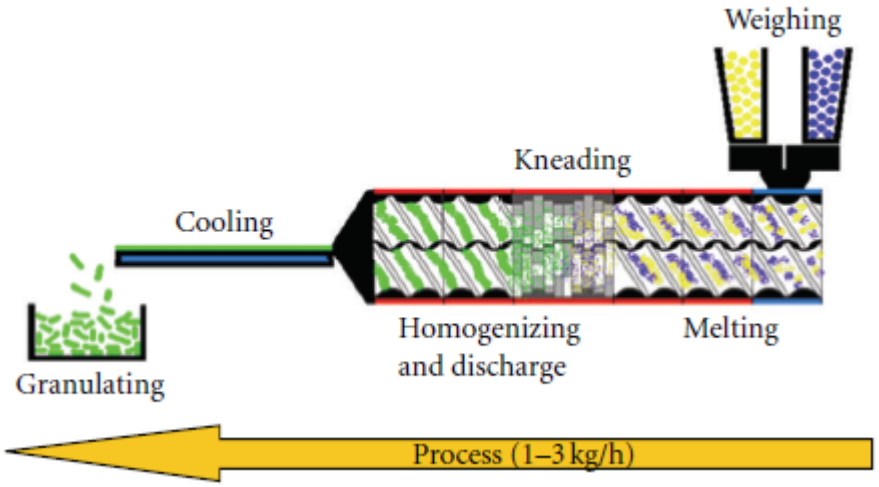

Figure 1.4. Twin-screw extruder and stages of a HME process. Reproduced from (Maniruzzaman, 2012)

The extruder can be equipped with one or two rotating screws located inside a cylindrical barrel. The most common configuration uses two screws and is called twin-screw extruder. In this case the screws can rotate in the same direction (co-rotating) or in the opposite direction (counter-rotating). Twin screws can also be intermeshing or non-intermeshing screws which helps increasing the conveying

degree and decreasing the residence time of the product (Crowley et al., 2007; Williams, 2010). The co-rotating twin-screw extruder with an intermeshing capacity is the preferred one within the pharmaceutical industry. Co-rotating screws which rotate in the same direction provide improved mixing properties than counter-rotating screws. In addition, transport and flow of material in the forward direction is dependent on the intermeshing capacity of the twin-screws and not dependant on material's properties (Andrews et al., 2009). Researchers such as Padmanabhan and Rauwendaal (Padmanabhan, 2008; Rauwendaal, 2005; Rauwendaal, 2008) have studied the influence of barrel screw design such as the introduction of barrel flights and channels as well as screw performance in HME processes. In addition, screws performance regarding the disposition of the melted material along the screw was investigated. Some of these new approaches include the addition of elongational and pin intermeshing mixing devices within the screw (Figures 1.5 and 1.6), providing a successful and homogeneous mixing device (Rauwendaal, 2008).

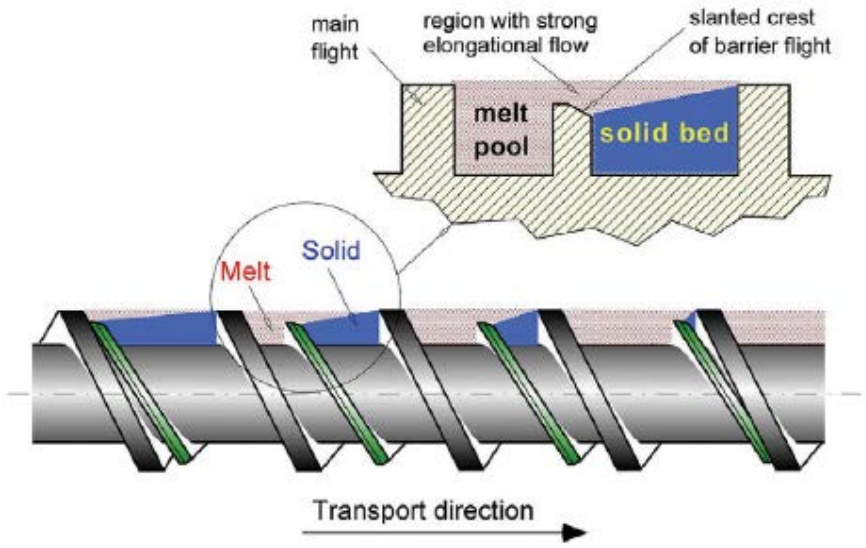

Figure 1.5. Transport of material inside a barrier screw. Reproduced from (Rauwendaal, 2008)

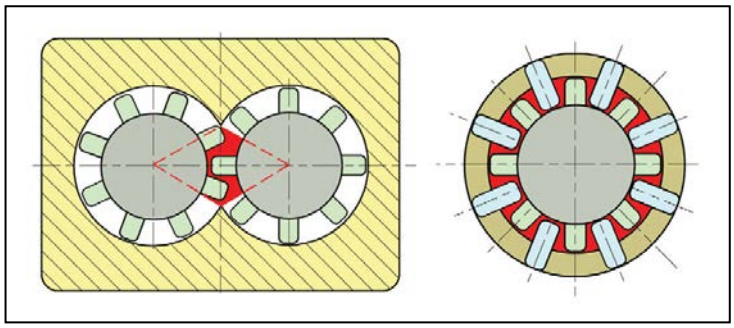

Figure 1.6. Pin intermeshing mixing screws. Reproduced from (Rauwendaal, 2008)

Initial HME studies focused on the production of modified release products in the form of granules, pellets or tablets (Repka et al., 2007). Currently, industry focuses on the development of this technique as a continuous manufacturing process for pharmaceutical products with the advantage that at the same time product quality is assessed by the introduction of PAT tools (Andrews et al., 2009).

It has been previously observed that the disposition and number of screw elements are key factors to achieve appropriate mixing and process performance (Mu and Thompson, 2012). Diverse studies (Lawal and Kalyon, 1995; Nakayama et al., 2011; Sarhangi Fard and Anderson, 2013; Van Zuilichem, 1999) have demonstrated the increased mixing capacity of twin-screw extruders compared to single screw extruders and high-shear mixers. Some of the main advantages of HME comprise bioavailability enhancement of poorly soluble drugs as well as the elimination of the drying step, as no solvent is required. In addition, production time and processing steps are reduced leading to a more economic process. In terms of pharmaceutical advantages, this method is suitable to obtain controlled release dosage forms with improved drug content uniformity. However, disadvantages such as the application of high temperatures (e.g. over 100 $^{\circ}$C) can compromise drug stability and therefore, the use of this technique can be limited in the case of thermally labile drugs.

Physical stability of the extruded material can be determined by characterisation techniques such as X-ray powder diffraction (XRPD). For example, Bruce et al., (Bruce et al., 2007) studied formulated tablets produced by HME containing guaifenesin and Acryl-EZE® or Eudragit® as main components. XRPD analysis in combination with SEM studies evidenced drug in crystalline form located in the surface while the rest of the extruded product remained in the amorphous state. This crystallisation event was correlated to an excess of drug content above the solubility limit of the drug in the polymer matrix. Despite the production of a drug delivery system where an amorphous state is obtained, there are recrystallisation processes that may occur after processing and that need to be monitored over time. Albers et.al., (Albers et al., 2009) studied the influence of the solid state of celecoxib and Eudragit® EPO extruded materials on the dissolution properties. The addition of another excipient like hydroxy-propyl methylcellulose (HPMC) was key to prevent the appearance of re-crystallisation phenomena.

The main components in HME formulations comprise the API and a polymer or if required, a plasticizer. Polymers such as polyvinylpyrrolidone (PVP), polyethylene glycols (PEG), cellulose ethers and polyethylene oxides (PEO) constitute some of the main carriers used in HME processes (Madan, 2012). Besides, plasticizers such as citrate esters, low molecular weight PEG or surfactants such as Poloxamer can also be added to improve the processing conditions and to obtain a more flexible strand. The selection of a plasticizer depends on the plasticizer-polymer compatibility and plasticizer stability. The plasticizer reduces the T_g of the polymer as well as improves the stability of the API and the carrier (Williams, 2010).

Assessment of drug-polymer miscibility:

It is necessary to evaluate the miscibility properties between the components of an amorphous solid dispersion prior to the application of a processing technique such as HME. The most common experimental techniques used are Hot-Stage Microscopy (HSM) and Differential Scanning Calorimetry (DSC). Physical mixtures drug-polymer at different drug loadings are characterised to determine the temperature at which both compounds are miscible. In recent studies, DSC together with a mathematical model was used to predict the solubility curve of a drug in a polymeric matrix (Bochmann et al., 2016; Kyerematenge et al., 2014). However, it is also possible to theoretically determine drug-polymer miscibility by the application of the Hoy and Hoftzyer/Van Krevelen method. A variant method is the Hansen solubility parameter method that calculates the solubility parameter difference ($\Delta\delta$) of the system based on the solubility parameters (δ) of each compound. The contribution of dispersive forces (E_d), polar interactions (E_p) and hydrogen bonds (E_h) are considered in the calculation (Equation 1.1) (Hansen, 2000).

$$\delta = \sqrt{{\delta_d}^2 + {\delta_p}^2 + {\delta_h}^2} \qquad \text{Equation 1.1}$$

A system is regarded miscible when the solubility parameter difference ($\Delta\delta$) values are <7 $MPa^{1/2}$. A glass solution appearance of the extruded material can also suggest successful miscibility. On the other hand, $\Delta\delta$ values >10 $MPa^{1/2}$ indicate absence of adequate miscibility (Forster, 2001). Both, drug and polymer must be similarly soluble in a way that their respective solubility do not differ over 2.0 $MPa^{1/2}$. The selection of polymers with high T_g value can be an approach to tailor components miscibility at a molecular level (Saerens et al., 2012).

1.2.3. Granulation techniques

1.2.3.1. Classic granulation methods

In the last decades the pharmaceutical industry has applied batch manufacturing for the production of intermediate and finished products. Intermediate products such as granules can be manufactured by different granulation techniques. This section will focus on wet granulation techniques. Some of the wet granulation methods currently used are high-shear wet granulation and fluid bed granulation. Both are well-known processing methods used to form particle agglomerates or granules by mixing at a specific rate and for a period of time. In this section both techniques will be introduced and compared as main wet granulation techniques that can be implemented for the production of solid oral dosage forms.

High-shear wet granulation:

Granulation processes that take place in high-shear wet granulation can be described by introducing the different stages involved. First of all, the powder and the sprayed liquid are mixed by the use of an impeller that rotates and applies high-shear forces. During this process, particle agglomerates are generated by the formation of liquid bridges and strong bonds between the powder and the liquid droplets. The next step involves the consolidation of the granules formed which is influenced by their strength properties. The effect that high-shear or stress has on the resulting granules has been related to factors such as the rotation speed of the impeller, the fill level of the vessel and material properties (Chan et al., 2013). Currently, the majority of studies are focused towards the understanding of the mixing mechanisms and the influence of different types of impeller on granules particle size and shape. Börner et al., and Mirza et al., (Börner et al., 2016; Mirza et al., 2015) have recently studied

the importance of the impeller geometry such as size and shape and suggest tailored approaches to improve mixing performance and robustness. Both studies demonstrated that a two-blade impeller with elongated side wings is able to produce homogeneous granules with better particle size and strength attributes when compared to a three-blade impeller. Ability to scale-up from laboratory to industrial scale is also shown for a two-blade impeller. Improved process performance and a better distribution of the kinetic energies involved demonstrated that the two-blade impeller can be a more suitable approach for high-shear granulation processes.

Other key property such as drug content uniformity has also been studied. Oka et.al., (Oka et al., 2015), reported a lack of adequate drug distribution when processing acetaminophen and microcrystalline cellulose in a high-shear granulator. Great differences in content uniformity between fines and coarse granules were attributed to powder segregation. These outcomes can compromise other important factors such as drug release properties.

High-shear wet granulation processes are influenced by processing parameters such as liquid to solid (L/S) ratio which can determine granule growth behaviour. Normally, it is considered that a higher L/S ratio and therefore higher water content results in coarser granules due to the formation of bigger nuclei. In granulation processes, the binder agent can be added as liquid form or as powder form. Different studies have related L/S ratio and binder content to granules attributes. For example Mangwandi et al., (Mangwandi et al., 2015) attributed better wettability properties and granulation performance to an increase in the content of liquid binder for a binary mixture formulation. Li et al., (Li et al., 2013) reported an increase in granules particle size when the solid state of a binder in powder form was changed

by high humidity conditions (e.g. over 90% RH). The binder in a rubbery-solution state can enhance granulation growth and rate processes due to improved adhesion properties compared to the same binder in a glassy state. Enhancement of particle size during high-shear wet granulation has also been attributed to delivery methods such as the pour-in method and the spray method (Tan et al., 2014).

Fluid bed granulation:

Another classical method for wet granulation of pharmaceuticals is fluid bed granulation. Wet granulation is performed in a fluid bed dryer where the binder liquid is sprayed to the powder bed at a constant flow rate and air flow is added at a constant inlet temperature to dry the granules once formed. Granules are formed by powder wetting mechanisms and formation of a liquid bridge that solidifies and therefore becomes a stable particle-particle bond. Processing parameters such as inlet temperature and air flow rate as well as pressure are constantly monitored to assure constant powder bed temperature. Most of the studies in fluid bed granulation have focused on granule attributes such as particle size, shape and flowability properties through the optimisation of processing conditions. Efforts have also been made to correlate granules growth rates, drug content uniformity and granules structure. To do so, the internal structure and porosity of the granules can be assessed by the application of novel techniques such as computed tomography (Micro-CT) (Hoffmann et al., 2015; Poutiainen et al., 2011). Micro-CT enables the visualisation and characterisation of the components by their differences in density. Further aspects of Micro-CT technique are reviewed in section 1.2.4.1 as part of the section entitled other analytical methods.

1.2.3.2. Novel granulation methods

In the last decade, wet granulation processes are evolving towards the optimisation of more flexible equipment that can be applied within continuous manufacturing platforms to deliver high quality medicines in a cost effective manner (Leuenberger, 2001; Vercruysse et al., 2012). Figure 1.7 below shows one of the current continuous manufacturing platforms of pharmaceuticals developed by GEA, the Consigma™-25 with integrated continuous wet granulation, drying and tableting equipment.

Figure 1.7. Continuous manufacturing platform Consigma™-25. 1) powder feeding system, 2) twin-screw granulator, 3) fluid bed dryer, 4 and 5) post-processing area of granules including sieving, 6 and 7) blenders for the addition of extragranular excipients and 8) tablet press. Reproduced from (Vercruysse et al., 2013)

Twin-screw granulation:

Twin-screw granulation is a novel granulation technique that the pharmaceutical industry is looking to implement due to the reduced time and cost associated with this technique. Moreover, it can be performed in continuous manufacturing

equipment as part of a continuous set-up such as the example in Figure 1.7. In twin-screw granulation there are subsequent growth stages involved that can occur at each of the screw regions within the barrel. Main granulation mechanisms that take place are wetting of the powder bed with the liquid droplets, nucleation to form initial nuclei, agglomeration of the particles through layering and coalescence and breakage phenomena (Figure 1.8) (Iveson, 2001). However, the mechanisms behind granule growth and the relations with granules final attributes are still not fully understood. Lee et al., (Lee et al., 2013) suggested that there were differences in the intra-granular structure of granules produced by high-shear granulation when compared to twin-screw granulation that leads to granules with very different shape and strength attributes.

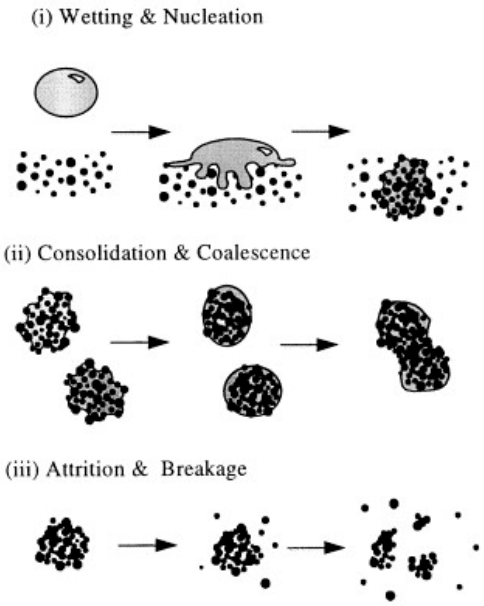

Figure 1.8. Granulation rate mechanisms involved in wet granulation. Reproduced from (Iveson, 2001)

A twin-screw granulator (TSG) is modular and flexible and is able to provide high-shear mixing to homogeneously mix the powder components of the formulation with

the granulation liquid to produce granules. High-shear is generated by the rotation of the twin-screws at a specific speed and the use of different conveying and mixing elements with diverse geometries, angles and configuration possibilities (Figure 1.9). Several studies have focused on the determination of the role that each screw element plays on final particle attributes such as granules size distribution (GSD), particle shape, homogeneity and porosity (El Hagrasy et al., 2013b; Sayin et al., 2015b; Thompson and Sun, 2010). There seems to be agreement on the fact that conveying elements provide coalescence properties whereas kneading elements provide mainly high-shear and breakage properties. A low degree of consolidation can also be provided by kneading elements due to the fact that both, fines and coarse granules are generated. Current pharmaceutical applications of twin-screw granulation as well as the main research outcomes towards enhancement of particle attributes are provided in section 1.2.4.2.

Figure 1.9. Example of two different screw configurations. Reproduced from (Dhenge et al., 2012)

In order to address the necessity for a fundamental understanding of twin-screw granulation processes and the influence of screw element configuration, different engineering approaches are reported in Chapter 5 of this thesis.

1.2.4. General applications of twin-screw equipment

1.2.4.1. Applications in the area of Hot-Melt Extrusion (HME)

HME is one of the processing routes that proved to be an alternative in the formulation stages of poorly water soluble drugs for immediate release and sustained release formulations.

Immediate release formulations for dissolution enhancement:

The production of amorphous solid dispersions by HME technique has been used to improve the dissolution rate and oral bioavailability properties of a wide number of poorly water soluble drugs, mainly those classified as BCS Class II (Kate et al., 2016; Lee et al., 2015; Palem et al., 2015).

Good drug-polymer miscibility properties are crucial to obtain a successful amorphous solid dispersion at a molecular level. The study performed by (Sathigari et al., 2012) evidenced the mechanisms behind the stability of immediate release formulations of efavirenz when applying polymers with different properties. Eudragit® EPO, a low glass transition polymer and Plasdone® S-630, a high glass transition polymer were used. Both formulations enhanced the dissolution rate of efavirenz as shown in Figure 1.10. The stability of formulations comprising Plasdone® S-630 was attributed to drug-polymer hydrogen bond interactions, whereas in the case of Eudragit® EPO, an antiplasticization effect contributed to the stability of the amorphous form. The mechanisms involved in the dissolution properties of amorphous solid dispersions were previously attributed to the solid state of the drug within the matrix (Albers et al., 2009). These polymeric carriers were also applied in the development of HME formulations of the poorly soluble compound Osthole that achieved successful bioavailability properties shown by in-

vivo studies (Yun et al., 2014). Other polymers that have successfully been used for HME amorphous solid dispersions are HPMC derivatives (Mitra et al., 2016). Adequate polymer selection depending on its physicochemical properties is crucial to obtain amorphous solid dispersions with increased dissolution properties. The combination of different polymeric carriers with known physicochemical properties is a suitable approach to achieve specific release rates (Kalivoda et al., 2012).

A similar result to Sathigari et.al., (Sathigari et al., 2012) was achieved by Pawar et.al., (Pawar et al., 2016) who developed amorphous solid dispersions of efavirenz in a blend of Soluplus and hydroxy-propyl methylcellulose acetate succinate (HPMCAS) applying a QbD approach. It was found that the ratio of Soluplus® with respect to HPMCAS was the key factor to significantly improve the dissolution rates. Contour plots in Figure 1.11 indicate that the saturation solubility of efavirenz increases at high ratios of Soluplus® as well as when using low ratios of HPMC-AS. The high hydrophilicity of Soluplus® and greater intermolecular interactions occurred between Soluplus® and Efavirenz may have caused improved wettability and dissolution properties. The combination of Eudragit® EPO with Kollidon® VA64 and Soluplus® was also studied by Liu et al., (Liu et al., 2013) as a method to produce amorphous solid dispersions of the thermally unstable drug carbamazepine. Based on these studies, the use of Soluplus® either alone or in combination with surfactants is one of the preferred approaches for the development of immediate release formulations by HME (Fule and Amin, 2014; Pina et al., 2014).

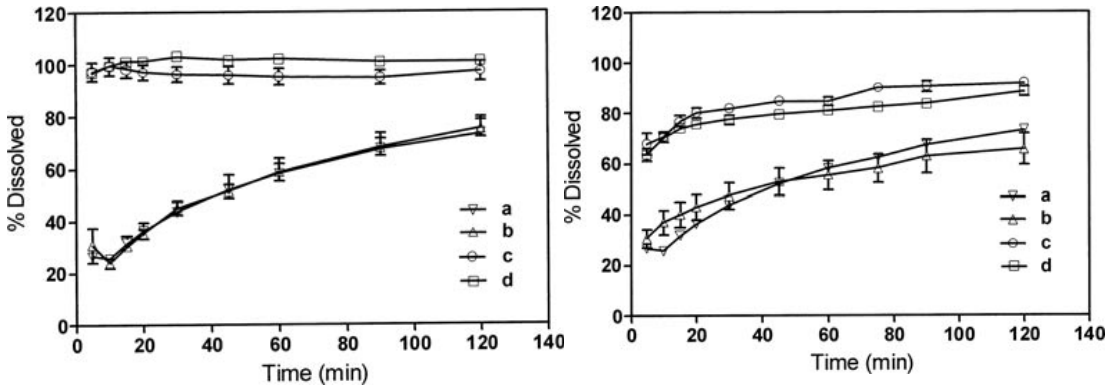

Figure 1.10. Dissolution profiles of Efavirenz - Eudragit® EPO mixtures (left) and Efavirenz - Plasdone® S630 (right); (a) Efavirenz, (b) physical mixture (1:1) of Efavirenz – polymer, (c) HME formulation time zero and (d) HME formulation (9 months). Reproduced from (Sathigari et al., 2012)

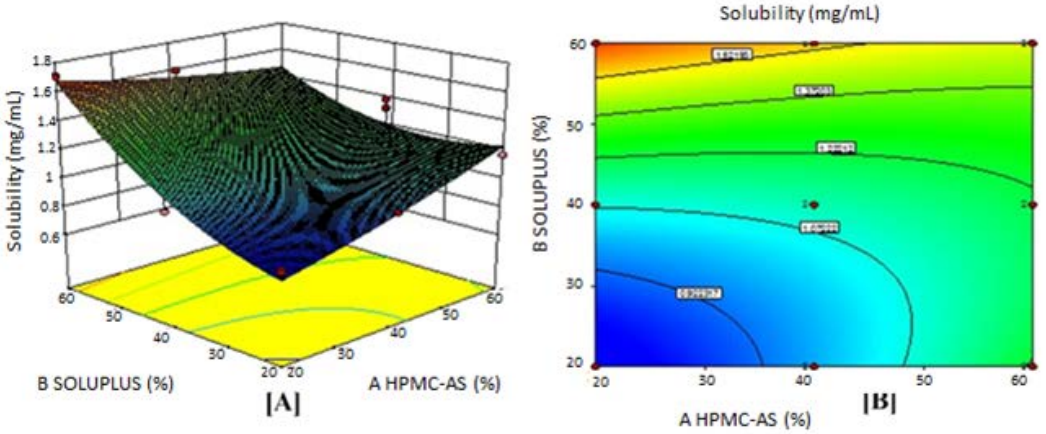

Figure 1.11. Effect of the ratio of Soluplus® and HPMCAS on the saturation solubility of Efavirenz. Reproduced from (Pawar et al., 2016)

Another antiretroviral drug, ritonavir, was formulated by HME as nano and micro-dispersions with Kollidon® VA-64 and a surfactant. After dispersion of the extruded materials in buffer media, the dispersed particles containing ritonavir were characterised. Analytical techniques such as Photon Correlation Spectroscopy (PCS) and Optical Particle Counting (OPC) were used to determine the particle size distribution of the micro-dispersed particles (Tho et al., 2010). Surfactants have also

demonstrated its utility in HME formulations to enhance the processability of highly viscous polymers such as Plasdone® S-630 or HPMC. A reduction of the polymer T_g enables a decrease of HME processing temperature (Ghebremeskel et al., 2007). In cases where the drug compound is miscible with low viscosity polymers that present a lower T_g value, the selection of this type of carrier must be considered. Low viscosity polymers such as Polyvinylpyrrolidone (PVP) have demonstrated ideal properties for HME processing due to their processability and stability properties. These will also be influenced by PVP molecular weight (Alsulays et al., 2015; Chan et al., 2015). On the other hand, PVP hygroscopicity can affect the polymer chains and free volume. This effect would cause stability issues due to a decrease of the material properties (Szakonyi and Zelkó, 2012). In order to avoid water intake when using PVP, it is recommended to store the samples in a sealed glass container and under controlled conditions. Poly (ethylene glycol) (PEG) is also a hygroscopic polymer that has been widely used as carrier in HME formulations (Alshehri et al., 2016; Bhagurkar et al., 2016; Douglas et al., 2016). For example Leonardi et al., (Leonardi et al., 2009) used PEG-6000 as hydrophilic carrier where it was observed that the higher the polymer content, the higher the dissolution rate of Albendazole. Drug delivery studies in infected mice proved the efficacy of these formulations through larvae inhibition. The impact of using hygroscopic polymers on the physicochemical properties of amorphous solid dispersions was reported by Feng et al., (Feng et al., 2016). Compounds or synthetic derivatives like Poly (vinyl alcohol) (PVA) are also suitable for HME application (De Jaeghere et al., 2015; Maniruzzaman et al., 2015).

Other manufacturing methods such as complexation by the addition of cyclodextrins constitute novel suitable approaches for dissolution enhancement (Miller et al., 2007). Therefore, HME application using cyclodextrins as carriers constitutes an interesting formulation approach. For example Fukuda et al., (Fukuda et al., 2008) incorporated chemically modified β-cyclodextrins such as sulfobutyl ether β-cyclodextrin (Captisol®) to obtain an extruded formulation of ketoprofen (Figure 1.12). This approach can lead to a great increase in dissolution rate and bioavailability of poorly soluble drugs (Fukuda et al., 2008).

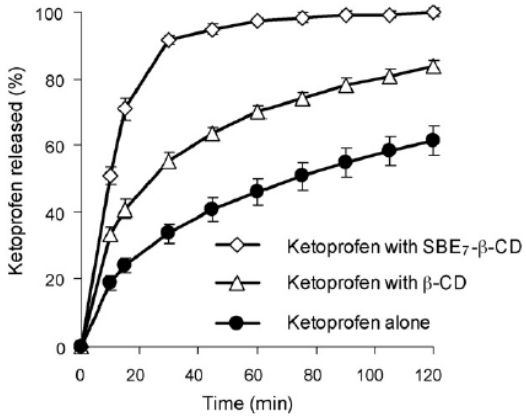

Figure 1.12. Impact of a cyclodextrin solid dispersion on ketoprofen dissolution rate. Reproduced from (Fukuda et al., 2008)

The HME formulations mentioned above have the potential to enhance oral bioavailability properties. However, in-vivo studies in those cases were not presented. Only a few researchers (Fu et al., 2016; Ma et al., 2016; Wang et al., 2016) have reported in-vivo studies to demonstrate increased bioavailability properties when compared to the commercial product. Moreover, the studies reported in this literature review were based on a laboratory scale production system. Therefore, more studies regarding scale-up of HME processes to an industrial level are required (Guns et al., 2012).

Controlled release formulations:

This section of the literature review highlights some of the findings of different types of controlled release formulations such as sustained release and delayed release formulations. The use of different excipients such as ethylcellulose (Ethocel® Standard 10 Premium), cellulose acetate butyrate (Eastman® CAB-171-15NF), polymethacrylates (Eudragit® RS100), polyvinylpyrrolidones (Kollidon® 30), cross-linked polyacrylates (Carbopol® 971), polyoxylglycerides (Gelucire® 50/13), HPMCAS (Affinisol® HPMCAS 912) and polyethylene oxides (Polyox® WSR N60K), among other excipients have been widely studied (Islam et al., 2014; Madan, 2012; Maniruzzaman et al., 2016). Some of the sustained release formulations developed by HME have been commercialised. For example, the first HME based marketed product for sustained release application was Isoptin®, a formulation of verapamil and HPC/HPMC (Andrews, 2008).

Some other examples of sustained release formulations comprise theophylline and the use of the methacrylic acid copolymer Acryl-EZE® (Young, 2005). Co-extrudates of theophylline for sustained release application were also developed by Quintavalle et al., (Quintavalle et al., 2008). It was observed that the shape and dimension of the co-extruded material had an impact on the percentage of drug released, where extrudates with smaller dimensions showed increased drug release.These extruded materials used microcrystalline wax as carrier in order to achieve theophylline sustained release for a period over 5h. Previous research comprising theophylline extrudates with stearic acid as carrier had shown an increase in drug release after 5h, therefore not maintaining sustained release properties. The selection of the optimal excipient was crucial to achieve a maintained effect in the

case of sustained release formulations (Figure 1.13, the arrow indicates the maintained effect achieved when changing excipient). Estimation of in-vivo results were obtained by the application of a mathematical model based on pharmacokinetic parameters.

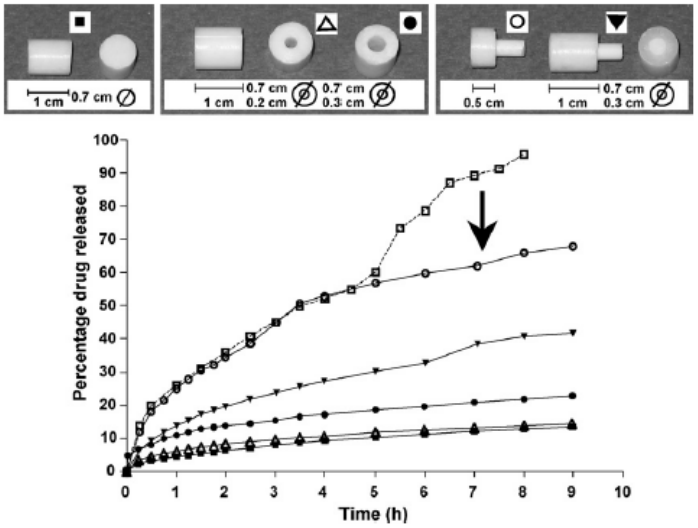

Figure 1.13. Dissolution profiles of co-extruded materials (40 % w/w theophylline) based on shape, dimension and excipient. Reproduced from (Quintavalle et al., 2008)

Besides Mehuys et al., (Mehuys et al., 2004) developed a matrix-in-cylinder system by HME. The combination of two sustained release excipients like HPMC and Gelucire® as core ingredients and the production of an ethylcellulose (EC) pipe by extrusion resulted in sustained release formulations with zero order drug release.

Other studies have developed metoprolol tartrate mini-matrices extrudates by incorporating dibutyl sebacate as a novel plasticizer and xanthan-gum as a modified drug release component. Process parameters as well as plasticizer suitability were evaluated through the manufacturing process. In addition, the assessment of the formulation properties was based on variables such as polymer properties and polymer content (Verhoeven et al., 2008; Verhoeven et al., 2009).

The evaluation of drug release from extruded metoprolol tartrate matrices was also performed by Almeida et al., (Almeida et al., 2011) considering different grades of ethylene vinyl acetate. The study revealed higher flexibility and amorphous behaviour proportional to vinyl acetate (VA) content. However, low proportions of VA polymers showed an increase in crystallinity. Other experimental work carried out by Dierickx et al., (Dierickx et al., 2012) suggested that multi-layered dosage forms can be processed by HME. Different release profiles (SR and IR) as well as bioavailability improvement were obtained due to a core and coat layers design where metoprolol tartrate and suitable polymers were selected.

In the last years the use of biological compounds as carriers for the formation of amorphous solid dispersions is gaining more interest due to their renewable properties and the cost reduction associated in comparison to synthetic polymers. For example, biopolymers such as xanthan gum in combination with chitosan have been previously used in the development of sustained release formulations (Fukuda et al., 2006). More recently, gum arabic was used as a biopolymer for the production of controlled release matrices containing Paracetamol. The mechanism of drug release through erosion of the matrix that is provided by this biopolymer was crucial to achieve sustained release properties as shown in Figures 1.14 and 1.15 (Kipping and Rein, 2016). Further sustained release formulations of Paracetamol were achieved recently by the use of hydrophilic polyurethanes with no further need to add release modifiers. The evaluation of the rheological properties of different polyurethanes and the determination of the adequate HME processing temperatures were key to achieve successful sustained release formulations with complete drug release (Verstraete et al., 2016).

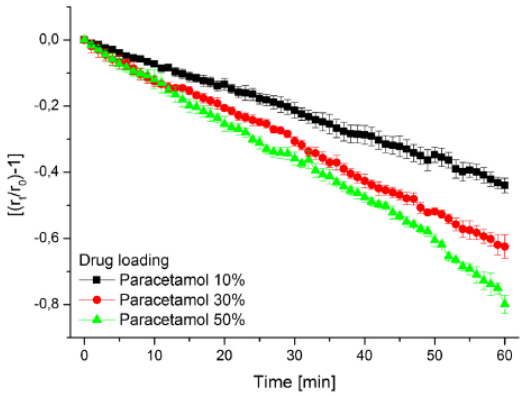

Figure 1.14. Erosion properties of Paracetamol in gum arabic matrices at different drug contents. Reproduced from (Kipping and Rein, 2016)

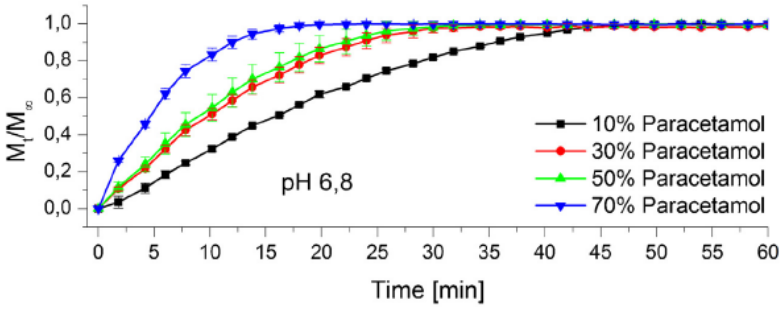

Figure 1.15. Controlled release profiles of Paracetamol in gum arabic matrices. Reproduced from (Kipping and Rein, 2016)

In the area of sustained release Lyons et al., (Lyons et al., 2006) compared agar and microcrystalline cellulose as filler compounds observing an impact of filler type and content on drug release. The use of agar increased the matrix viscosity and showed a comparable decrease of dissolution rates. Therefore, agar can be an alternative for the production of sustained release dosage forms. In addition Özgüney et al., (Özgüney et al., 2009) correlated an increase in HME processing temperature with a decrease of the extended drug release rate of theophylline formulations. Controlled release formulations produced by HME comprise as well applications such as sustained release formulations with dual drug release (Laukamp et al., 2015), delayed release formulations (Wiederhold, 2016) and novel floating controlled release

systems (Vo et al., 2016). Delayed release formulations of multiparticulate systems and specifically the extent of drug release are influenced by the type of polymer and not by the mechanical strength properties (Schilling and McGinity, 2010).

Oral Disintegrating Tablets (ODT) and taste-masking applications:

Several researchers have studied amorphous solid dispersions for taste-masking applications in the case of bitter tasting drugs and novel applications such as ODT tablets. In most of these cases, the selected carrier for the development of amorphous solid dispersions was Eudragit® EPO in combination with further excipients (Alshehri et al., 2015; Gryczke, 2011; Maniruzzaman et al., 2012). Processing conditions such as the screw element configuration and the length of the twin-screw shafts were used to maintain the drug in crystal form but achieving good homogeneity properties due to the mixing degree applied by twin-screw extruders (Morott et al., 2015).

Application of supercritical fluid:

The application of an inert gas such as CO_2 can be a suitable approach in the development of HME processes due to its ability to act as plasticizer, leading to the reduction of polymer viscosity, T_g and T_m values (Sauceau et al., 2011). Studies comprising a formulation of carvedilol as well as PEG and polydimethylsiloxane showed viscosity reduction with consequent decrease of the die head pressure and torque resistance (Lyons et al., 2007). By adding a supercritical fluid, not only polymers viscosity is reduced but also the need for additional plasticizers (Verreck et al., 2006b). HME is not a suitable manufacturing process for thermally labile products such as p-ASA. However, the addition of CO_2 can lead to a significant

processing temperature decrease and constitute a major improvement within extrusion processing (Verreck et al., 2006a).

Manufacturing of fixed-dose combination solid dosage forms:

The combination of at least two drugs or active compounds in a single dosage form is considered a fixed-dose drug combination (FDC). It is possible to produce FDC products comprising poorly soluble drugs by the application of a hot-melt co-extrusion process. This application has recently been used in the case of antimalarial drugs such as artemether and lumefantrine (Fule et al., 2015) as well as in the case of atovaquone and proguanil (Kate et al., 2016). Both studies proved the transformation of the crystalline compound into amorphous form and the consequent increase in drug release which was superior to the respective commercialised combined drug products. Moreover, co-extrusion enables the incorporation of drugs with different solubility properties as part of a multi-layer system (Dierickx et al., 2014; Vynckier et al., 2015a). Polymers with different properties can be included depending on their function as part of the nucleus or the coating layer of the system.

Characterisation techniques used in HME processing:

In this section of the literature review two types of analytical techniques will be covered. Some analytical techniques are used in-line to monitor HME processes such as PAT tools and other techniques are used off-line to characterise product properties. Main PAT tools used to take real-time measurements of HME processes are NIR and Raman spectroscopy which application is reviewed in the following section. On the other hand, the main analytical techniques used to monitor product characteristics after HME processing are Differential Scanning Calorimetry (DSC), Scanning Electron Microscopy (SEM), Thermal Gravimetric Analysis (TGA), X-Ray

Powder Diffraction (XRPD), Fourier Transformed Infrared (FTIR) and Near-infrared (NIR) spectroscopy, Raman spectroscopy, High-Performance Liquid Chromatography (HPLC) and UV-spectrophotometry (Dong et al., 2008; Madan, 2012; Qi et al., 2008; Sathigari et al., 2012; Singhal, 2011; Zhang et al., 2004). More recently, the possibility to perform micro-structural x-ray surface analysis of materials with pharmaceutical application has gained interest (Alhijjaj et al., 2016; Kašpar et al., 2013; Vynckier et al., 2015b).

Near-infrared and Raman spectroscopy:

Most of the research studies related to HME applications include analytical characterisation of the extruded materials by different spectroscopic techniques such as near-infrared (NIR) and Raman spectroscopy. In-line measurements using these techniques can be performed by linking a probe to the die located at the end of the barrel. Monitoring conditions are set up for either on-line or in-line measurements. The scan range, resolution, average scan and length time of the assay are the main important parameters for NIR. NIR data suggests that blend content uniformity is highly influenced by the screw speed and also but at lower degree by the feed rate (Chirkot, 2009). Recently, Raman spectroscopy has reached a particular interest in this field as another PAT tool that can be implemented in HME manufacturing processes (Netchacovitch et al., 2016). The aim of this application is to assess drug content and the appropriate solid dispersion obtained through the entire process (De Beer et al., 2011; Saerens et al., 2012). Both analytical methods, NIR and Raman spectroscopy, can be applied as in-line measurement tools to determine product homogeneity and API solid-state transformations. Other parameters such as moisture content and particle size distribution obtained from granulation and drying

processes are usually quantified by NIR (De Beer et al., 2011). These techniques were also used to analyse metoprolol tartrate and ethylene vinyl-acetate (EVA) extrudates. A set of temperature ranges and screw speeds in HME were carried out at laboratory and pilot scale. The application of these techniques revealed that API crystallinity decreases as the HME process temperature increases. However, the information provided by Raman spectroscopy clusters suggest that the main factor involved may be screw speed (Almeida et al., 2012). In-line NIR can be used to measure drug concentration as well as any drug-polymer interaction occurring during HME processes (Saerens et al., 2012).

Other analytical methods:

As mentioned above, computed tomography (Micro-CT) can be applied as a useful characterisation tool to determine the differences in density of pharmaceutical products such as extruded materials, granules or tablets comprised by API and excipients (Busignies et al., 2006; Crean et al., 2010; Sinka et al., 2004). Moreover, it can also determine if there is any phase separation occurring within the amorphous system as depicted in Figure 1.16 (Alhijjaj et al., 2016). This technique can also determine the internal porosity (%) of a product and correlate it to the pores size (Figure 1.17) (Verhoeven et al., 2009).

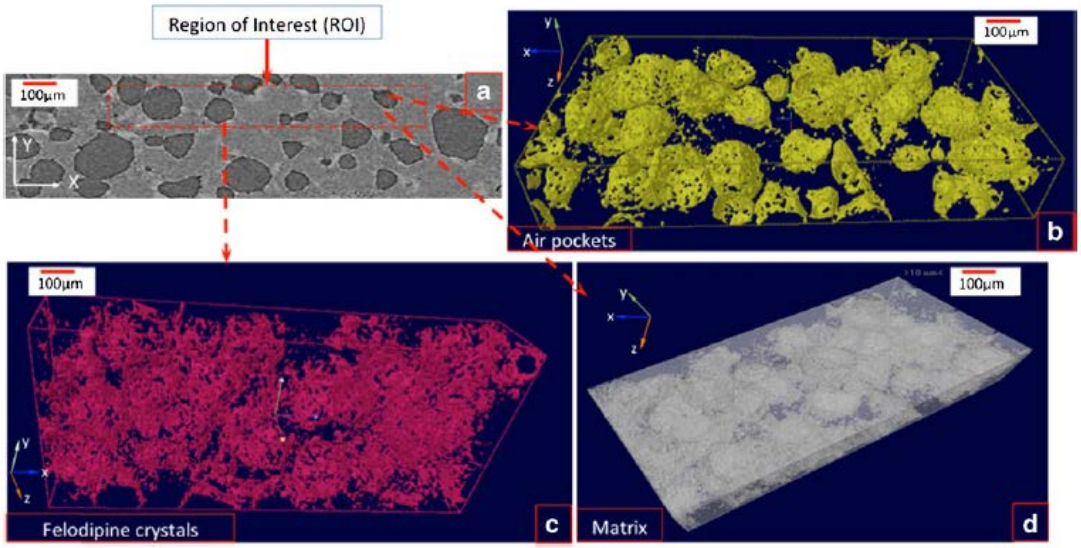

Figure 1.16. Micro-CT images of 30 % (w/w) felodipine solid dispersions indicating phase separation of crystalline drug (c). Reproduced from (Alhijjaj et al., 2016)

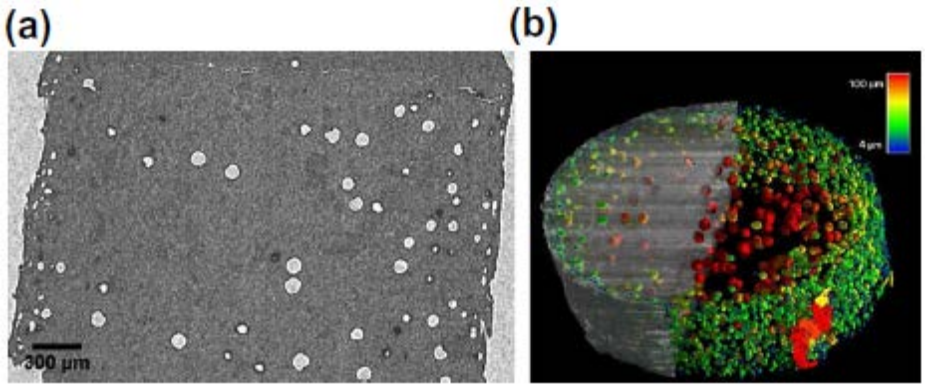

Figure 1.17. Micro-CT images of extruded mini-matrices of metoprolol tartrate and PEO 10 % (w/w). (a) Porosity at time 0h; (b) 3D image of the pores. Reproduced from (Verhoeven et al., 2009)

Another useful technique for the detection of possible recrystallisation events of amorphous solid dispersions as well as to detect drug-polymer phase separations is solid-state Nuclear Magnetic Resonance (NMR) (Ito et al., 2010; Yang et al., 2016). It calculates the correlation of a short relaxation time with the drug being at a separated phase. However, this method is not suitable to accurately determine the

crystalline or amorphous state of the drug during the process due to the close relaxation time values that are normally obtained at room temperature (Qi et al., 2010).

SEM is another technique used to characterize surface properties of amorphous solid dispersions. An example of SEM picture of an extruded material comprised of HPMCAS is depicted in Figure 1.18 (Dong et al., 2008). It is possible to observe the birefringence property exhibited by the crystalline material causing the light to split in two directions.

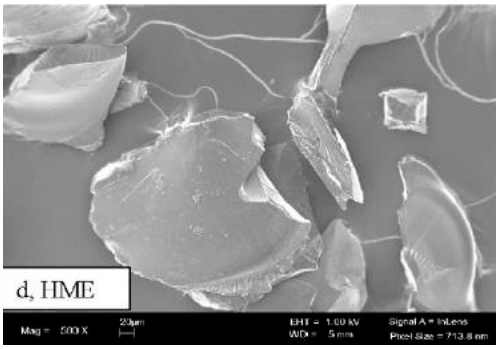

Figure 1.18. SEM micrograph of extruded material of HPMCAS. Reproduced from (Dong et al., 2008)

The main current pharmaceutical applications of twin-screw equipment in the area of HME were described above. As mentioned earlier in the introduction, the application of twin-screw equipment for the production of pharmaceuticals is broad due to the flexibility of the equipment and its components. As such, another application of twin-screw equipment comprises a common manufacturing process like wet granulation, achieved by the conversion of a twin-screw extruder into a twin-screw granulator. The following sections of this literature review will highlight the most recent advances reported in the area of twin-screw granulation (TSG).

1.2.4.2. Applications in the area of Twin-Screw Granulation (TSG)

One of the first reports of a successful and consistent twin-screw granulation process that was able to run in a continuous manner for several hours was reported by Keleb et al., (Keleb et al., 2004). Since then, several researchers have investigated twin-screw granulation as a possible continuous manufacturing technique such as Djuric et al., and Vercruysse et al., (Djuric et al., 2009; Vercruysse et al., 2015b) among others.

The transition from batch to continuous granulation processes requires the understanding of the differences in product properties as well as growth mechanisms that take place in each of these processes. It is important to consider that powder and liquid addition for a wet granulation process in a batch set-up is not the same as the addition mode when a continuous process such as twin-screw granulation is used (Meier et al., 2016). Different studies have clearly evidenced the great differences present in granules size distribution, densification and porosity attributes between a batch and a continuous granulation process (Beer et al., 2014; Lee et al., 2013). An increment on L/S ratio and a higher mixing degree provided by kneading elements, suggests that bigger and denser granules are produced in twin-screw granulation, leading to decreased porosity properties (Beer et al., 2014). In a similar line, Lee et al., (Lee et al., 2013) highlighted that the densification degree and porosity of granules produced by these two methods is highly influenced by the growth mechanisms involved. The consolidation degree within the process, the residence time and size of the initial nuclei before agglomeration, determine the densification properties of the granules.

Assessment of hydrophobic formulations and binder delivery:

Another interesting critical quality attribute (CQA) to consider in twin-screw granulation is drug content uniformity. It can be an issue in the case of hydrophobic drugs. However, the use of a foam binder in TSG has shown to improve the dispersion of the components involved (Li et al., 2015; Yu et al., 2014). Binder addition and delivery is a current interesting topic that many researchers are investigating. Correlations between the binder addition method and granules properties can also contribute to further understand overall granule growth mechanisms. Initial studies were performed by El Hagrasy et al., (El Hagrasy and Litster, 2013a) looking to binder distribution of granules in a 16 mm TSG and using one block of kneading elements (KE). It was found that the addition of a liquid binder compared to a solid form binder can produce less number of fines. However, some findings suggest that narrow particle size distributions can be obtained when the binder is added in powder form. The application of Particle Image Velocimetry (PIV) successfully correlated binder spreading time with liquid penetration and its influence on granules size distribution (Saleh et al., 2015).

Evaluation of particle attributes based on screw configuration:

An important factor of granule growth mechanisms in TSG processes is screw element configuration and the function of each element in the different stages of granule growth. Several screw configurations were studied to determine the role of each element. Configurations based on a screw formed by CE and KE elements have been commonly used as a flexible approach. Most of these studies (Dhenge et al., 2012; Dhenge et al., 2013; Van Melkebeke et al., 2008) concluded that CE elements provide the ideal *nucleation* or *wetting zone* for initial nucleation and

formation of agglomerates, whereas KE enhance binder distribution through coalescence and growth mechanisms. It was also suggested that KE elements provide high shear that cause deformation of bigger agglomerates and therefore breakage phenomena to occur, leading to smaller fine granules. Within nucleation mechanisms it is important to consider the method of addition of the granulation liquid. In TSG processes, the spraying method has some advantages compared to the pouring method. The spraying method creates smaller liquid droplets to be dispersed with the powder bed and therefore, dispersion mechanisms are favourable in the nucleation phase. Moreover, it is considered that nucleation is governed by two main parameters, the contact angle between the powder and the liquid droplet as well as the spreading coefficient of the liquid over the solid (Dhenge et al., 2012; Iveson, 2001).

A study carried out by Lute et al., (Lute et al., 2016) established the granulation mechanisms of separate screw configurations where an increase in the number of KE and CE with different pitch and conveying degrees were characterised. It was observed that granules increased their size and densification properties due to higher shear and compaction provided by an increased number of kneading elements. Moreover, an increase in the amount of fines was proportionally related to an increase in screw speed. The following addition of a short pitch (1D) conveying element to the previous KE block produced more spherical granules. These granules presented decreased size properties due to a cutting and shearing function provided by the CE pitch (Figure 1.19).

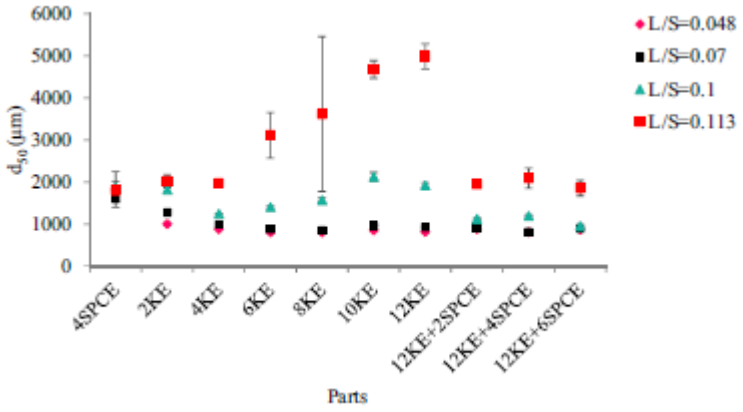

Figure 1.19. Representation of average particle size (d_{50}) achieved with screw configurations comprising kneading elements (KE) and short pitch conveying elements (SPCE) at different liquid to solid (L/S) ratios. Each point is the average of three replicates. Reproduced from (Lute et al., 2016)

These results agree with Liu et al., (Liu et al., 2015) who observed that the location of a CE element after KE block had a great impact on granules particle size, shape and strength properties, also due to the pitch of the CE.

Impact of DFS and DME screw elements on particle attributes:

As mentioned above, several studies have provided a rational behind twin-screw granulation and granules properties based on screw element configuration. Most of those studies evaluated the effect of CE and KE as main screw elements used in twin-screw granulation processes. The generation of multimodal particle size distributions can be addressed by the use of elements that apply less shear forces. For example Sayin et al., (Sayin et al., 2015b) studied the particle size distributions obtained when using a distributive feed screw (DFS) in comparison to a KE block configuration. It was observed that the amount of coarse granules obtained by DFS element was slightly higher than the configuration comprising KE. Therefore, KE

showed better efficiency in the breakage of coarse granules. Compared to the distributive mixing element (DME), Sayin et al., (Sayin et al., 2015a) found its capability to break coarse granules but also to form agglomerates through layering mechanisms of fines. It was one of the first studies to demonstrate a mono-modal particle size distribution achieved in TSG processes.

Most of the studies described above have assessed individual screw element performance and its impact on granules attributes. However, some studies have recently been published to understand the global impact of these elements when combined in a single screw configuration. Vercruysse et al., (Vercruysse et al., 2015a) observed that the addition of several DFS elements to a screw configuration formed by CE and KE considerably reduced the number of coarse granules achieved by CE and KE. This is preferred to have adequate flowability properties and to facilitate further processing steps such as tableting. It was also observed that when comparing the fractions of fines with those achieved by KE, this fraction was increased in the case of DFS elements. Moreover, DME proved to be successful on the reduction of fines when compared to CE and KE. The use of a narrow DME showed better particle size distribution results than the wide DME. The wide DME resulted not just on a reduction of fines but also in an increase of coarse granules.

Assessment of liquid distribution in TSG:

Previously in this review, different growth mechanisms that take place within TSG processes were mentioned. These studies focused on nucleation regimes and the effect of processing variables such as binder distribution and screw element performance. Liquid distribution in TSG processes provides an insight of the mixing degree between the powder bed and the liquid to form agglomerates.

Therefore, it can have a great impact on granules attributes such as particle size distribution and shape. In the initial mixing stages of the powder and the liquid, nuclei are formed during the nucleation stage (Figure 1.20). Then nuclei develop into agglomerates or granules through coalescence and layering mechanisms.

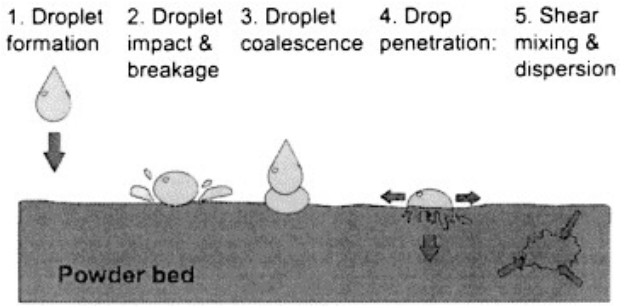

Figure 1.20. Steps involved in the nucleation stage. Reproduced from (Litster, 2001)

Nuclei formation is mainly influenced by drop penetration speed and drop spray flux. The spray flux (ψ) is a dimensionless parameter that controls nucleation phenomena and was first described by Litster et al., (Litster, 2001). Depending on the spray flux value, which depends on processing parameters such as powder and liquid feed rate, the formation of initial nuclei can be controlled. Appropriate control of nucleation mechanisms in TSG can be crucial to obtain granules with adequate shape and a narrow particle size distribution. Mixing behaviour and liquid distribution can be influenced by the length of time required for TSG, which is the residence time of the product in the barrel. Several studies have focused on the correlation between liquid distribution, mixing performance, residence time and granules properties by the application of NIR chemical imaging (Kumar et al., 2016; Kumar et al., 2014; Vercruysse et al., 2014). However, it is also possible to accurately determine liquid distribution by adding a dye or tracer to the granulation liquid. Dye concentration in the granules can be measured by UV-Vis spectrophotometry. Recent studies (El

Hagrasy et al., 2013b; Sayin et al., 2015a; Sayin et al., 2015b) have successfully correlated dye concentration with the liquid distribution achieved by mixing elements (Figure 1.21). A similar approach is applied in the study included in chapter 5 of this thesis.

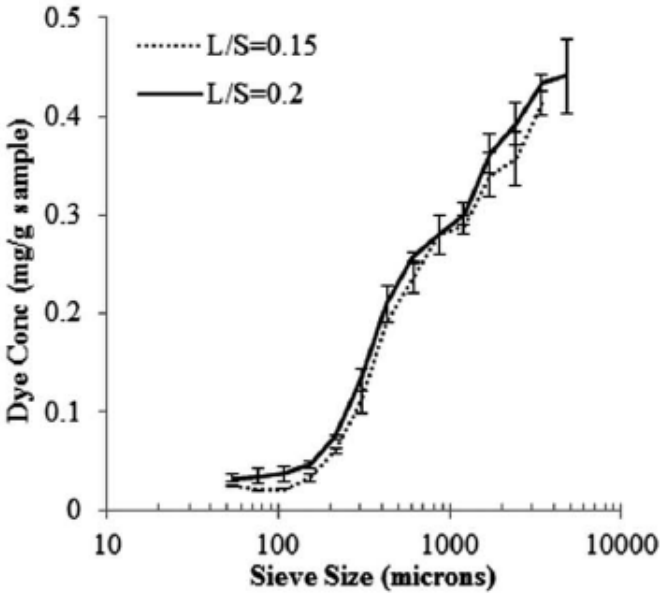

Figure 1.21. Liquid distribution represented by dye concentration as a function of particle size. Reproduced from (El Hagrasy and Litster, 2013b)

1.3. Project aims

It was outlined above that the pharmaceutical industry requires flexible and reduced cost manufacturing processes to produce high-quality medicines. The implementation of continuous manufacturing can be an alternative approach to batch manufacturing. Processes such as HME and TSG can be easily integrated as part of a continuous production line delivering intermediate products that are processed to tablets. This PhD project comprises the development of two types of intermediate products by the application of HME and TSG techniques. Therefore, this PhD

project covers twin aims based on the application of twin screw processing equipment and the product properties arising.

1.3.1. Aims in the area of HME

The main aim comprised the development of HME stable amorphous solid dispersions of a poorly soluble drug in order to potentially enhance its oral bioavailability properties. The drug molecule selected was albendazole (ABZ) (Figure 1.22) which is classified as BCS Class II due to its low solubility and high permeability properties (Kasim, 2004). It is widely known that the low solubility and dissolution rate of ABZ lead to erratic absorption (below 5 %) from the gastrointestinal tract mainly observed through pharmacokinetic studies (Jung et al., 1998; Marriner, 1986). ABZ is an anthelmintic drug for human and veterinary use indicated for the treatment of hydatid disease, amongst other parasitic worm infestations. Moreover Newman et al., (Newman et al., 2012) classified ABZ as one of the poorly soluble drugs where a solid phase transformation using a hydrophilic polymer such as PVP K12 could be a suitable approach to enhance ABZ bioavailability. Based on the work published by Torrado et al., (Torrado, 1996b), amorphous solid dispersions of ABZ in PVP K12 were manufactured by the classic solvent evaporation method. These formulations showed a high increase in the dissolution rate of ABZ and later Torrado et al., (Torrado, 1997) demonstrated an increase of its oral bioavailability. To our knowledge, there are no previous evidences of amorphous solid dispersions of ABZ manufactured by HME process.

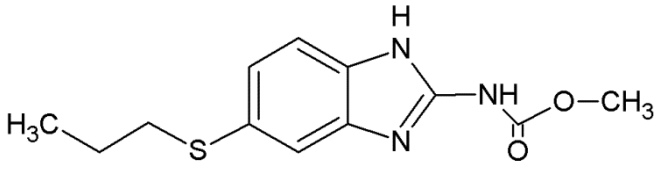

Figure 1.22. Molecular structure of ABZ

Two hydrophilic polymers that present different physicochemical properties were used as carriers in the development of amorphous solid dispersions of ABZ. The first one, Polyvinylpyrrolidone (PVP K12) is an amorphous polymer with low viscosity properties that is produced by a synthetic route and is frequently used as a binder excipient in oral formulations. The second polymer used, Polyethylene glycol (PEG 6000) is a plasticiser excipient which in solid form can be used as carrier to enhance the dissolution properties of poorly soluble drugs. It is known by its crystalline structure which is confirmed by an endothermic event in thermal analysis. Their molecular structures are depicted in Figures 1.23 and 1.24.

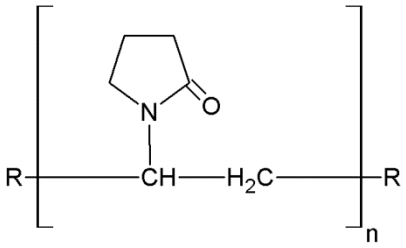

Figure 1.23. Molecular structure of PVP K12, value of n indicates molecular weight of the PVP grade (molecular weight of 2500 for PVP K12)

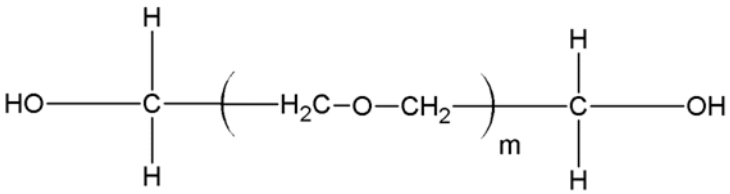

Figure 1.24. Molecular structure of PEG, value of m indicates the average number of oxyethylene groups and is related to the molecular weight of the PEG grade (molecular weight of 5000-7000 for PEG 6000)

Both polymers are considered as highly hydrophilic and have low toxicity. They are commonly used as excipients and carriers in the development of solid oral dosage

forms for diverse pharmaceutical applications. Previous studies of successful amorphous solid dispersions of ABZ comprising PVP K12 and PEG 6000 developed by the solvent evaporation method were mentioned above. The physicochemical properties of amorphous solid dispersions such as solid state and dissolution behaviour are assessed in chapters 2 and 3 of this thesis.

1.3.2. Aims in the area of TSG

The main aim was to understand the impact of processing conditions on final product attributes in TSG from an engineering perspective. The information obtained can be included within the design of space of TSG processes. As indicated above, many studies have focused on evaluating the influence of screw configuration and processing conditions on product attributes. However, there is still a lack of understanding of the mechanisms behind granule formation, granule rupture and the relationship between these mechanisms and processing variables in TSG. The results of this project are presented in chapter 5 of this thesis.

2. Development of HME formulations of Albendazole using PVP K12

2.1. Introduction

In this chapter, HME technique is used to produce amorphous solid dispersions of ABZ with the polymeric carrier PVP K12 which was described in chapter 1. The mixing degree provided by the twin-screw extruder and the use of a hydrophilic polymeric carrier has previously shown to enhance the dissolution properties of poorly soluble drugs (BCS Class II) (Shah et al., 2013). As described in chapter 1 of this thesis, the transformation of the drug's solid form from an ordered crystalline structure to an amorphous disordered structure can greatly increase its dissolution properties. The characterisation of the extruded materials by the application of diverse solid state characterisation techniques enabled the determination of the physicochemical properties of amorphous solid dispersions. This chapter provides a better understanding of drug-polymer behaviour in amorphous solid dispersions and also the effects observed after storage of the extruded materials under specific conditions.

2.2. Aims and objectives

The aim of this chapter comprised the development and characterisation of ABZ formulations manufactured by HME processing to improve ABZ dissolution properties, and potentially its oral bioavailability properties. Solid state and physicochemical properties of the developed formulations are evaluated to understand the role of the polymeric matrix on the stabilisation of amorphous solid dispersions of ABZ.

2.3. Materials and methods

2.3.1. Materials

Poorly water soluble drug Albendazole (ABZ) was selected as our drug molecule in order to improve its solubility and dissolution properties by conversion to the amorphous state using a novel technique such as HME processing. The hydrophilic polymer PVP K12 was selected as carrier due to its adequate physicochemical properties such as melting temperature (T_m) and glass transition temperature (T_g). The physicochemical properties of both drug and polymer are shown in Table 2.1.

Albendazole (ABZ, ≥98 %) was purchased from Sigma-Aldrich Company Ltd. (Gillingham, Dorset, United Kingdom). Pharmaceutical grade polyvinylpyrrolidone K12 (PVP K12 PF), was kindly donated by BASF (Cheshire, United Kingdom). Other reagents such as methanol (HPLC grade, ≥99.5 %), potassium chloride AR grade, sodium dihydrogen phosphate (>99.0 %) and glacial acetic acid (ACS reagent, ≥99.7 %) were obtained from Sigma-Aldrich.

Table 2.1. Physicochemical properties of formulation materials according to Mahlin et al., and Reintjes (Mahlin et al., 2013; Reintjes, 2011)

Material	**T_m (°C)**	**T_g (°C)**
ABZ	210[a]	60
PVP K12	135[a]	90

[a]Experimental data

2.3.2. Miscibility studies

Miscibility properties of ABZ and PVP K12 were theoretically assessed using the Hansen solubility parameter calculations. The results were confirmed by hot-stage microscopy (HSM) using a Reichert-Jung® polyvar optical microscope fitted with a hot-stage and a Fisher Scientific® 16 mm diameter circle glass slide and cover slip

(Leicestershire, United Kingdom). Raw materials and physical mixtures (PM) comprising 1 %, 5 %, 10 % and 20 % (w/w) were studied using a heating rate of 10 °C/min.

2.3.3. Formulations obtained by Hot-Melt Extrusion (HME)

Amorphous solid dispersions of formulations comprising ABZ and PVP K12 (total sample weight of 50 g) with drug contents of 1 %, 5 %, 10 % and 20 % (w/w) were developed by HME process (Table 2.1) (Jones et al., 2014; Kelly et al., 2015). Previous sieving of PVP K12 through a mesh of 250 µm was carried out for particle size homogenisation purposes. Physical mixtures of ABZ – PVP K12 (F1 to F3 as in Table 2.2) were manually blended with the help of a recipient for 2-5 minutes prior to extrusion. Following formulations F4 to F7 were blended for 20 minutes using a Turbula® T2F mixer (Glen Mills Inc., New Jersey, United States) at a speed of 46 rpm. Formulations were manufactured using two different processing temperatures, 70-145 °C and 70-135 °C (Table 2.3). Degassing during HME process (zone 6 of the barrel) was carried out to manufacture formulations F4 to F7 in order to decrease the porosity of the extruded materials. All formulations were processed by HME using a Thermo Scientific® Process 11 co-rotating twin-screw extruder (40L/D) (Karlsruhe, Germany). The 11 mm screw diameter extruder was fitted with a single orifice die of 2.0 mm diameter.

Processing of the materials in the twin-screw extruder was performed once all barrel temperatures reached steady state and extruded materials were collected after 2 minutes. The processing parameters are presented in Table 2.3 and the screw configuration is depicted in Table 2.4. Cooling of the strands was performed at room temperature and then stored in a sealed glass container under temperature

controlled conditions of 25 °C and 50 °C. The storage chambers were not humidity controlled but moisture content (%) was measured at samples collection time. Stability studies of all extruded materials were performed after 6 months storage under the conditions indicated in the text.

Figure 2.1. Set-up of Thermo Scientific® 11 mm twin-screw extruder

Table 2.2. Formulations manufactured by HME

Formulation	**Ratio of ABZ / PVP K12 (% w/w)**
F1	1/99
F2	5/95
F3	10/90
F4	1/99
F5 (a, b, c)	5/95
F6	10/90
F7	20/80

Table 2.3. HME processing parameters of ABZ – PVP K12 formulations

HME formulation	Barrel temperatures (°C, zones 1, 2, 3 and 4-8)	Melt temp. (°C)	Screw speed (rpm)	Torque (Nm)	Throughput (kg/h)
F1	70, 120, 140, 145	142 - 145	100	1.2 - 3	0.10 - 0.15
F2	70, 120, 140, 145	140 - 144	100	1.2 - 3	0.15
F3	70, 120, 140, 145	142 - 144	100	1.2 - 2.7	0.10 - 0.15
F4	70, 140, 140, 140	134 - 139	100	5.4 - 10.0	0.20
F5a	70, 120, 130, 135	130 - 133	100	3.0 - 10.5	0.20
F5b	70, 120, 130, 135	133 - 136	100	3.0 - 10.5	0.23
F5c	70, 120, 130, 135	135 - 136	100	2.4 - 10.3	0.13
F6	70, 120, 130, 135	132 - 135	100	1.8 - 8.8	0.14
F7	70, 120, 130, 135	132 - 134	100	0.7 - 9.1	0.10 - 0.11

Figure 2.2. Image of 11mm screw configuration used in HME process

Table 2.4. Detailed screw configuration used in HME process

Formulation	Screw configuration
F1 to F7	*(CE 11/40) x 7 + (KE 10/90°) x 8 + (KE 10/60°) x 4(F) + (CE 11/40) x 8 + (KE 10/60°) x 6(F) + (CE 11/40) x 7 + (KE 10/90°) x 4 + (KE 10/60°) x 3(F) + (KE 10/30°) x 5(F) + (CE 11/40) x 9

*Where CE 11/40 is conveying element with a pitch of 11 mm and length of 40 mm; KE 10/90°: kneading element with thickness of 10 mm and 90° offset angle; KE 10/60°: kneading element with thickness of 10 mm and 60° offset angle; KE 10/30°: kneading element with thickness of 10 mm and 30° offset angle and F means forward direction.

2.3.4. Scanning Electron Microscopy (SEM)

HME formulations containing ABZ – PVP K12 were analysed by SEM for surface characterisation purposes. Gold-coated samples of extruded materials (F1 to F3) were mounted on the sample holder using silver paint. Uncoated samples of extruded materials (F4 to F7) and uncoated samples of pure ABZ and physical mixtures ABZ – PVP K12 were mounted using double-sided conductive tape. Measurements were performed using a Hitachi® SU 6600 high-resolution analytical FE-SEM (Tokyo, Japan) at 5.00 and 20.00 kV, a Zeiss® IS50 (Oberkochen, Germany) at 20.00 kV and a Hitachi® TM 1000 table top microscope (Tokyo, Japan) at 15.00 kV.

2.3.5. X-Ray Powder Diffraction (XRPD)

All extruded materials, physical mixtures and raw materials were analysed by XRPD in order to determine the molecular transformation of the drug from crystalline to amorphous state. A Bruker® AXS D8 advanced transmission diffractometer and a Bruker® D2 Phaser diffractometer (Karlsruhe, Germany) were used. Bruker® D8 diffractometer used theta-theta geometry, primary monochromatic radiation (Cu Kα1λ = 1.54056 Å), a Vantec 1D position sensitive detector and an automated multi-position x-y sample stage. Bruker® D2 Phaser diffractometer used theta-theta geometry, primary monochromatic radiation (Cu Kα1,2 = 1.5406 Å line focused), a LynxEye 1D detector and an automated 6 sample auto changer carousel. Data were collected in the range 4-35° 2θ with a 0.017° 2θ step size (Bruker® D8), a 0.014° 2θ step size (Bruker® D2) and 1 s step^{-1} count time.

2.3.6. Differential Scanning Calorimetry (DSC)

Thermal analysis of the extruded materials, physical mixtures drug-polymer and raw materials was performed using a Mettler Toledo® DSC 822^e (Greifensee, Switzerland) differential scanning calorimeter. A standard In/Zn calibration was performed and an inert gas such as N_2 was used to purge throughout the equipment at 150 mL/min. Samples were ground using a mortar and pestle then introduced into 40 µL sealed aluminium crucibles with a pierced lid. All samples were heated from 25 to 250 °C, melting temperature (T_m) of ABZ (208-210 °C), at a heating rate of 10 °C/min, data was evaluated using the Star®e software.

2.3.7. Karl-Fischer (KF) studies

A Mettler Toledo® DL-39 Karl-Fischer instrument (Schwerzenbach, Switzerland) was used to assess the water content of the extruded materials after 6 months storage. Previous sample preparation required grinding of the sample using a mortar and a pestle followed by dissolution of 10 mg of extruded material in 1 mL of methanol.

2.3.8. In-vitro dissolution studies

Dissolution studies of the extruded materials and physical mixtures were carried out using a Sirius T3 measurement system (East Sussex, United Kingdom). Sample preparation required manual grinding using a mortar and a pestle to a fine powder, followed by the formation of a 3 mm diameter tablet by weighing between 7 to 12 mg of ground material. Tablets were pressed using a custom made die and a Specac® manual hydraulic press (Kent, United Kingdom) to 80 kilogram-force (kgf). A Sirius T3 measurement system was then used to obtain material dissolution profiles between pH values of 2 to 7 (data at pH 2 is shown). A stationary disk apparatus was used consisting of a tablet holder where die and tablet were inserted

and analysed using 15 mL of acetate phosphate buffer dissolution media. The buffer media was used to simulate in-vitro gastrointestinal conditions by pH automatic adjustment from 2.0-3.7 (time 0-30min), 3.7-5.2 (time 30-60min), 5.2-7.1 (time 60-90min), and 7.1 (time 90-130min) and tablet surface facing the media to facilitate tablet erosion. PM as well as extruded materials produced were analysed under sink conditions by a titration method. Data points were collected every 30 seconds by a spectroscopic UV dip-probe at a wavelength of 250 nm and transformed using pKa values (4.08; 10.34) and Molar Extinction Coefficient (MEC) into dissolution profile curves representing drug release (%) over time. Data points (amount of drug released, µg) were normalised by the exact drug content in each tablet, taking into account the weight (mg) of each individual tablet. This value was then used to calculate the maximum concentration in solution (µg/mL) as well as % of drug released (details of these calculations can be found in the appendix).

2.3.9. Particle size analysis

Particle size analysis of physical mixtures and ground extruded materials were measured (sample measurement time of 3 s) using a Malvern® Mastersizer 3000 (Worcestershire, United Kingdom) fitted with the *Aero S* dry dispersion unit, a micro tray and air pressure adjusted to 1 bar.

2.3.10. Determination of drug content by UV spectrophotometry

An off-line Varian Cary® 50 UV-spectrophotometer (California, United States) was used to determine the % of drug content within the extruded materials. A λ_{max} of 295.0 nm and a glass cuvette of 1.0 cm path length were used. Calibration standards of ABZ in methanol (HPLC grade) at concentrations of 0.10, 0.20, 0.50 and 0.75 mg/mL were prepared from an ABZ stock solution of 1 mg/mL. Then, samples of

the extruded materials of 0.20 mg/mL were prepared from stock solutions of 1 mg/mL. All samples, including calibration standards were diluted (1 mL of solution in a 10 mL volumetric flask) in order to obtain readable absorbance values. Total % of ABZ in the extruded materials was calculated using the calibration curve obtained from the calibration standards.

2.4. Results and discussion

2.4.1. Assessment of product attributes and physicochemical properties

2.4.1.1. Miscibility studies

The application of the *Hoy and Hoftzyer/Van Krevelen* method through the Hansen solubility parameter calculation evidenced that ABZ and PVP K12 are highly miscible, with a solubility parameter difference ($\Delta\delta$) of 0.18 $MPa^{1/2}$. Individual solubility parameter value (δ = 21.12 $MPa^{1/2}$) for ABZ was calculated (Equation 2.1) based on the contribution of dispersive forces (F_d), polar interactions (F_p) and hydrogen bonds (E_h) as shown in Equations 2.2 to 2.4. Molar volume of ABZ (203.2 cm^3) was considered. The solubility parameter value (δ = 21.3 $MPa^{1/2}$) of PVP K12 was taken from literature (Forster, 2001). PM of ABZ and PVP K12 were also characterised by Hot-Stage Microscopy (HSM) to assess the miscibility properties of the two components and also their suitability for HME processing. Figures 2.3 to 2.6 illustrate ABZ sample alone and images 2.7 to 2.9 the results of PM of ABZ – PVP K12 at 10 % (w/w) under different temperature conditions.

$$\delta_{total} = \sqrt{{\delta_d}^2 + {\delta_p}^2 + {\delta_h}^2} \qquad \text{Equation 2.1}$$

$$\delta_d = \frac{\sum_i F_{di}}{\sum_i V_i} \qquad \text{Equation 2.2}$$

$$\delta_p = \frac{\sqrt{\sum_i {F_{pi}}^2}}{\sum_i V_i} \qquad \text{Equation 2.3}$$

$$\delta_h = \frac{\sqrt{\sum_i E_{hi}}}{\sqrt{\sum_i V_i}}$$ Equation 2.4

i: structural group within the molecule

F_d: group contributions to dispersion forces

F_p: group contributions to polar forces

E_h: group contributions to hydrogen bond energy

V_i: group contributions to molar volume

Table 2.5. ABZ group contributions to calculate F_d, F_p and E_h

Functional group	**F_{di}**	**F_{pi}**	**E_{hi}**
CH_3 (2x)	420	0	0
CH_2 (2x)	270	0	0
CH (3x)	80	0	0
S (1x)	440	-	-
NH (2x)	160	210	3100
N (1x)	20	800	5000
C (4x)	70	0	0
CO (1x)	290	770	2000
O (1x)	100	400	3000
Total	3070	2390	16200

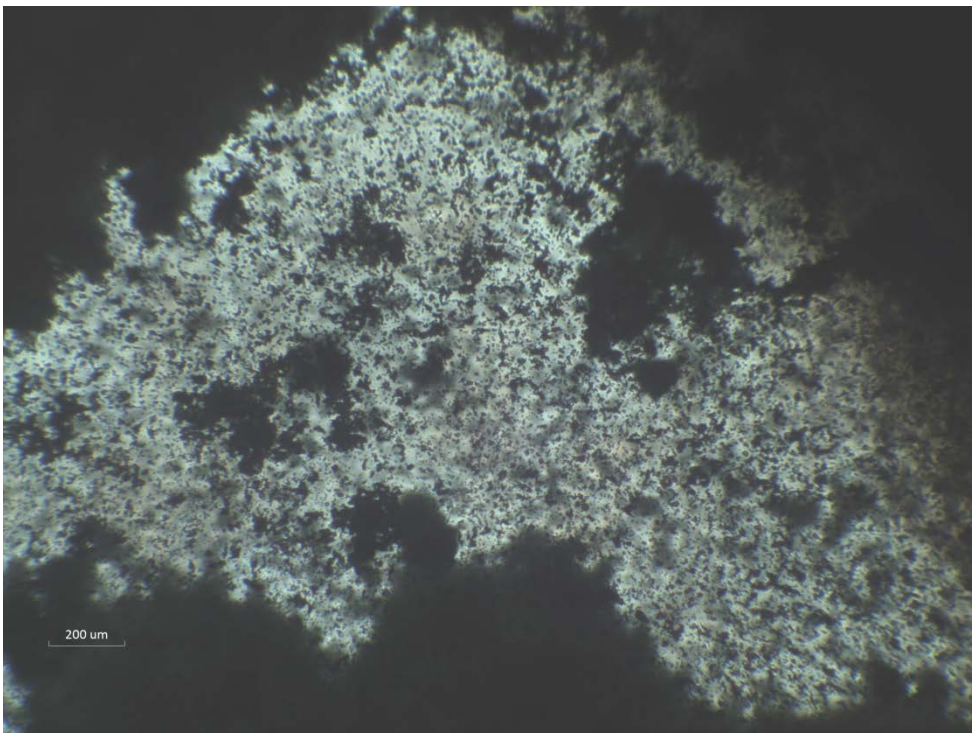

Figure 2.3. HSM image (10X) of ABZ alone at 80 °C

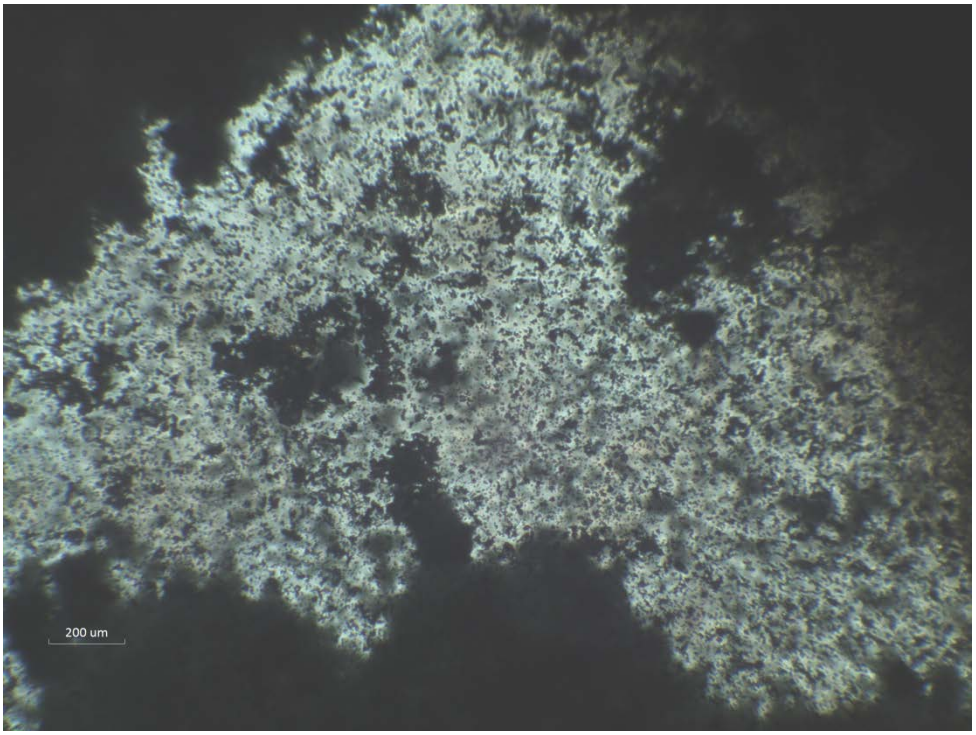

Figure 2.4. HSM image (10X) of ABZ alone at 145 °C

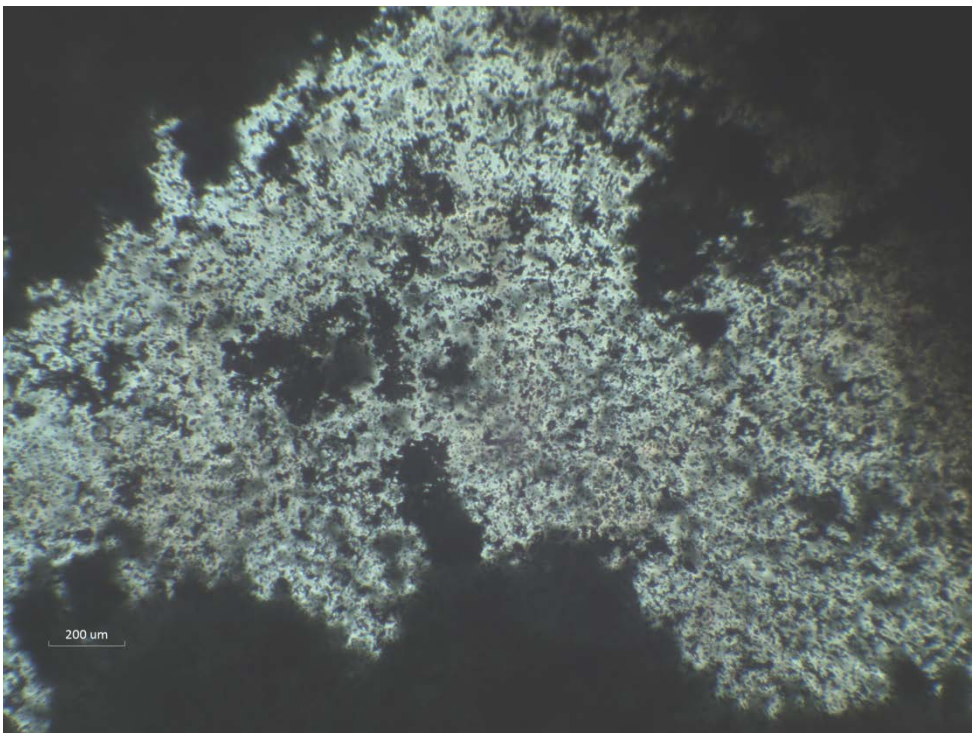

Figure 2.5. HSM image (10X) of ABZ alone at 180 °C

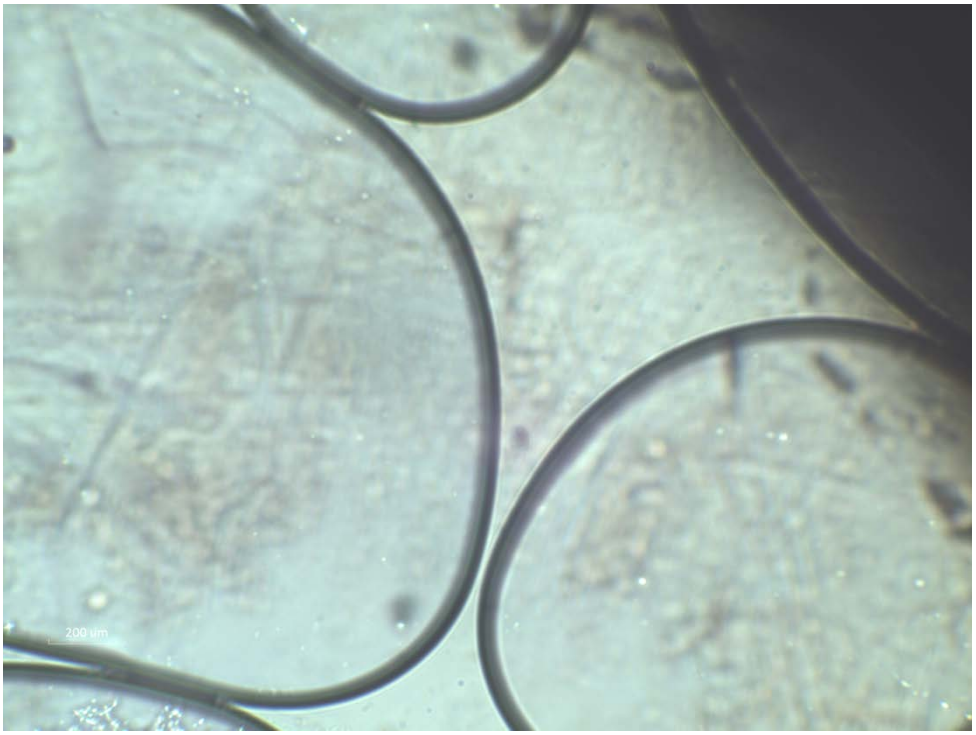

Figure 2.6. HSM image (10X) of ABZ alone at 210 °C

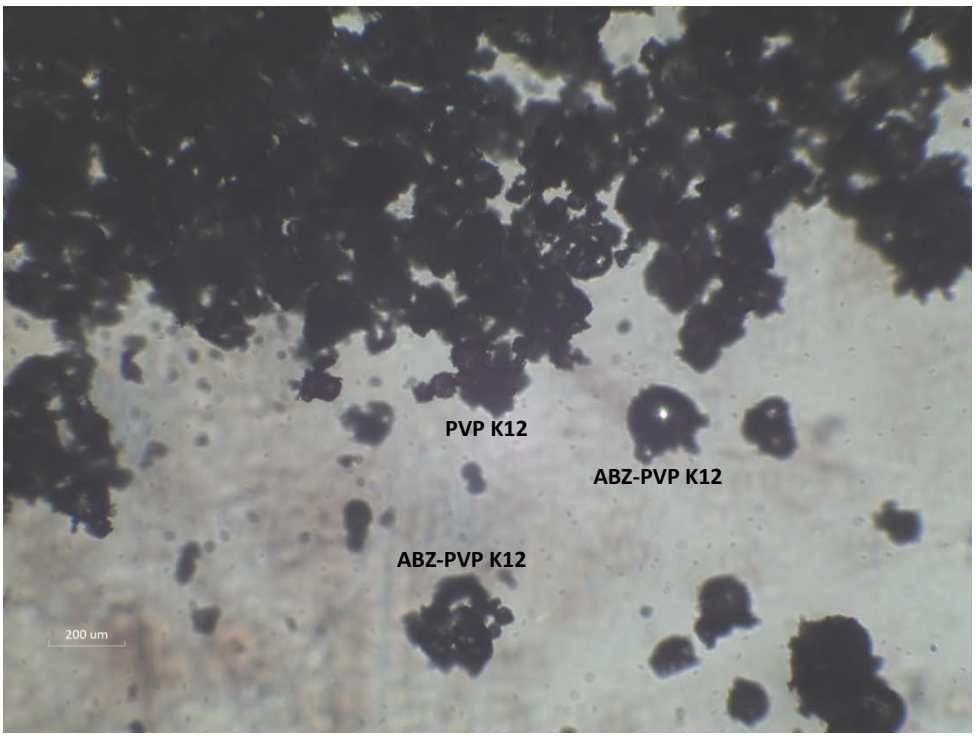

Figure 2.7. HSM image (10X) of PM ABZ-PVP K12 (10 % w/w) at 80 °C

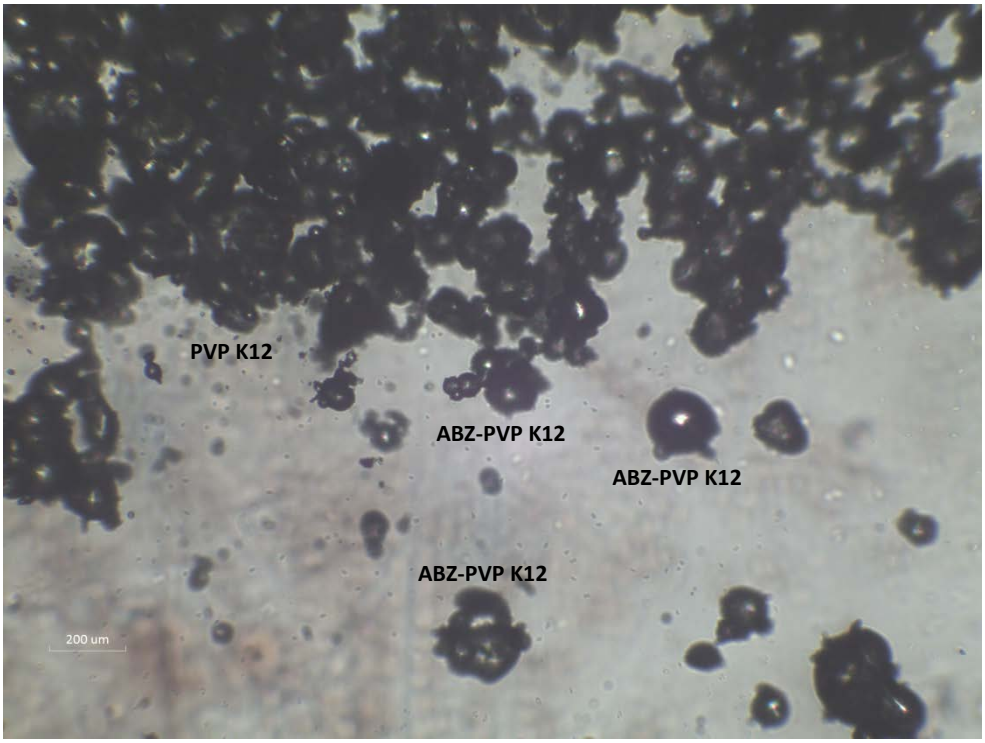

Figure 2.8. HSM image (10X) of PM ABZ-PVP K12 (10 % w/w) at 145 °C

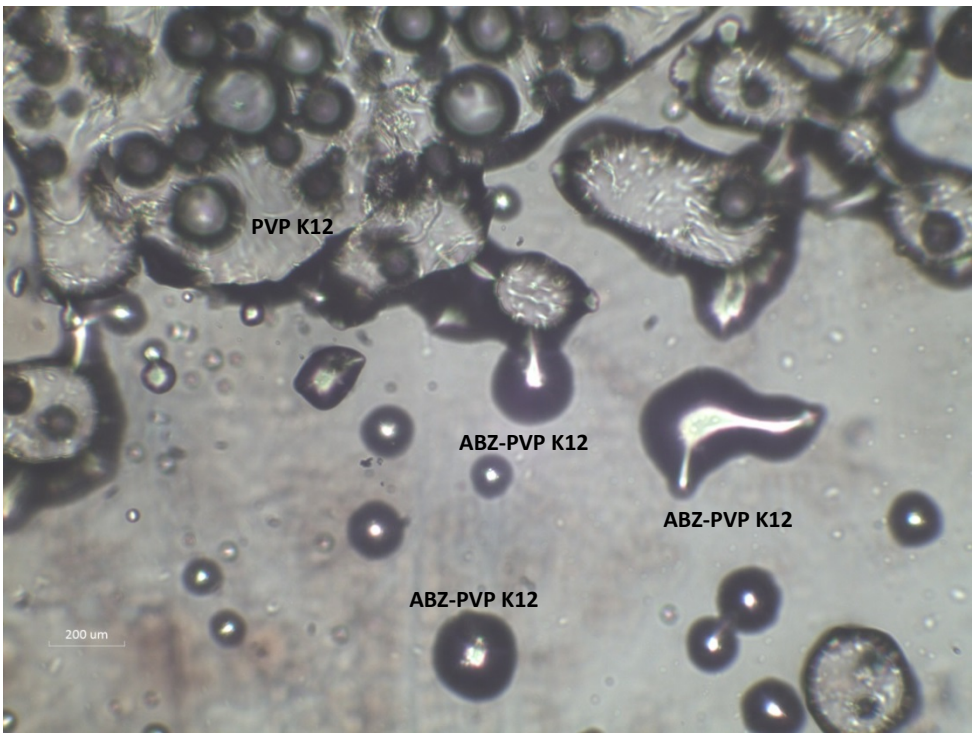

Figure 2.9. HSM image (10X) of PM ABZ-PVP K12 (10 % w/w) at 180 °C

Solid ABZ appears as dark crystals using a 10X magnification lens, similar to the results observed by Moyano et al., (Moyano, 2014) using 100X magnification. In their study, commercial ABZ melting event is characterised at an onset temperature of 186 °C and complete melting is observed at 216 °C. Similar results are shown in Figures 2.3 to 2.6, where commercial ABZ particles are stable at temperatures between 45 to 180 °C but complete melting event is shown at 210 °C. A physical mixture, ABZ – PVP K12 at 10 % (w/w), shows a characteristic birefringence property that allows the differentiation between amorphous polymer and ABZ crystals (Figures 2.7 to 2.9). Initial stages of polymer melting can be observed at a temperature of 145 °C (Figure 2.8) similar to DSC thermal analysis behaviour observed by Baird and Taylor (Baird and Taylor, 2012) and at 180 °C, drug crystals dissolve within the polymer indicating the miscibility properties of the two materials (Figure 2.9). These results confirm the ability of ABZ and PVP K12 to form a

miscible system when temperatures above the T_g of the polymer are applied (T_g of PVP K12 = 90 °C) (Reintjes, 2011). Similar results were observed for the other PM samples of ABZ – PVP K12.

2.4.1.2. Scanning Electron Microscopy (SEM)

Formulations F1 to F7 processed by HME were characterised by SEM microscopy to assess the physical state of the drug within the polymeric matrix. Extruded materials F1 to F3 appear to be homogeneous when compared to the physical mixtures (Figure 2.10). It was also observed that as the amount of drug increased, the porosity within the samples also increased which suggests that HME processing temperature was high for PVP K12. It also indicates that there is a correlation between PVP K12 and the proportion of ABZ in the system with the relaxation properties exhibited by the extruded materials (Sarode and Kumbharkhane, 2012). Moreover, analysis of extruded materials (Figure 2.10, e to g) suggests the presence in all samples of a laminated and fractured surface that agrees with the findings reported in previous research on PVP K12 matrices (Okwuosa, 2016; Pina et al., 2014; Sun et al., 2008). In order to decrease the porosity and possible presence of air bubbles within the extruded materials, formulations were extruded at 145 $^{\circ}$C (same as F1 to F3) but degassing by opening the top-barrel at zone 6. It was observed (visually and using computed tomography, data not shown) that only degassing was not enough to produce extrudates with uniform shape and decreased porosity. Therefore, optimisation of processing temperature was performed by extruding at 140 $^{\circ}$C (F4) and 135 $^{\circ}$C (F5 to F7).

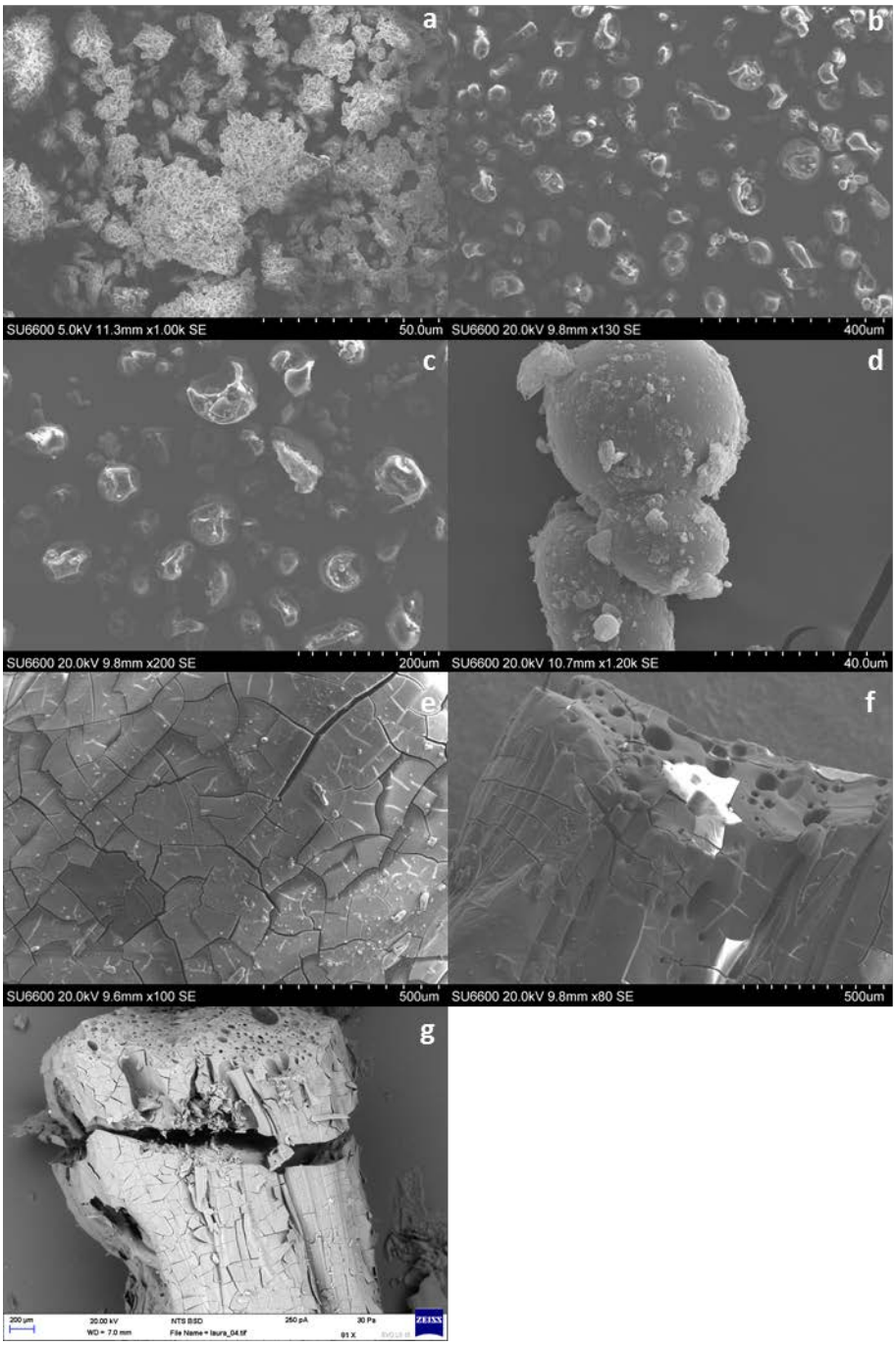

Figure 2.10. SEM images of ABZ alone (a), physical mixtures ABZ–PVP K12 at 1 %, 5 % and 10 % (w/w) (b–d) and extruded materials of ABZ–PVP K12 (post extrusion), F1 to F3 (e–g)

SEM images of formulations F4 to F7 (produced by HME at 135 °C) indicate that at this optimised processing temperature the porosity of ABZ extruded materials is still

present (Figures 2.11 to 2.18). It can be observed that at lower drug contents such as 5 % and 10 % (w/w), there are almost no internal pores present while at 20 % (w/w) drug content, the number of internal pores increases. When the samples are analysed after 6 months storage (Figures 2.12, 2.14, 2.16 and 2.18), it is observed that the polymer matrix formed by PVP K12 present altered surface features such as cracks (Feng et al., 2013).

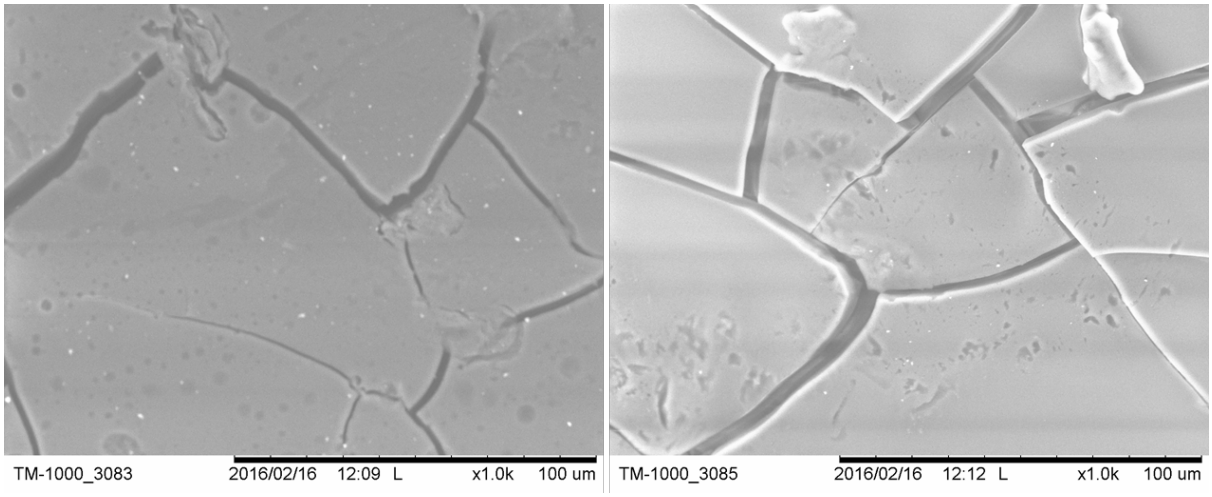

Figure 2.11. SEM images, side view (left) and top view (right) of F4 extruded material (post extrusion)

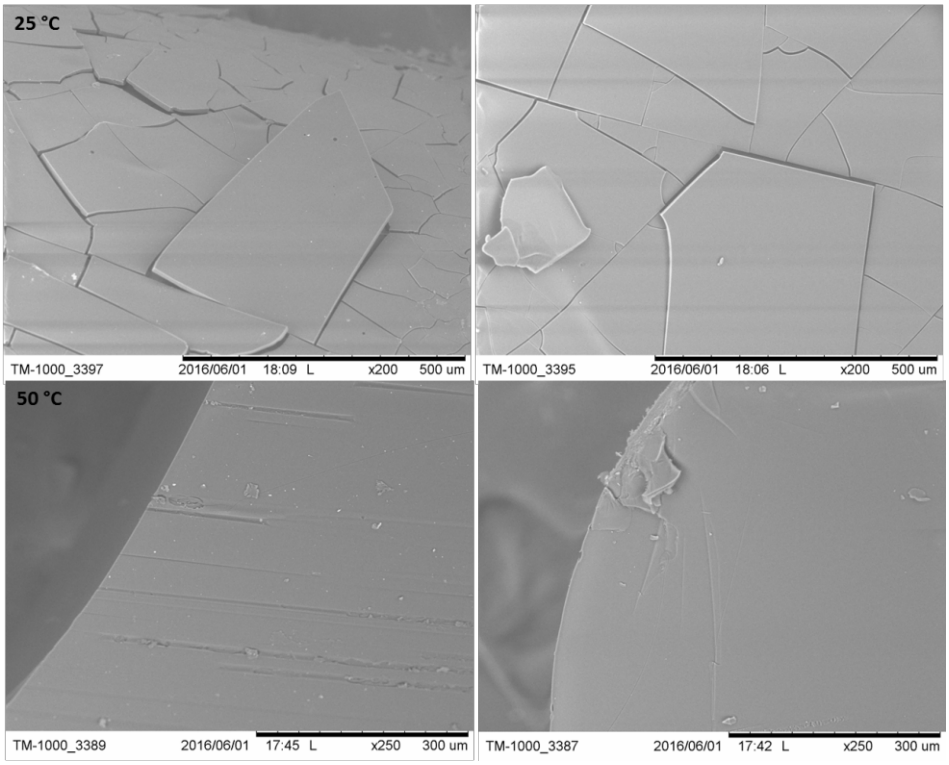

Figure 2.12. SEM images after 6 months storage at 25 °C and 50 °C, side view (left) and top view (right) of F4 extruded material

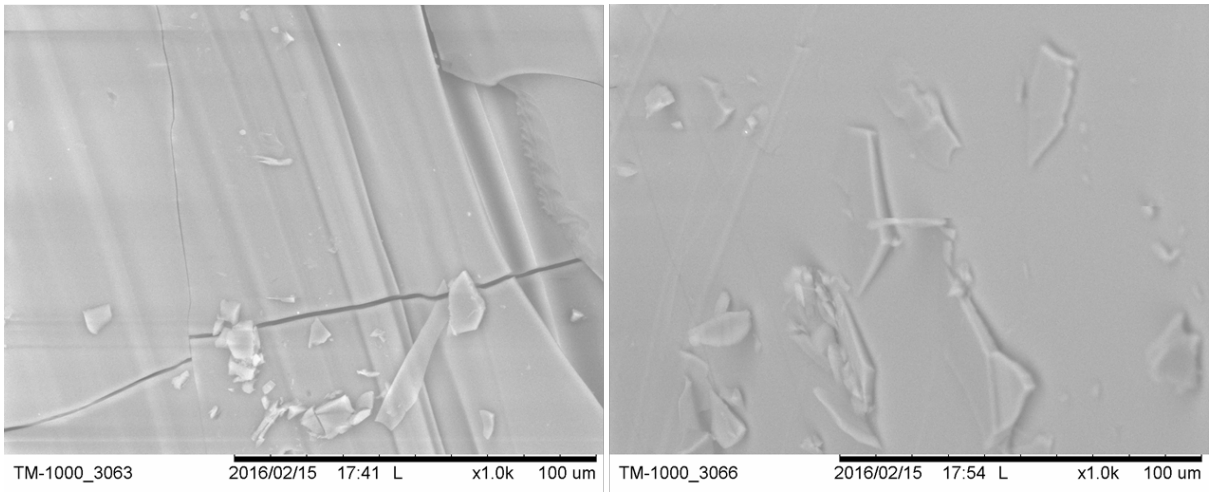

Figure 2.13. SEM images, side view (left) and top view (right) of F5 extruded material (post extrusion)

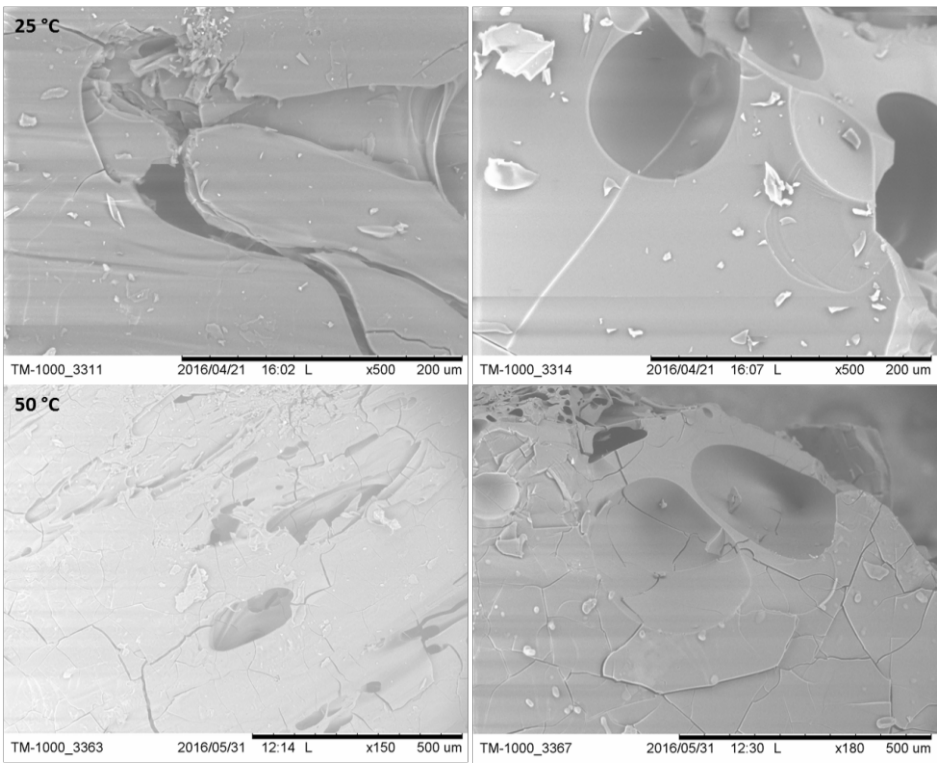

Figure 2.14. SEM images after 6 months storage at 25 °C and 50 °C, side view (left) and top view (right) of F5 extruded material

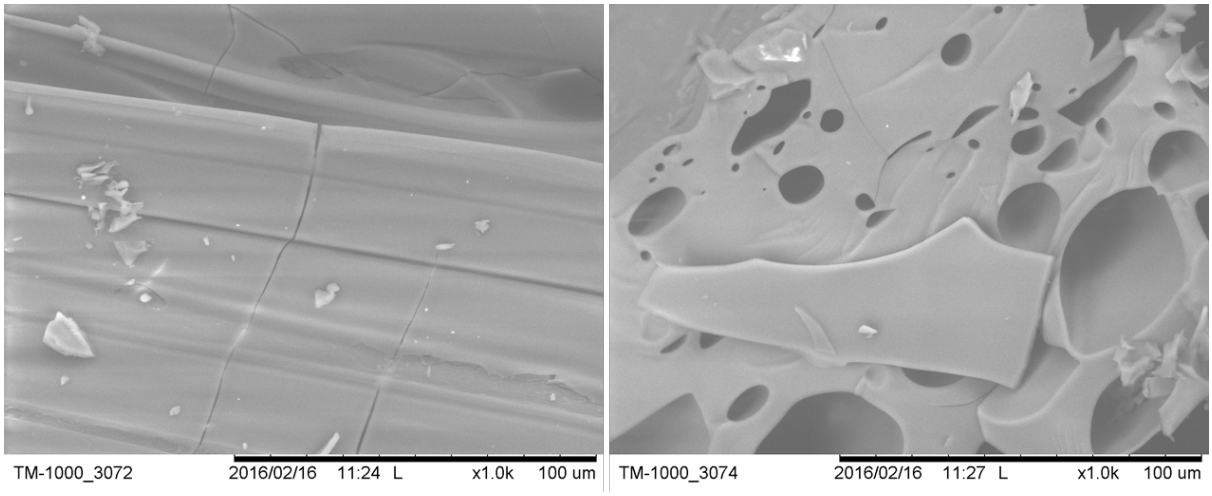

Figure 2.15. SEM images, side view (left) and top view (right) of F6 extruded material (post extrusion)

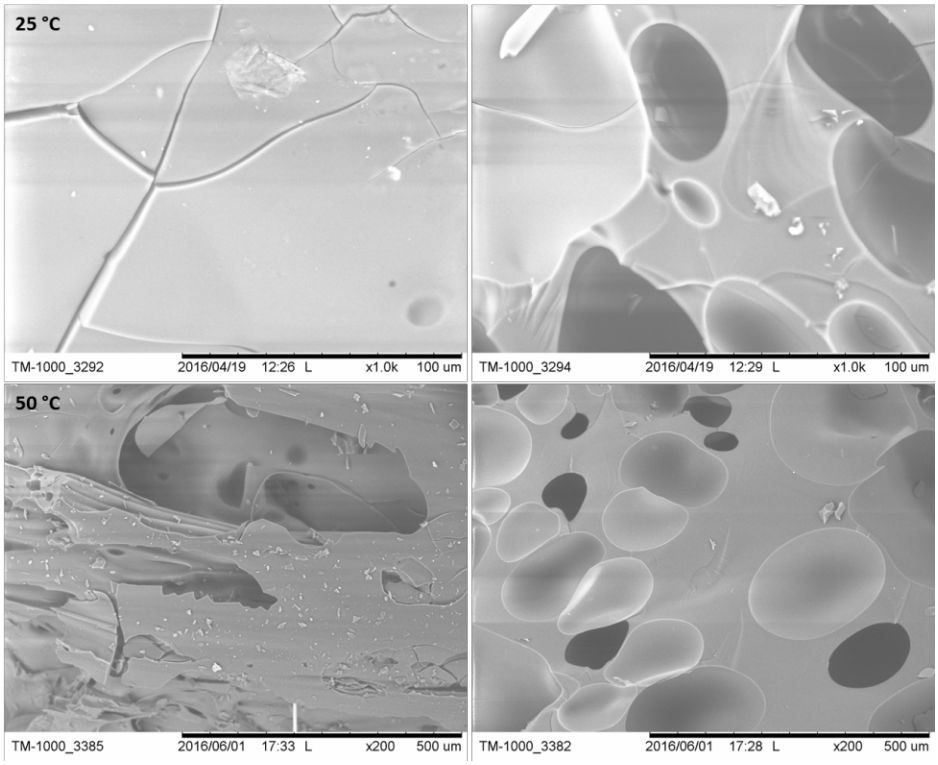

Figure 2.16. SEM images after 6 months storage at 25 °C and 50 °C, side view (left) and top view (right) of F6 extruded material

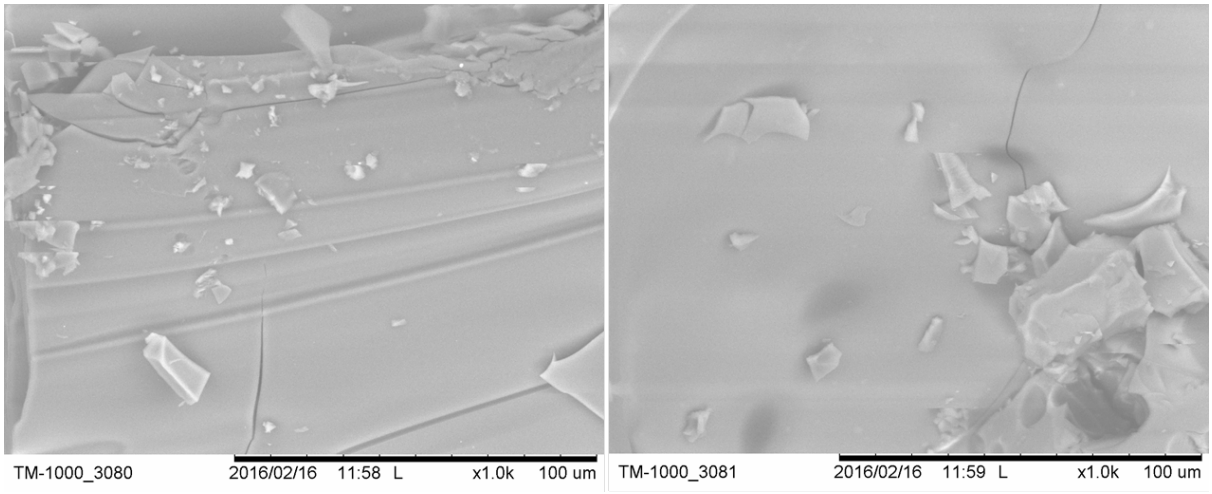

Figure 2.17. SEM images, side view (left) and top view (right) of F7 extruded material (post extrusion)

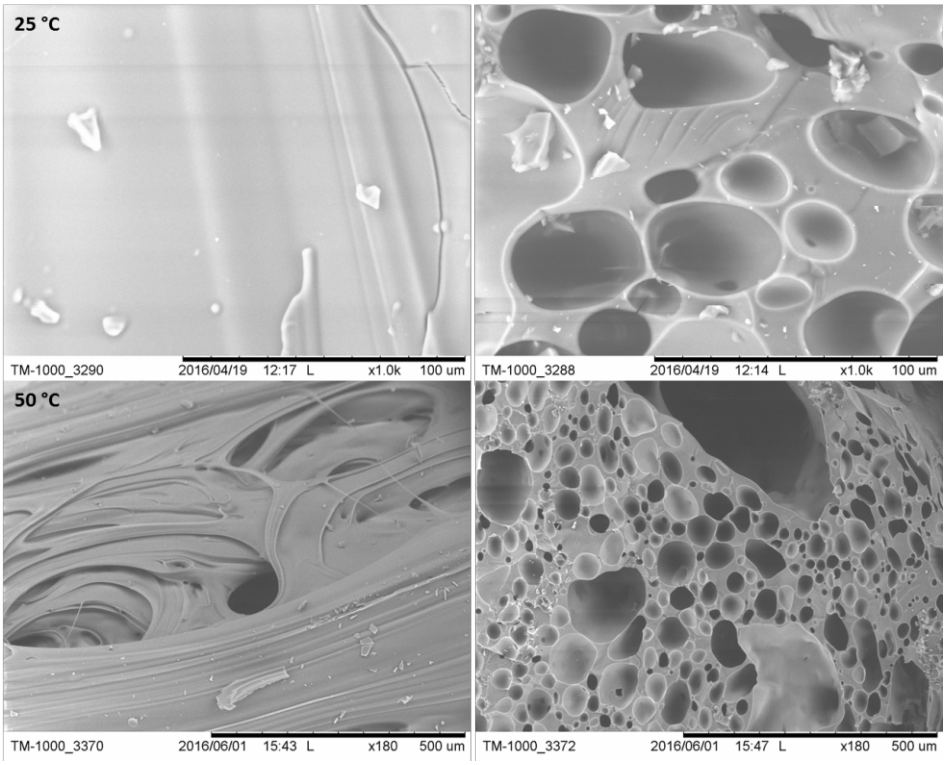

Figure 2.18. SEM images after 6 months storage at 25 °C and 50 °C, side view (left) and top view (right) of F7 extruded material

2.4.1.3. X-Ray Powder Diffraction (XRPD)

The XRPD patterns of ABZ – PVP K12 extruded formulations F1 to F3, physical mixtures (PM), ABZ and PVP K12 alone are presented in Figures 2.19 to 2.21. The XRPD pattern of ABZ shows intensity peaks at 2θ angles of 6.91, 11.32, 13.83, 17.97, 19.51, 19.99, 20.75, 22.19, 23.85, 24.47, 24.72, 25.05, 26.08, 26.23, 27.21, 28.73, 29.06, 30.00, 30.52 and 31.05° that correspond to ABZ crystalline form I (Pranzo et al., 2010). However, the intensity of the peak observed at 25° 2θ is lower compared to the one observed by Pranzo et al., (Pranzo et al., 2010). This may be due to specimen preparation errors in the commercial ABZ pattern reported by Pranzo et al., such as crystals non-random preferred orientation (Jenkins, 1996).

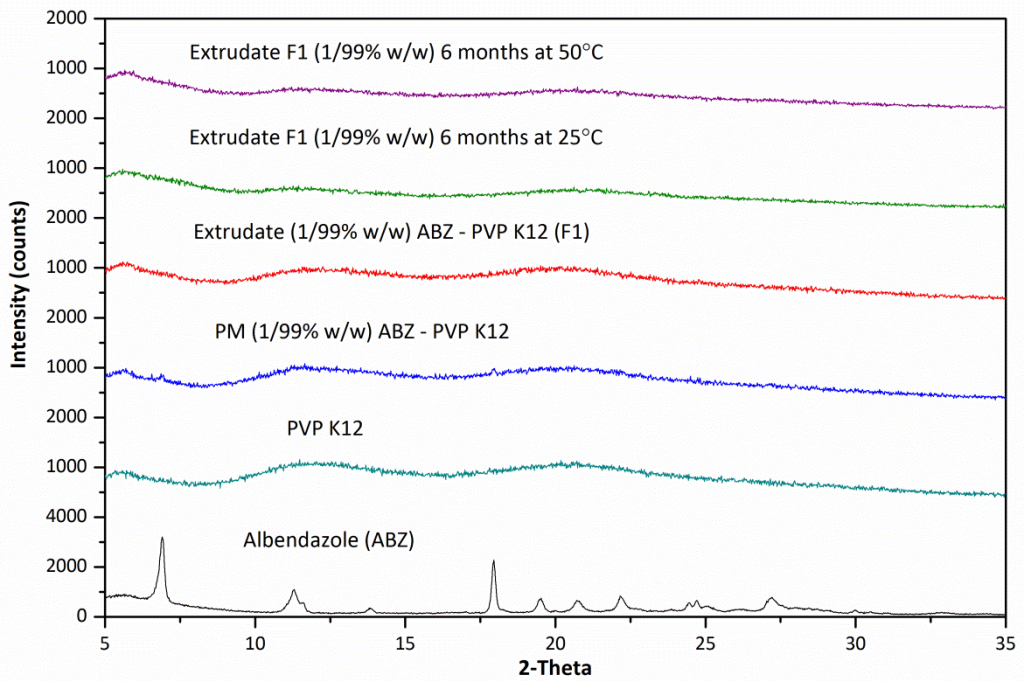

Figure 2.19. Diffractogram of formulation F1 ABZ–PVP K12

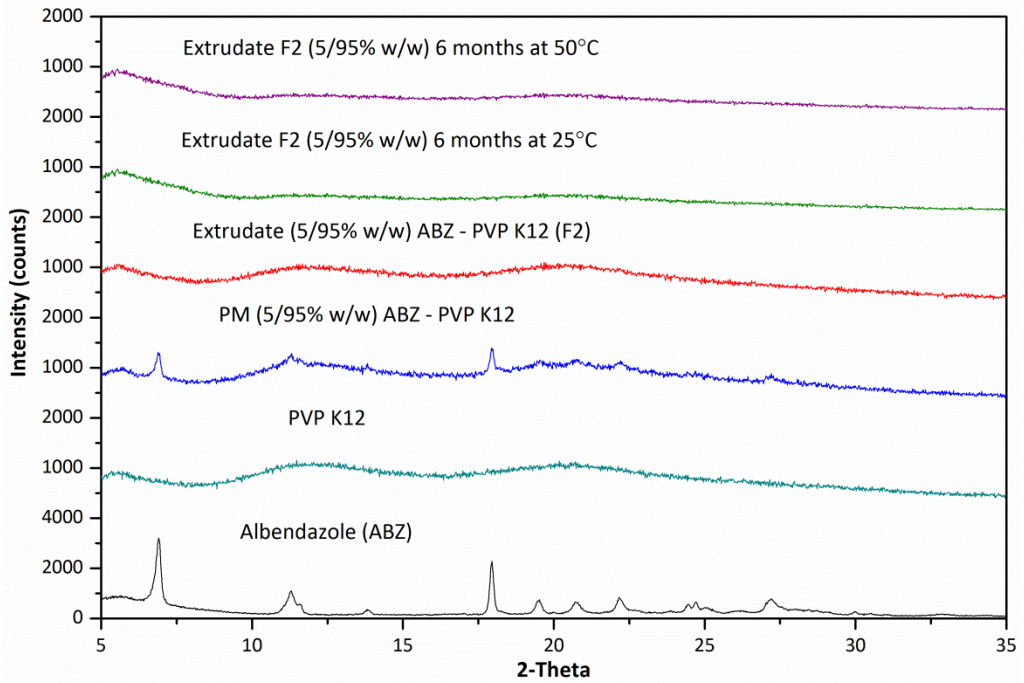

Figure 2.20. Diffractogram of formulation F2 ABZ–PVP K12

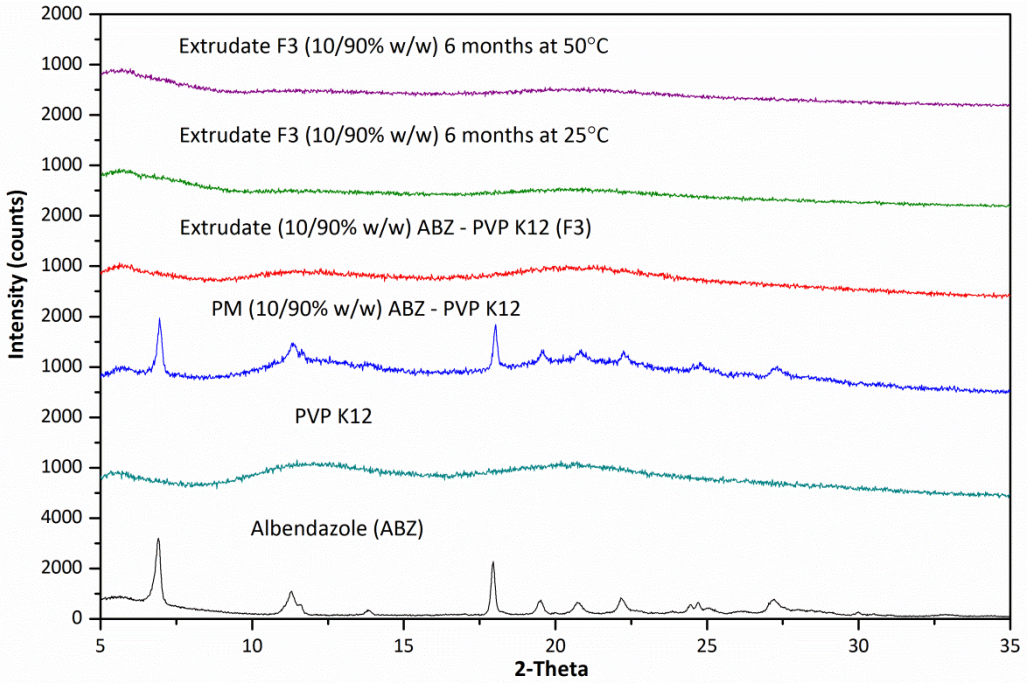

Figure 2.21. Diffractogram of formulation F3 ABZ–PVP K12

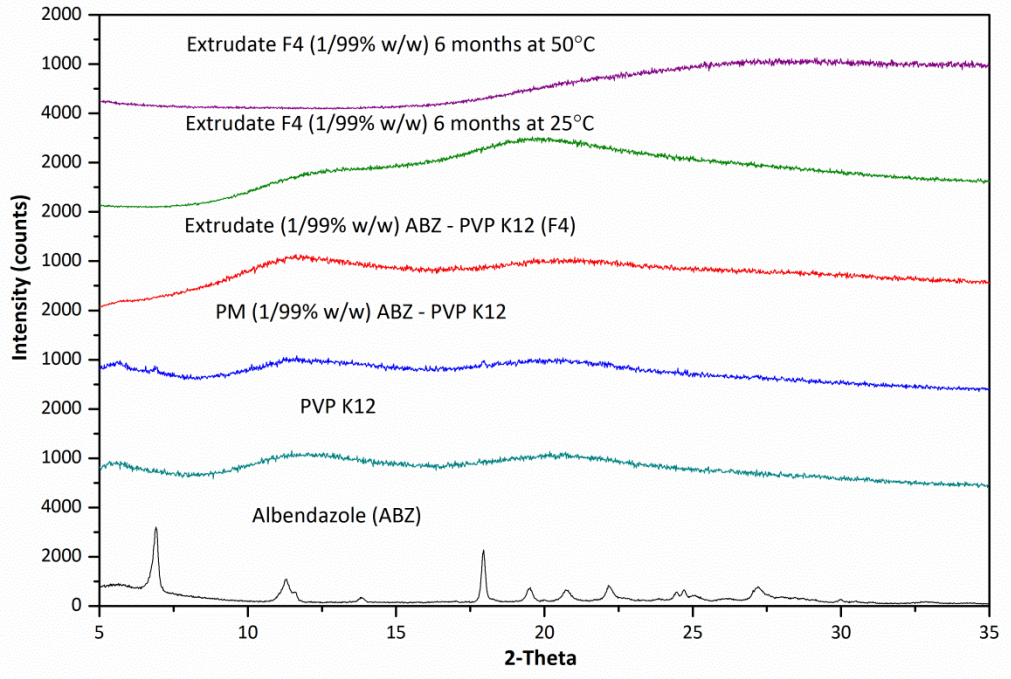

Figure 2.22. Diffractogram of formulation F4 ABZ–PVP K12

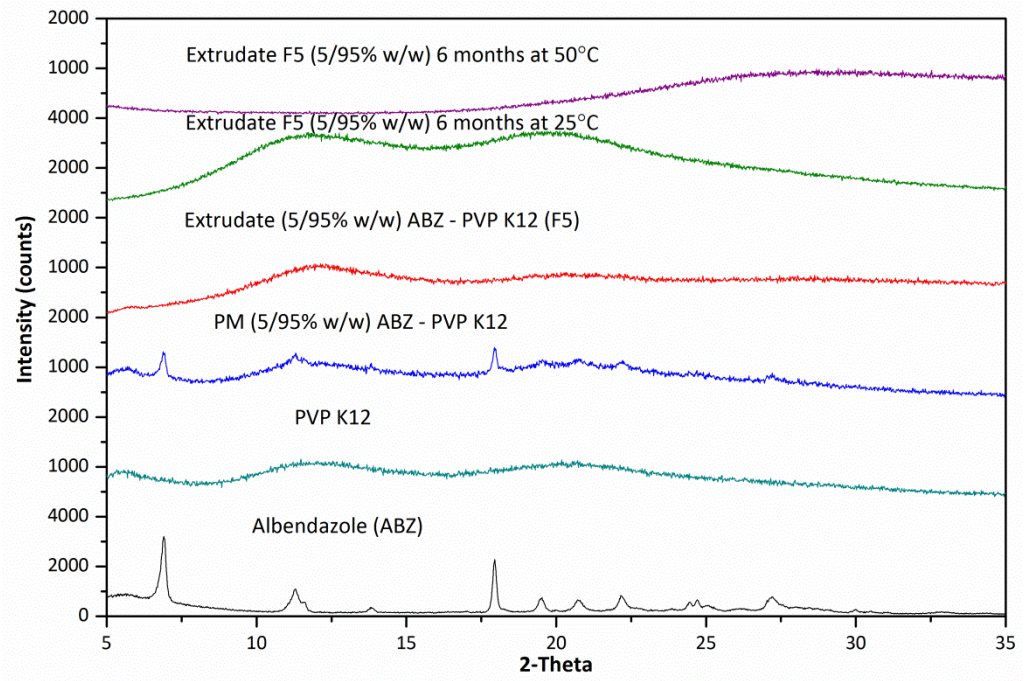

Figure 2.23. Diffractogram of formulation F5 ABZ–PVP K12

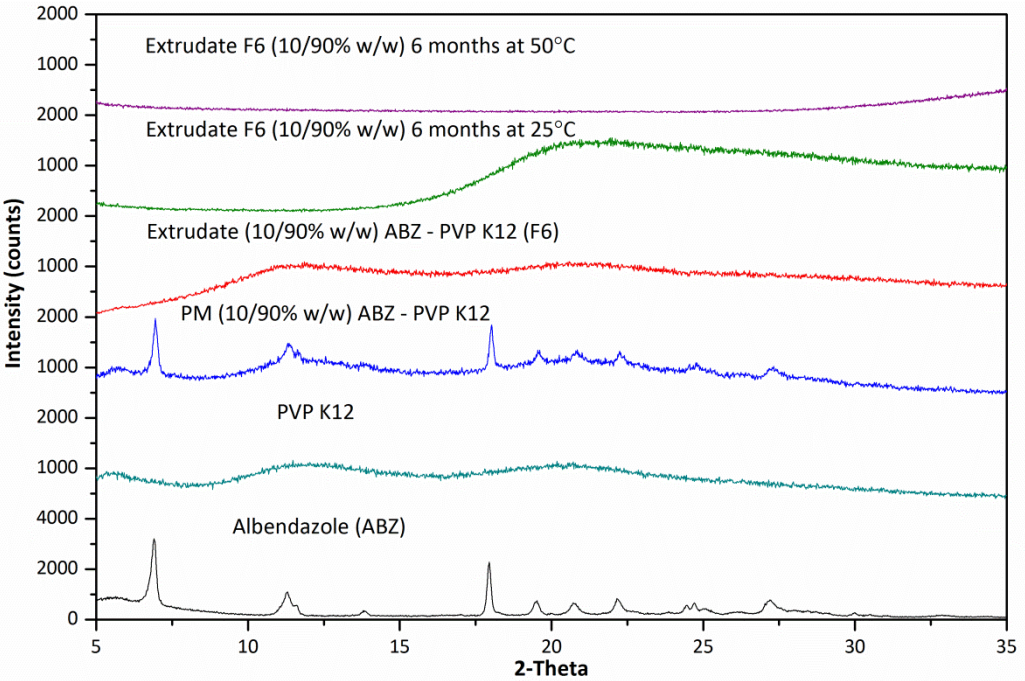

Figure 2.24. Diffractogram of formulation F6 ABZ–PVP K12

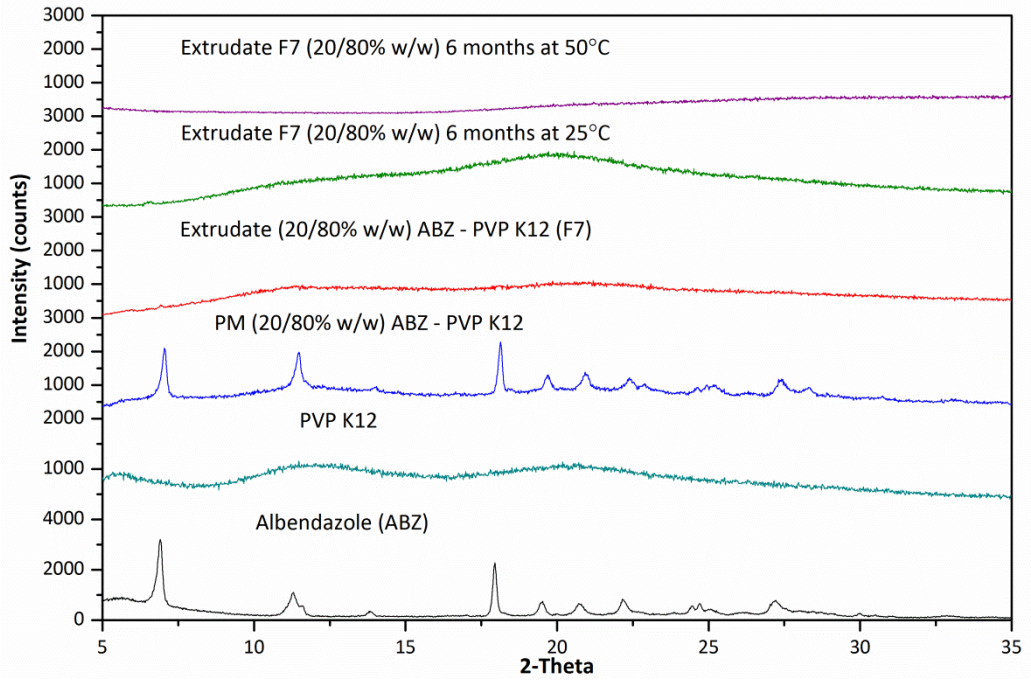

Figure 2.25. Diffractogram of formulation F7 ABZ–PVP K12

The XRPD patterns of the physical drug-polymer mixtures and the extruded materials of formulations F1 to F3, suggest the absence of a crystalline ordered structure of ABZ and the formation of an amorphous solid dispersion of the drug within the extruded polymer matrix. It can also be observed that by increasing ABZ content in PM samples, the height of the intensity peaks registered also increased (Figures 2.19 to 2.21). In contrast, the extruded materials do not show any intensity peaks relative to crystalline structures but a halo pattern characteristic of amorphous materials. By looking to the XRPD patterns obtained after 6 months storage of all extruded materials, we can conclude that the materials are stable and there is no re-crystallisation events registered over time. Therefore, these results suggest that stable amorphous solid dispersions of ABZ in PVP K12 for all formulations were achieved. In the case of formulations F4 to F7, it is observed that after 6 months storage at 50 °C, the characteristic amorphous halo pattern of PVP K12 is lost (Figures 2.22 to 2.25), indicating a possible alteration phenomena of the polymer.

This type of polymer property modification was previously observed when amorphous excipients were stored with the addition of water at a temperature of 25 °C (Airaksinen et al., 2005).

2.4.1.4. Differential Scanning Calorimetry (DSC)

Characterisation of the polymeric carrier PVP K12 alone (Figure 2.26) and initial studies between ABZ and PVP K12 were performed in the ratios indicated in Figure 2.27, using a heating/cooling/heating cycle (Bikiaris et al., 2005). Figure 2.26 shows PVP K12 amorphous behaviour. The T_g value of PVP K12 (90 °C) was not directly calculated but taken from literature (Reintjes, 2011). However, the literature value matches with the middle temperature value observed from the curve. It can be observed in Figure 2.27 an endothermic peak corresponding to the melting point of ABZ which is clearly shown at 30 % ABZ (w/w) compared to the curve of 10 % ABZ (w/w). This result suggests that detection of ABZ by DSC technique may be limited, especially at low drug contents as observed in the DSC thermograms of other PM samples (e.g. 1 % and 5 % w/w). DSC analysis of the extruded materials, PM and raw materials was carried out to determine the formation of amorphous solid dispersions and also evaluate the presence of glass transition (T_g) events (Figures 2.28 to 2.33). Differences between the T_g values of the extruded ABZ formulations and PM drug-polymer (differences in scale to be considered) indicated that a solid form transformation of the ABZ crystals occurred during HME. According to the DSC thermograms, there is no evidence of endothermic events due to melting of crystalline material. Also, differences regarding T_g appearance is observed and is normally considered a middle value comprised by the T_g values of the raw materials involved (Baird and Taylor, 2012; Maru et al., 2011). The

presence of two T_g events for some of the curves in Figures 2.28 and 2.29, suggests that the material could have evolved to a solid glassy suspension (Qi et al., 2008). However, there is no evidence of recrystallisation events. Therefore we can conclude that the extruded materials are stable over time.

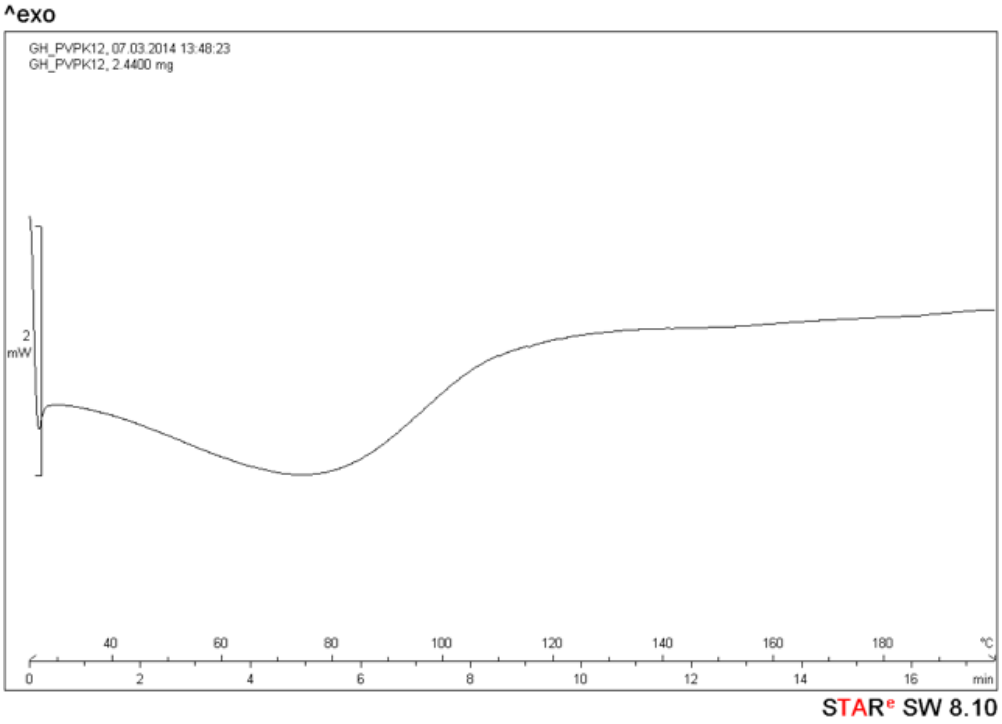

Figure 2.26. DSC thermogram of PVP K12 alone

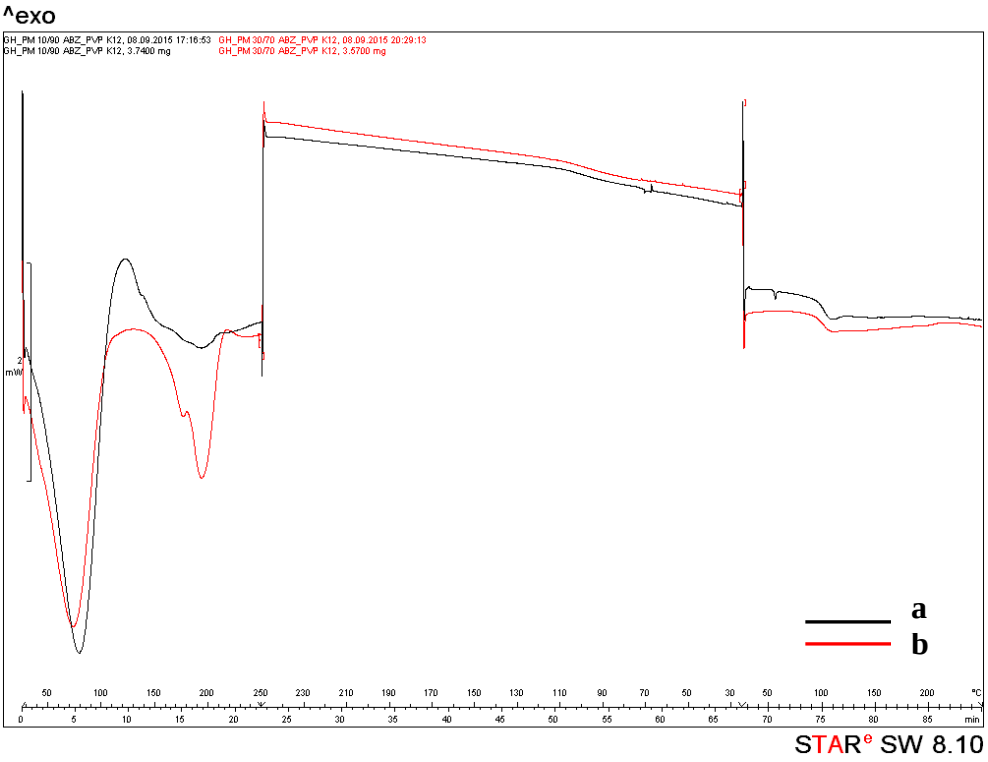

Figure 2.27. DSC thermograms of ABZ – PVP K12 physical mixtures comprising (a) 10 % and (b) 30 % ABZ (w/w)

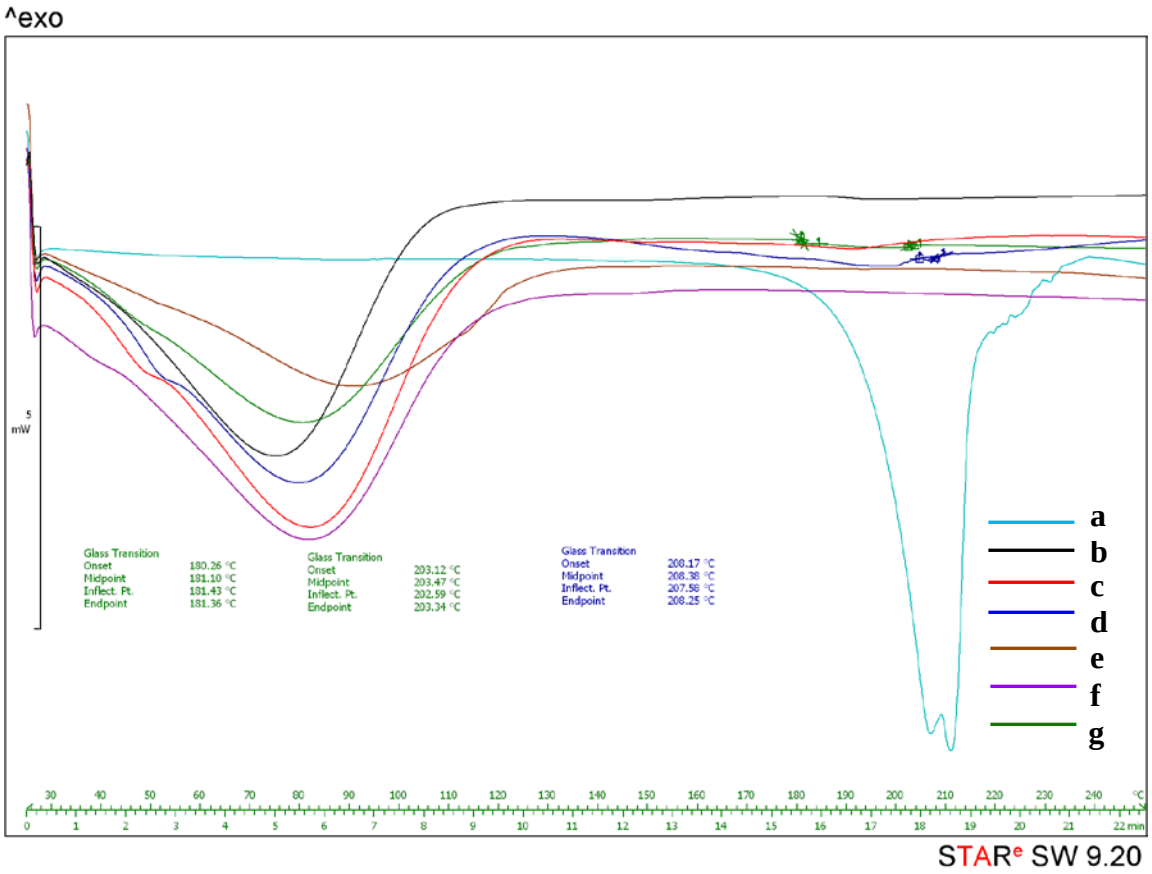

Figure 2.28. DSC thermograms of (a) ABZ alone, (b–d) physical mixtures (PM) of ABZ–PVP K12 at 1 % , 5 % and 10 % (w/w) and (e–g) extruded materials of ABZ–PVP K12 (F1, F2, F3) at 1 %, 5 % and 10 % (w/w) post extrusion

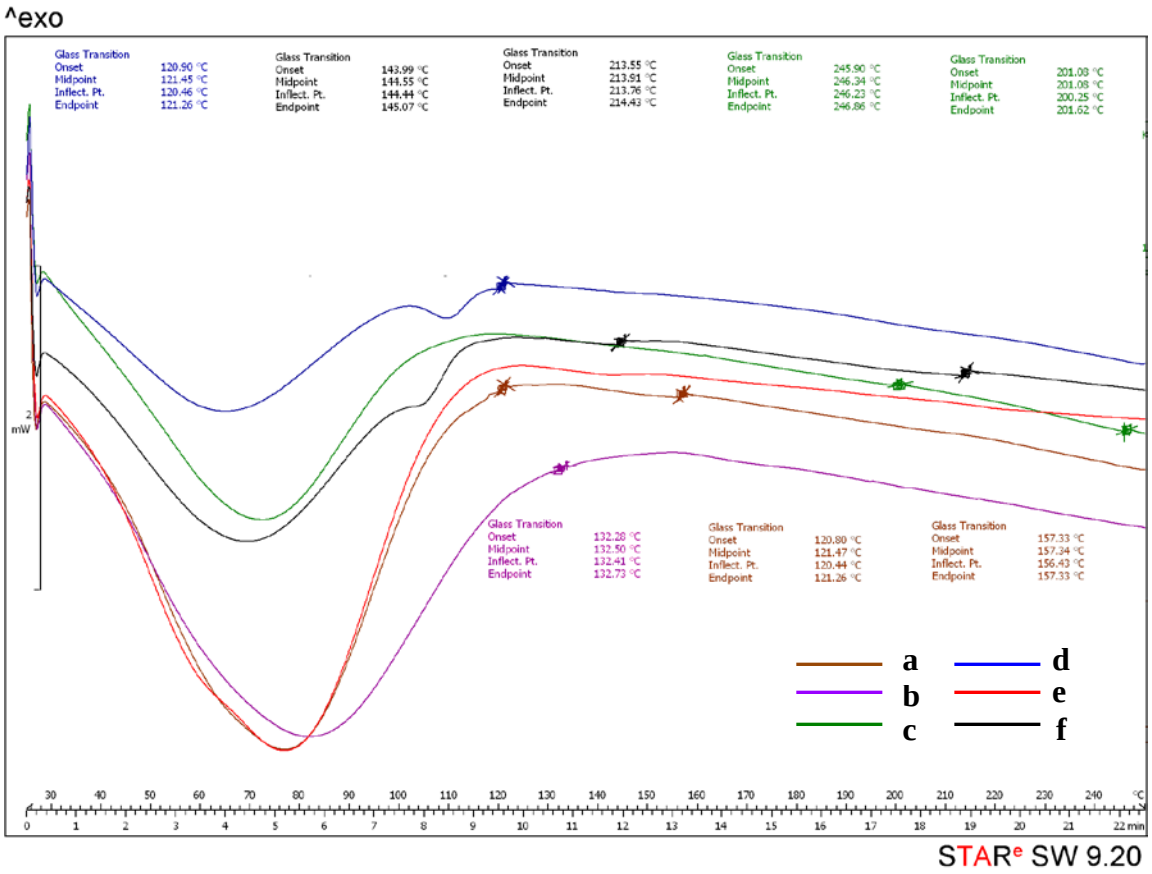

Figure 2.29. DSC thermograms after 6 months storage where: (a) extruded material F1 at 25 °C, (b) F1 at 50 °C, (c) extruded material F2 at 25 °C, (d) F2 at 50 °C, (e) extruded material F3 at 25 °C and (f) F3 at 50 °C

Figures 2.30 to 2.33 show the DSC thermograms of ABZ – PVP K12 extruded materials produced at 135 °C. Visually it is not possible to distinguish a T_g event either post extrusion or after 6 months storage. A possible explanation is that HME processing temperature was at the limit of the extrudable temperature for PVP K12 since it was not possible to melt the polymer and extrude below 135 °C. Therefore, this temperature was not high enough for the extruded material to clearly show a thermal event or T_g (it is normally recommended to extrude approximately 30 – 50 °C above the polymer T_g to ensure formulation stability (Baird and Taylor, 2012; LaFountaine et al., 2016)). Despite this, amorphous solid dispersions of ABZ in

PVP K12 were achieved as indicated by XRPD and DSC analysis. Another possibility could be that the physicochemical properties of PVP K12 are easily altered when processed at 135 °C, resulting in absence of a T_g in extruded materials. This would agree with the XRPD patterns of formulations F4 to F7, where absence of the characteristic halo pattern of PVP K12 is observed (Figures 2.22 to 2.25). These events occurred after exposure of PVP K12 polymeric matrix to 50 °C for 6 months and suggest that physical changes of the polymer chains can be caused leading to alteration of polymer properties.

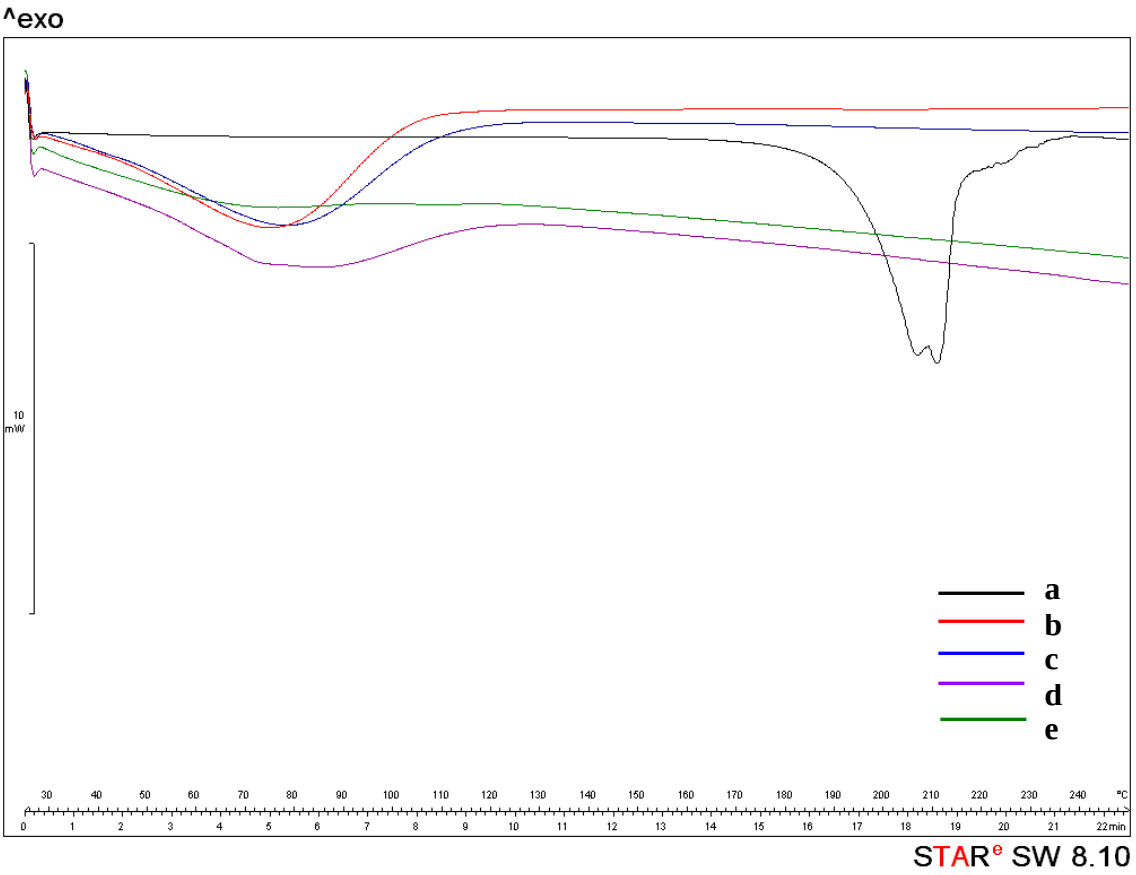

Figure 2.30. DSC thermograms of (a) ABZ alone, (b) physical mixture (PM) of ABZ–PVP K12 at 1 % (w/w), (c) extruded material F4 post extrusion, (d) F4 after 6 months at 25 °C and (e) F4 after 6 months at 50 °C

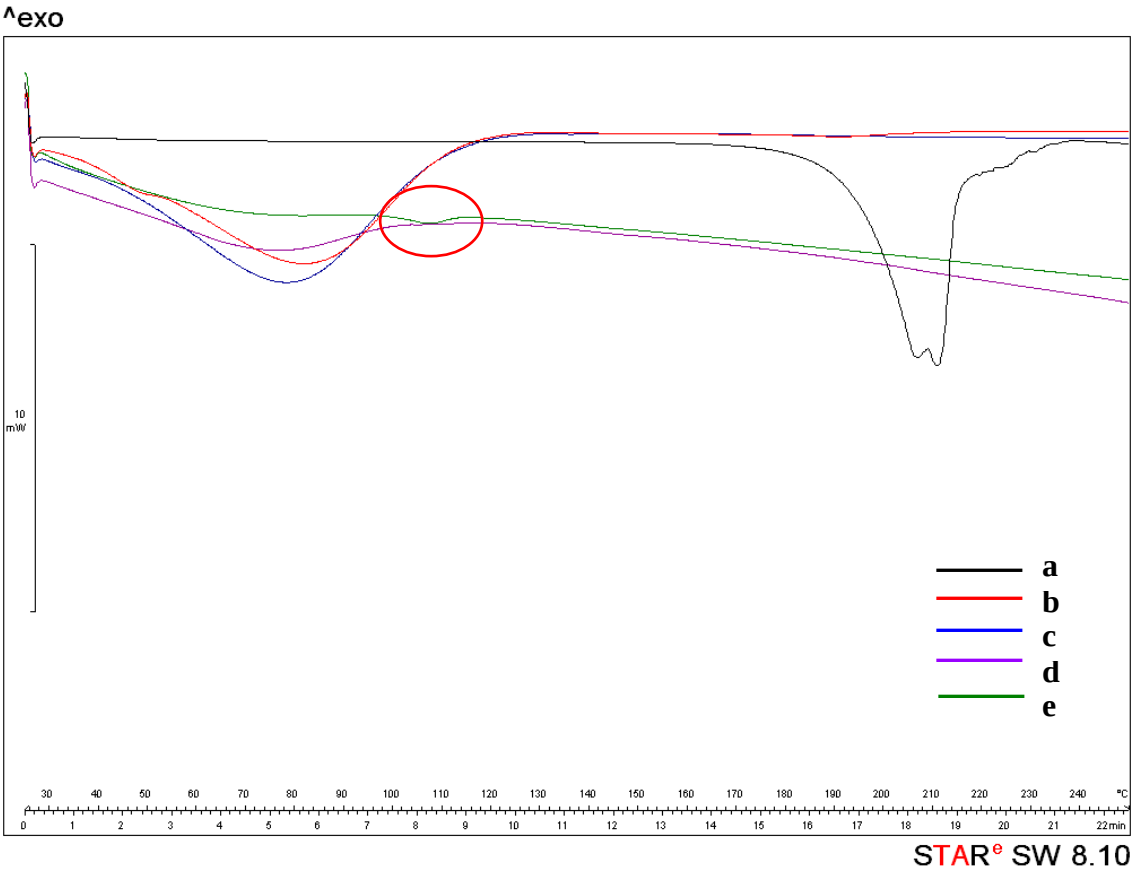

Figure 2.31. DSC thermograms of (a) ABZ alone, (b) physical mixture (PM) of ABZ–PVP K12 at 5 % (w/w), (c) extruded material F5 post extrusion, (d) F5 after 6 months at 25 °C and (e) F5 after 6 months at 50 °C (red circle indicates the presence of a small trace)

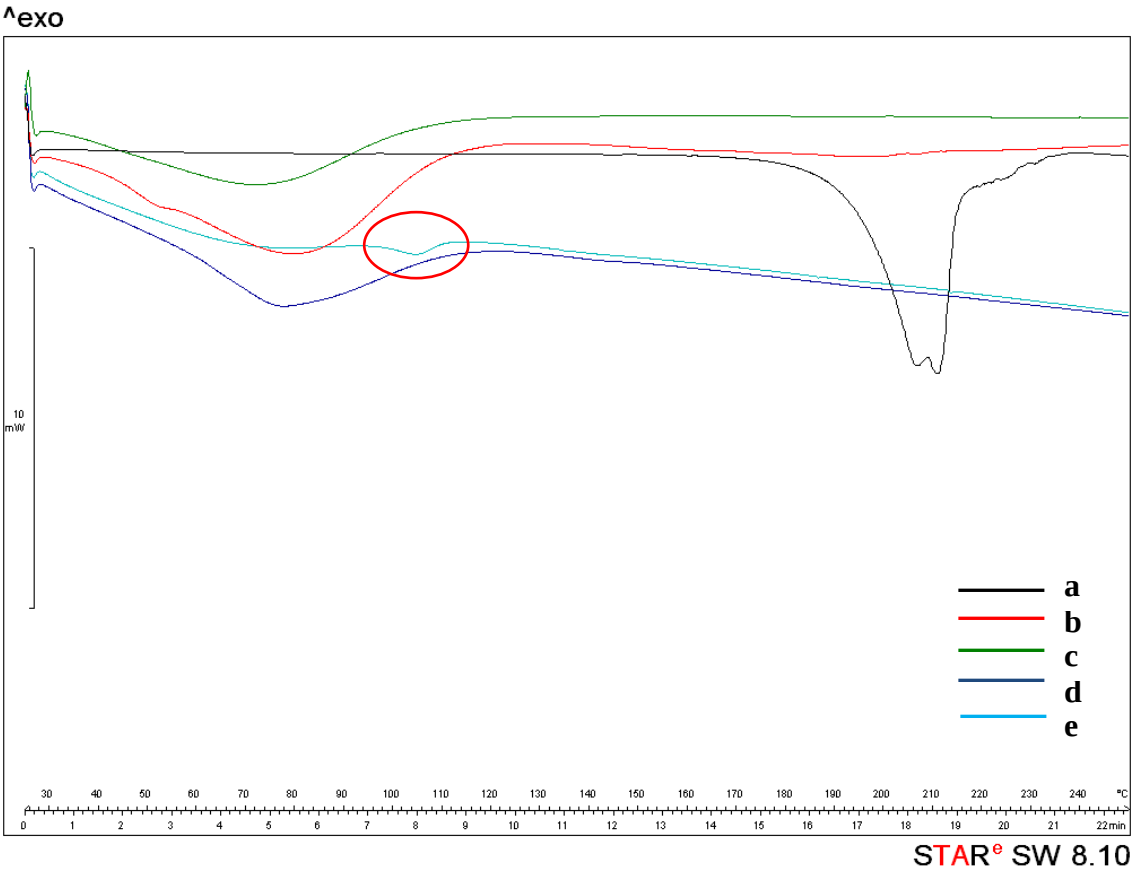

Figure 2.32. DSC thermograms of (a) ABZ alone, (b) physical mixture (PM) of ABZ–PVP K12 at 10 % (w/w), (c) extruded material F6 post extrusion, (d) F6 after 6 months at 25 °C and (e) F6 after 6 months at 50 °C (red circle indicates the presence of a small trace)

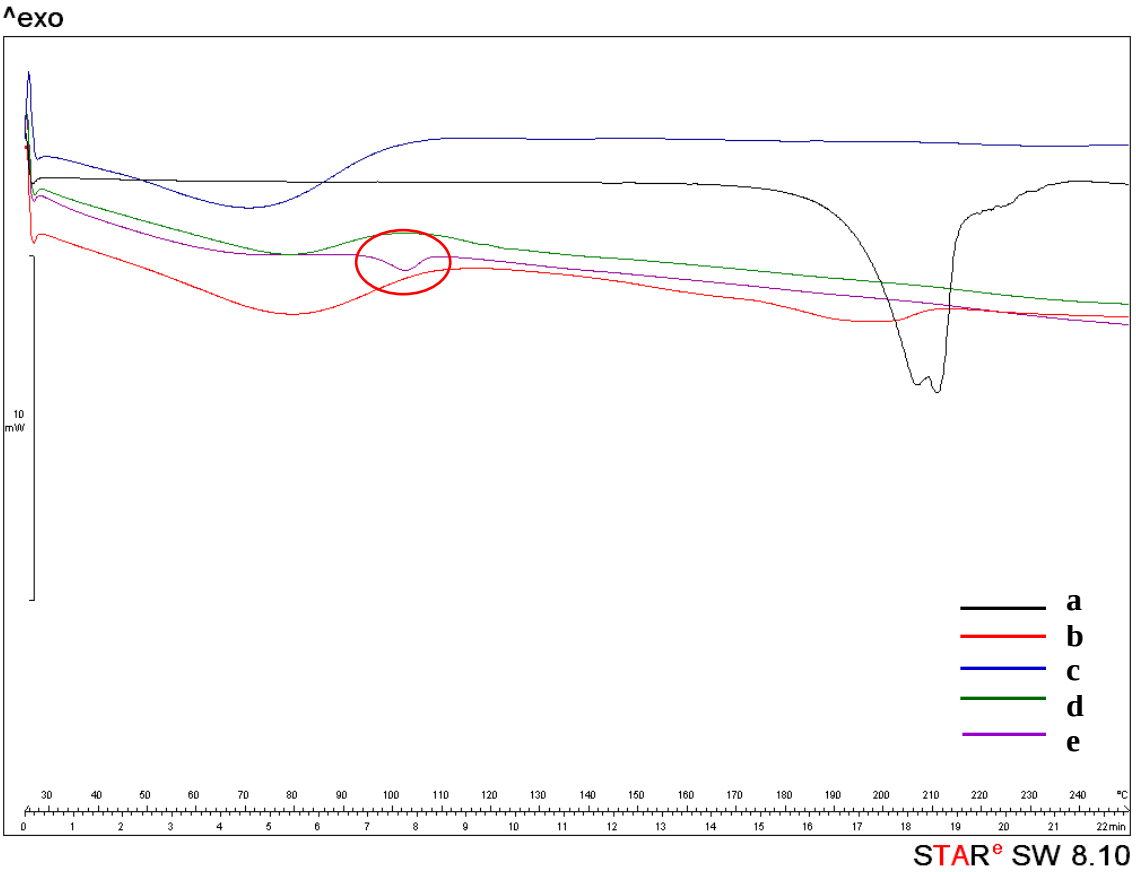

Figure 2.33. DSC thermograms of (a) ABZ alone, (b) physical mixture (PM) of ABZ–PVP K12 at 20 % (w/w), (c) extruded material F7 post extrusion, (d) F7 after 6 months at 25 °C and (e) F7 after 6 months at 50 °C (red circle indicates the presence of a small trace)

DSC thermograms of formulations F5 to F7 (Figures 2.31 to 2.33) show a small trace (indicated with a red circle) in the case of extruded materials (e) 6 months storage at 50 °C. This event may indicate an alteration of the polymer properties during storage and would agree with the XRPD results reported above.

2.4.1.5. Karl-Fischer (KF) studies

All the raw materials and extruded samples were analysed by Karl-Fischer titration to determine the water content, since the well-known hygroscopicity of some pharmaceutical grade polymers such as PVP can be a limitation due to its influence

on the stability of amorphous solid dispersions (Bianco et al., 2013). Low water content values of dosage forms containing hygroscopic polymeric materials such as PVP constitute a crucial parameter to be evaluated. There is evidence indicating that intramolecular bonds of polymeric materials and therefore the polymer free volume and other properties like plasticity or elasticity can be affected by increases in water content (Szakonyi and Zelko, 2012). The water content within the samples is a quality attribute to ensure product stability and to preserve the product from degradation phenomena, often known as drug-polymer phase separation events (Rumondor and Taylor, 2009). Figure 2.34 shows the water content (% w/w) of all extruded materials observed post extrusion and after 6 months storage. Mean standard deviations of 3 replicates calculated for each sample are represented by error bars. Water content of samples post extrusion was <0.3 % (w/w) except in the case of formulation F5, with a water content of 2.12 % (w/w). This material, in comparison to the other formulations, was manufactured during a warm and humid season and therefore humidity levels at room temperature may lead to an increase in water content. All samples were stored for 6 months and did not show water content increase higher than 0.2 % despite the high hygroscopicity properties of PVP. Non-parametric ANOVA (Kruskal-Wallis) test was also performed indicating that temperature changes do not have a significant influence in samples water content ($P>0.05$) for formulations F1, F3 and F6. However, temperature does have a significant influence ($P<0.05$) on the water uptake of formulations F4, F5 and F7 (indicated by * symbol). These results are at the limit of the significance and present low variance values. Despite samples being stored in glass sealed containers, PVP K12 is hygroscopic and chambers were not humidity controlled.

Low water content values of 0.2 % are considered optimum for oral dosage forms in order to be stable and preserve their physicochemical properties. Solid dosage forms with water content values below 2.0 % are considered acceptable (Gerhardt, 2009) for a commercial pharmaceutical product although these values may differ depending on the type of product and specifications required.

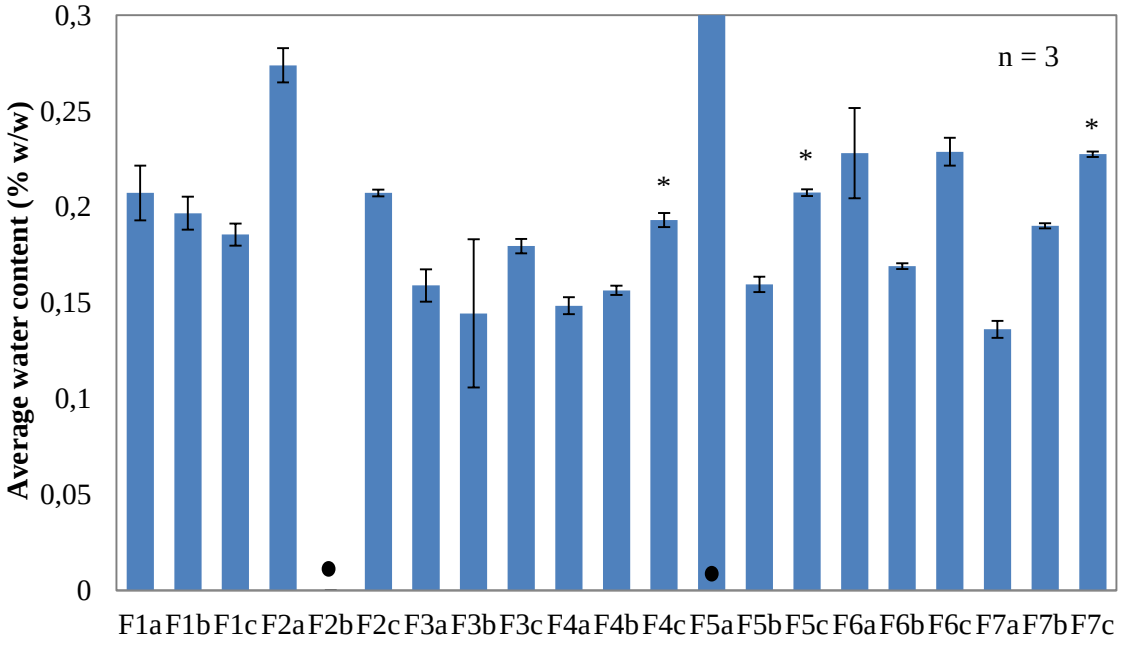

● F2b: Karl-Fischer not performed, not enough sample
F5a: Average water content (% w/w) of 2.1239 ± 0.0187

Figure 2.34. Karl-Fischer results of formulations F1 to F7 post extrusion (a), 6 months at 25 °C, 20 % RH (b) and 6 months at 50 °C, 3 % RH (c). * symbol represents statistically significant differences obtained from a non-parametric Kruskal-Wallis test with 0.05 significance level (n = 3). Error bars represent standard deviation.

2.4.1.6. In-vitro dissolution studies

Drug release of the extruded materials was characterised using a Sirius T3 measurement system under sink conditions and simulating gastrointestinal pH conditions. ABZ is a weak base which solubility is pH dependent as can be

observed in Figure 2.35 (Torrado, 1996a). Therefore, it is important to consider the pH value during dissolution studies. Figure 2.35 shows that ABZ maximum solubility is achieved at acid pH values (1-2), whereas basic pH (6-7) lead to the lowest solubility. Tablets used for dissolution studies did completely dissolved in the buffer media after 15 minutes (pH 2.0 from 0 to 30 minutes), indicating that maximum dissolution is already achieved. Taking this into account, dissolution profiles of our materials are plotted at pH 2.0 for a total time of 30 minutes.

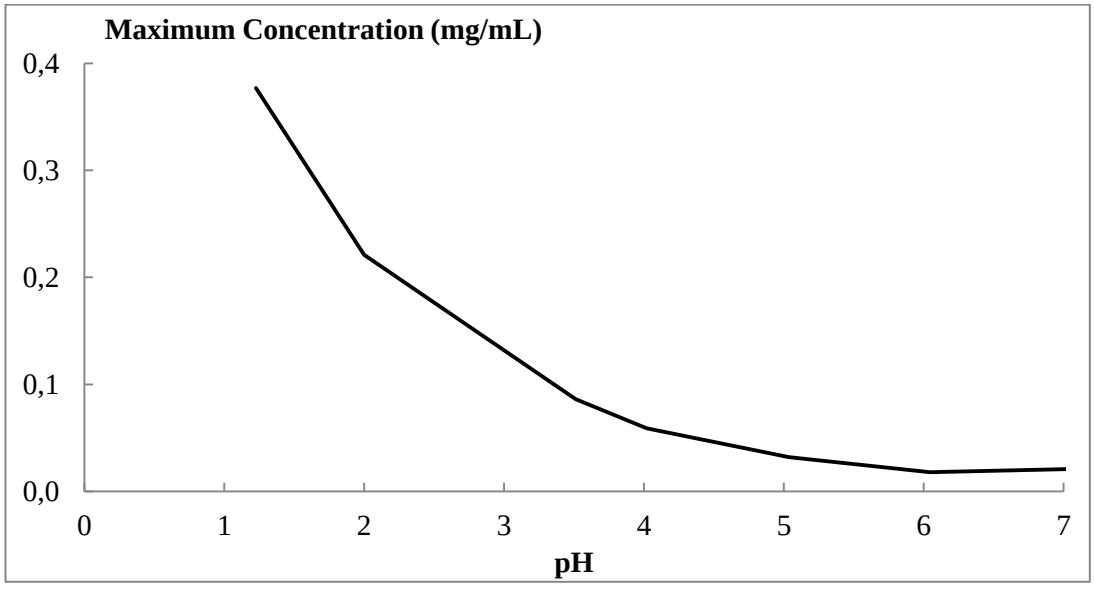

Figure 2.35. Solubility (mg/mL) of ABZ in buffer solution. Data reproduced from (Torrado, 1996a).

As can be observed in Figures 2.36 and 2.38, extruded materials of F1 and F3 formulations show increased drug release compared to ABZ alone with values of 89 % and 56 % drug release, respectively. Extrapolated dissolution rates of 45.09 µg min^{-1} and 148.80 µg min^{-1} are reached. Drug release of 67 % and extrapolated dissolution rate of 171 µg min^{-1} were achieved by formulation F2 (Figure 2.37). Solid dispersions of a BCS Class II drug into a PVP matrix manufactured by the spray drying solvent evaporation technique showed such an increase in drug

dissolution rate and similar dissolution profiles (Frizon et al., 2013). Dissolution profiles of the extruded materials of ABZ – PVP K12 at 1 %, 5 % and 10 % (w/w) did not achieve supersaturation (maximum concentrations achieved are shown in Table 2.6).

Table 2.6. Maximum concentration values of ABZ in solution from amorphous solid dispersions

Post Extrusion	**Concentration (µg/mL)**	**6 months at 25 °C**	**Concentration (µg/mL)**	**6 months at 50 °C**	**Concentration (µg/mL)**
F1	0.0600	F1	0.0474	F1	0.0461
F2	0.0450	F2	0.0290	F2	0.0298
F3	0.0379	F3	0.0429	F3	0.0542
F4	0.0593	F4	0.0491	F4	0.0613
F5	0.0533	F5	0.0496	F5	0.0463
F6	0.0368	F6	0.0361	F6	0.0412
F7	0.0155	F7	0.0194	F7	0.0153

It is of note in Figures 2.36 to 2.38 the increased and fast drug release profile (or also called “spring”) of the extruded materials that does not exhibit under the test conditions the characteristic “parachute” effect observed by Brouwers et al., (Brouwers et al., 2009). In our studies, an optimum drug release profile close to 100 % was not achieved and possible influence of the polymeric material PVP K12 needs to be further studied (Kothari et al., 2015). The differences in drug released observed (indicated by the length of the error bars) together with higher drug release after 6 months storage (Figures 2.38, 2.41 and 2.42), suggest a possible cross-linking effect of PVP. These effects as well as the ability of PVP to form complexes by hydrogen bonding were previously described as beneficial to overcome solubility although it can also lead to bioavailability issues if interactions are very strong (Bühler, 2005; Haaf, 1985). This effect may prevent the complete dissolution of

ABZ leading to different % of drug released over time, although this needs to be further studied. Dissolution studies of the extruded materials stored for 6 months at 25 °C and 50 °C revealed that the formulations were stable over time. In these profiles, it is considered that ABZ content in the extruded materials is stable and does not degrade during storage. Extruded materials comprising 1 % (w/w) show a similar dissolution profile after 6 months storage in comparison to 5 % and 10 % (w/w) which show variations of 10 % drug release. In the case of F2 formulation, drug release decreases 20 %, in contrast to F3 where 6 month sample shows an increase of drug release of 10 to 30 % compared to the material post extrusion.

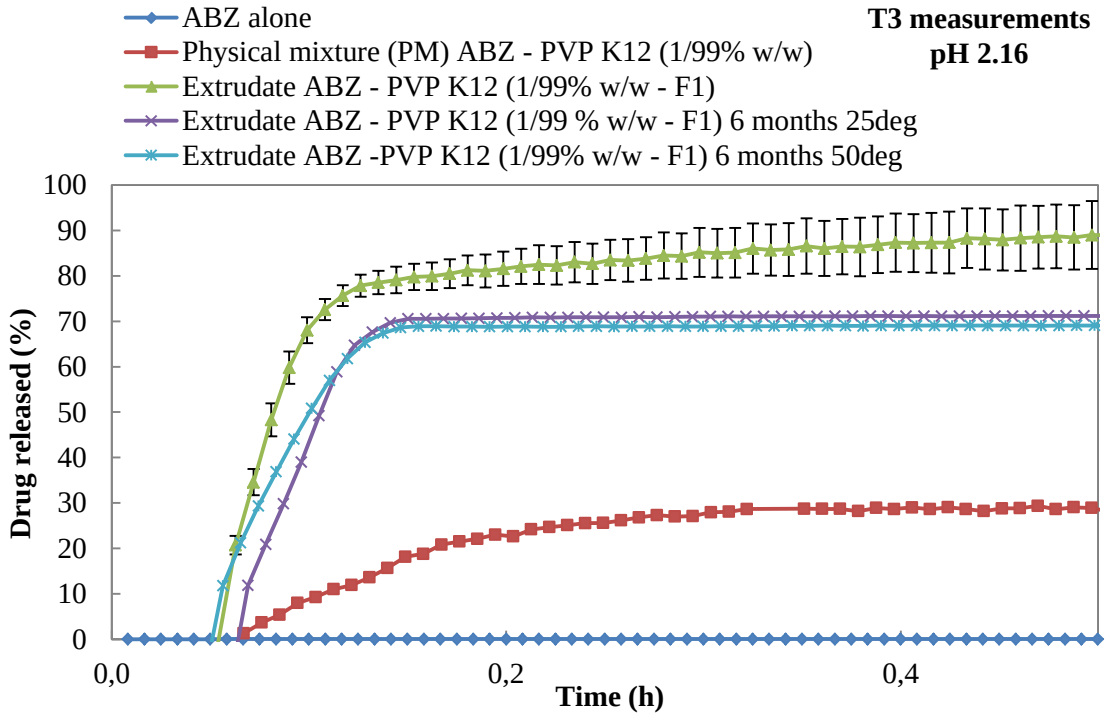

Figure 2.36. Dissolution profiles of F1 extruded material. Standard error of the mean bars are based on 2 tests per sample.

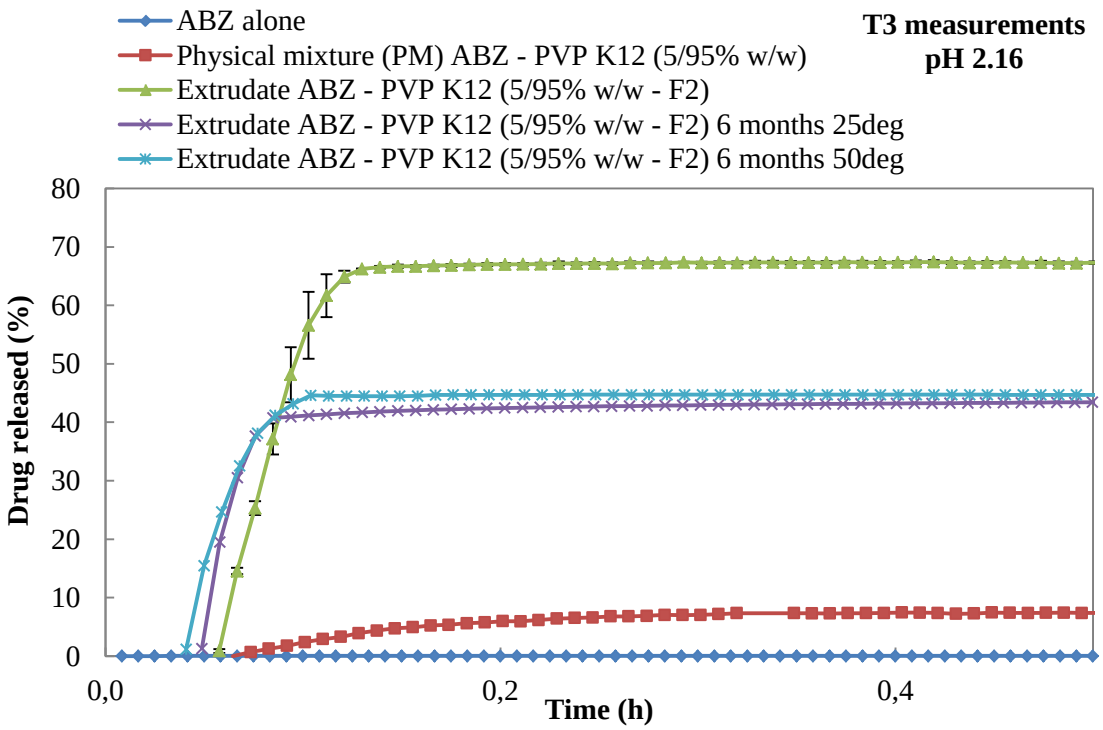

Figure 2.37. Dissolution profiles of F2 extruded material. Standard error of the mean bars are based on 2 tests per sample.

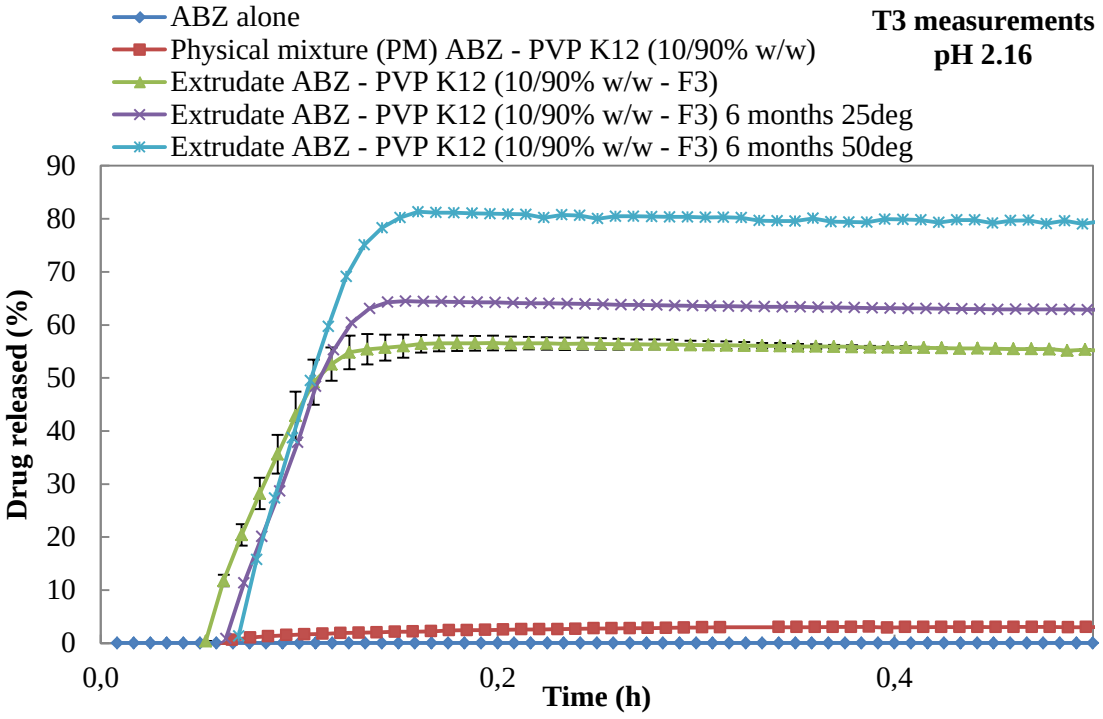

Figure 2.38. Dissolution profiles of F3 extruded material. Standard error of the mean bars are based on 2 tests per sample.

Amorphous solid dispersions of extruded materials produced at 135 °C (formulations F4 to F7) show increased drug release profiles when compared to drug alone with a similar "spring" release as materials produced at 145 °C (formulations F1 to F3) (Figures 2.39 to 2.42). Formulation F4 (post extrusion) achieves up to 88 % drug release in 30 minutes time. Formulation F5 (post extrusion) achieves up to 79 % drug release. Formulation F6 (post extrusion) achieves up to 55 % drug release and formulation F7 (post extrusion) achieves up to 15 % drug release. After 6 months storage at the conditions detailed above, formulations F3, F6 and F7 indicate that a higher drug release is achieved after storage at 50 °C. Karl-Fischer analysis proves that there was no significant uptake of water during storage. Therefore, these differences in drug release may be due to an interaction effect between ABZ and PVP K12, as previously mentioned. It is of note in Figure 2.42 a lower % of drug released as well as a delayed release profile with a less characteristic "spring", except in the case of the extruded material after 6 month storage at 50 °C. More interestingly, the sample after 6 month storage at 25 °C, shows an altered drug release profile already observed in previous solid dispersions with PVP (Frizon et al., 2013). In addition, the porosity degree of this formulation is very high, as observed by Micro-CT analysis (see chapter 4 for reference). High porosity degree in this case may have influenced the differences observed in the physical performance of the tablet in these studies. However, the slow dissolution profiles obtained may be also explained by a lower polymer content as previously seen with PVP matrices (Andrews et al., 2010).

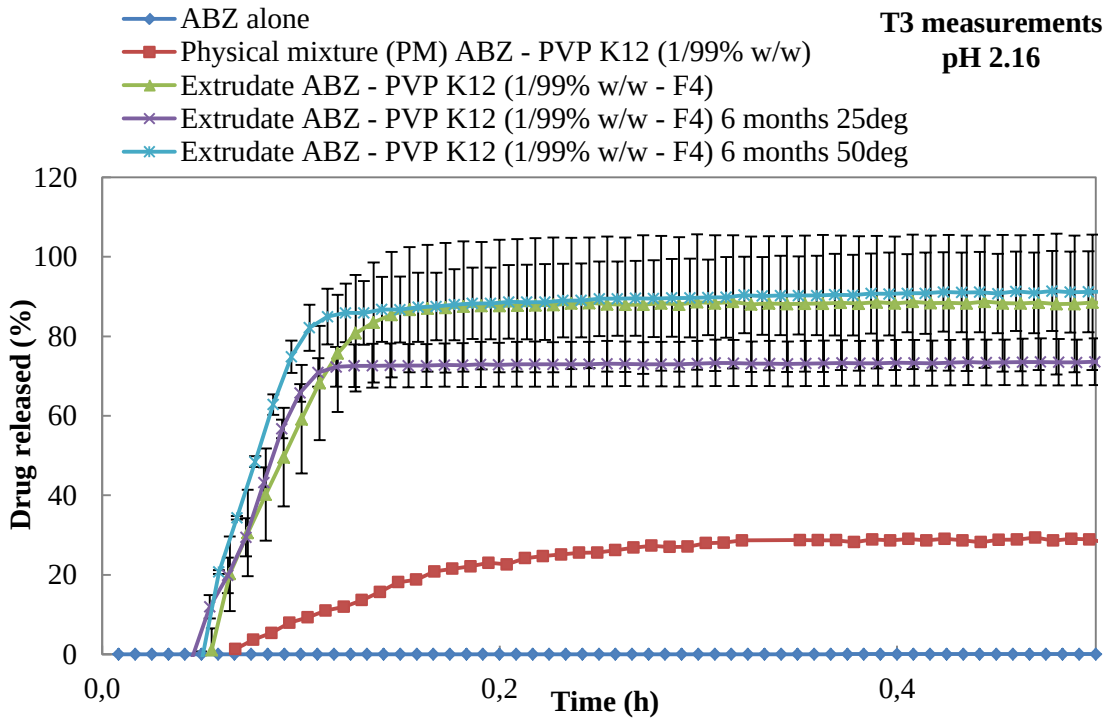

Figure 2.39. Dissolution profiles of F4 extruded material. Standard error of the mean bars are based on 2 tests per sample.

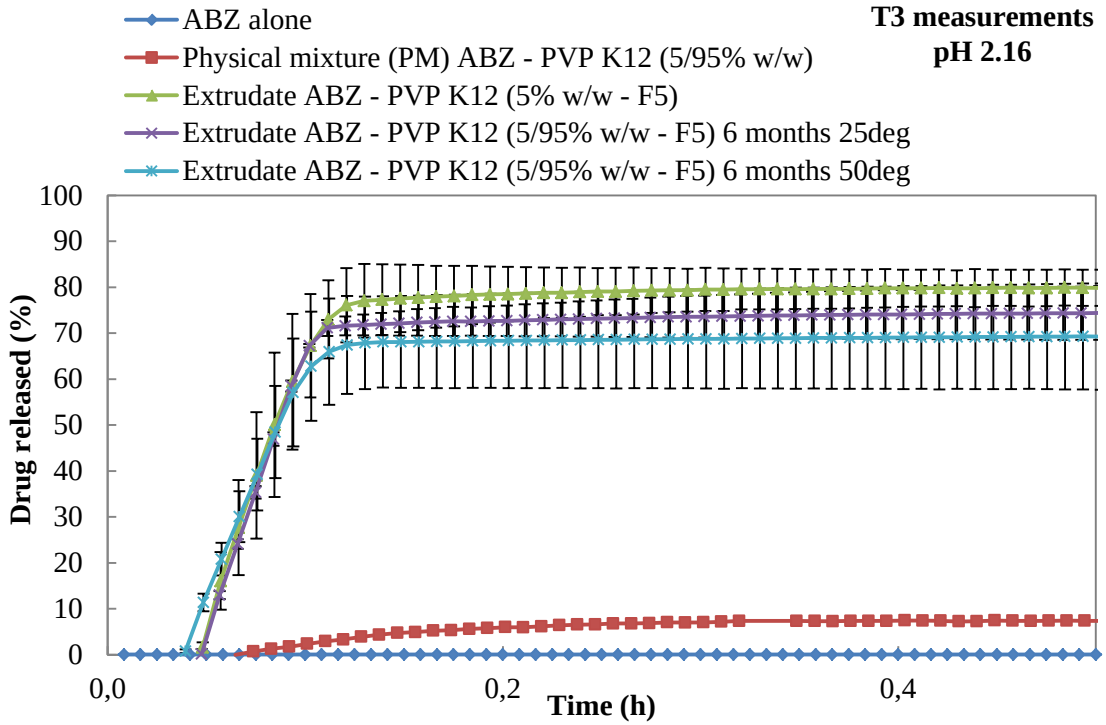

Figure 2.40. Dissolution profiles of F5 extruded material. Standard deviation bars are based on 3 replicates.

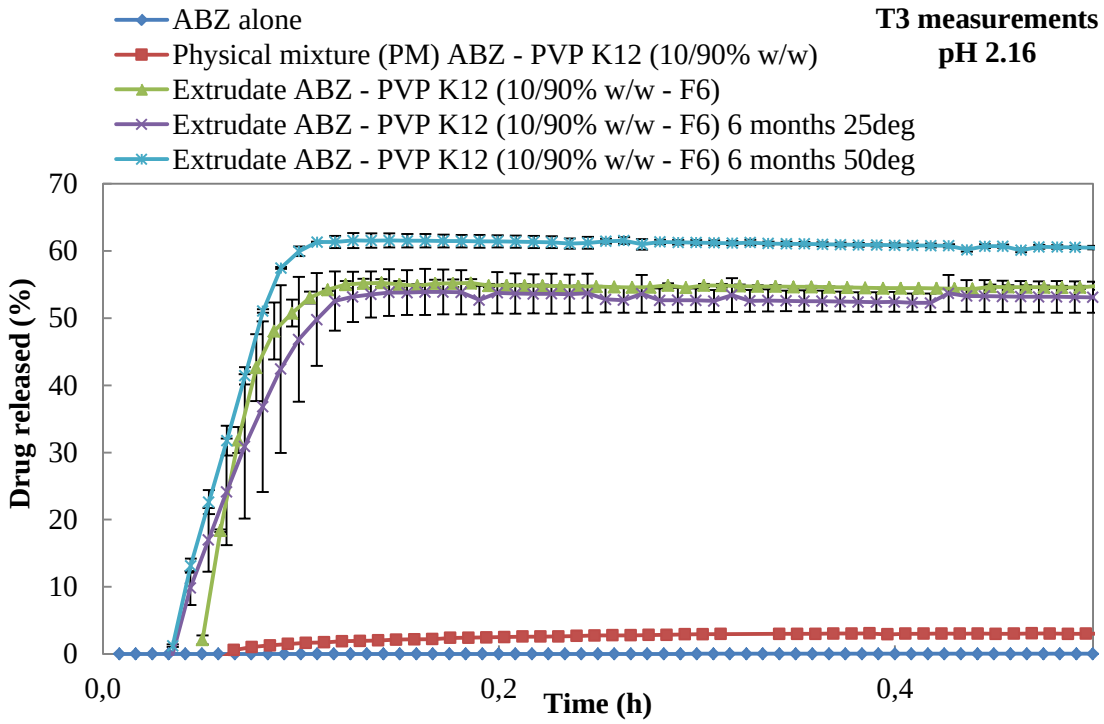

Figure 2.41. Dissolution profiles of F6 extruded material. Standard error of the mean bars are based on 2 tests per sample.

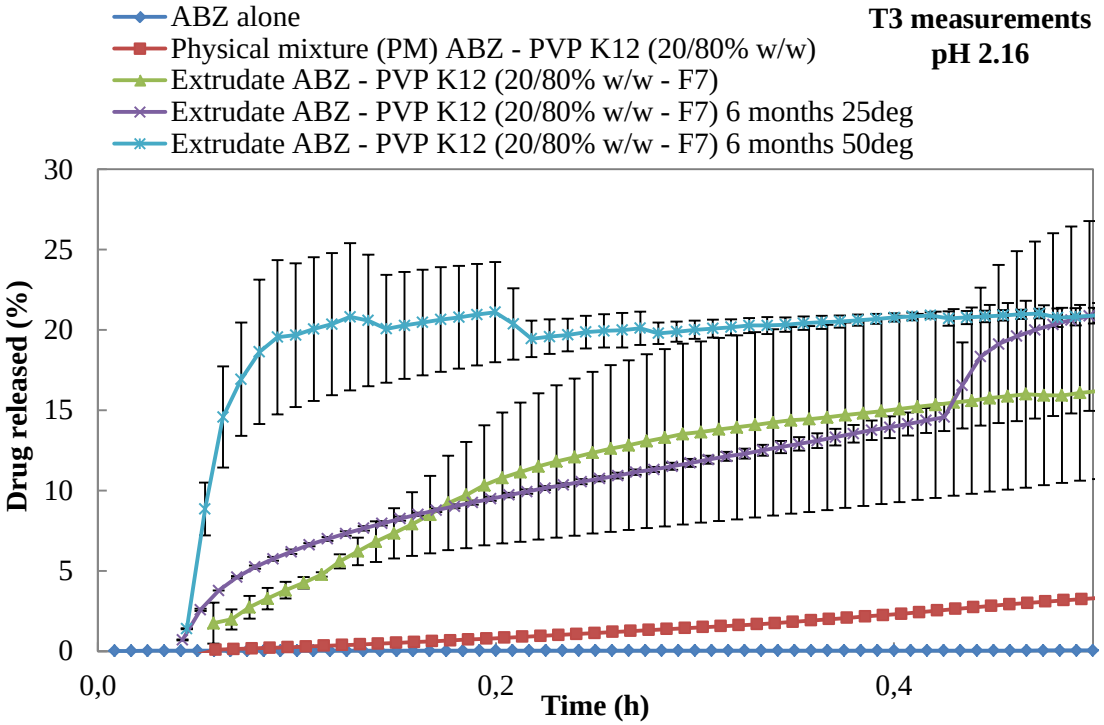

Figure 2.42. Dissolution profiles of F7 extruded material. Standard error of the mean bars are based on 2 tests per sample.

Similar improvements towards ABZ dissolution rate were achieved by Torrado et al., (Torrado, 1996b) that manufactured successful amorphous solid dispersions of ABZ in PVP K12 by the classic solvent evaporation method and also carried out bioavailability studies in animals. The dissolution studies above show that ABZ dissolution rate is dependent on ABZ solid form (amorphous vs crystalline), possible cross-linking interactions and storage conditions such as temperature. We demonstrate the suitability of a lab scale HME process to obtain stable amorphous solid dispersions of ABZ with enhanced dissolution properties that could lead to novel formulations with enhanced oral bioavailability.

2.4.1.7. Particle size analysis

Particle size of ground extruded materials used for dissolution studies were determined by laser diffraction. The mean values (d_{10}, d_{50}, d_{90}) obtained for PM and extruded materials are depicted in Tables 2.7 and 2.8. It can be observed that d_{50} (µm) of ground samples correspond to particle size values below 100 µm, except in case of F1, F2, F5 (post extrusion) and F4 (6 months at 25 °C) where d_{50} (µm) was between 150 - 250 µm. It is well-known (Anderberg, 1988; Chu et al., 2012) that the smaller the particle size, the higher increase in surface area and therefore a greater increase in dissolution rate can be achieved.

Table 2.7. Particle size values (d_{10}, d_{50}, d_{90}) of ground materials post extrusion

Sample name	d_{10} (µm)	d_{50} (µm)	d_{90} (µm)
PM 1/99 % (w/w)	22.5	65.1	117
PM 5/95 % (w/w)	16.5	53.8	104
PM 10/90 % (w/w)	11.3	49.1	96.1
PM 20/80 % (w/w)	6.35	46.8	467
F1	36.2	212	492
F2	23.3	172	1650
F3	9.21	94.6	489
F4	11.9	90.3	293
F5	42.3	150	442
F6	9.24	74.7	294
F7	5.53	45	177

Table 2.8. Particle size values (d_{10}, d_{50}, d_{90}) of ground materials after 6 months storage

Sample name	d_{10} (µm)	d_{50} (µm)	d_{90} (µm)
F4 at 25 °C	34.8	235	614
F4 at 50 °C	10.9	83.2	421
F5 at 25 °C	11.2	98.8	443
F5 at 50 °C	7.26	44.9	183
F6 at 25 °C	10.7	73.1	295
F6 at 50 °C	10.9	79.7	347
F7 at 25 °C	11.5	79.2	336
F7 at 50 °C	9.16	51.1	194

2.4.1.8. Determination of drug content by UV spectrophotometry

Quantification of drug content in all extruded materials was performed by UV spectrophotometry analysis. The calibration curve representing the calibration standards of ABZ at 0.10, 0.20, 0.50 and 0.75 mg/mL can be observed in Figure 2.43. This calibration curve is representative of the two calibrations performed, in all cases R^2 >0.99. Moreover, the results of drug content of all extruded materials are represented in Table 2.9.

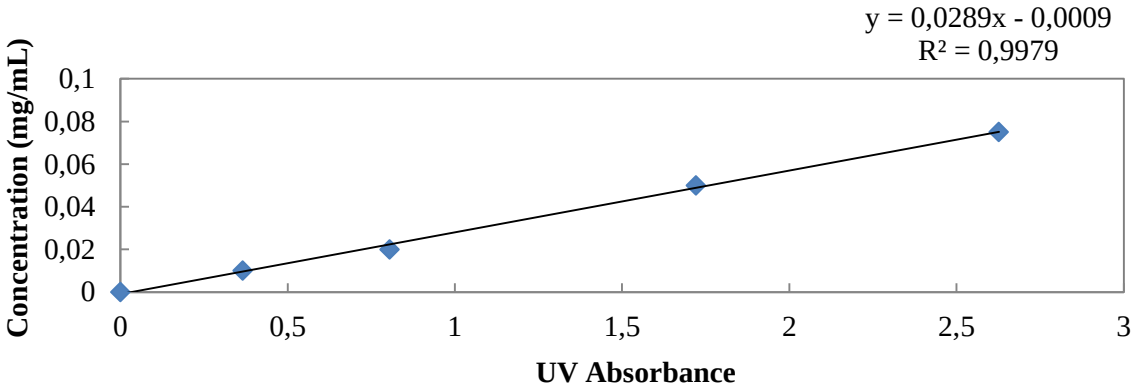

Figure 2.43. Calibration curve of ABZ calibration standards measured by UV spectrophotometry

Table 2.9. ABZ drug content (%) of extruded materials measured by UV spectrophotometry. Absorbance values are the average of 3 measurements and standard deviations are included (± symbol).

Sample name	Absorbance	Concentration (mg/mL)	% drug content*
F1	0.6622 ± 0.0034	0.0182	91.18
F2	0.6583 ± 0.0045	0.0181	90.62
F3	0.7094 ± 0.0029	0.0196	98.01
F4	0.6124 ± 0.0073	0.0167	83.99
F5a	0.7097 ± 0.0084	0.0196	98.05
F5b	0.6263 ± 0.0012	0.0162	81.47
F5c	0.6407 ± 0.0008	0.0166	83.27
F6	0.6971 ± 0.0089	0.0192	96.23
F7	0.7335 ± 0.0045	0.0202	101.49

*The drug content (%) reported represents total ABZ content respect to the theoretical content of ABZ within each extruded material (e.g. 1 %, 5 %, 10 % and 20 %).

It can be observed that formulations F3 (10 % w/w produced at 145 °C), F5, F6 and F7 (5 % w/w, 10 % w/w and 20 % w/w produced at 135 °C) show drug contents between 95 % and 101 %. The drug content value achieved in the case of formulation F7 of 101 % may be due to analytical error. On the other hand,

formulations F1, F2 (1 % w/w and 5 % w/w produced at 145 °C) and F4 (1 % w/w produced at 140 °C) show drug contents of 91 %, 90 % and 84 %, respectively.

2.5. Conclusions

Amorphous solid dispersions or also called amorphous solid solutions of ABZ in a PVP K12 matrix were produced by HME technique. Evidence of a change in the physical solid state of ABZ is proved by characterisation of the extruded materials using SEM, XRPD and DSC all of which indicate the formation of amorphous systems, or where possible crystalline material is below the limit of detection. Analysis of the samples after 6 months storage did not indicate any drug re-crystallisation events, which suggest that the samples were stable over time. However, in some cases polymer stability was compromised as evidenced by XRPD diffractograms performed after 6 months storage. These events do not seem to be due to an increase in water content, as these values are kept low (<1.0 % w/w). The use of a polymeric material with high T_g such as PVP K12 plays a key role in the stabilisation of the amorphous form of the drug. High dissolution rate increase of ABZ in gastrointestinal simulated media was achieved in all cases with values of 55 to 89 % drug release post extrusion. Six months storage under temperature controlled conditions did not greatly affect drug release. However, there are some differences that may be explained due to physicochemical interactions that control the amount of drug released due to strong linking mechanisms. To conclude, HME can be applied as a manufacturing technique to improve dissolution and potential bioavailability properties of ABZ without the need of further processing techniques. The possible presence of molecular interactions between PVP K12 and ABZ would

need to be further studied. More details on possible experimental methods that can be used to assess these interactions are provided in chapter 6 of this thesis.

3. Development of HME formulations of Albendazole using PEG 6000

3.1. Introduction

This chapter introduces the use of a partially crystalline polymer such as PEG 6000 in the production of amorphous solid dispersions of ABZ. The hydrophilicity and high stability of PEG provide good properties that are required for carriers to be used for pharmaceutical applications (Rowe, 2009). It is also used as ointment base for topical formulations due to its non-irritant and washable properties (Bhagurkar et al., 2016). The HME processing temperature required to melt and process this polymer is much lower compared to the polymer used in chapter 2 providing ease of processability. In addition, PEG 6000 has previously shown to be suitable for the development of amorphous solid dispersions of ABZ and other APIs by the application of HME, solvent evaporation and melt fusion methods (Khan et al., 2011; Leonardi et al., 2007; Leonardi et al., 2009; Lin and Cham, 1996). Polymer properties such as the absence of electrostatic effects that were observed when using PVP K12 are also considered. The use of PEG 6000 can also enhance the surface properties of the extruded materials by providing a non-fractured and smooth surface which can also enhance the aspect and porosity properties of the matrix (Leonardi et al., 2007).

3.2. Aims and objectives

The aim of this chapter comprised the development, characterisation and understanding of the physicochemical properties of amorphous solid dispersions of ABZ manufactured by HME using a partially amorphous and partially crystalline polymer, such as PEG 6000. Secondly, the optimisation of extruded materials to obtain strands with enhanced porosity properties was considered.

3.3. Materials and methods

3.3.1. Materials

PEG 6000 was selected as an alternative carrier to manufacture HME formulations comprising ABZ. The ease of processability of this polymer due to a low melting temperature required to extrude was the main criteria used for its selection. Moreover, the use of an alternative polymer was required in order to decrease the porosity properties of previously extruded materials (see chapter 2 and 4 for reference).

Albendazole (ABZ, ≥98 %) was purchased from Sigma-Aldrich Company Ltd. (Gillingham, Dorset, United Kingdom). Pharmaceutical grade polyethylene glycol 6000 (PEG 6000) was kindly donated by CRODA International Plc. (East Yorkshire, United Kingdom) in the form of flakes. These were milled before HME processing using a Fitzpatrick® L1A mill apparatus at a speed of 2500 rpm to obtain granules of 1.60 mm diameter (see Figure 3.1). Other reagents such as methanol (HPLC grade, ≥99.5 %), chloroform, potassium chloride AR grade, sodium dihydrogen phosphate (>99.0 %) and glacial acetic acid (ACS reagent, ≥99.7 %) were obtained from Sigma-Aldrich. The physicochemical properties of PEG 6000 are depicted in Table 3.1.

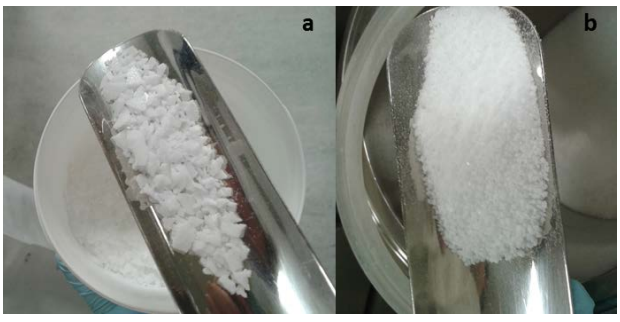

Figure 3.1. Image of PEG 6000 as flakes before milling (a) and as granules after milling (b)

Table 3.1. Physicochemical properties of formulation materials according to Mahlin et al., and PerkinElmer® (Mahlin et al., 2013; PerkinElmer®, 2011)

Material	T_m (°C)	T_g (°C)
ABZ	210[a]	60
PEG 6000	58[a]	-22

[a]Experimental data

3.3.2. Miscibility studies

The miscibility of ABZ and PEG 6000 was assessed by the Hansen solubility parameter calculation as well as HSM and DSC experiments as described in chapter 2.

3.3.3. Formulations obtained by Hot-Melt Extrusion (HME)

Extruded materials comprising ABZ and PEG 6000 produced by HME technique using the blending conditions, twin-screw extruder and set-up already described in chapter 2. In this case, all formulations were manufactured by degassing at zone 6 of the twin-screw extruder. Initial experiments with polymer alone were performed in order to optimise the processing parameters such as barrel temperature (°C), screw speed (rpm) and powder feed rate (kg/h). In addition, feeding properties were also optimised by using a feeding screw more suitable for pellets (Figure 3.2). Drug-polymer ratios used are shown in Table 3.2 and the optimised processing parameters for these formulations are depicted in Table 3.3. Extruded materials were stored at 25 °C and 37 °C in glass sealed containers and then put into a desiccator with drying pearls to avoid water uptake during storage. Stability studies were carried out after 6 months storage at the conditions just mentioned.

Figure 3.2. Feed screw used in HME process

Table 3.2. Formulations manufactured by HME

Formulation	Ratio of ABZ / PEG 6000 (% w/w)
F1	1/99
F2 (a, b, c)	5/95
F3	10/90
F4	20/80

Table 3.3. HME processing parameters of ABZ – PEG 6000 formulations

HME formulation	Barrel temperatures (°C, zones 1, 2, 3 and 4-8)	Melt temp. (°C)	Screw speed (rpm)	Torque (Nm)	Throughput (kg/h)
F1	30, 40, 55, 58	55 - 56	50	0.2 - 4.4	0.20
F2a	30, 40, 55, 58	54 - 55	50	0.3 - 3.9	0.15 - 0.16
F2b	30, 40, 55, 58	55 - 57	50	0.3 - 3.8	0.17
F2c	30, 40, 55, 58	55 - 57	50	0.8 - 4.3	0.17
F3	30, 40, 55, 58	54 - 57	50	0.2 - 3.6	0.12
F4	30, 40, 55, 58	54 - 57	50	0.2 - 1.4	0.09

Table 3.4. Detailed screw configuration used in HME process

Formulation	Screw configuration
F1 to F4	*(CE 11/40) x 7 + (KE 10/90°) x 8 + (KE 10/60°) x 4(F) + (CE 11/40) x 8 + (KE 10/60°) x 6(F) + (CE 11/40) x 7 + (KE 10/90°) x 4 + (KE 10/60°) x 3(F) + (KE 10/30°) x 5(F) + (CE 11/40) x 9

*Where CE 11/40 is conveying element with a pitch of 11 mm and length of 40 mm; KE 10/90°: kneading element with thickness of 10 mm and 90° offset angle; KE 10/60°: kneading element with thickness of 10 mm and 60° offset angle; KE 10/30°:

kneading element with thickness of 10 mm and 30° offset angle and F means forward direction.

3.3.4. Physicochemical and surface characterisation

The characterisation of the physicochemical and surface properties of the extruded materials was carried out by SEM, XRPD, DSC, KF, in-vitro dissolution studies, particle size analysis and UV spectrophotometry analysis. The detailed description of these methods is specified in chapter 2. The main specifications used to measure drug content by UV spectrophotometry are also described there, with the exception in this case of the use of chloroform as solvent due to the high solubility of both PEG 6000 and ABZ. In the case of in-vitro dissolution studies, the tablet used for the experiments was compressed to 40 kilogram-force (kgf).

3.4. Results and discussion

3.4.1. Assessment of product attributes and physicochemical properties

3.4.1.1. Miscibility studies

The miscibility properties of ABZ and PEG 6000 were assessed by the application of the *Hoy and Hoftzyer/Van Krevelen* method through the Hansen solubility parameter calculation. The solubility parameter of PEG 6000 (δ = 21.44) was obtained from literature (Kitak et al., 2015) and the solubility parameter of ABZ was calculated (value can be found in chapter 2). A solubility parameter difference ($\Delta\delta$) between both components of 0.32 $MPa^{1/2}$ was obtained, indicating they are miscible (see chapter 1 for reference). Further description of the method and considerations used to perform the calculations as well as microscope images of ABZ alone are provided in materials and methods section of chapter 2. Microscopic images obtained by HSM technique (see chapter 2), were obtained to assess ABZ and PEG 6000

miscibility properties. Figures 3.3 to 3.6 show the HSM results obtained for PM 5 % (w/w) of ABZ – PEG 6000 at temperatures of 26 °C, 57 °C and 62 °C. It can be observed that above 57 °C, ABZ starts solubilising into PEG 6000 and is completely miscible over 62 °C (see image annotations).

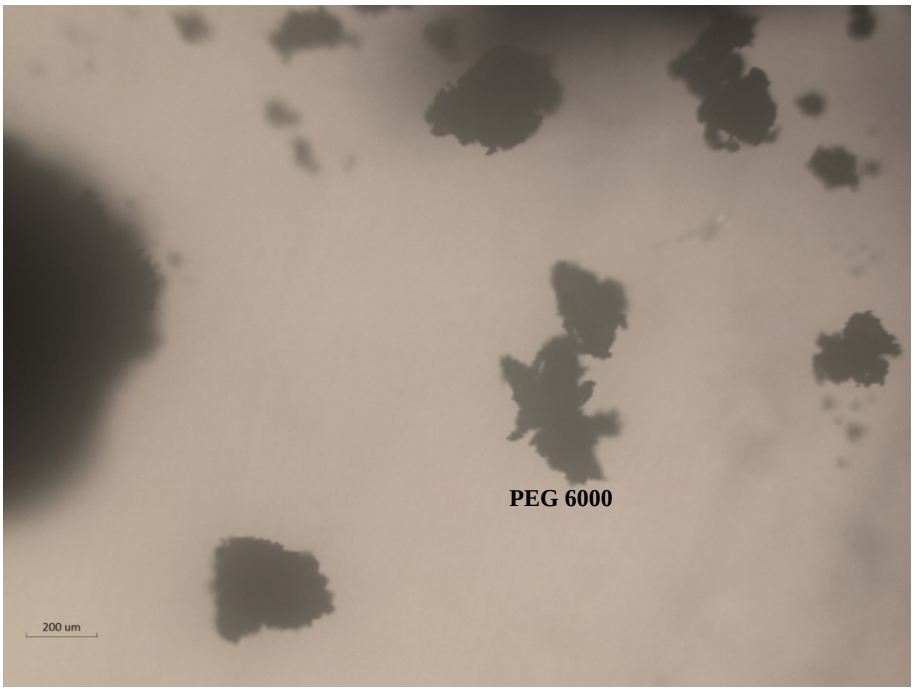

Figure 3.3. HSM image (10X) of PM ABZ-PEG 6000 (5 % w/w) at 26 °C

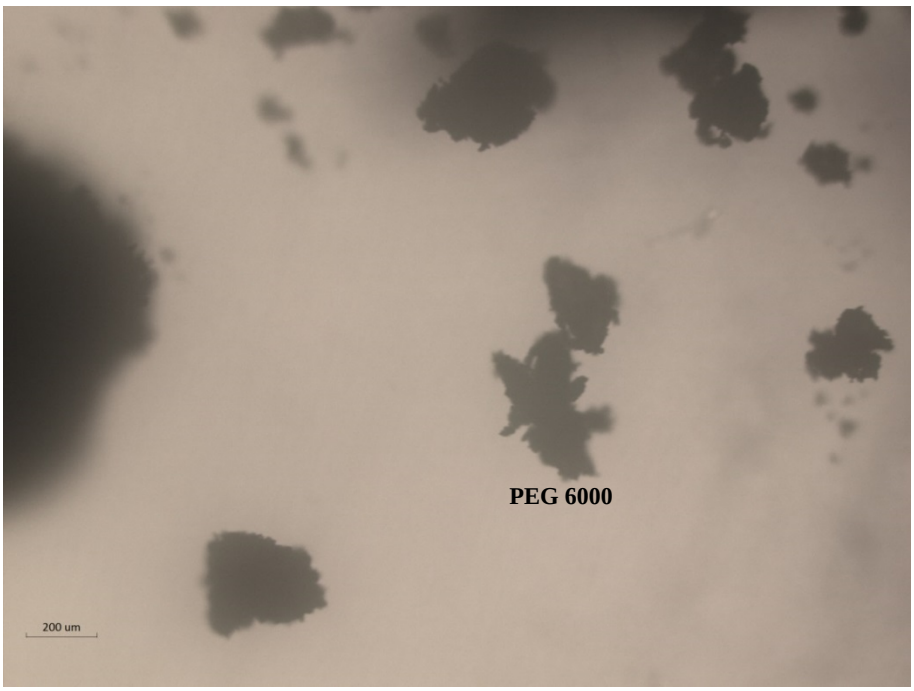

Figure 3.4. HSM image (10X) of PM ABZ-PEG 6000 (5 % w/w) at 57 °C

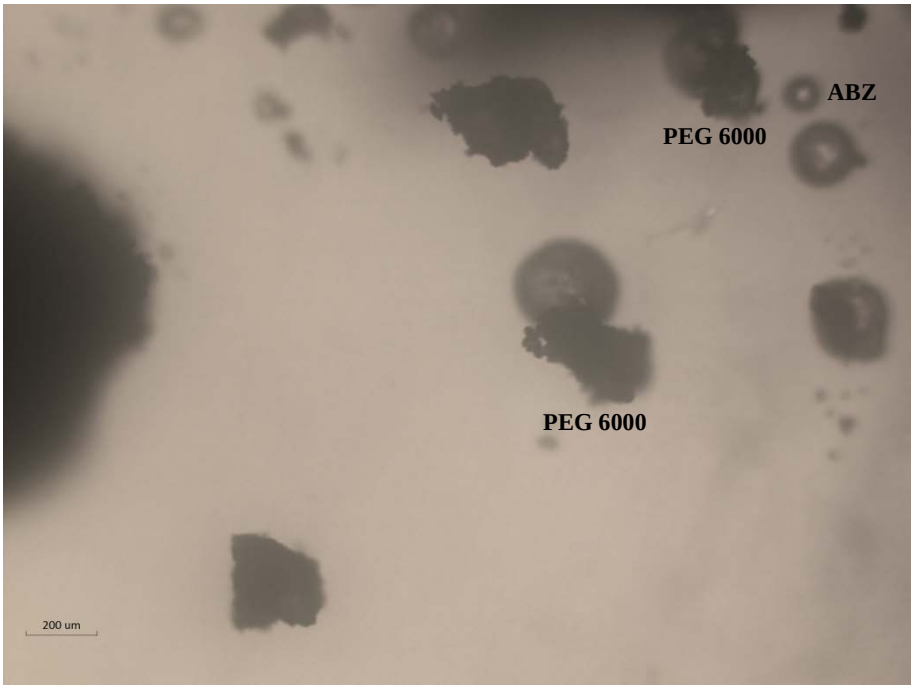

Figure 3.5. HSM image (10X) of PM ABZ-PEG 6000 (5 % w/w) at 62 °C

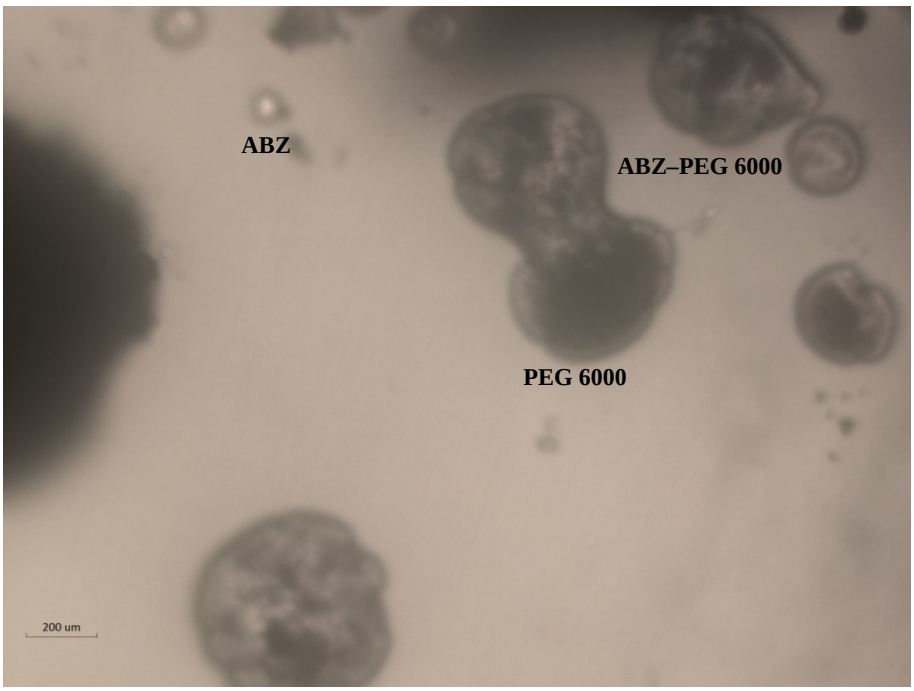

Figure 3.6. HSM image (10X) of PM ABZ-PEG 6000 (5 % w/w) over 62 °C

3.4.1.2. Scanning Electron Microscopy (SEM)

Images of raw materials, physical mixtures and extruded materials were taken using SEM technique. Visual comparison between ABZ alone (Figure 3.7), PM at different drug contents (Figure 3.8) and extruded materials (Figures 3.9, 3.10, 3.12 and 3.14) indicate the absence of crystalline ABZ in the surface of the extruded materials post extrusion. Moreover, the polymeric matrix of these formulations is clearly different to the ones produced in chapter 2 when using PVP K12. In this case, PEG 6000 forms a plastic type of material with no brittleness properties. In addition, side view images depict a homogeneous polymer matrix with no de-laminated zones. The extruded materials after 6 months storage at 25 and 37 °C (Figures 3.11, 3.13 and 3.15) show specific points of reflectance (indicated by a red circle) that is characteristic of crystalline materials. This crystallinity degree could be due to crystalline ABZ but also to particles of PEG 6000. Regarding the porosity

properties of PEG 6000 extruded materials, few internal pores are observed from the top view as seen in Figures 3.9 to 3.15.

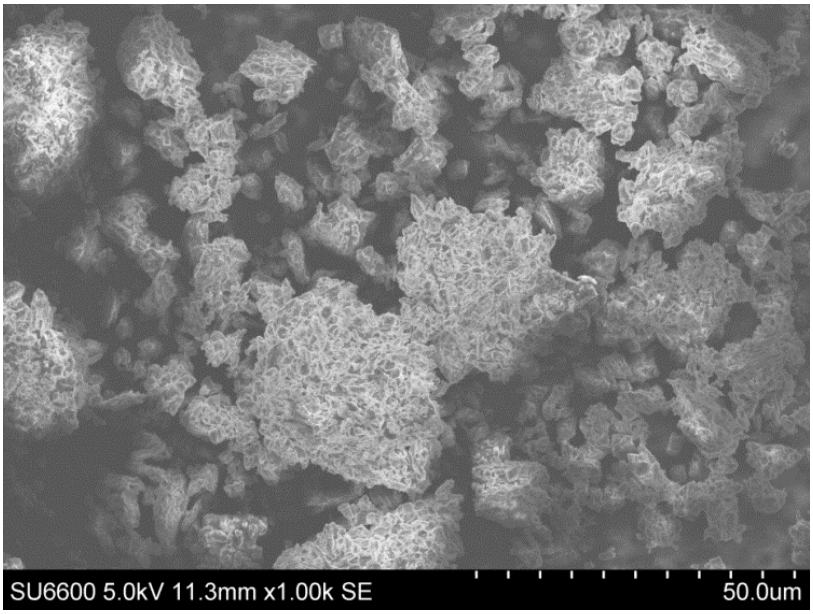

Figure 3.7. SEM image of ABZ alone

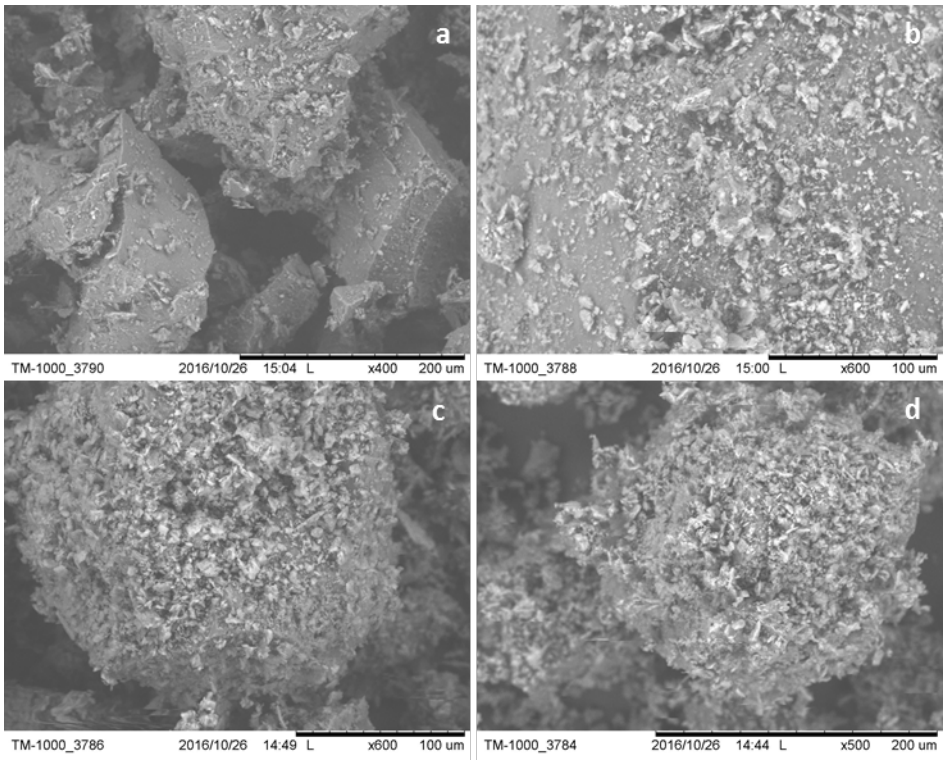

Figure 3.8. SEM images of PM ABZ–PEG 6000 at (a) 1 %, (b) 5 %, (c) 10 % and (d) 20 % (w/w)

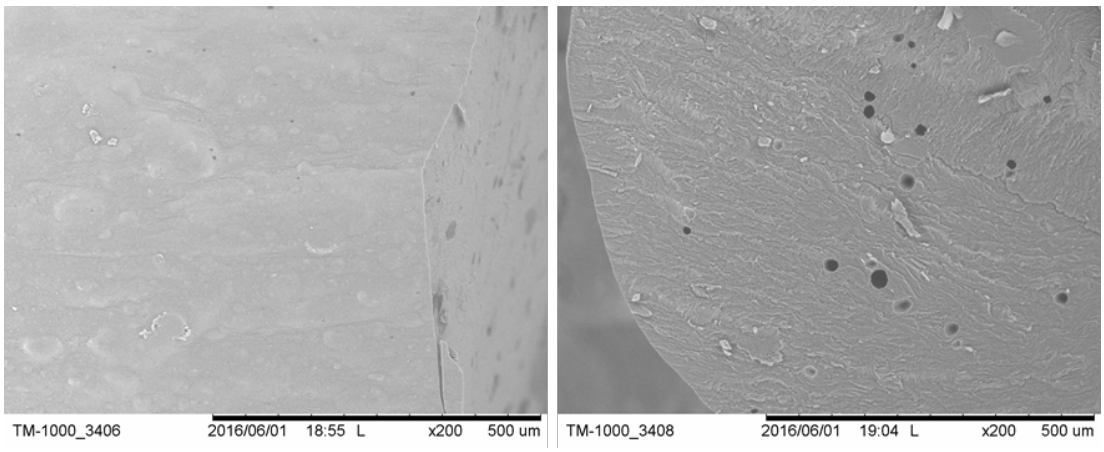

Figure 3.9. SEM images, side view (left) and top view (right) of F1 extruded material (post extrusion)

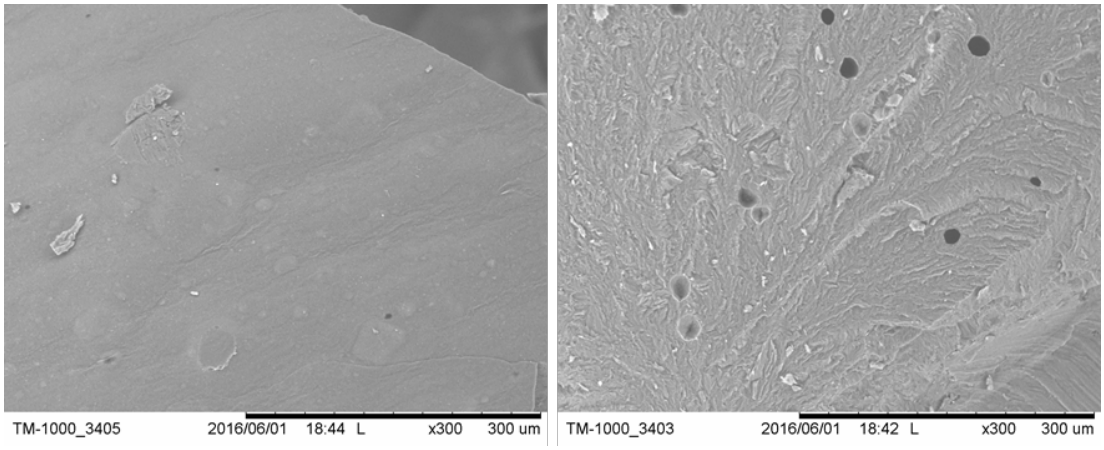

Figure 3.10. SEM images, side view (left) and top view (right) of F2 extruded material (post extrusion)

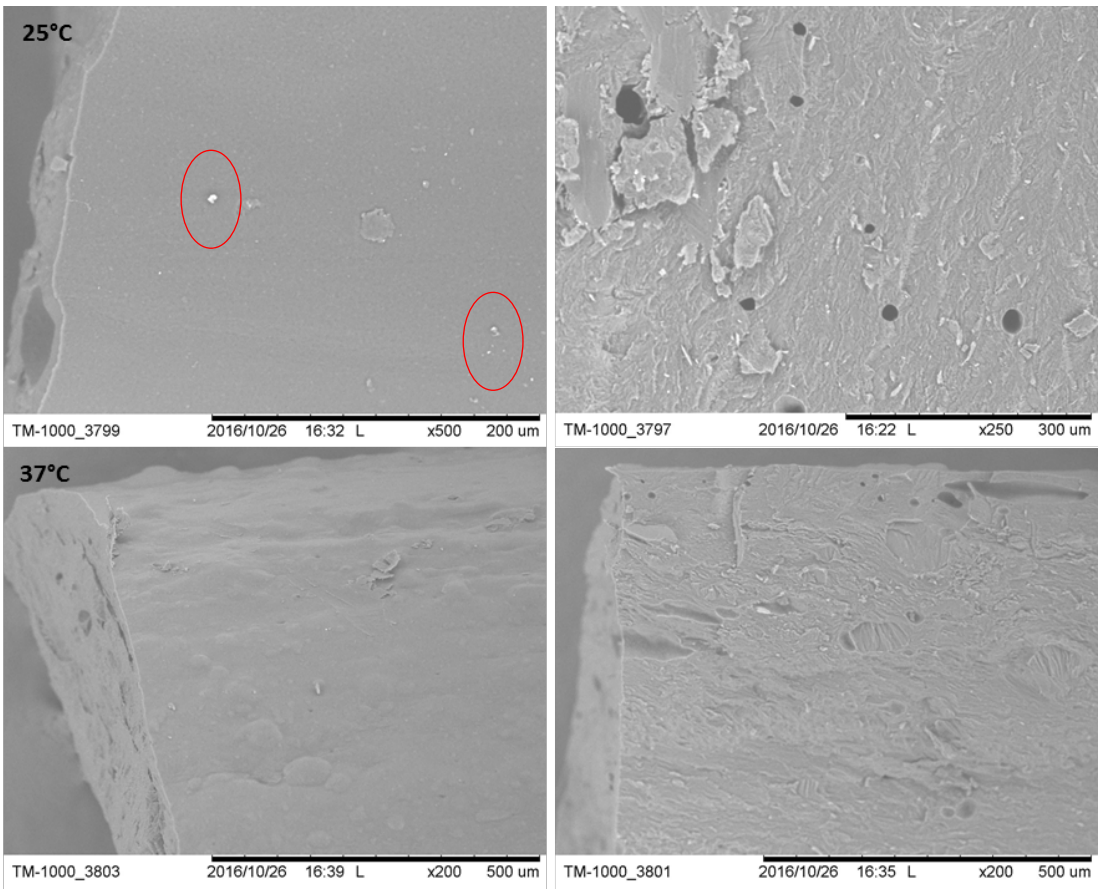

Figure 3.11. SEM images after 6 months storage at 25 °C and 37 °C, side view (left) and top view (right) of F2 extruded material

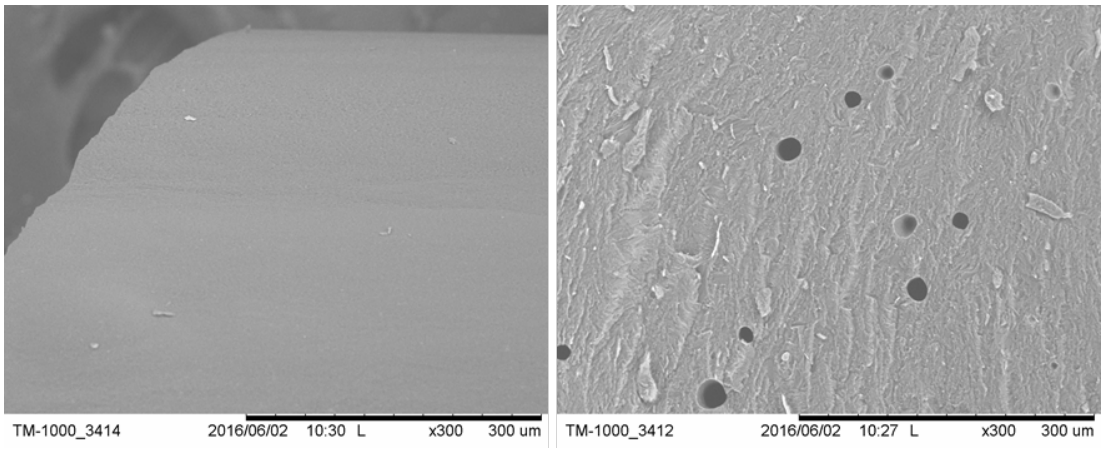

Figure 3.12. SEM images, side view (left) and top view (right) of F3 extruded material (post extrusion)

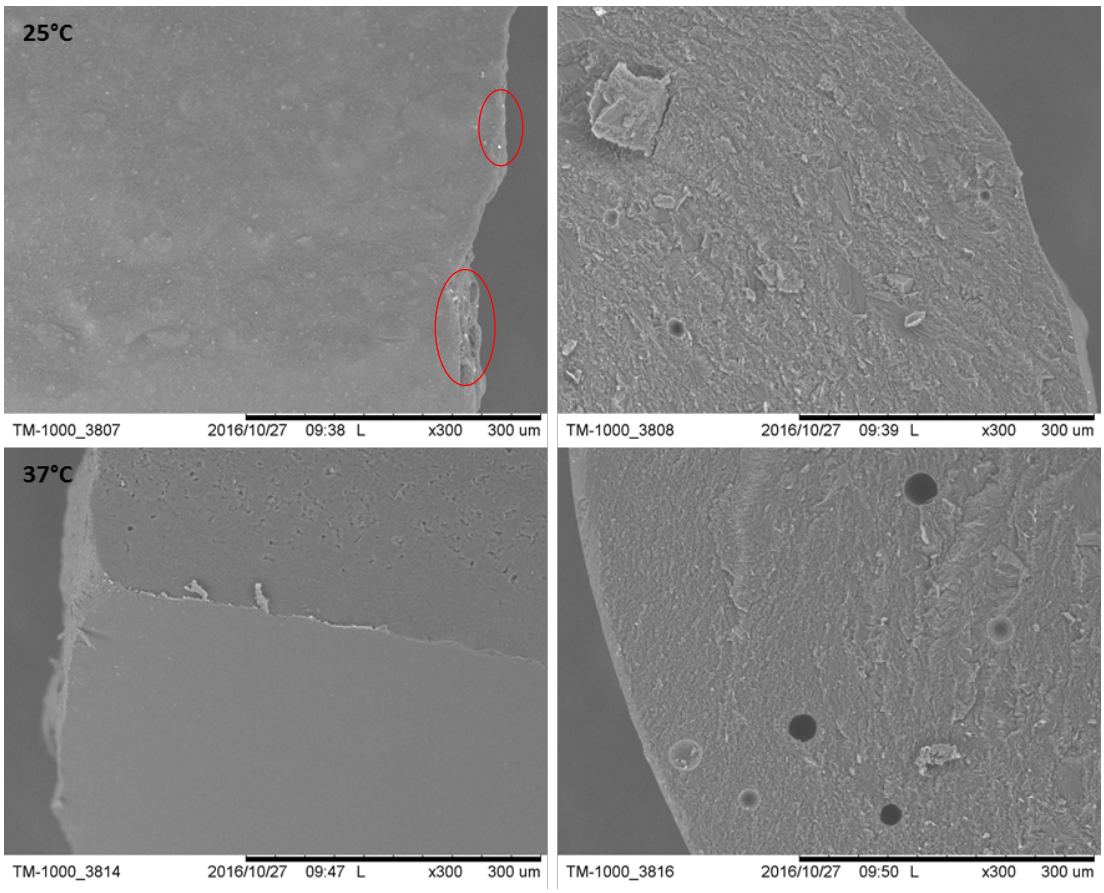

Figure 3.13. SEM images after 6 months storage at 25 °C and 37 °C, side view (left) and top view (right) of F3 extruded material

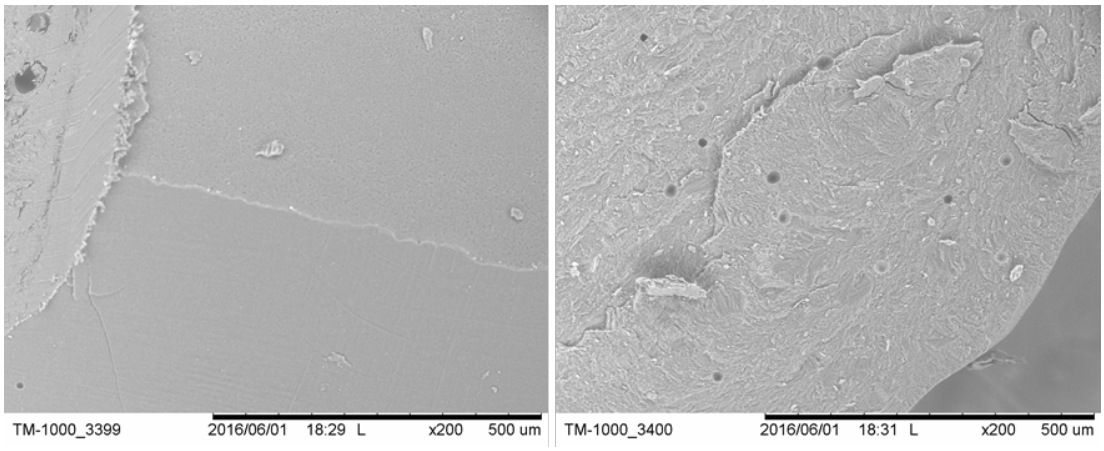

Figure 3.14. SEM images, side view (left) and top view (right) of F4 extruded material (post extrusion)

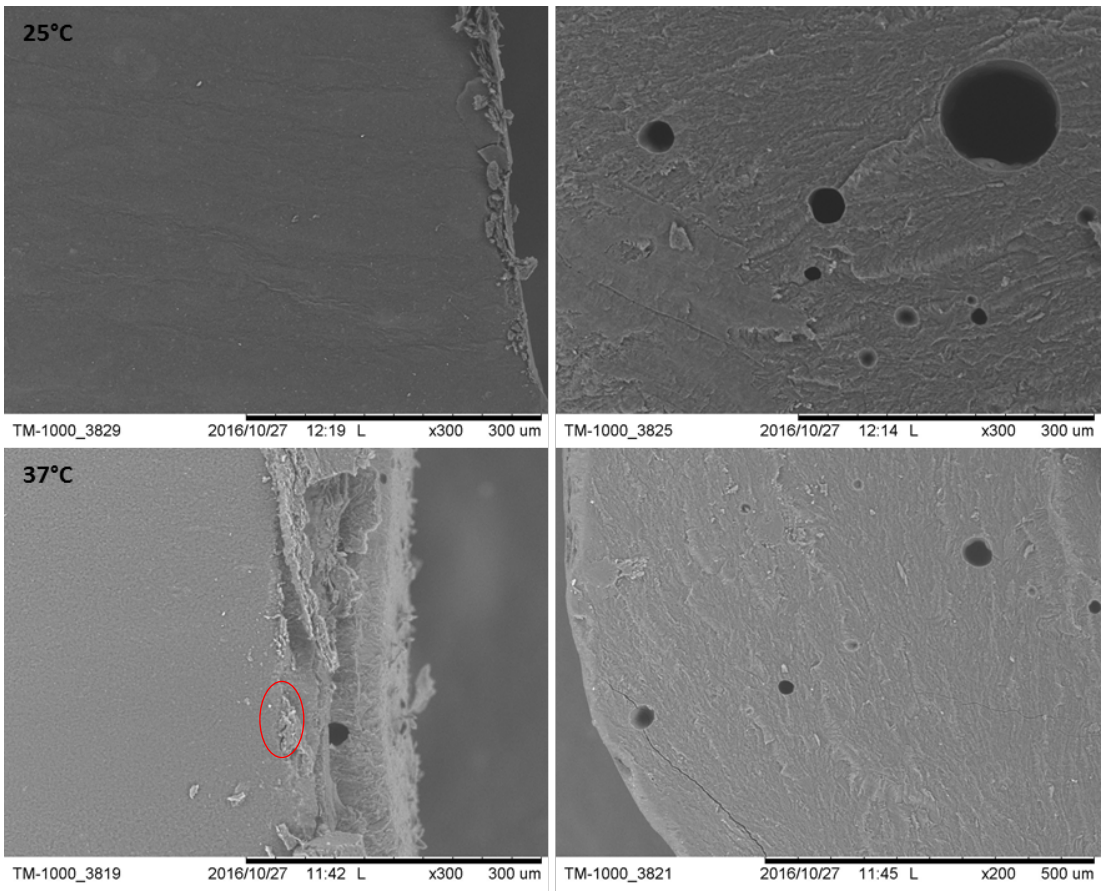

Figure 3.15. SEM images after 6 months storage at 25 °C and 37 °C, side view (left) and top view (right) of F4 extruded material

3.4.1.3. X-Ray Powder Diffraction (XRPD)

The XRPD patterns of ABZ and PEG 6000 alone, PM and ABZ – PEG 6000 extruded materials (Figures 3.16 to 3.19) are shown below. The XRPD pattern of ABZ shows intensity peaks at 2θ angles of 6.91, 11.32, 13.83, 17.97, 19.51, 19.99, 20.75, 22.19, 23.85, 24.47, 24.72, 25.05, 26.08, 26.23, 27.21, 28.73, 29.06, 30.00, 30.52 and 31.05° that correspond to ABZ crystalline form I (Pranzo et al., 2010) as previously described in chapter 2. The XRPD pattern of PEG 6000 alone shows two main intensity peaks at 2θ angles of 18.83 and 22.90 and peaks of much lower intensity at 2θ angles of 12.93, 13.27, 14.41, 14.82, 25.90, 26.54 and 27.52. PM at different drug contents (1 % to 20 % w/w) show two main crystalline peaks of PEG

6000 and also ABZ peaks of low intensity. All extruded materials post extrusion show two main crystalline peaks at 2θ angles of 18.42 and 22.46 which are really close to the peaks reported above, corresponding to PEG 6000. Therefore, ABZ was successfully converted to amorphous form. However, when the extruded materials are characterised after 6 months storage at 25 and 37 °C, it can be observed a certain crystallinity degree that corresponds to both, polymer and drug. For example, formulation F2 shows intensity peaks at 2θ angles of 7.03, 11.48, 13.26, 13.67, 14.78, 15.25, 18.11, 18.79, 19.33, 22.23, 23.47, 26.40, 27.11, 28.06, 30.52, 31.02 and 32.91 (Figure 3.17). These results (▼) indicate recrystallisation events and therefore partial transformation of ABZ from amorphous to crystalline form. Diffractograms of extruded materials after 6 months storage also exhibit increased intensities of the crystalline peaks corresponding to ABZ as the drug content of extruded materials also increases. Further investigations such as HSM studies would be required to exactly determine the crystallinity degree of the stored samples (Urbanetz and Lippold, 2005).

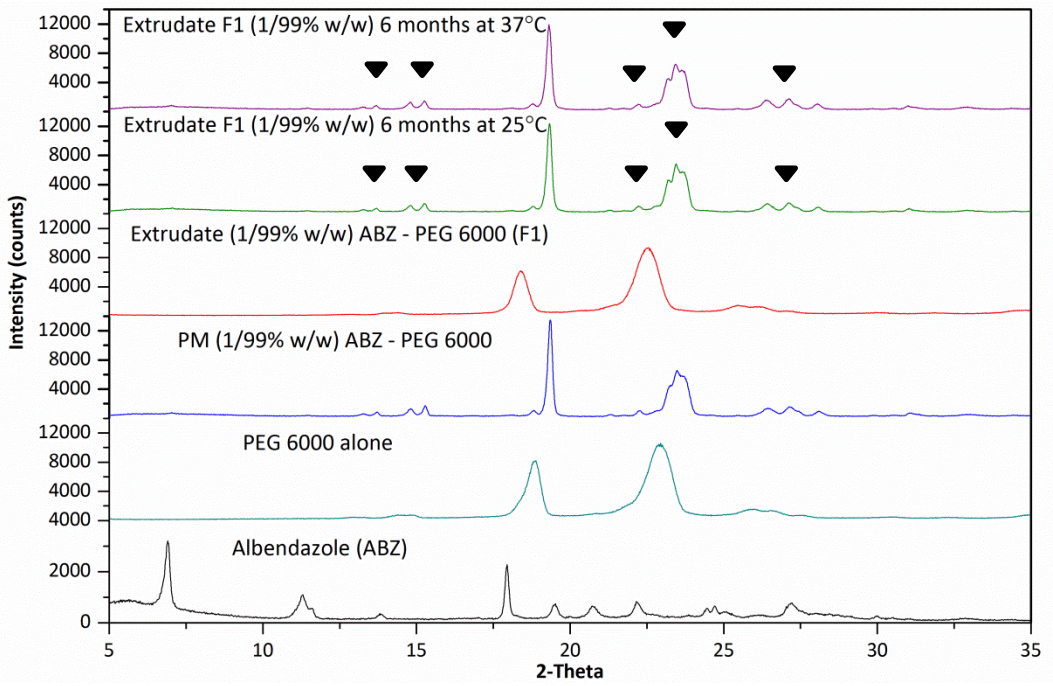

Figure 3.16. Diffractogram of formulation F1 ABZ – PEG 6000

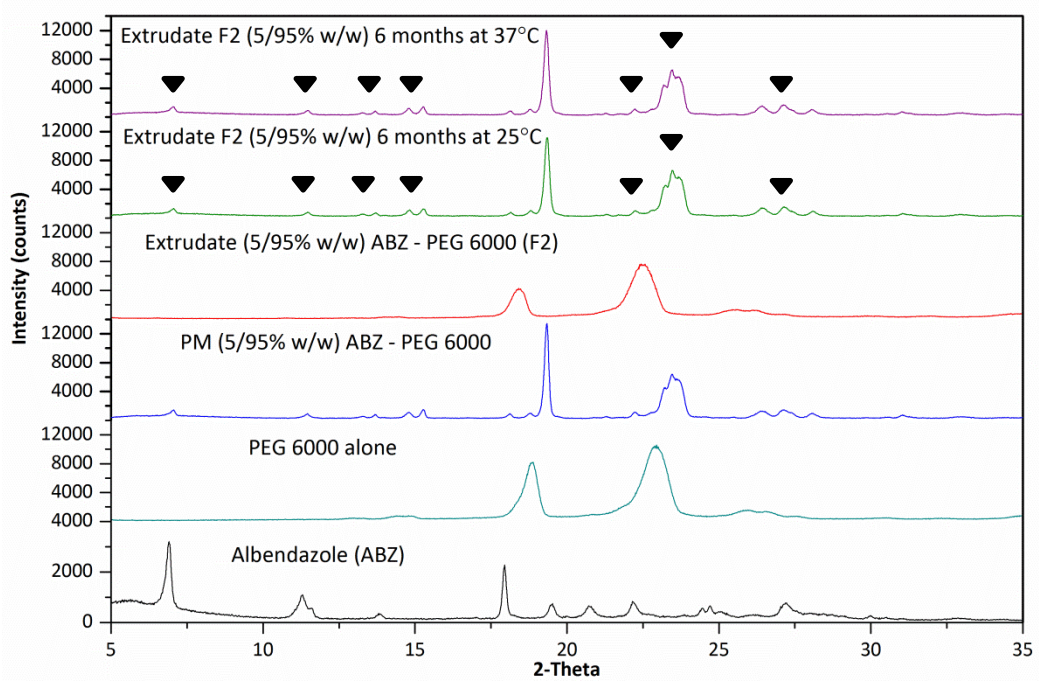

Figure 3.17. Diffractogram of formulation F2 ABZ – PEG 6000

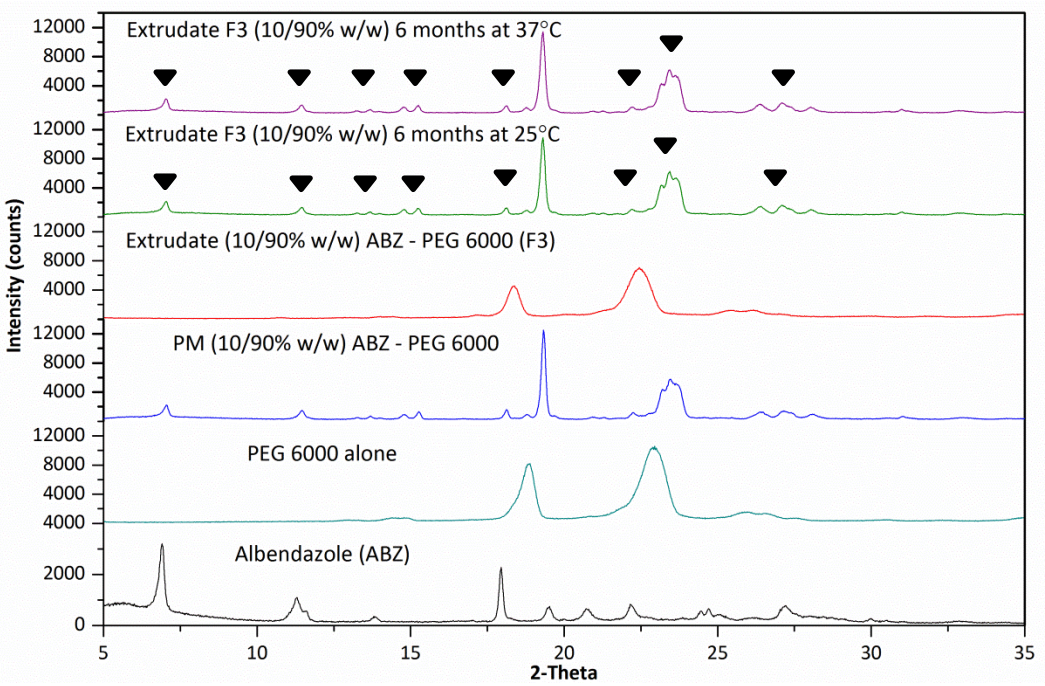

Figure 3.18. Diffractogram of formulation F3 ABZ – PEG 6000

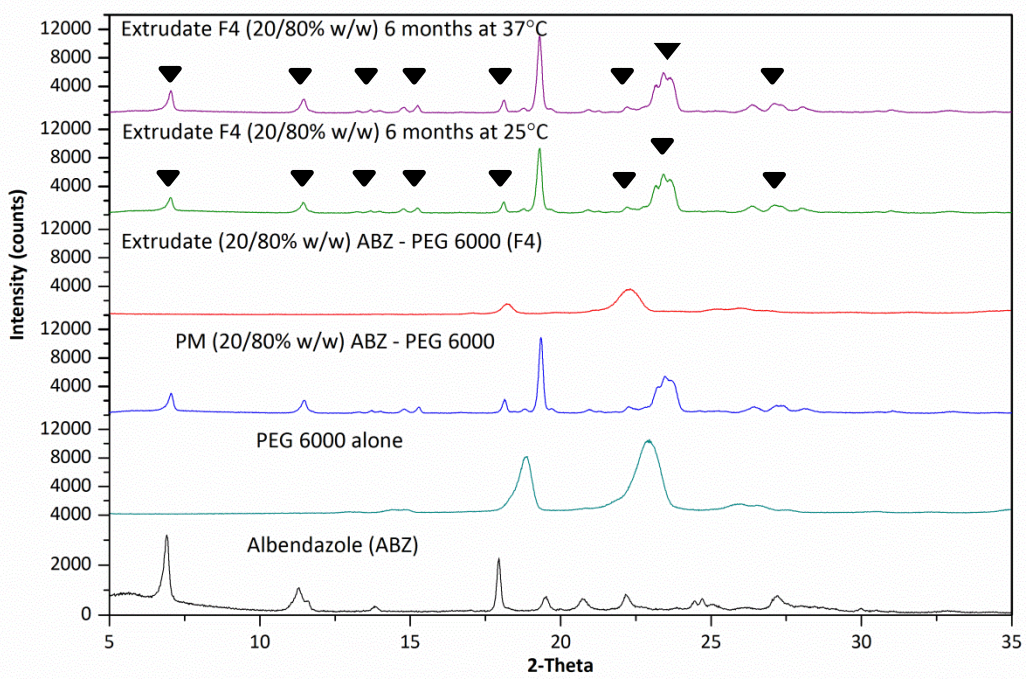

Figure 3.19. Diffractogram of formulation F4 ABZ – PEG 6000

3.4.1.4. Differential Scanning Calorimetry (DSC)

DSC analysis of the raw materials, PM and extruded materials was performed post extrusion and also after 6 months storage of the samples. Assessment of the

formation of amorphous solid dispersions and absence of crystalline drug was carried out. Extruded materials show an endothermic event at 62 °C that corresponds to the melting point of PEG 6000 (Figure 3.20) and also a glass transition event (T_g) which suggests that ABZ is in amorphous form. The exact value of the extruded materials T_g was calculated in each case using the inflection point method (Figures 3.21 to 3.24). For example, formulation F1 shows a small T_g event of 140.11 °C after 6 months storage at 25 °C (Figure 3.21). The extruded material post extrusion and after 6 months storage at 37 °C, do not show a T_g event. This behaviour has been previously associated to the influence of a slow heating rate (10 °C/min) on the low detection of T_g events due to very small temperature differences between the sample and the reference (Kerč and Srčič, 1995).

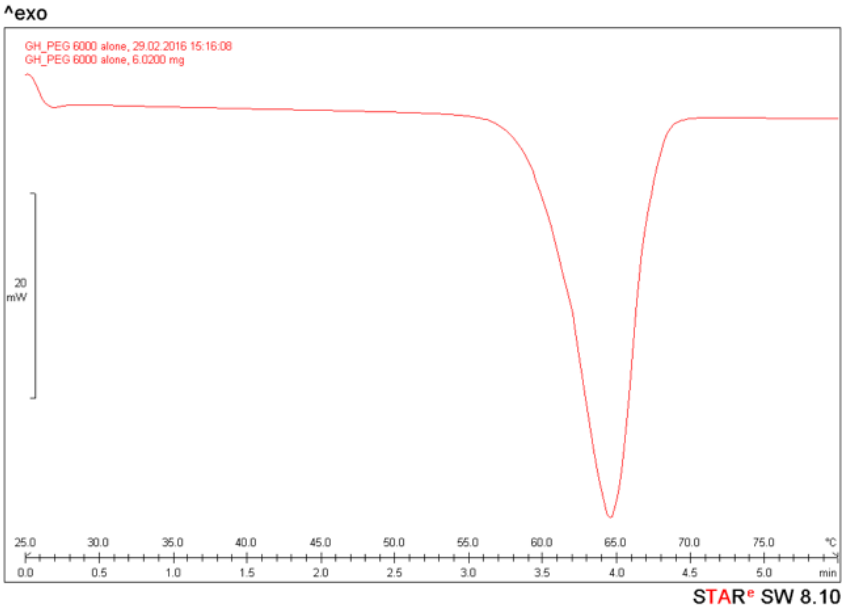

Figure 3.20. DSC thermogram of PEG 6000 alone

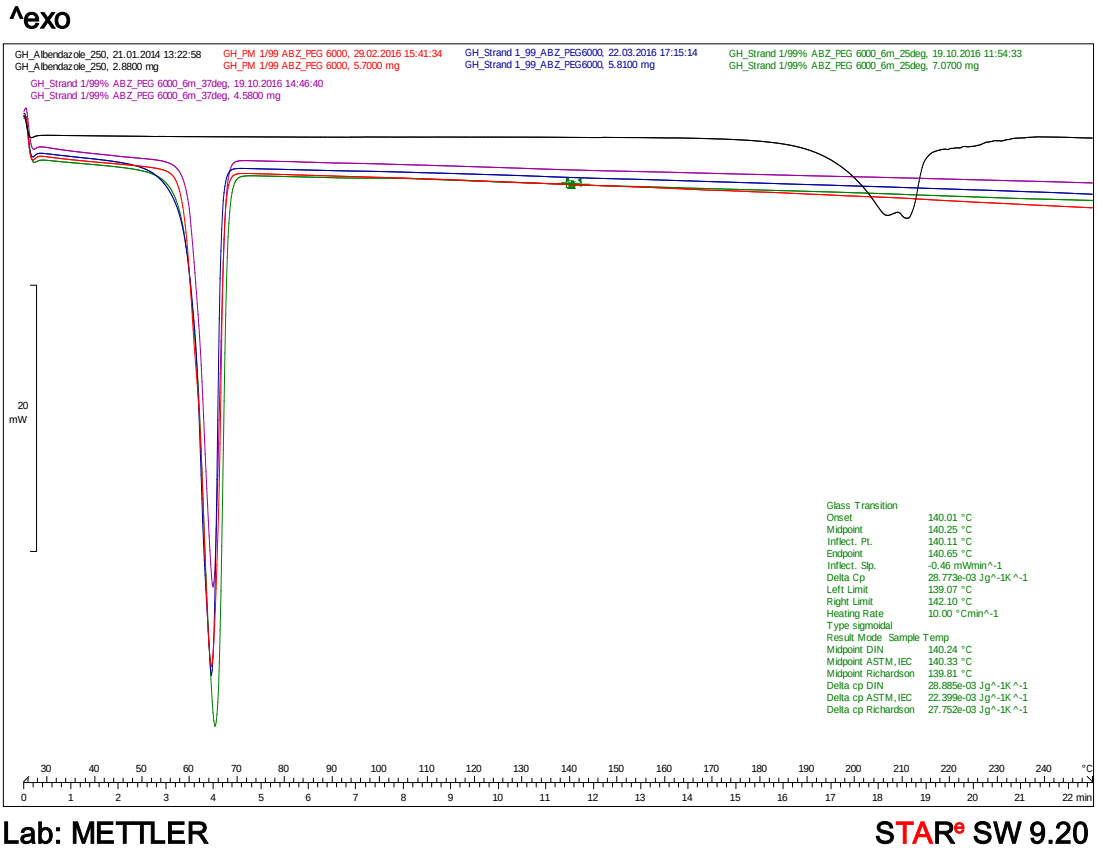

Figure 3.21. DSC thermograms of (a) ABZ alone, (b) physical mixture (PM) of ABZ–PEG 6000 at 1/99 (% w/w), (c) extruded material F1 post extrusion, (d) F1 after 6 months at 25 °C and (e) F1 after 6 months at 37 °C

In the case of formulations F2, F3 and F4, DSC thermograms indicate similar results to F1, amorphous form of ABZ with no recrystallisation events occurring after 6 months storage (Figures 3.22 to 3.24). All show one single T_g event that is characteristic of each extruded material and indicates the formation of miscible amorphous solid dispersions. In addition, extruded materials show broader T_g event shifts as the drug content in the formulation increases (Damian et al., 2000). The values of the T_g events obtained for each formulation are depicted in Table 3.5. The absence of melting endotherm peaks relative to crystalline ABZ in the case of samples stored for 6 months, is not in agreement with the results observed above by

XRPD analysis. In order to determine the solid state of these formulations, further experiments such as HSM analysis could be performed (Vasa et al., 2014).

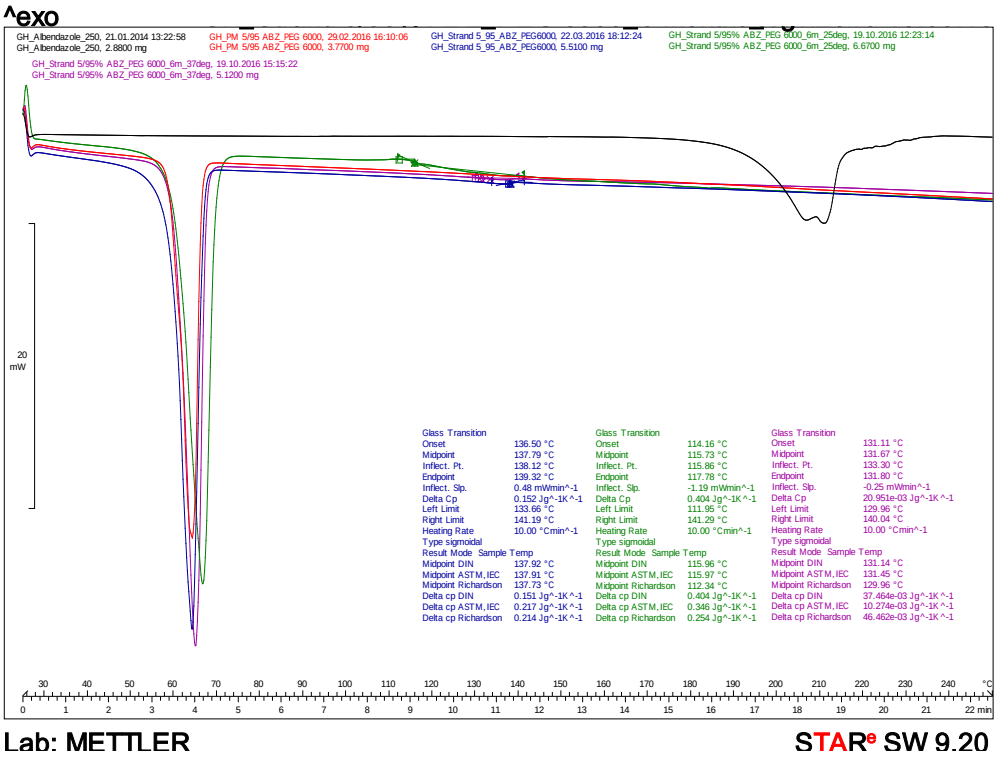

Figure 3.22. DSC thermograms of (a) ABZ alone, (b) physical mixture (PM) of ABZ–PEG 6000 at 5/95 (% w/w), (c) extruded material F2 post extrusion, (d) F2 after 6 months at 25 °C and (e) F2 after 6 months at 37 °C

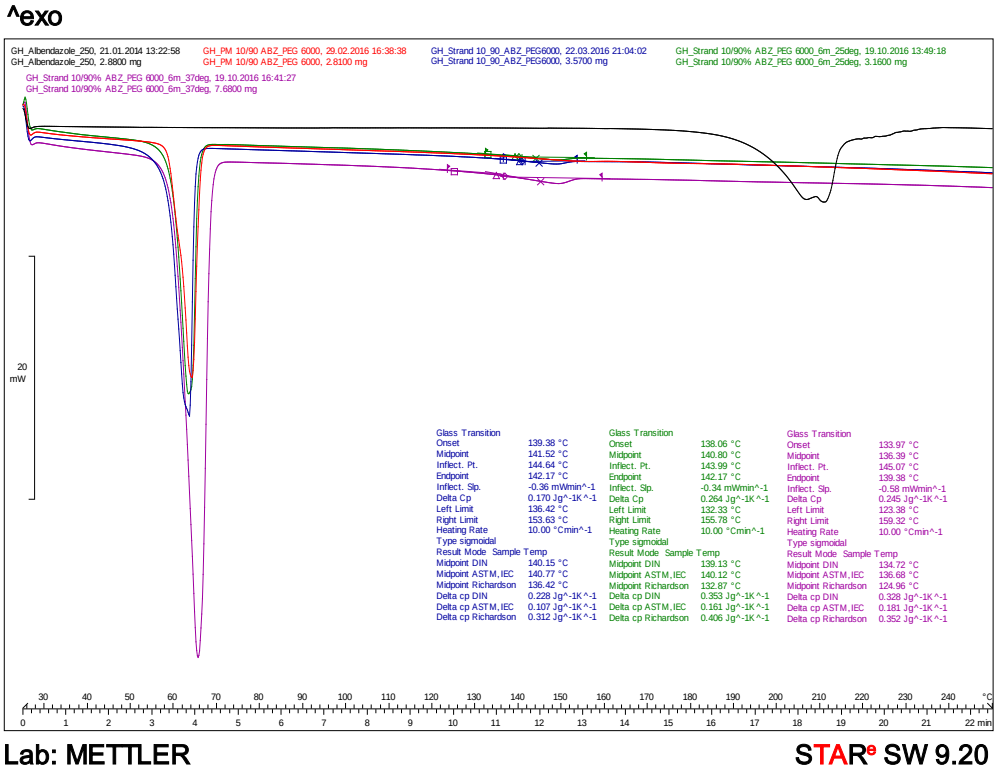

Figure 3.23. DSC thermograms of (a) ABZ alone, (b) physical mixture (PM) of ABZ–PEG 6000 at 10/90 (% w/w), (c) extruded material F3 post extrusion, (d) F3 after 6 months at 25 °C and (e) F3 after 6 months at 37 °C

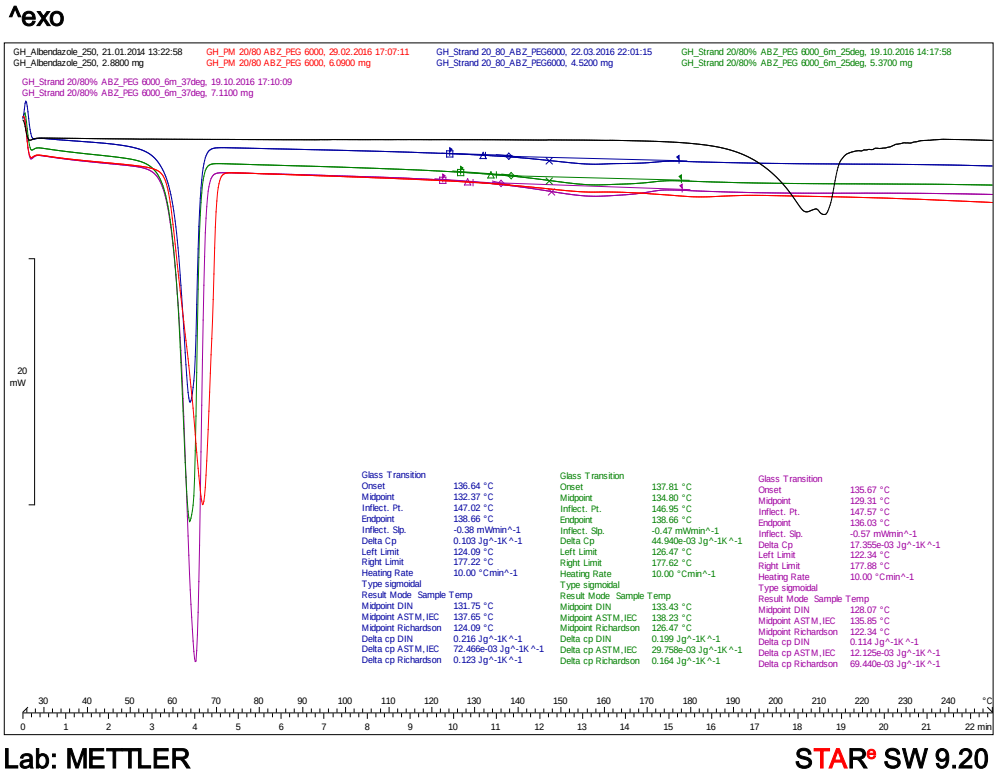

Figure 3.24. DSC thermograms of (a) ABZ alone, (b) physical mixture (PM) of ABZ–PEG 6000 at 20/80 (% w/w), (c) extruded material F4 post extrusion, (d) F4 after 6 months at 25 °C and (e) F4 after 6 months at 37 °C

Table 3.5. Measured T_g values of extruded materials post extrusion and after 6 months storage

Formulation	Sample	T_g (°C)	Onset (°C)	Endpoint (°C)
F1	6m at 25 °C	140.11	140.01	140.65
F2	Post extrusion	138.12	136.50	139.32
	6m at 25 °C	115.86	114.16	117.78
	6m at 37 °C	133.30	131.11	131.80
F3	Post extrusion	144.64	139.38	142.17
	6m at 25 °C	143.99	138.06	142.17
	6m at 37 °C	145.07	133.97	139.38
F4	Post extrusion	147.02	136.64	138.66
	6m at 25 °C	146.95	137.81	138.66
	6m at 37 °C	147.57	135.67	136.03

3.4.1.5. Karl-Fischer (KF) studies

Extruded materials of ABZ – PEG 6000 were characterised by Karl-Fischer post extrusion and also after 6 months storage to evaluate possible water intake. It is known that PEG is a very hygroscopic polymer which can undergo a phase transformation known as deliquescence, when a critical relative humidity (RH %) value is reached (Baird et al., 2010; Rumondor and Taylor, 2009). The importance of possible water content uptake by a hygroscopic polymeric material was already discussed in chapter 2 of this thesis. The water content (% w/w) obtained for all ABZ – PEG 6000 extrudates post extrusion and after storage are depicted in Figure 3.25. Mean standard deviation (SD) values of 3 replicates calculated for each sample are represented by error bars. It is observed that extruded materials water content increased from ≤ 0.1 % post extrusion to ≤ 0.27 % (6 months at 25 $^{\circ}$C) and to ≤ 0.51 % (6 months at 37 $^{\circ}$C). The water content increase observed is higher than the water content uptake described in chapter 2, indicating that PEG 6000 is more hygroscopic than PVP K12. Moreover, non-parametric ANOVA (Kruskal-Wallis) test indicates that temperature changes do have a significant influence in samples water content ($P<0.05$) in all formulations (indicated by * symbol).

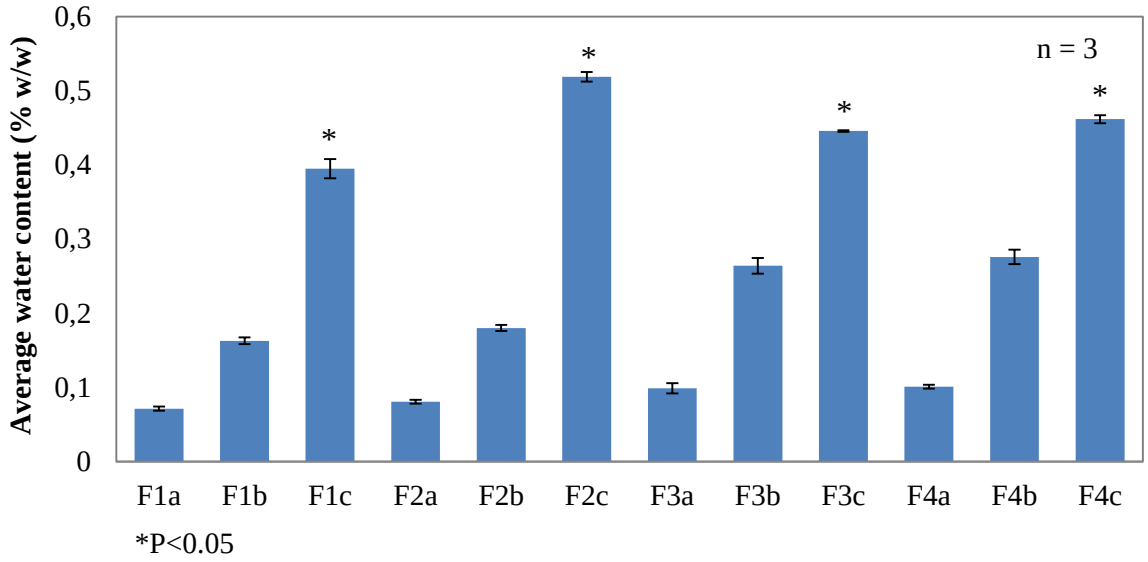

Figure 3.25. Karl-Fischer results of formulations F1 to F4 post extrusion (a), 6 months at 25 °C, 20 % RH (b) and 6 months at 37 °C, 9 % RH (c). * symbol represents statistically significant differences obtained from a non-parametric Kruskal-Wallis test with 0.05 significance level (n = 3). Error bars represent standard deviation.

3.4.1.6. In-vitro dissolution studies

Initial dissolution profile experiment of formulation F2 within the full pH range (2.0 – 7.0) indicated that extruded materials comprising ABZ – PEG 6000 were in solution for 30 minutes at pH 2.1. At higher pH, ABZ precipitation is observed as shown in Figure 3.26 (red circle). Therefore, further T3 experiments were performed just at pH 2.0 for 30 minutes. This effect was previously observed in PEG formulations, due to the high affinity of PEG for water, leading to a conversion of the drug solid state from amorphous to crystalline (Gullapalli and Mazzitelli, 2015; Quinn et al., 2012).

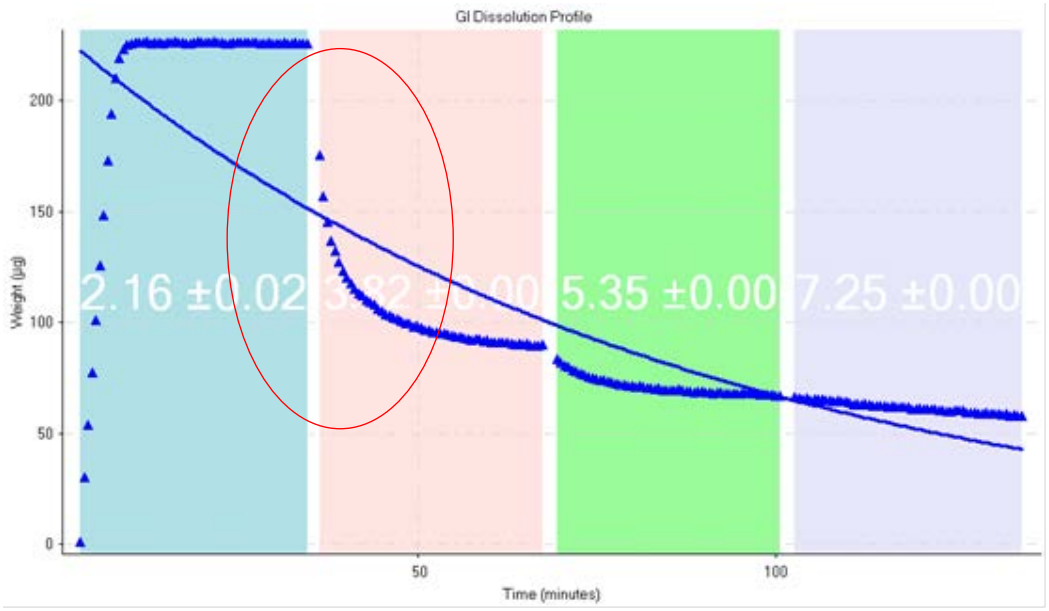

Figure 3.26. Dissolution profile at pH range 2 – 7 of formulation F2

Dissolution curves shown in Figures 3.27 to 3.30 were normalised by the drug content of each formulation and also in each tablet sample measured (calculations are detailed in the appendix).

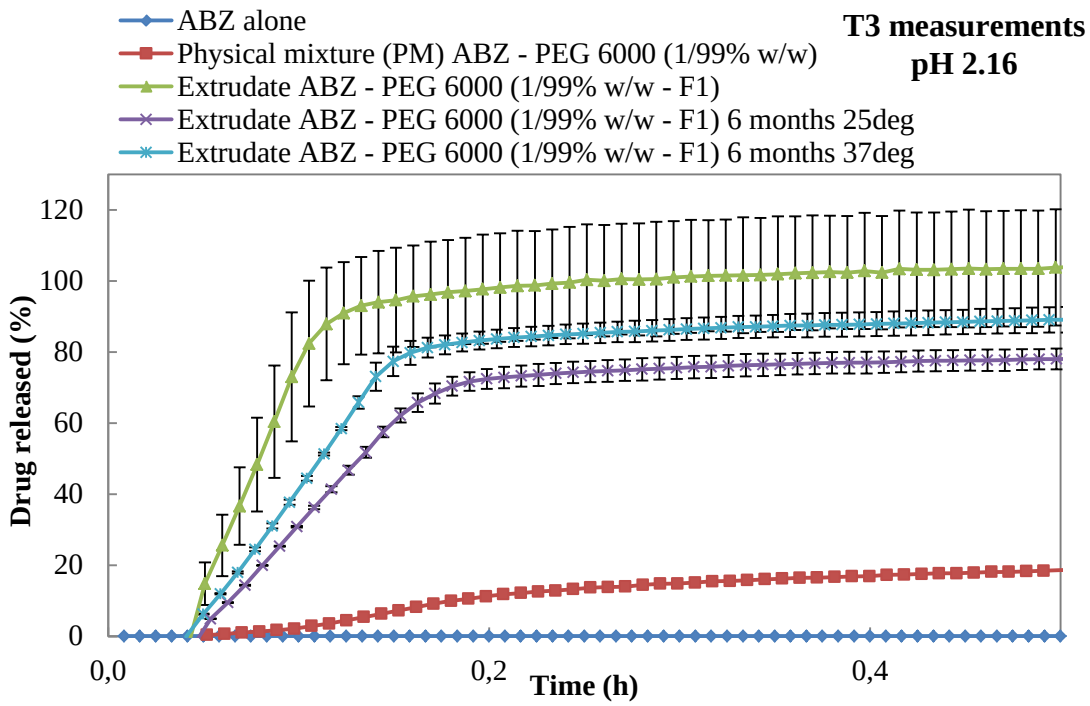

Figure 3.27. Dissolution profiles of F1 extruded material. Standard error of the mean bars are based on 2 tests per sample.

Amorphous solid dispersions of ABZ - PEG 6000 show maximum drug release of 100 % (F1), 50 % (F2), 21 % (F3) and 13 % (F4) over a period of 30 minutes. In the case of formulation F1 (Figure 3.27), the extruded material shows a decrease from 100 % drug release (post extrusion) to 78 % (6 months at 25 °C) and 89 % (6 months at 37 °C). This could be due to higher humidity conditions in the storage chambers. It is known that the chamber at 25 °C has a higher relative humidity (RH 20 %) than the chamber at 37 °C (RH 9 %) and Karl-Fischer results reported above suggest there is an increase in water content (%) after storage of the samples. As mentioned already in chapter 2, water uptake can provide a higher molecular mobility leading to possible drug recrystallisation. The XRPD diffractogram (Figure 3.16) suggests there is ABZ recrystallisation after 6 months storage that can explain the dissolution profiles achieved. It is also interesting to note that DSC thermogram does not show any evidence of ABZ recrystallisation over time. This could be due to the crystalline material being below the limit of detection.

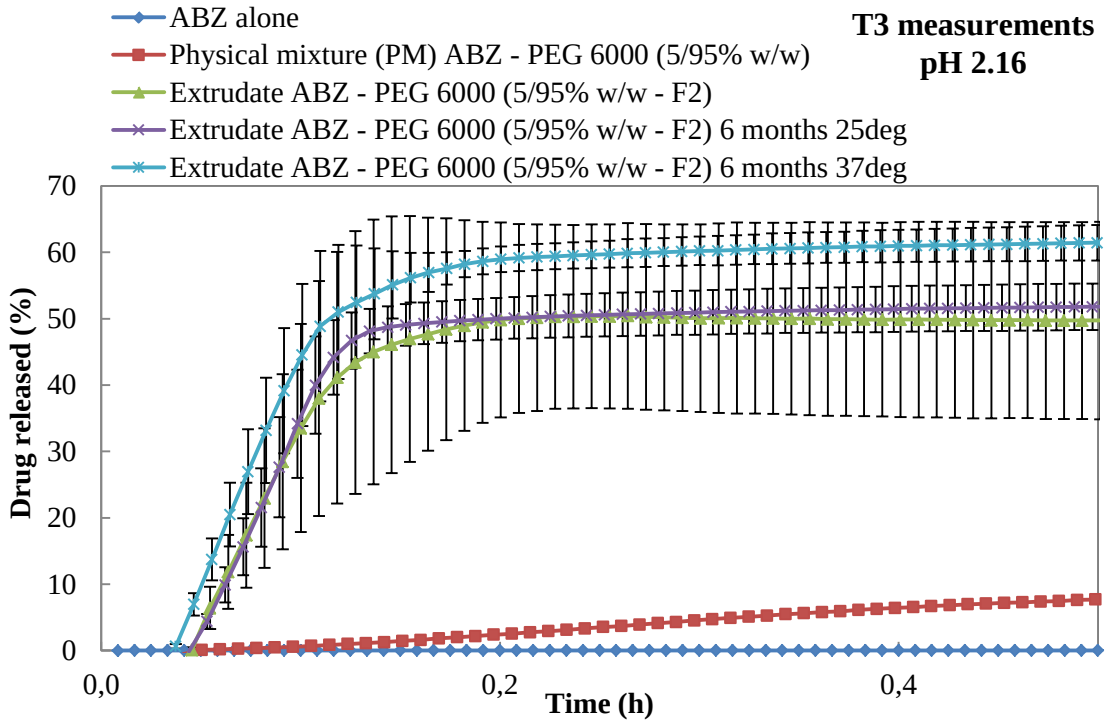

Figure 3.28. Dissolution profiles of F2 extruded material. Standard deviation bars are based on 3 replicates.

The dissolution profiles obtained in case of formulation F2 (Figure 3.28) show an increase in drug release for the amorphous form post extrusion of 50 %. When this formulation is compared to F1 results, it is observed that formulation F2 comprising 5 % (w/w) ABZ in comparison to 1 % (w/w), exhibits a considerable decrease in maximum drug release achieved. This result indicates that formulations where PEG 6000 acts as polymeric carrier, perform differently depending on drug and polymer ratios. It is known that some polymeric carriers can promote carrier-controlled mechanisms as main factor influencing drug dissolution behaviour (Albers et al., 2009). Previous solid dispersions comprising PEG and manufactured by the solvent and fusion methods indicated a carrier-controlled mechanism, especially observed in the case of dispersions with high PEG and low drug levels (Corrigan, 1979; Dubois, 1985; Özkan, 2000). Similar findings to our results were reported by Perissutti et

al., (Perissutti, 2002) when analysing extruded materials comprised by PEG 4000, lactose and carbamazepine at different ratios. However, the extent of decrease in drug release as PEG content decreased was found to be different. In this case it could be attributed to the absence of further excipients in our formulations, being dissolution behaviour of the matrix dependent on PEG hydrophilic properties. Moreover Windbergs et al., (Windbergs et al., 2009) observed lower drug release of tripalmitin with decreased PEG ratios and attributed these to drug particles being completely surrounded by PEG molecules. This phenomena would have inhibited the formation of big pores within the matrix which have shown to govern the dissolution rate of these materials. Similar results of solid dispersions comprising a poorly soluble drug and PEG 6000 where a decrease in polymer content leads to decreased drug release profiles were previously reported (Khan et al., 2011; Leonardi et al., 2007; Leonardi et al., 2009; Lin and Cham, 1996). As can be observed in Table 3.6, the maximum concentration of drug in solution (calculated from the average of two tests) is much lower than the maximum solubility (220 µg/mL) of ABZ at pH 2. Therefore, extruded materials F1 to F4 did not achieve supersaturation.

Table 3.6. Maximum concentration values of ABZ in solution from amorphous solid dispersions

Post Extrusion	**Concentration (µg/mL)**	**6 months at 25 °C**	**Concentration (µg/mL)**	**6 months at 37 °C**	**Concentration (µg/mL)**
F1	0.0698	F1	0.0523	F1	0.0596
F2	0.0337	F2	0.0346	F2	0.0411
F3	0.0145	F3	0.0163	F3	0.0217
F4	0.0094	F4	0.0121	F4	0.0101

Regarding F2 stability after 6 months storage, it is evidenced a similar drug release profile for the sample stored at 25 °C. However, there is an increase in drug release up to 60 % for the sample stored at 37 °C. This can be explained due to smaller particle size of the ground sample d_{50} = 454 µm compared to the sample post extrusion where d_{50} = 525 µm (Tables 3.7 and 3.8) (Lin and Cham, 1996).

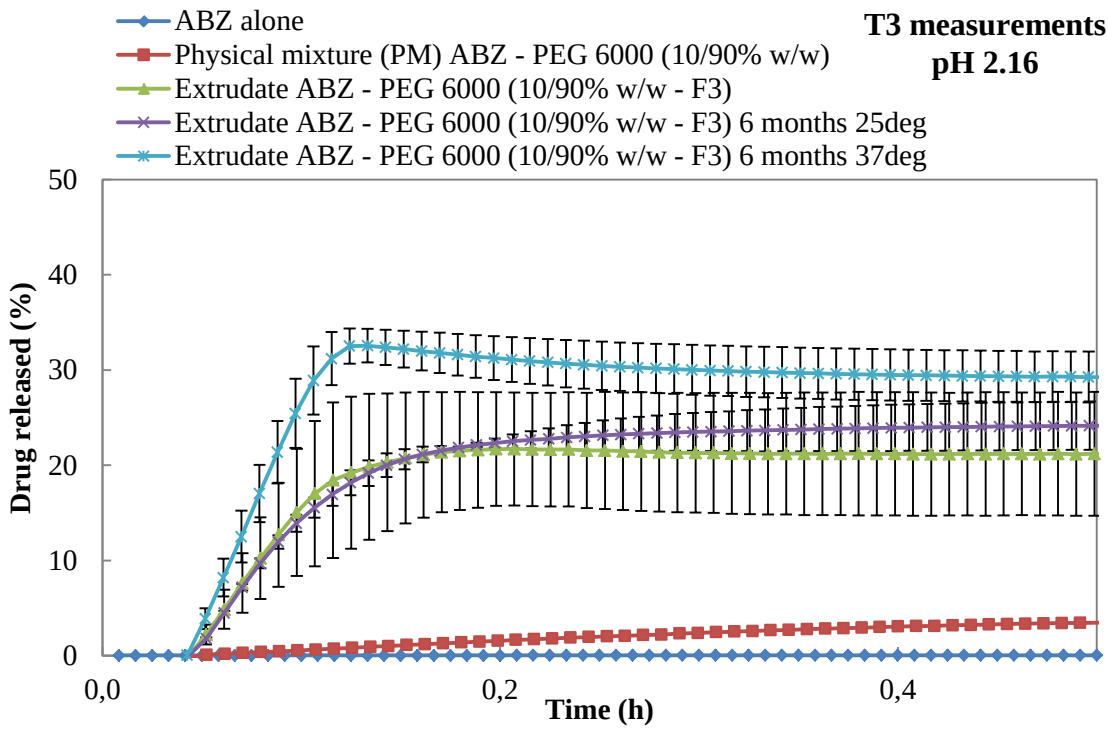

Figure 3.29. Dissolution profiles of F3 extruded material. Standard error of the mean bars are based on 2 tests per sample.

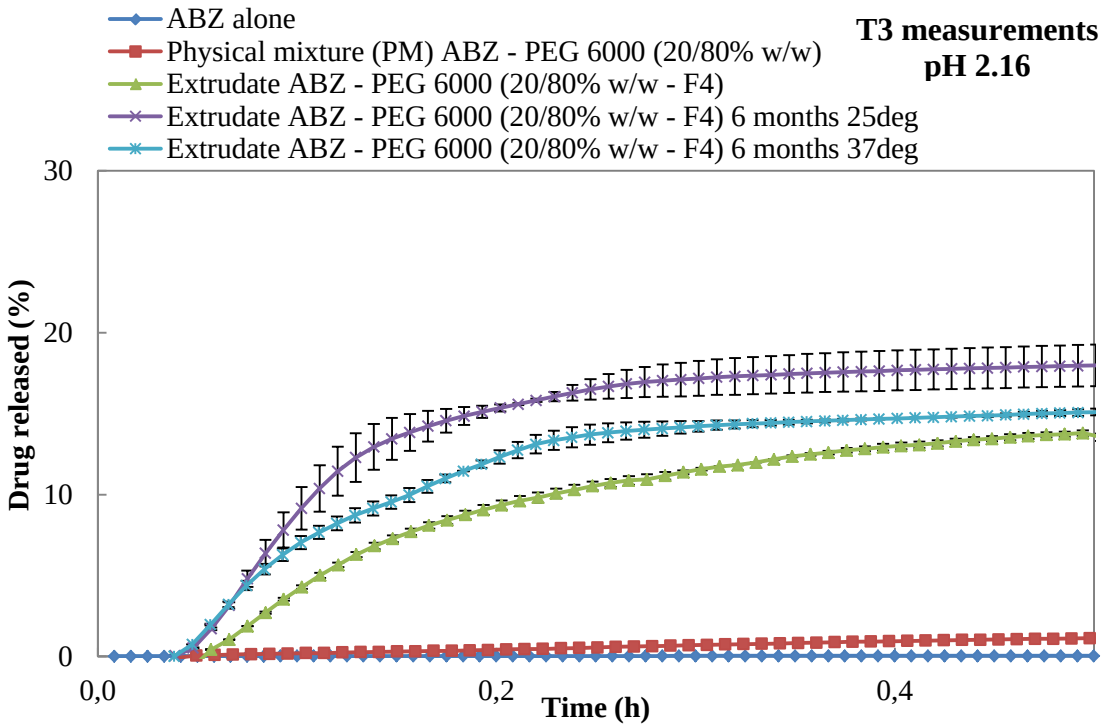

Figure 3.30. Dissolution profiles of F4 extruded material. Standard error of the mean bars are based on 2 tests per sample.

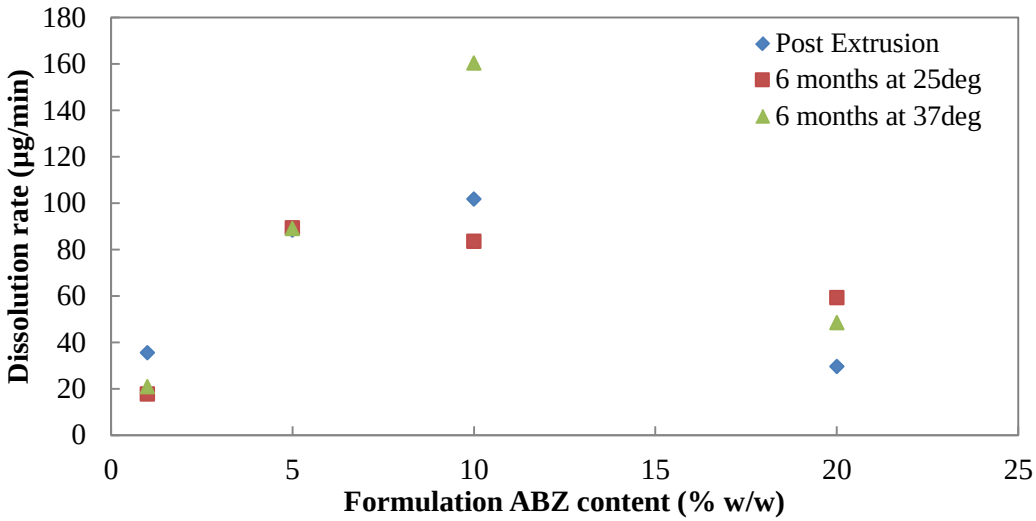

Figure 3.31. Extrapolated dissolution rate (µg/min) of extruded materials as a function of ABZ content (% w/w)

Formulations F3 and F4 with 10 % and 20 % (w/w) ABZ (Figures 3.29 and 3.30) clearly show that as drug content increases within the different formulations, % of

drug release decreases as mentioned above. The influence of ABZ and PEG 6000 content on the extent of drug release is shown in Figure 3.31. It can be observed a linear profile up to a maximum drug content, from which dissolution rate starts to decrease as it was previously reported by several researchers (Dubois, 1985; Franco, 2001). F3 formulation post extrusion releases up to 21 %, sample after 6 months at 25 °C releases up to 24 % and after 37 °C releases up to 32 % which slowly decreases to 29 %. Differences in drug release between the samples post extrusion and after 6 months are not significant ($P>0.05$). It is observed a similar pattern as described in the case of Figure 3.28, where the sample after 6 months storage at 37 °C shows a slight increase in drug release ($P>0.05$). In the case of F4 (Figure 3.30), a low drug release of 13 % post extrusion is achieved. When the extruded material is analysed after 6 months storage, similar drug release profiles of 15 % and 18 % are obtained. All dissolution profiles presented are plotted at pH 2.1 and do not follow the behaviour observed in Figure 3.26, where drug precipitation occurred at pH 3.0. Overall, solid dispersions F1 to F4 show an improvement in ABZ dissolution rates compared to ABZ alone at pH 2.1 and therefore potential enhancement of ABZ oral bioavailability. The use of hydrophilic PEG 6000 can improve drug solubilisation as well as its wettability and dispersibility properties, leading to improved ABZ dissolution properties (Özkan, 2000; Trapani, 1999; Verheyen, 2002). However, the dissolution behaviour of ABZ – PEG 6000 formulations are clearly dependant on the pH, as ABZ can precipitate at pH 3.0. Therefore the use of these formulations can be limited to the pH of the media.

3.4.1.7. Particle size analysis

Particle size of ground extruded materials used for dissolution studies were determined by laser diffraction. The mean values (d_{10}, d_{50}, d_{90}) obtained for PM and extruded materials are depicted in Tables 3.7 and 3.8. Mean particle size (d_{50}) values of all ground extruded materials are above 250 µm, reaching also in case of physical mixtures, values above 1000 µm. The method applied to grind the extruded materials was the same as the one used in chapter 2. However, the plasticity of PEG 6000 may have influenced grinding performance leading to bigger particle size.

Table 3.7. Particle size values (d_{10}, d_{50}, d_{90}) of ground materials post extrusion

Sample name	**d_{10} (µm)**	**d_{50} (µm)**	**d_{90} (µm)**
PM 1/99 % (w/w)	400	830	1480
PM 5/95 % (w/w)	620	1100	2090
PM 10/90 % (w/w)	345	1080	2210
PM 20/80 % (w/w)	11.2	919	2150
F1	NA[1]	NA[1]	NA[1]
F2a	144	525	1700
F2b	259	596	1120
F2c	159	476	1150
F3	115	379	857
F4	99.4	284	542

NA[1]: Not available

Table 3.8. Particle size values (d_{10}, d_{50}, d_{90}) of ground materials after 6 months storage

Sample name	**d_{10} (µm)**	**d_{50} (µm)**	**d_{90} (µm)**
F1 at 25 °C	134	569	1420
F1 at 37 °C	126	562	1430
F2 at 25 °C	107	489	1310
F2 at 37 °C	118	454	1350
F3 at 25 °C	159	550	1130
F3 at 37 °C	101	445	1080
F4 at 25 °C	85.2	350	815
F4 at 37 °C	128	472	1100

3.4.1.8. Determination of drug content by UV spectrophotometry

Quantification of drug content in all extruded materials was performed by UV spectrophotometry analysis. The calibration curves representing the calibration standards of ABZ at 0.10, 0.20, 0.50 and 0.75 mg/mL can be observed in Figure 3.32. This calibration curve is representative of the two calibrations performed due to F1, F2a and F4 being repeated, in all cases R^2 >0.99.

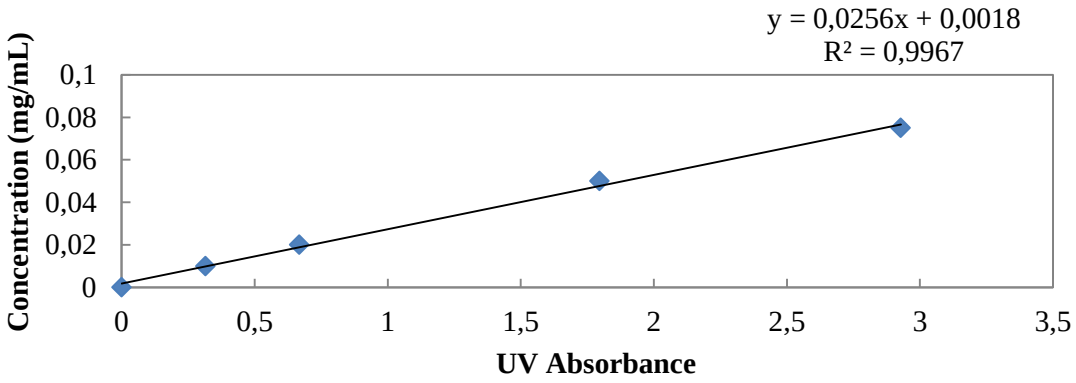

Figure 3.32. Calibration curve of ABZ calibration standards measured by UV spectrophotometry

Drug content values obtained for all extruded materials are shown in Table 3.9. As it can be observed, ABZ content of the extruded materials is between 87 – 90 % (w/w) of the total ABZ content (%) in each extruded material.

Table 3.9. ABZ drug content (%) of extruded materials measured by UV spectrophotometry. Absorbance values are the average of 3 measurements and standard deviations are included.

Sample name	Absorbance	Concentration (mg/mL)	% drug content*
F1	0.7222 ± 0.0015	0.0174	87.41
F2a	0.7264 ± 0.0008	0.0175	87.90
F2b	0.6087 ± 0.0042	0.0173	86.91
F2c	0.6100 ± 0.0035	0.0174	87.08
F3	0.6397 ± 0.0328	0.0181	90.88
F4	0.7297 ± 0.0010	0.0176	88.28

*The drug content (%) reported represents total ABZ content respect to the theoretical content of ABZ within each extruded material (e.g. 1 %, 5 %, 10 % and 20 %).

3.5. Conclusions

Amorphous solid dispersions of the poorly soluble drug, ABZ, in a matrix of PEG 6000 were produced by HME technique. The processing conditions required for this polymer such as a low barrel temperature lead to ease of processability by HME, in comparison to PVP K12 materials. In addition, the aspect and internal porosity properties were enhanced by using a plasticiser polymer such as PEG 6000. Dissolution profiles obtained for extruded materials with drug contents from 1 % to 20 % (w/w) lead to higher drug release than ABZ alone, which appears to be maintained for a period of 30 minutes before drug precipitation occurs. It was also evidenced a carrier-controlled mechanism that seems to govern the dissolution process. The production of amorphous solid dispersions of ABZ and PEG 6000 together with a possible increase of ABZ wettability properties can greatly affect the dissolution properties observed at pH 2.1. Extruded materials were stored for 6 months under temperature controlled chambers at 25 and 37 $^{\circ}$C. XRPD diffractograms of these samples show crystalline peaks that correspond to both PEG 6000 and ABZ. The higher the drug content within the extruded materials, the higher the intensity of the crystalline peaks observed after 6 months storage. These results are supported by SEM pictures showing crystalline ABZ particles on the surface of the extruded materials. On the other hand, DSC analysis indicate that successful amorphous solid dispersions were produced although it does not evidence any endothermic peak characteristic of crystalline ABZ after 6 months storage. This

could be due to crystalline material which is below the limit of detection. In summary, PEG 6000 can be used as a successful carrier for HME processing to enhance dissolution and also porosity properties of ABZ, although its use may be limited to the drug release required.

4. Application of computed tomography as homogeneity indicator of extruded materials

4.1. Introduction

Several characterisation techniques can be used off-line to measure different physicochemical properties of extruded materials. One of the main properties that a pharmaceutical product may comply with is an adequate drug content uniformity, where drug is equally distributed through the full matrix or final dosage form (Karande et al., 2010; Pharmacopeia, 2011; Zaid et al., 2013). A novel characterisation technique for medical and pharmaceutical applications is computed tomography (Micro-CT). This technique enables the visualisation and determination at a micro-molecular level of the overall density and internal micro-structure of the dosage form. The first report of distribution properties within a solid dosage form by Micro-CT technique was performed by Ozeki et al., (Ozeki, 2003) and followed by further studies looking to assess the drug content uniformity within HME systems by incorporating a fluorescent dye (Park et al., 2013). The characterisation of materials internal structure by computed tomography has gained popularity as a useful tool to examine solid dosage forms (Russe et al., 2012; Zeitler and Gladden, 2009). Some of the recent applications include tablets or capsules (Martins de Oliveira Jr., 2010), granule intermediates (Crean et al., 2010; Kašpar et al., 2013), coated materials for pharmaceutical application (Perfetti et al., 2010; Sondej et al., 2015; Tokudome et al., 2009) and more recently, multi-phase materials (Alvarez-Murga et al., 2012) as well as co-extruded materials (Vynckier et al., 2015). The use of Micro-CT offers some advantages such as being a non-destructive and non-contact method as well as small size sample requirements (e.g. maximum 5 cm length filament). On the other hand, it is limited by the radio-opacity properties of the

material as more radio-opaque materials exhibit high X-ray attenuation coefficient and therefore are preferred for better visibility (Sharma et al., 2016).

4.2. Aims and objectives

The aim of this chapter was to determine the differences in density and the internal structure properties of the different polymeric matrices produced by HME technique (see chapters 2 and 3). This chapter is also focused on the understanding of the influence of processing temperature on the density properties. Different ABZ contents (% w/w) within the extruded materials are studied and its influence in relation to the internal porosity is evaluated. The differences in density between the drug and the polymer can highlight possible drug distribution throughout the extruded material.

4.3. Materials and methods

4.3.1. Materials

The details of the drug and polymeric materials used are specified in chapters 2 and 3 under the materials and methods section.

4.3.2. Scanning procedure by computed tomography

Cross-sections of the extruded materials were analysed by Micro-CT x-rays scanning to assess the internal void content (porosity) at a microstructural level, as well as sample uniformity by the characterisation of the average molecular densities. A Bruker® high resolution X-ray Micro-CT SkyScan 1172 (Kontich, Belgium) with an X-ray source voltage of 80 kV was used. The system was equipped with an 11 Mp CCD detector. Sample preparation required the introduction of a piece of extruded material inside a drinking straw to avoid any interference due to sample movement during measurement. All extruded materials were analysed using a rotation step of

0.2°. Exposure time for PVP K12 extruded materials were 380 ms (F1 to F3 formulations) and 190 ms (F4 to F7 formulations) due to equipment set-up. In the case of PEG 6000 materials, exposure time was also 190 ms. The scanned images were reconstructed using the NRecon software (version 1.6.9.18, Bruker® Micro-CT, Kontich, Belgium). A calibration was performed by scanning a sample of deionised water inside a drinking straw and calculating the Hounsfield Units (HU) for that sample as reference, which was used as the HU calibration number to convert greyscale values (0 to 255) to HU values (Table 4.1). The minimum and maximum values of mean density (HU) corresponding to air and water were included in the calibration equation provided by CTAn software (section 4.4.1.1). The calibration equation was applied to all extruded materials to obtain the respective mean density values. To visualise and analyse the data, CTAn software (version 1.14.4.1, Bruker® Micro-CT, Kontich, Belgium) was used. A set of calculations within CTAn including image thresholding were applied to determine a region of interest (ROI) within the cross section of the extruded material and avoid any interference caused by the straw. Porosity calculations were performed considering the volume of internal closed pores which are completely surrounded by solid material.

4.4. Results and discussion

4.4.1. Evaluation of homogeneity by density characterisation

4.4.1.1. Extruded materials of ABZ and PVP K12

Extruded materials comprising ABZ – PVP K12 at ratios of 1/99, 5/95, 10/90 and 20/80 (% w/w) produced by HME technique were analysed by Micro-CT (Figures 4.1 to 4.8). It is important to consider that different processing temperatures were used for suitable extrusion of materials with varied drug contents (see materials and

methods section in chapter 2 for reference). The cross-section of the extruded materials inside the drinking straw is shown in each image. Drug-polymer homogeneity within the extruded materials can be visualised by density characterisation and assessed based on the differences on density, where the drug is the compound with higher density and the polymer has a lower density. The coloured bar located at the left side of each image represents the corresponding colour to the degree of density, from low density (red and orange colours) to high density (blue colour). Water was also scanned using the same device to act as a "phantom" for the correlation of greyscale values to density values expressed as Hounsfield Units (HU). The mean density value obtained from the scan of water sample is called the *HU calibration number*. This value, 657 HU was added in CTAn software to perform density calculations for each extruded material (Table 4.1). However, the light contrast and intensity adjustments carried out for reconstruction of the scans into visual images can also influence density results (Bruker, 2014).

Table 4.1. Calibration set used by CTAn software

Calibration unit	**Minimum value**	**Maximum value**
Index	0	255
HU	-1000	657

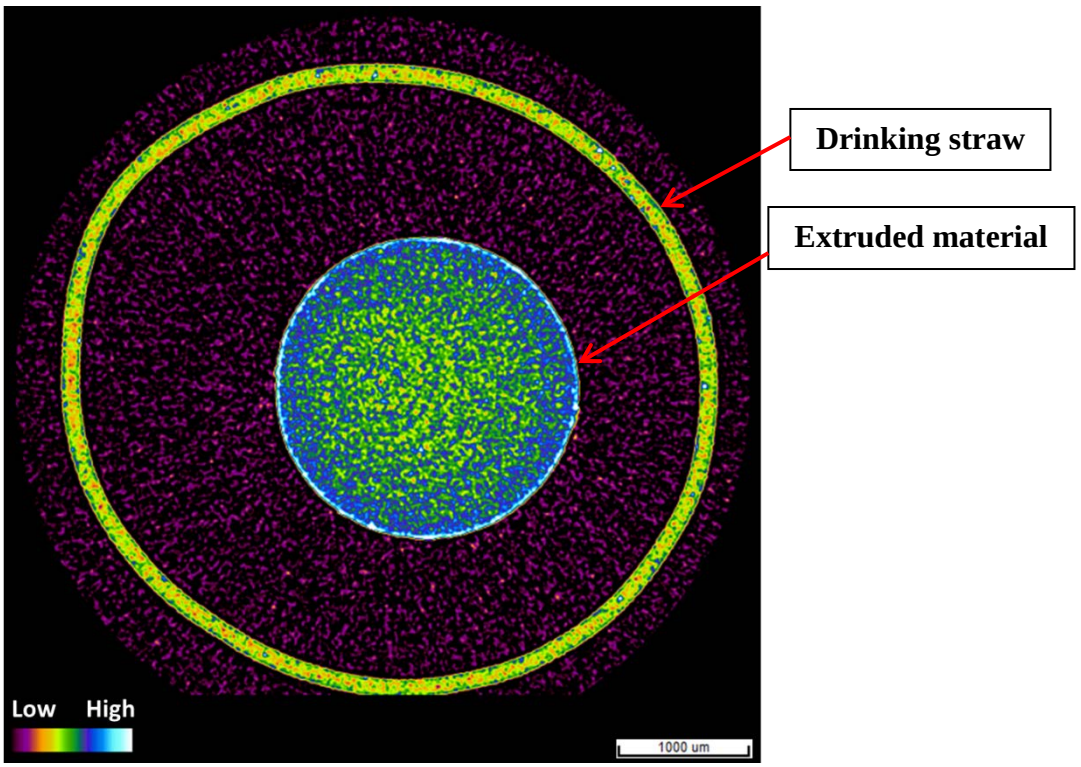

Figure 4.1. Micro-CT scanned image of extruded material of PVP K12 alone, processing temperature of 140 °C.

Figure 4.1 shows two different colours, blue and green that refer to zones with high and low density properties. Interestingly, this figure corresponds to the extruded material that contains PVP K12 alone, therefore it would be expected to have just one colour corresponding to PVP K12 density. This change in density between the surface and the inner part of the extruded material suggests possible sudden changes from high to low temperatures that occurred while cooling of the surface can affect density properties. This material was extruded by HME at 140 °C and cooling of the extruded material took place at room temperature (22 °C) without the aid of cooling air. A big temperature change within few minutes could lead to the formation of a film or "skin" at the outer layer or surface of the extruded material. This phenomenon could be a result of cooling happening at a faster rate at the surface in contrast to the inner core which cooled down at a slower rate. Differences in

density could also be explained by a free volume increase of the extruded material at the die section due to polymer swelling. Changes in free volume and density are expected to be higher for crystalline than for amorphous polymers and is also dependent on the cooling temperature and rate applied after extrusion. This is the first report of differences in density throughout extruded materials due to processing conditions such as temperature, that show the influence of a rapid decrease of temperature on the materials properties. Differences in density of pharmaceutical tablets due to high humidity conditions or friction mechanisms during tabletting were previously reported (Otsuka et al., 2009; Sinka et al., 2004). Therefore, Micro-CT technique can be used as a complimentary tool to assess the impact of different processing and storage conditions that can affect product quality and performance (Hancock, 2005).

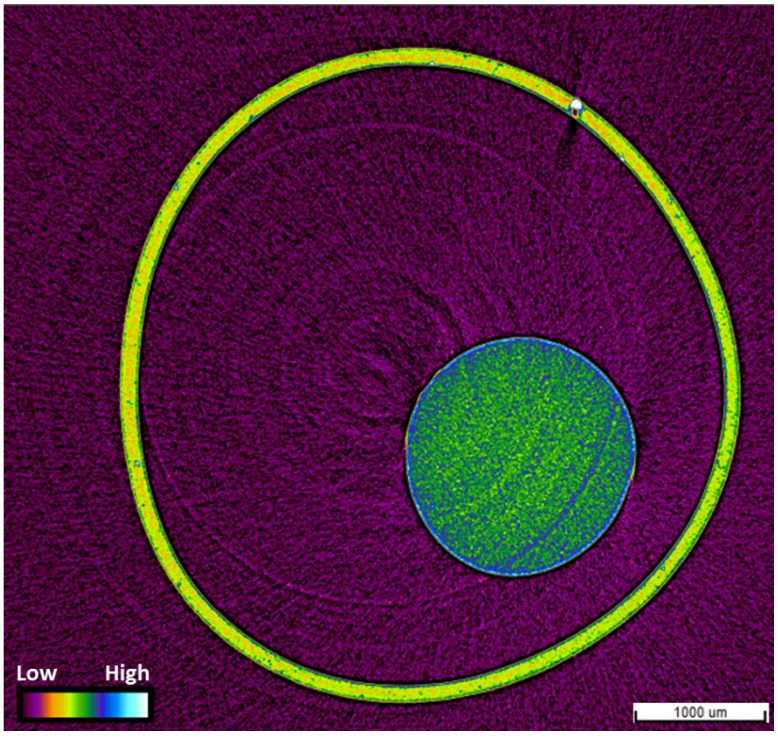

Figure 4.2. Micro-CT scanned image of extruded material of formulation F1 (ABZ – PVP K12 at 1/99 % w/w), processing temperature of 145 °C.

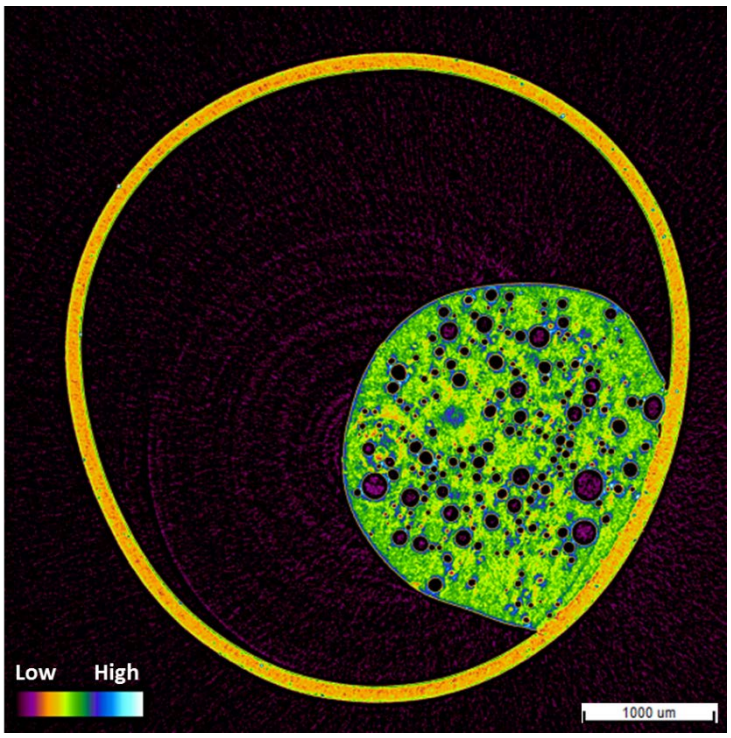

Figure 4.3. Micro-CT scanned image of extruded material of formulation F2 (ABZ – PVP K12 at 5/95 % w/w), processing temperature of 145 °C.

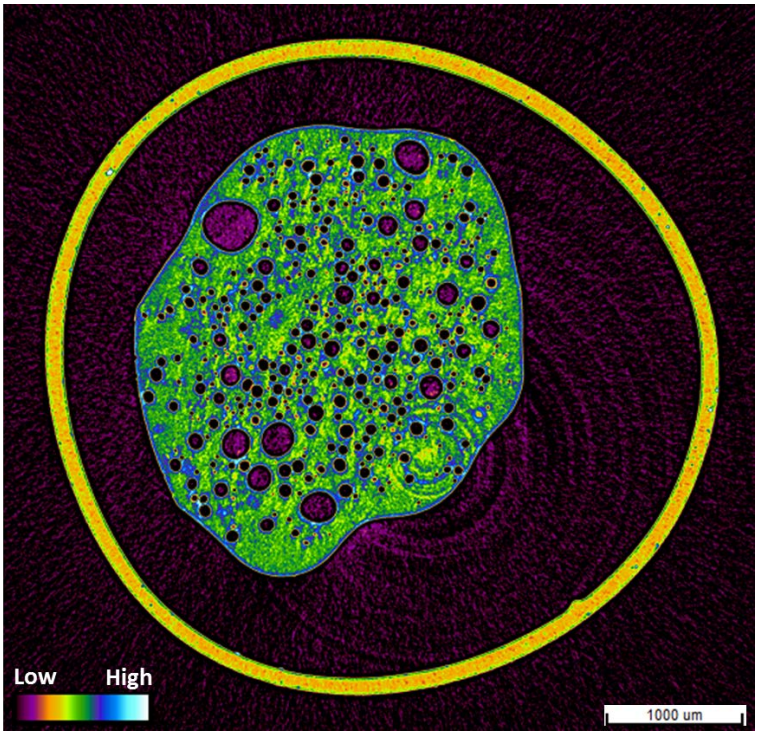

Figure 4.4. Micro-CT scanned image of extruded material of formulation F3 (ABZ – PVP K12 at 10/90 % w/w), processing temperature of 145 °C.

The Micro-CT scans of formulations F1 to F3 (Figures 4.2 to 4.4) show that extruded materials present an irregular shape which is not completely circular and also high porosity properties as well as possibly the presence of air bubbles. In the case of Figure 4.2 the appearance of ring artefacts from the void (purple colour) between the straw and the extruded material that continue within the extruded material, indicate the limitations of this technique. Overall, the cross-section visualised by density characterisation shows an increase in porosity as well as different density levels from low (purple) to medium (orange-yellow) and high (green-blue) density. These values correspond to the densities of air, polymeric material such as PVP K12 and the drug molecule ABZ. The porosity degree achieved in these initial formulations could be explained by the processing temperature used (145 $^{\circ}$C) but also by the presence of entrapped air. To assess the influence of temperature, all formulations were extruded again at a lower temperature of 135 $^{\circ}$C. This decrease in temperature greatly decreased the porosity degree and improved the shape of the extruded materials.

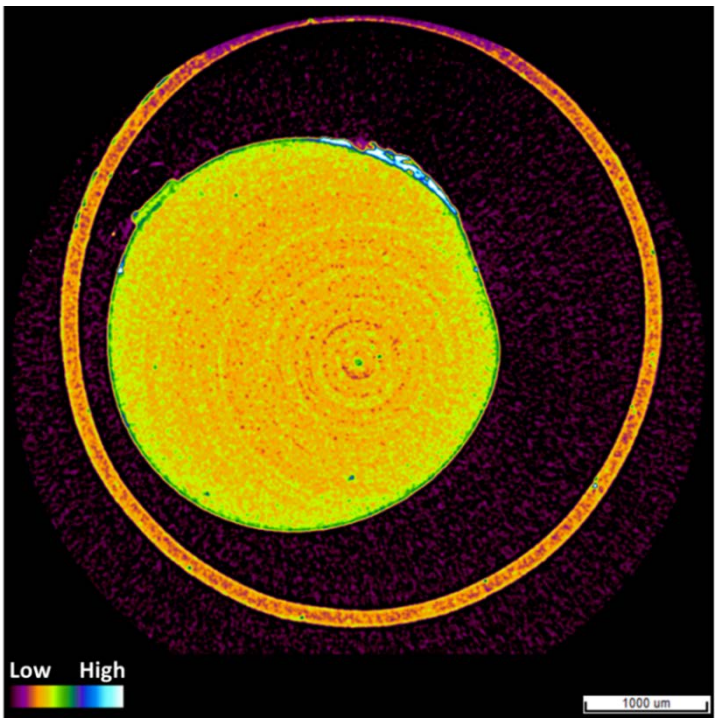

Figure 4.5. Micro-CT scanned image of extruded material of formulation F4 (ABZ – PVP K12 at 1/99 % w/w), processing temperature of 140 °C.

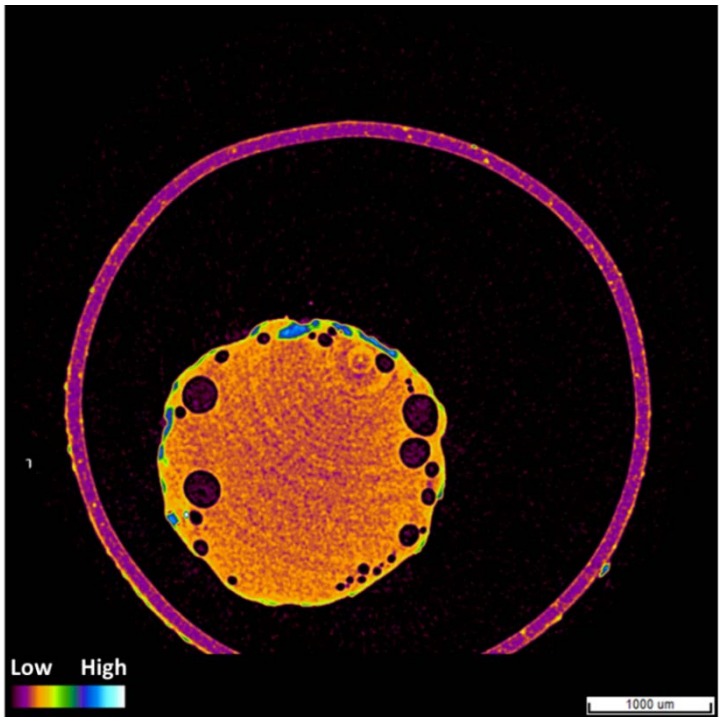

Figure 4.6. Micro-CT scanned image of extruded material of formulation F5 (ABZ – PVP K12 at 5/95 % w/w), processing temperature of 135 °C.

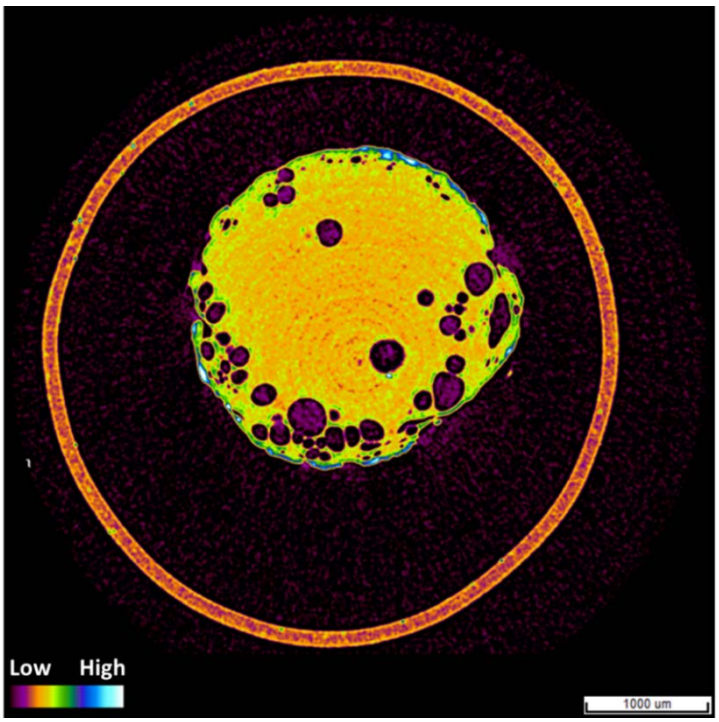

Figure 4.7. Micro-CT scanned image of extruded material of formulation F6 (ABZ – PVP K12 at 10/90 % w/w), processing temperature of 135 °C.

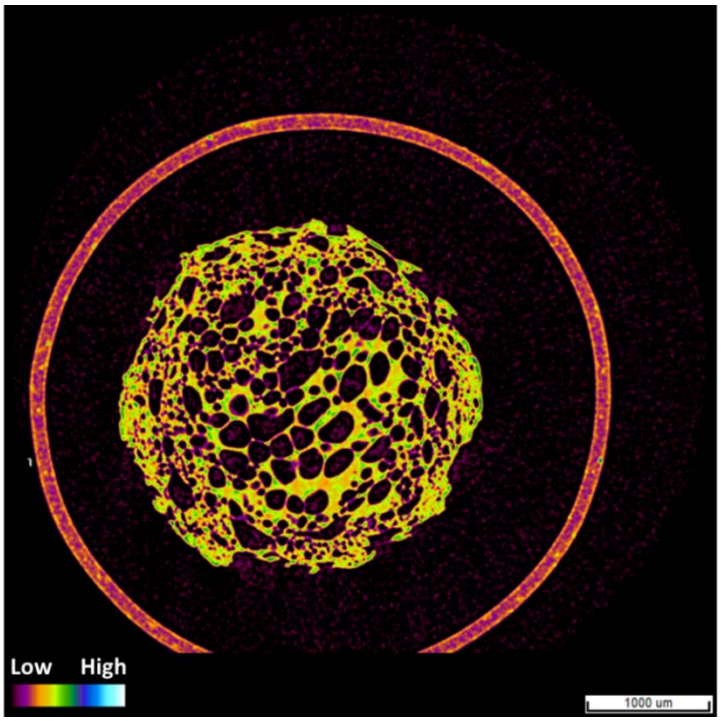

Figure 4.8. Micro-CT scanned image of extruded material of formulation F7 (ABZ – PVP K12 at 20/80 % w/w), processing temperature of 135 °C.

The images depicted in Figures 4.5 to 4.8 (extruded materials produced at 135 °C) show that extruded materials manufactured at lower temperature present a better defined circular shape, in comparison to formulations F1 to F3. In the case of Figure 4.6 (formulation F5), the differences in density observed between the voids and the matrix are not as apparent as in previous images, due to a characteristic purple colour. This difference in density and also the different straw densities observed can be due to image reconstruction being performed differently, by applying different contrast adjustments between samples. Figures 4.5, 4.7 and 4.8 show a main yellow-orange colour of lower density and a green colour of higher density. Solid state characterisation by XRPD and DSC techniques as described in chapter 2 suggest the formation of molecular solid dispersions of ABZ in PVP K12 and absence of crystalline material in the case of PVP K12 extrudates. According to Alhijjaj et al., (Alhijjaj et al., 2016) molecular dispersions of an API in a polymer that have not undergone phase separation, show an even distribution with higher density due to the presence of electronegative groups in the drug molecule such as oxygen and sulphur in the case of ABZ. Micro-CT can then be used to show the materials distribution within extruded matrices and also a porosity degree that seems to increase with drug content (Martinez-Marcos et al., 2016). In addition, Figure 4.8 does show high density areas (green colour) distributed more in the core than just at the sides as in previous figures, together with big and small pores present. This degree of porosity may mask the results and therefore can make difficult to perform an accurate interpretation. Further evaluation of porosity is detailed in section 4.4.2. The mean densities (HU) and standard deviations measured for PVP K12 extruded materials are depicted in Table 4.2. It can be observed that the standard deviations

are bigger than the absolute values of mean density due to large data scattering between positive and negative values.

Table 4.2. Mean density values of ABZ – PVP K12 extruded materials

HME formulation	Mean density (HU)	Standard deviation
PVP K12 alone	-59.56	249.93
F1	-87.19	100.12
F2	-213.23	146.26
F3	-134.47	156.56
F4	-395.91	140.29
F5	-275.20	179.35
F6	-379.87	154.33
F7	-330.18	143.70

4.4.1.2. Extruded materials of ABZ and PEG 6000

The scanned images of the extruded materials comprising ABZ and PEG 6000 were collected and reconstructed as mentioned in the materials and methods section. Selected cross-section images are shown in Figures 4.9 to 4.13.

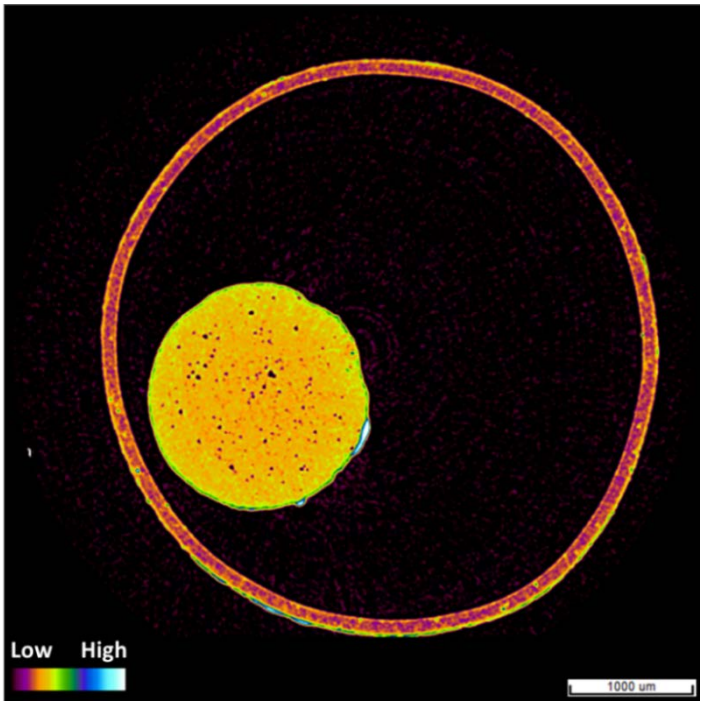

Figure 4.9. Micro-CT scanned image of extruded material of PEG 6000 alone, processing temperature of 58 °C.

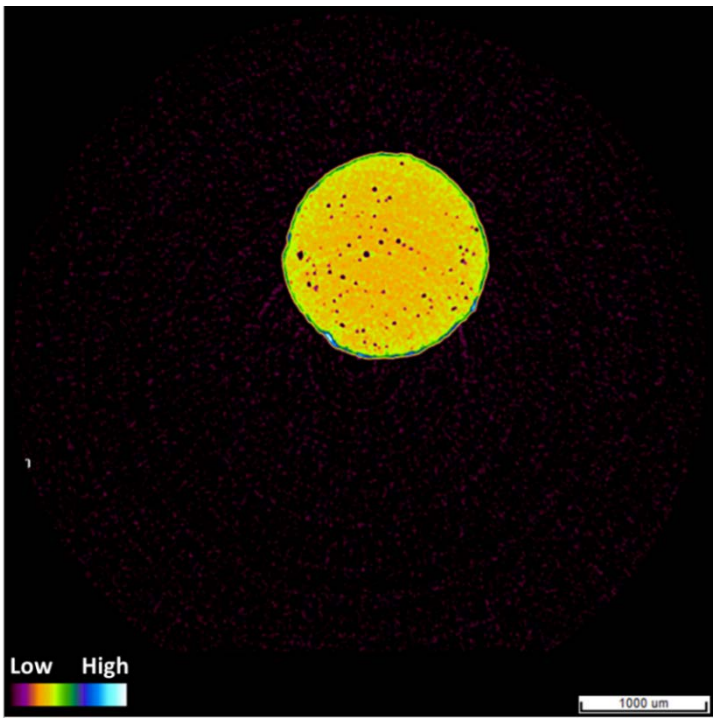

Figure 4.10. Micro-CT scanned image of extruded material of formulation F1 (ABZ – PEG 6000 at 1/99 % w/w), processing temperature of 58 °C.

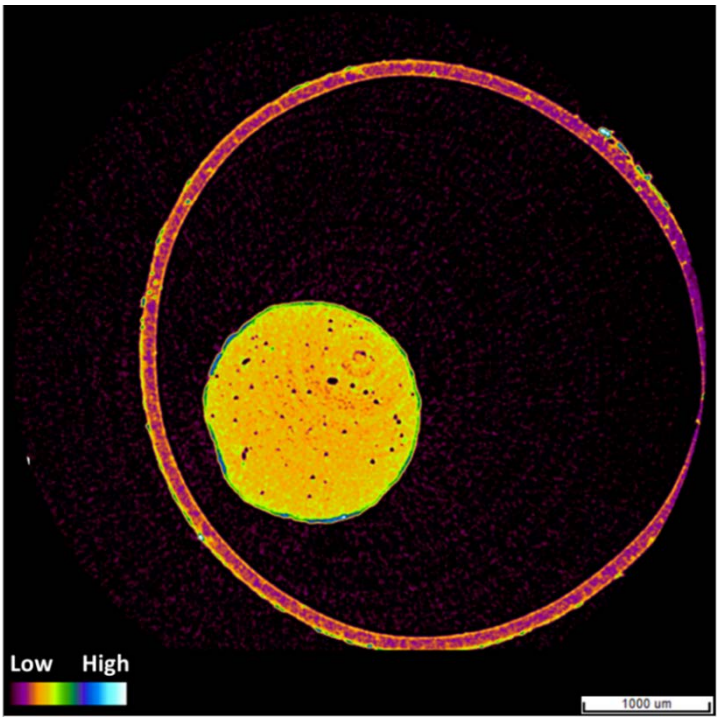

Figure 4.11. Micro-CT scanned image of extruded material of formulation F2 (ABZ – PEG 6000 at 5/95 % w/w), processing temperature of 58 °C.

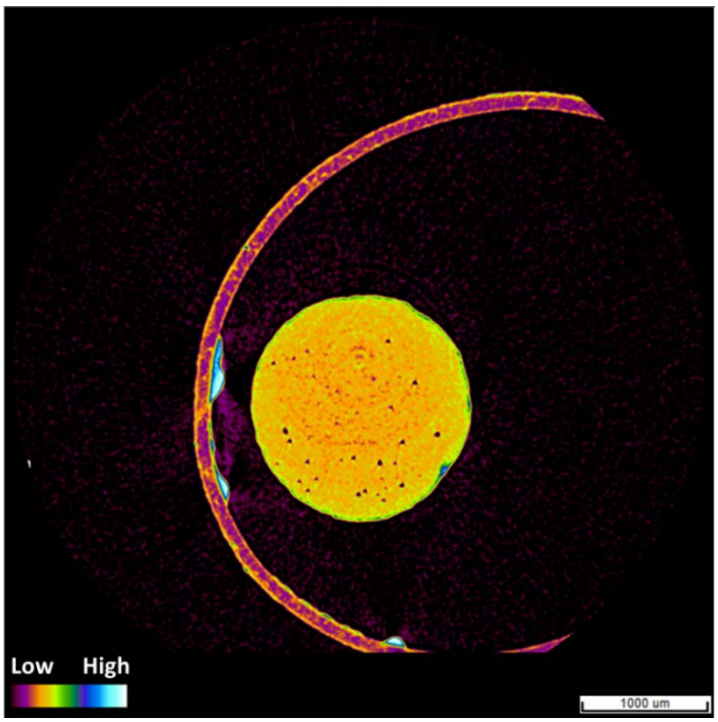

Figure 4.12. Micro-CT scanned image of extruded material of formulation F3 (ABZ – PEG 6000 at 10/90 % w/w), processing temperature of 58 °C.

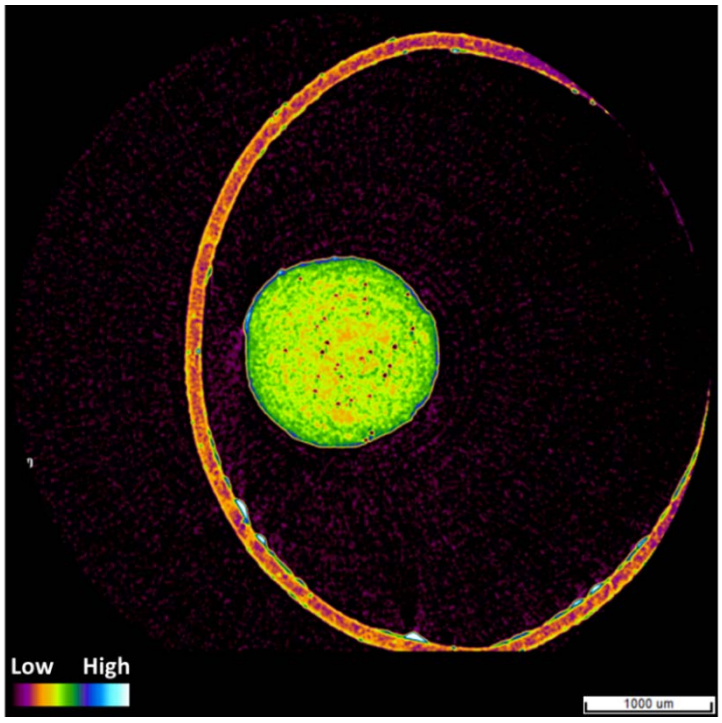

Figure 4.13. Micro-CT scanned image of extruded material of formulation F4 (ABZ – PEG 6000 at 20/80 % w/w), processing temperature of 58 °C.

The scanned images above represent the images captured at the middle part of the respective extruded materials. Material's density between drug and polymer differ, where the drug in this case ABZ is considered to be of higher density than the polymer PEG 6000 (Alhijjaj et al., 2016; Traini, 2008). The colour density scale shown in the figures enables the visual characterization of these results by the differences in density. Therefore, based on this scale, the polymer is shown in orange-yellow colour and the drug in green colour. It can be observed that the matrix has a medium density in orange-yellow colour and some high density in green colour is present at the outer surface and slightly in inner areas of the matrix (Figures 4.11 and 4.12). In comparison to the Micro-CT scans of PVP K12 matrices described above, PEG 6000 matrices were extruded at a low temperature (58 $^{\circ}$C) and therefore cooling after extrusion should have not influenced density differences throughout the material. These results agree with reports from Busignies et al., (Busignies et al., 2006) where cylindrical tablets presented higher densities in the outer surface or peripheral areas due to possible friction generated during the manufacturing process. Characterisation of PEG 6000 extruded materials by XRPD and DSC suggest the formation of amorphous solid dispersions of ABZ in a crystalline matrix (see chapter 3 for reference). In these cases, the location and distribution of green and orange-yellow densities suggest the heterogeneity of these matrices. Moreover, there are not significant differences of the mean density (HU) between materials comprising 1, 5 and 10 % (w/w) ABZ content as depicted in Table 4.3. Further studies would be required to accurately determine drug distribution within the matrices.

Figure 4.13 shows an increase in high density with mainly green colour present in the extruded material (20 % (w/w) ABZ content). Further focus is shown in Figure 4.14. Analysis was performed by capturing images at 3 points of the extruded material (lower, middle and upper sections). It appears to be a more homogeneous distribution throughout the extruded material in comparison to the extruded materials with lower drug content. Visual characterisation suggests there is a better distribution possibly of ABZ in PEG 6000 located at the upper section of the extruded material compared to the middle and lower sections.

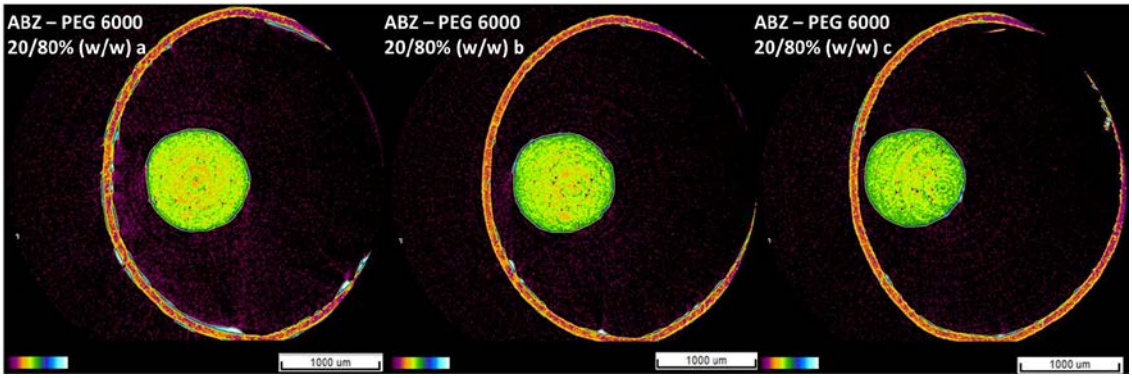

Figure 4.14. Distribution of ABZ through cross-sections of extruded material ABZ – PEG 6000 20/80 % (w/w) at lower section (a), middle section (b) and upper section (c)

Table 4.3. Mean density values of ABZ – PEG 6000 extruded materials

HME formulation	Mean density (HU)	Standard deviation
PEG 6000 alone	-364.99	213.94
F1	-364.93	190.24
F2	-396.40	155.90
F3	-405.94	132.22
F4	-315.41	124.62

4.4.2. Characterisation of internal porosity

4.4.2.1. Extruded materials of ABZ and PVP K12

Porosity of all extruded materials was measured using the CTan software as described in the materials and method section of this chapter. Figures 4.1 to 4.7 show an increase in porosity of post extrusion samples as the drug content increases. These differences in porosity could be explained by entrapped air and bubble formation. Moreover, 3D analysis and differences in the morphometric parameters obtained for formulations F1 to F7 comprising PVP K12 can be observed in Table 4.4 below.

Table 4.4. Morphometric parameters of ABZ - PVP K12 extruded materials

HME formulation	**Object volume (mm^3)**	**Volume closed pores (mm^3)**	**Closed porosity (%)**	**Total porosity (%)**
PVP K12 alone	46.31	5.98	0.13	22.91
F1	19.10	1.30	0.00	49.98
F2	19.77	5.57	21.98	52.40
F3	40.60	11.05	21.39	58.35
F4	38.22	3.50	0.09	63.86
F5	31.32	2.60	7.66	51.53
F6	40.45	3.13	7.20	50.17
F7	39.65	7.16	1.77	57.37

The total porosity values indicate that the overall porosity of the extruded material increases as the drug content also increases, especially in the case of formulations F1 to F3. It appears that drug content does not directly affect total porosity in the case of the extruded materials produced at 135 $^{\circ}$C. For example, formulations F5 and F6 present porosity values of approximately 50 % and a difference of 5 % (w/w) drug content. This could be due to the fact that these formulations were extruded at a lower temperature than F1 to F3. Total porosity (%) measured using 3D analysis

considers both, closed and open pores. The closed pores are located in the inner side and therefore surrounded by drug-polymer matrix and the open pores connect to the outer surface of the extruded material. They are part of a total volume of interest (VOI). Moreover, the application of Micro-CT allows an in-depth analysis of the materials providing pores size distribution as well as interconnected porosity (Farber et al., 2003). These results indicate that despite the known mixing ability of twin-screw processing equipment (Crowley et al., 2007) standard techniques for assessing homogeneity may not be adequate.

4.4.2.2. Extruded materials of ABZ and PEG 6000

Porosity calculations obtained for extruded materials comprising ABZ and PEG 6000 are depicted in Table 4.5.

Table 4.5. Morphometric parameters of ABZ - PEG 6000 extruded materials

HME formulation	**Object volume (mm^3)**	**Volume closed pores (mm^3)**	**Closed porosity (%)**	**Total porosity (%)**
PEG 6000 alone	29.09	1.21	0.41	25.58
F1	15.93	1.44	0.89	51.85
F2	19.27	1.28	0.66	43.98
F3	22.86	1.25	0.54	43.17
F4	23.18	6.26	0.26	33.62

In the case of ABZ – PEG 6000 extruded materials, the 3D porosity analysis suggests that the porosity degree is also influenced by an increase in drug content, compared to the extruded material of PEG 6000 alone. However, the total porosity (%) of most of the extruded materials containing PEG 6000 as carrier are overall less porous than the extruded materials comprising PVP K12. The possible increase in free volume of PVP K12 extruded materials could have also influenced the porosity degree and formation of air bubbles.

4.5. Conclusions

Density differences within the extruded materials comprising ABZ were evaluated by Micro-CT analysis as well as internal porosity properties. Formulations where PVP K12 was used as carrier showed density differences that possibly suggest a poor drug distribution at the inner part of the extruded materials. It was also observed that a decrease in temperature from 145 to 25 °C during extrusion processing resulted in clear density differences exhibited by polymer alone. This is the first reported case in extruded materials regarding density variations due to high temperature differences. Moreover, these materials were found to be very porous. Porosity appears to increase as drug content also increases. The presence of high porosity in the extruded materials can determine later physicochemical properties of the final dosage form such as possible increase in dissolution rate and water adsorption properties. When PEG 6000 was used as matrix carrier, extruded materials showed similar properties regarding density location and potential drug distribution properties. However, the extruded material with highest drug content (20 % w/w) presents high density properties which appear to be more homogeneous in the upper section. These formulations did show an important decrease of total porosity as well as internal pores size in comparison to PVP K12 extruded materials.

5. Understanding and optimisation of initial liquid distribution in twin-screw granulation

5.1. Introduction

Twin-screw wet granulation is one of the current techniques for particle enlargement purposes to produce agglomerates also called granules. A twin-screw granulator (TSG) applies high-shear, a high-deformability property governs granule growth where granules have been formed by deformation of the powder mass (Parikh, 2005). However, there are many factors involved in twin-screw granulation process. Processing parameters such as powder feed rate, liquid feed rate, screw speed and screw configuration have been shown to affect granule attributes and growth behaviour such as particle size, morphology and strength properties (Dhenge et al., 2012; El Hagrasy et al., 2013b; Vercruysse et al., 2015a; Vercruysse et al., 2012). This chapter investigates the influence of constant feed rate to screw speed ratios, which visually confirmed to yield similar degrees of barrel fill, on granule liquid distribution and particle size properties. A dye or tracer in solution is used in all TSG experiments for characterisation purposes (El Hagrasy and Litster, 2013b; Sayin et al., 2015a). This part of the thesis was performed as an industrial placement at GlaxoSmithKline (GSK, Stevenage).

5.2. Aims and objectives

The aims and objectives of this project can be divided into two main focus or streams.

The first study comprised the investigation and understanding on the effect of feed rate to screw speed ratio on liquid distribution using a 16 mm twin-screw granulator (TSG) with a screw configuration based only on conveying elements (CE). These elements are normally used as transport or transfer elements that convey the blend material through the barrel. However, these elements can also provide certain

mixing degree at the intermeshing region of the twin-screws when these rotate. Main particle attributes such as granules particle size was also evaluated using particle size analysis.

A second study focused to de-couple the effect of screw configuration previously observed (GSK data) where a high population of fines was formed during granulation experiments. The screw configuration in these experiments was comprised of different mixing and conveying elements such as kneading elements (KE), distributive feed screws (DFS) and distributive mixing elements (DME). These results are valuable to further understand the impact of screw elements and screw configuration in the area of twin-screw granulation.

5.3. Materials and methods

5.3.1. Materials

A placebo formulation (Dhenge et al., 2010) comprised of lactose monohydrate (Pharmatose 200, 73.5 % w/w; DFE Pharma, Goch, Germany), microcrystalline cellulose (Avicel PH101, 20 % w/w; FMC Biopolymer, Philadelphia, United States), hypromellose 2910 (Pharmacoat 603, 5 % w/w; Shin Etsu, Tokyo, Japan) and croscarmellose sodium (Ac-Di-Sol, 1.5 % w/w; FMC Biopolymer, Philadelphia, United States) was used in twin-screw granulation studies. A stock solution of quinoline yellow (tracer) in deionised water at a concentration of 5 mg/mL was used as granulation liquid. Studies were performed at a liquid to solid (L/S) ratio of 17.5 %. Powder and liquid feed rates were calculated based on L/S ratio.

5.3.2. Twin-screw granulation experiments

All solid materials were pre-blended in batches of 700 g using a Turbula® T2F mixer (Glen Mills Inc, New Jersey, United States) at a speed of 39 rpm for 10 minutes.

Density of the blend (bulk) was 0.4860 g/cc (Pharmacopeia, 2012). A Flexwall® 20 gravimetric feeder (Brabender Technologie GmbH, Duisburg, Germany) was used to feed the powder. The granulation liquid, a solution of quinoline yellow (Lot: A0344650) (Acros Organics, Fair Lawn, NJ, United States) in deionised water at a concentration of 5 mg/mL was pumped using a MasterFlex® L/S pump (Cole-Parmer Instrument Co., Illinois, United States). A 16 mm with a 25:1 L/D twin-screw granulator (Eurolab 16, Thermo Fisher Scientific, Karlsruhe, Germany) was used to perform all granulation experiments. The screw elements used in studies 1 and 2 are shown in Figure 5.1 and full screw configurations are depicted in Table 5.1. Processing parameters used corresponding to feed rate to screw speed ratios are shown in Tables 5.2 and 5.3. Feeding ports for liquid and powder feeding were located at zones 2 and 4 of the barrel from outlet, respectively. Initial granulation runs comprised control experiments with no tracer and granulation experiments with tracer. In order to evaluate the influence of drying conditions on granules during sieving analysis, two samples were collected from each run. One sample was directly dried overnight in a vacuum oven at 40 °C (SH – short hold) and the other was kept at room temperature for 24 hours and then placed overnight in a vacuum oven at 40 °C (LH – long hold). Drying conditions were evaluated just for initial runs during study 1 (Figures 5.2 to 5.5) as no substantial difference was observed.

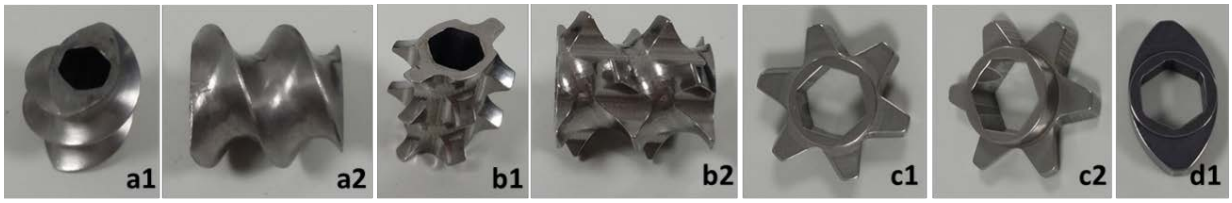

Figure 5.1. 16 mm screw elements; a1-2: top and side view of conveying element (CE), b1-2: top and side view of distributive feed screw (DFS), c1-2: two sides of distributive mixing element (DME) and d1: kneading element (KE0°)

Table 5.1. Screw configuration used in studies 1 and 2

Study	Screw configuration
1	All conveying elements (CE)
2 (a)	19 CE, 9 KE, 1 DME, 3 DFS
2 (b)	18 CE, 9 KE, 1 DME (without DFS)
2 (c)	15 CE, 9 KE (without DFS and DME)

Table 5.2. TSG initial processing parameters of studies 1 and 2

Experiment reference number	Screw speed (rpm)	Powder feed rate (kg/h)	Liquid feed rate (g/min)	Feed rate to screw speed ratio
EE862698 1.5T500	500	1.5	4.375	0.03
EE862698 1.5T60	60	1.5	4.375	0.26

Table 5.3. TSG processing parameters of later experiments of study 1

Experiment reference number	Screw speed (rpm)	Powder feed rate (kg/h)	Liquid feed rate (g/min)	Feed rate to screw speed ratio
EE862698 1.0T333	333	1.0	4.375	0.03
EE862698 6.0T240	240	6.0	4.375	0.26

5.3.3. Water content analysis by Karl-Fischer and Loss on Drying

Granules samples were dried overnight using a vacuum oven at 40 °C to avoid any change in properties of the product. Karl-Fischer (KF) studies of each sample were

performed using a Metrohm® 756 KF coulometer (Metrohm, Herisau, Switzerland) at a temperature of 110 °C. Samples were prepared by weighing 100 mg of granules in a sealed glass vial. To confirm these results, the water content was also measured by Loss on Drying (LOD) technique using a Mettler Toledo® HR-83 moisture analyser (Greifensee, Switzerland) at a temperature of 130 and 105 °C using an aluminium pan and weighing 1.0 g of granules sample.

5.3.4. Sieving analysis

Granules were collected after drying (water content below 2.0 % w/w) and split to obtain representative samples using a Retsch® RT 6.6 riffler (Retsch GmbH, Haan, Germany) in case of study 1 granules and a Laborette® 27 rotary cone sample divider (Fritsch GmbH, Idar-Oberstein, Germany) in the case of study 2 granules. Sieving analysis was then performed using a Fritsch® Analyssete Pro A3 sieve shaker (Fritsch GmbH, Idar-Oberstein, Germany) with sieve fractions of 2.0 mm, 1.4 mm, 1.0 mm, 850 µm, 500 µm, 212 µm, 125 µm, 75 µm and 45 µm mesh size. A sample weight of approximately 30 g of granules was used to perform sieving analysis. Processing conditions comprised an amplitude value of 1.5 and 5 min duration. Following US Pharmacopeia, sieving analysis was performed until steady state was achieved based on the weight difference between sieve fractions. Final mass frequency and the logarithm of particle size are considered for plotting purposes using Equation 5.1 (Allen, 2003).

$$\boldsymbol{fi(lnx)} = \frac{y_i}{\ln\left(\frac{X_i}{X_i{-}1}\right)} \qquad \text{Equation 5.1}$$

where, y_i is the mass fraction in size interval i and X_i corresponds to the upper limit of the size interval.

5.3.5. Liquid distribution studies

Liquid distribution was studied by measuring the absorbance of the tracer quinoline yellow in solution and calculating the dye concentration (mg of dye/g of sample) following a mass balance approach. A PerkinElmer® Lambda 35 UV-spectrophotometer (PerkinElmer Inc., Waltham, United States) was used to characterise the samples from study 1 and a Varian Cary® 50 UV-Vis spectrophotometer (Cary UV-Vis, Agilent, Wilmington, DE) to characterise the samples from study 2, at λ_{max} of 412.5 nm. Previous calibration standards of quinoline yellow were prepared at concentrations of 0.020 mg/mL, 0.010 mg/mL, 0.005 mg/mL and 0.001 mg/mL. Granules samples from each sieve fraction were collected and dissolved using deionised water to obtain a dye solution concentration between 0.018 – 0.005 mg/mL. The required volumes were calculated considering the amount of granules (g) collected per sieve fraction and a theoretical content of 0.875 mg of dye per 1.0 g of powder at L/S ratio of 17.5 % and assuming a dye solution density of 1 g/cc. Once dissolved, samples were centrifuged for 5 minutes in order to remove insoluble excipients prior to UV analysis. A Thermo Fisher Scientific® Heraus multifuge X3R (Thermo Fisher Scientific, Langenselbold, Germany) at a speed of 4000 rpm was used in study 1 and an Avanti® J-E high performance centrifuge (Beckman Coulter Inc., Brea, United States) at a speed of 5400 rpm was used in study 2. In both cases, a relative centrifugal force (RCF) of 3,488 x *g* was applied.

5.4. Results and discussion

5.4.1. Understanding liquid distribution in TSG using conveying elements (Study 1)

The experiments performed in the initial stage of this study comprised a powder feed rate of 1.5 kg/h and screw speeds of 500 and 60 rpm (EE862698 1.5T500 and 1.5T60). Later studies comprised powder feed rates of 1.0 and 6.0 kg/h and screw speeds of 333 and 240 rpm (EE862698 1.0T333 and 6.0T240) which yielded equivalent feed rate to screw speed ratios.

5.4.1.1. Water content analysis by Karl-Fischer and Loss on Drying

Prior to sieving analysis, the water content of dry granules was assessed using Karl-Fischer (KF) and Loss on Drying (LOD) (Table 5.4).

Table 5.4. Water content of EE862698 samples assessed by KF and LOD. Values are the result of one measurement per sample.

Sample name	Water content KF (% w/w)	Water content LOD (% w/w)
EE862698 SH – 1.5T500 (Water)	3.68	2.30
EE862698 SH – 1.5T500 (Dye)	2.34	1.23
EE862698 LH – 1.5T500 (Water)	2.86	NA[1]
EE862698 LH – 1.5T500 (Dye)	2.19	1.17
EE862698 SH – 1.5T60 (Water)	3.06	1.94
EE862698 SH – 1.5T60 (Dye)	2.31	1.05
EE862698 LH – 1.5T60 (Water)	2.85	NA[1]
EE862698 LH – 1.5T60 (Dye)	2.26	0.79
EE862698 SH – 1.0T333 (Dye)	3.67	1.39
EE862698 SH – 6.0T240 (Dye)	3.41	1.13

[1]NA: Not available

5.4.1.2. Sieving analysis

Particle size distribution (PSD) of all granule samples was determined off-line by sieving analysis. PSD of EE862698 samples produced at 1.5 kg/h and speed of 500 and 60 rpm are shown in Figures 5.2 to 5.5. Comparative studies between a control sample where the granulation liquid was water and the sample produced with dye in solution are shown below.

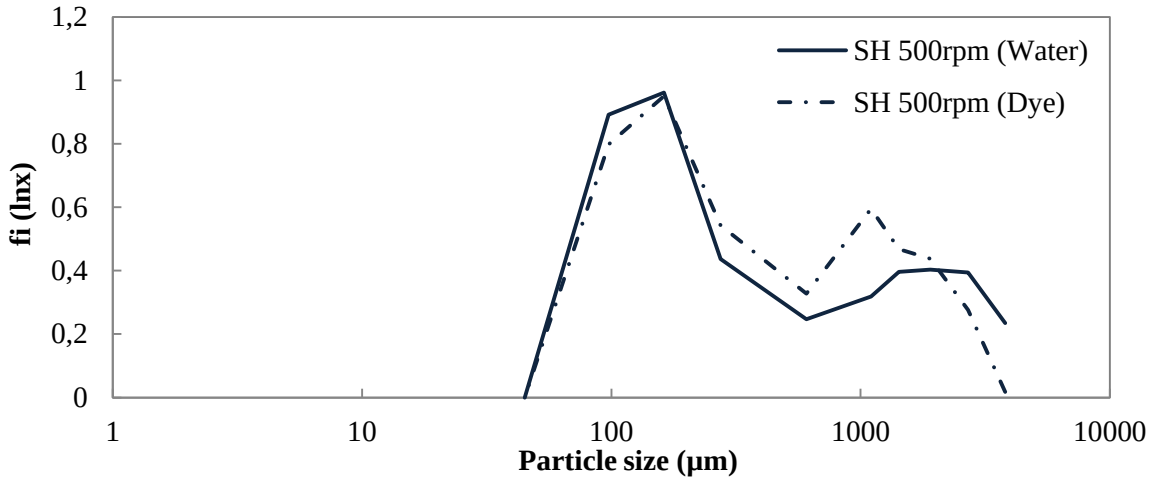

Figure 5.2. Comparative PSD of control and tracer samples of EE862698 SH at 500 rpm

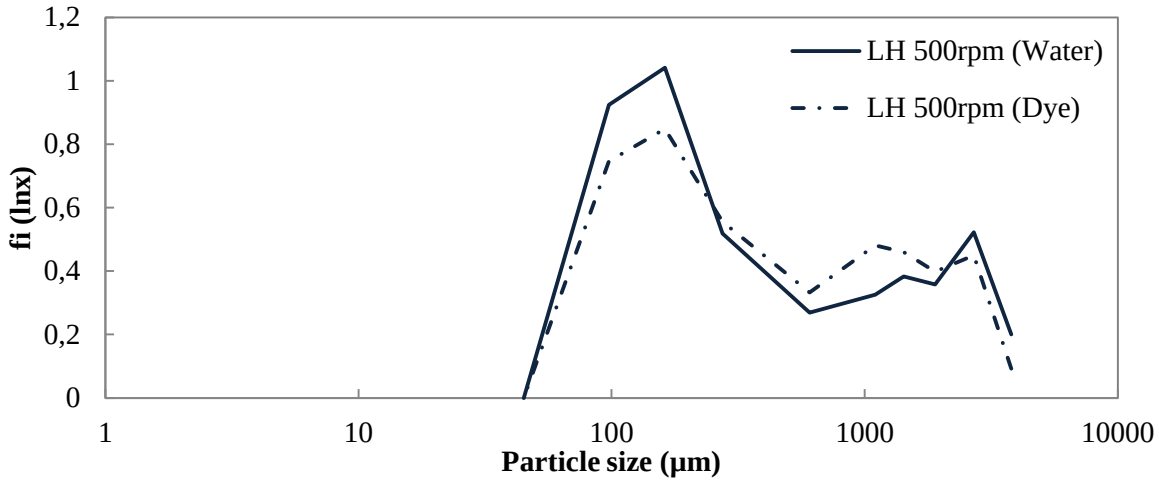

Figure 5.3. Comparative PSD of control and tracer samples of EE862698 LH at 500 rpm

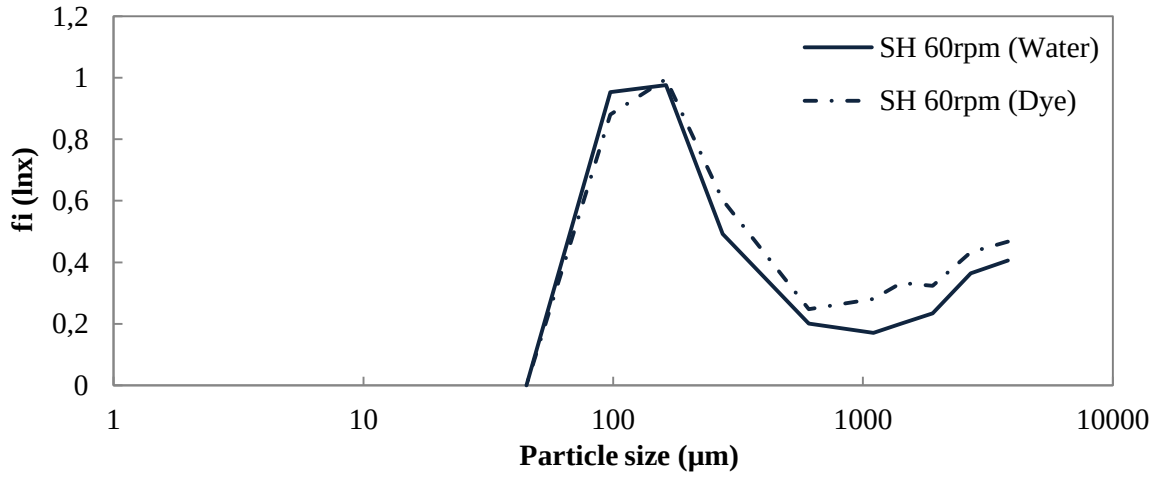

Figure 5.4. Comparative PSD of control and tracer samples of EE862698 SH at 60 rpm

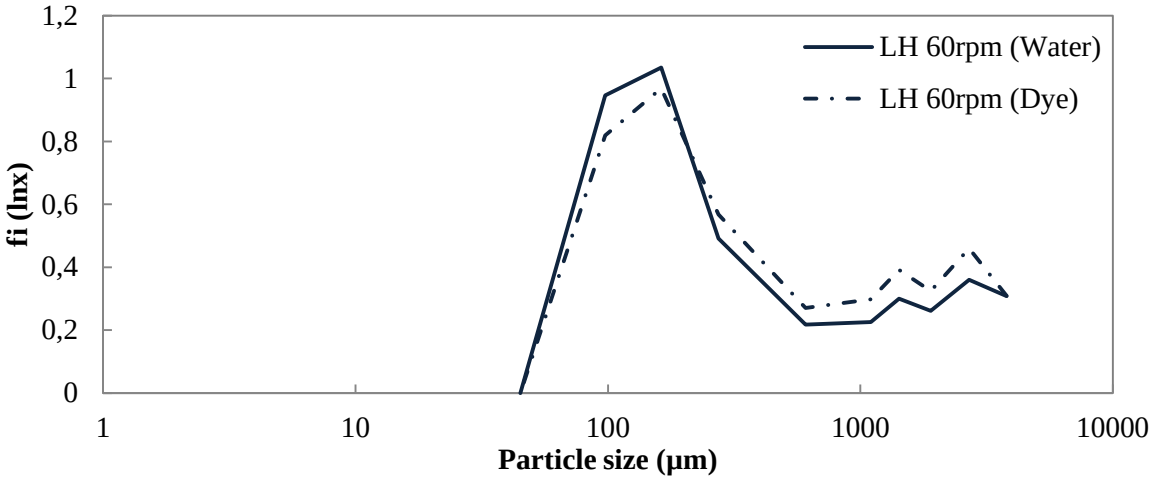

Figure 5.5. Comparative PSD of control and tracer samples of EE862698 LH at 60 rpm

The PSD obtained for the control and tracer samples show similar patterns with little difference between short and long hold times. In all cases, a bi-modal size distribution is achieved, with a big population of fines (<500 µm) and a smaller population of coarse granules (>1000 µm). The use of CE only which are known by their transport or conveying role exert a low shear regime in twin-screw granulation processes. Low shear can lead to the formation of weak agglomerates or nuclei.

Screw geometry and in specific short pitch CE elements (1D) generate low filling degree of material within the screw channels (Thompson and Sun, 2010). Clearance performance of CE elements from one screw to the other cause segregation of particles and asymmetric material distribution within the screws, generating a bi-modal distribution (Chan Seem et al., 2016). Moreover, the filling degree of material can impact the torque generated during TSG experiments. These parameters are directly related to the stresses involved in the formation of granules and therefore can influence granule strength properties (Dhenge et al., 2013). An increase in granules porosity could also explain the production of fines due to low strength properties of the granules. Porosity and drying temperature are parameters that can induce stresses during the drying process, causing the granules to break (Mezhericher, 2014). In our studies, SH and LH conditions were introduced to confirm the likely range of drying process that had a limited impact on granule breakage during sieving analysis. However, PSD plots show comparable results between SH and LH granules where similar amount of fines are produced. The generation of a higher amount of coarse granules at increased screw speed (500 rpm) could be explained by the generation of higher shear forces between the barrel and the screws.

A second part of the study was performed as an attempt to elucidate liquid distribution phenomena. In this case, feed rate to screw speed ratio was maintained but screw speeds of 333 rpm and 240 rpm were used. PSD of these studies are compared to previous results in Figure 5.6.

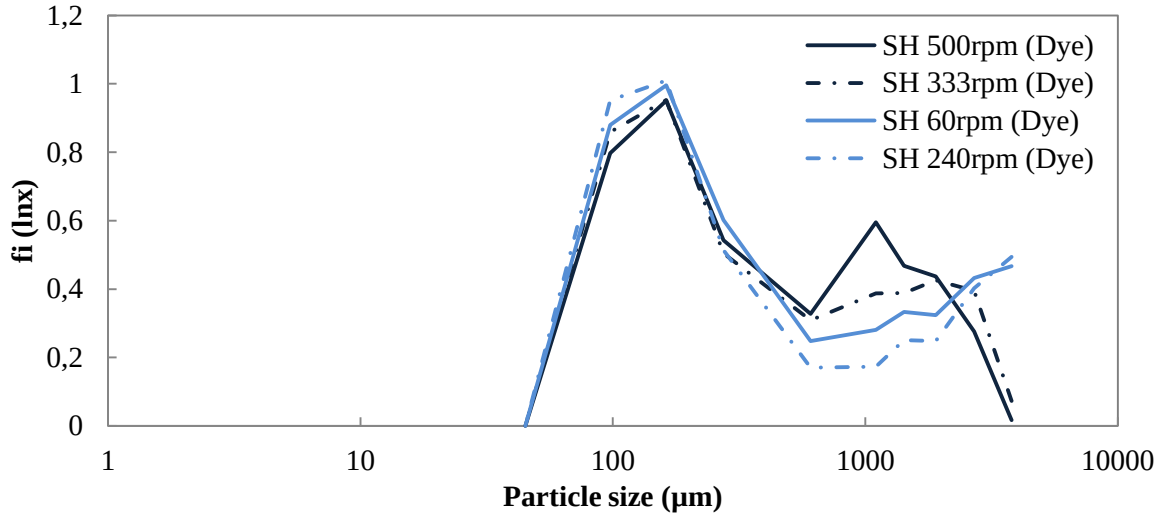

Figure 5.6. Comparative PSD of EE862698 SH tracer samples at 500 rpm, 333 rpm, 60 rpm and 240 rpm

Although similar bi-modal broad distributions are obtained, there is a difference that seems to correlate with mass flow to screw speed ratio. The application of low shear forces by CE elements mainly results in weak nuclei with minimum growth due to the absence of coalescence mechanisms. This phenomena was previously reported by Dhenge et al., (Dhenge et al., 2013) who observed the formation of weak nuclei due to the low shear of CE elements at different powder feed rates.

5.4.1.3. Liquid distribution studies

Liquid distribution studies using a screw configuration of CE are depicted in Figures 5.7 and 5.8 where dye concentration (mg of dye/g of granules) is plotted as a function of particle size.

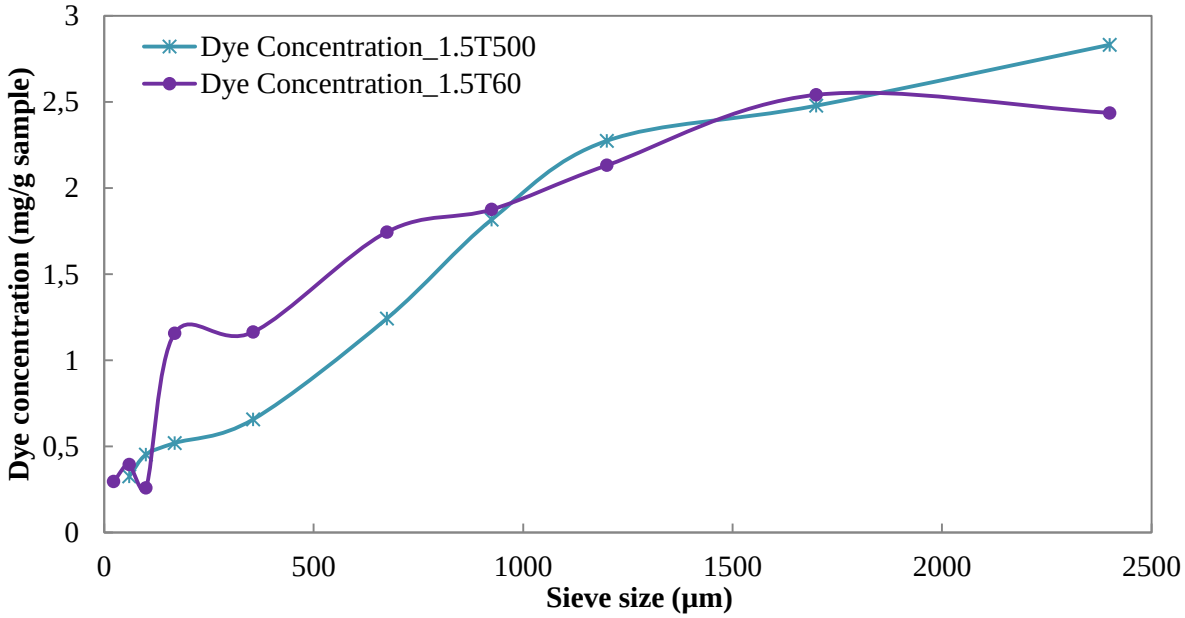

Figure 5.7. Liquid distribution of EE862698 SH at 500 and 60 rpm. Target dye concentration of 0.875 mg/g sample.

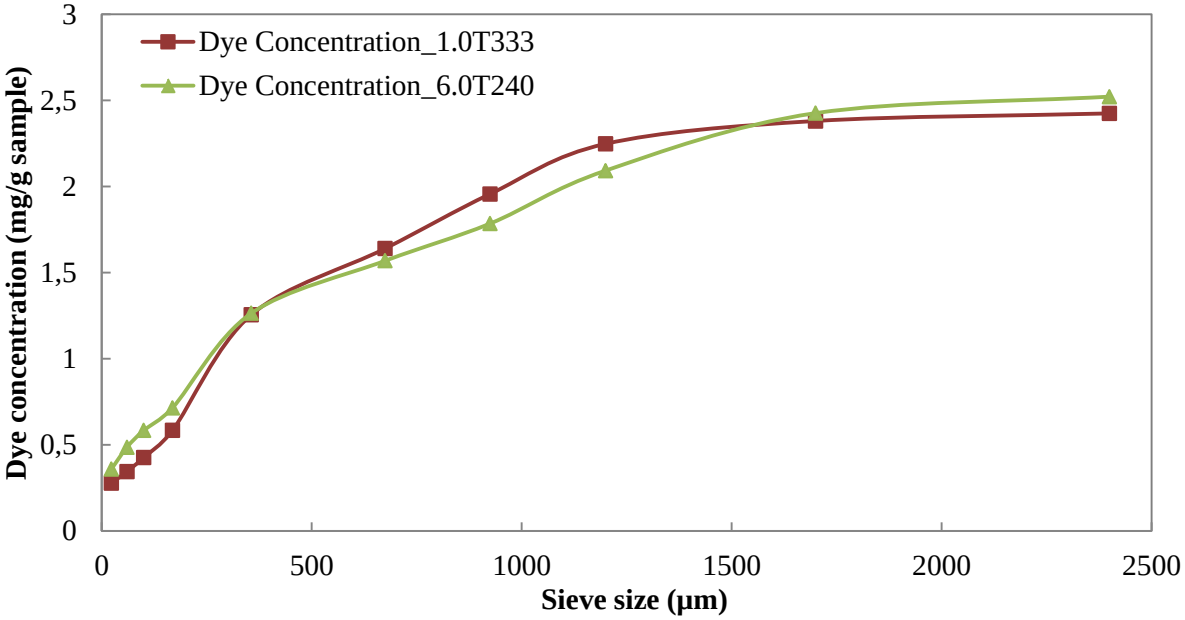

Figure 5.8. Liquid distribution of EE862698 SH at 333 and 240 rpm. Target dye concentration of 0.875 mg/g sample.

Both figures show a gradual increase in dye concentration as particle size increases, which suggests that a poor liquid distribution and therefore poor homogeneity

between components is achieved. Also, Figure 5.7 shows a little difference regarding liquid distributions of granules performed at 60 rpm (full condition) and 500 rpm (starved condition). Dye concentration of granules between 125-1000 µm seems to increase at 60 rpm more than at 500 rpm. The terms full and starved are used to indicate if there is a high or low filling degree of the blend inside the barrel. When comparing these results to the experiments performed at 333 and 240 rpm (Figure 5.8), we can see a similar trend. Statistical analysis using a non-parametric test (Kruskal-Wallis) suggests that dye concentration values are significantly different between them ($P<0.05$). This suggests that the application of different process parameters (shear) and barrel fills had limited effect on granule formation. In twin-screw granulation, the application of different material throughputs and screw speeds translates into different filling degrees of the screw channels. Kumar et al., evaluated the effect of material throughput on the mixing properties and residence time of the material within the granulator. It was observed that a lower filling degree of material resulted in a less compacted product and a better transport within the TSG (Kumar et al., 2016; Kumar et al., 2014). However, these experiments used a KE configuration which suggests that mixing properties in TSG are governed not just by material throughput but also by screw element performance. In our study, the use of only CE produced granules with poor liquid distribution and evidenced a lack of mixing efficiency when compared to screw elements such as KE, DME or DFS. Studies by Dhenge et al., using CE and granulation liquid with different viscosity properties suggest that water as granulation liquid produces more cohesive granules due to a short penetration time where the powder bed becomes wet more rapidly and liquid distribution should improve (Dhenge et al., 2013). It is

known that CE elements apply limited shearing, leading to nuclei or agglomerates that are not developed further to bigger granules. This can lead to granules with poor liquid distribution. Moreover, granule growth or deformation properties are influenced by the stresses generated by the torque as well as the material filling degree. Therefore, these parameters can also have an influence on liquid distribution.

5.4.2. De-coupling of screw element configuration (Study 2)

A second study focused to investigate the key screw element causing a high population of fines or under-granulation phenomena to appear when using a screw configuration formed by KE, DME, DFS and CE elements (see Table 5.1 for reference). Sieving analysis and liquid distribution studies were carried out to characterise granules properties as above.

5.4.2.1. Water content analysis by Karl-Fischer and Loss on Drying

The water content of granules after drying was measured by Karl-Fischer (KF) technique and Loss on Drying (LOD). These results are depicted in Table 5.5. Water content (% w/w) values measured by LOD technique appear to be lower than KF values in all cases (equipment issue).

Table 5.5. Water content of EE867000 granules assessed by KF and LOD

Sample name	Water content KF (% w/w)	Water content LOD (% w/w)
EE867000 – 1.5T500 Dye (a)	3.76	1.82
EE867000 – 1.5T60 Dye (a)	3.76	1.70
EE867000 – 1.5T500 Dye (b)	4.48	2.21
EE867000 – 1.5T60 Dye (b)	3.86	1.99
EE867000 – 1.5T500 Dye (c)	3.69	2.19
EE867000 – 1.5T60 Dye (c)	4.41	2.37

5.4.2.2. Sieving analysis

PSD of EE867000 samples produced at 1.5 kg/h and speeds of 500 and 60 rpm using three types of screw configuration (*a*, *b*, *c*) are shown in Figures 5.9, 5.10 and 5.11. A comparison of the ratio between the upper population (1.0 mm – 500 µm) and the lower population (75 – 45 µm) of granules produced at the lower speed condition (60 rpm) is depicted in Figure 5.12.

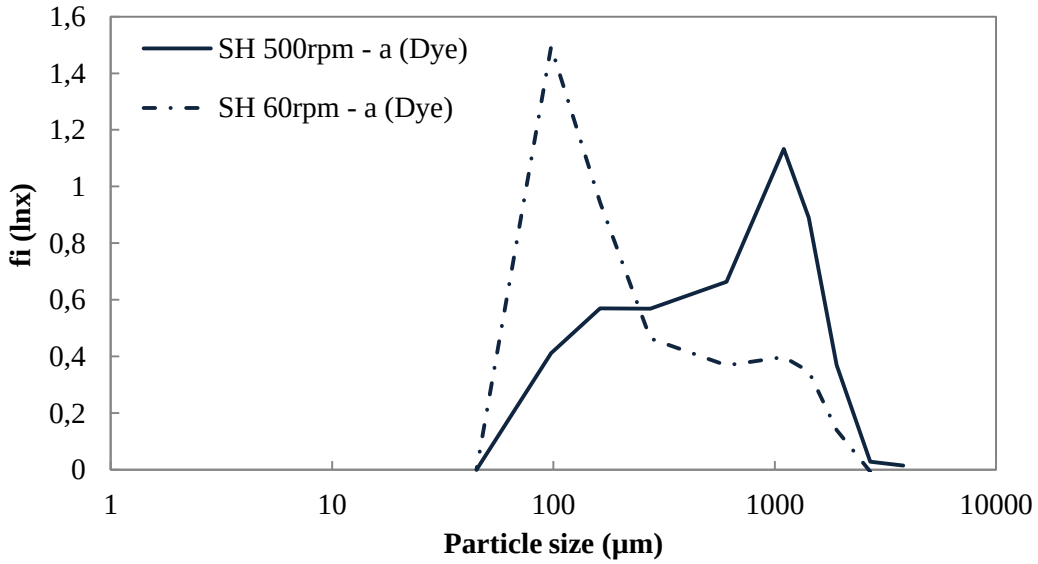

Figure 5.9. Comparative PSD of screw configuration a at 500 and 60 rpm

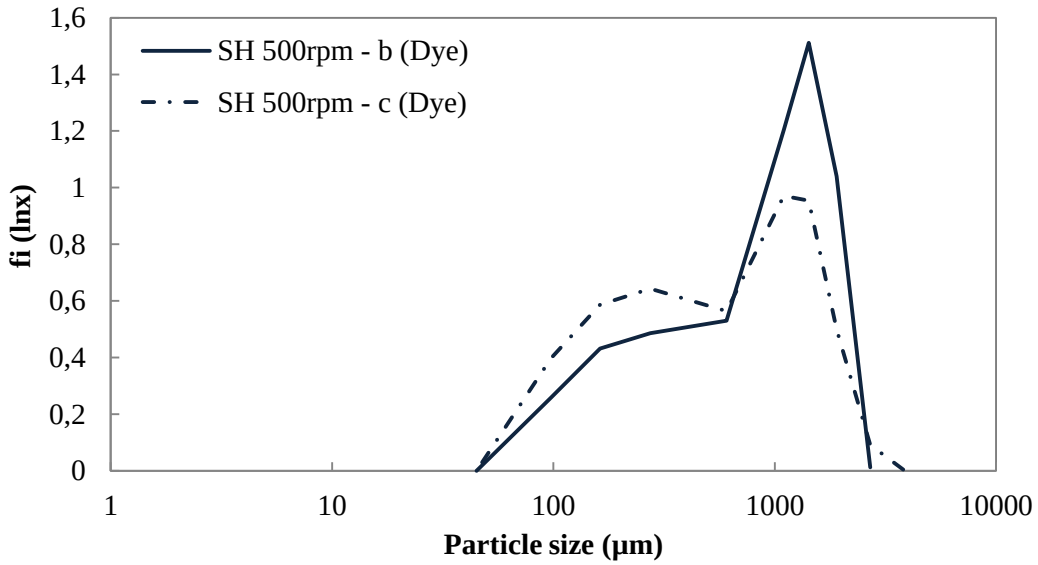

Figure 5.10. Comparative PSD of screw configurations b and c at 500 rpm

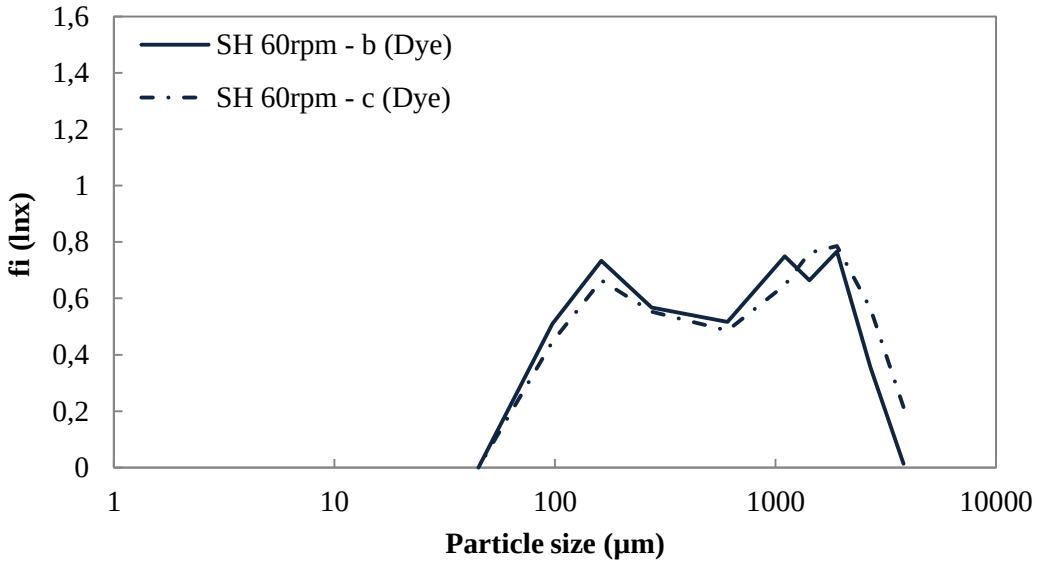

Figure 5.11. Comparative PSD of screw configurations b and c at 60 rpm

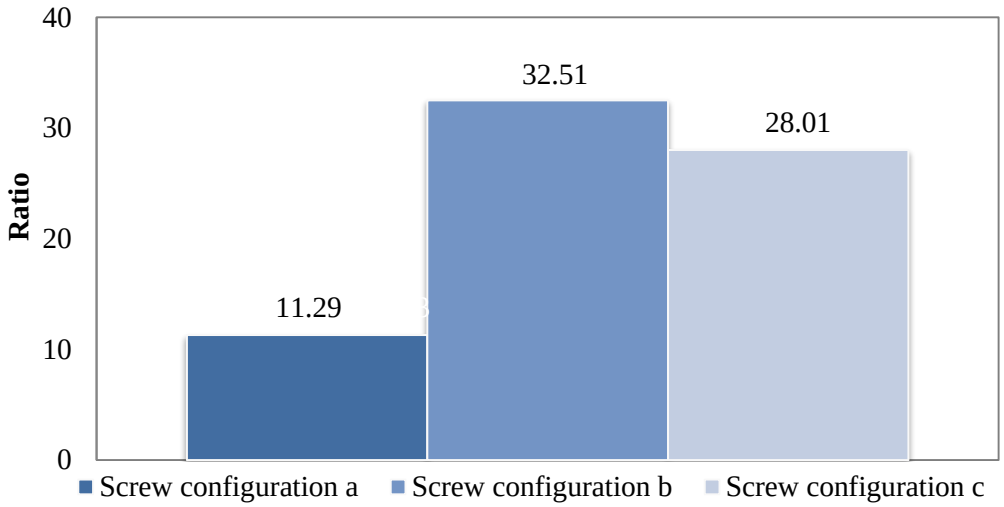

Figure 5.12. Ratio between population >500 and <75 µm for a, b, c configurations at 60 rpm

The populations depicted in Figures 5.9, 5.10 and 5.11 show a clear impact of screw element design and mass flow to screw speed ratio on the PSD achieved by the three different screw element configurations. Figure 5.9 shows that screw configuration *a* which includes the DFS element, produces coarse granules and fines at 500 rpm while a main population of fines (particle size below 500 µm) and almost no coarse granules are obtained at 60 rpm. When screw configurations *b* and *c* were run at 500 rpm (starved configuration) (Figure 5.10), similar PSD results with similar spans and broad distributions of fines and coarse granules were obtained, indicating granule growth. On the other hand, Figure 5.11 of screw configurations *b* and *c* at 60 rpm indicate that at this screw speed, breakage is the main mechanism taking place due to the production of less number of coarse granules and more fines. Compared to configurations *b* and *c*, where bi-modal distributions of coarser granules are observed, we can conclude that DFS is the main element causing a big population of fines through breakage mechanism which is driven by barrel fill rather than shear. These results are simplified in Figure 5.12 where the ratio of particles

>500 and <75 µm for each case is shown. It can be observed that all three ratios calculated for a population between 500 and 75 µm have different values. The ratio corresponding to screw configuration *a* is clearly lower than the other two ratios for *b* and *c*, which show also slightly different values between them. Previous studies we performed with Sayin et al., and other studies by Djuric et al., already described that DFS can generate more fines and less coarse granules due to higher densification properties provided by their longitudinal slots (Djuric and Kleinebudde, 2008; Sayin et al., 2015b). Its characteristic shape allows more material to pass through and therefore, increases the filling degree within the barrel. Combined mixing elements within a twin-screw configuration in twin-screw wet granulation were already studied (Lute et al., 2016; Thompson and Sun, 2010). Interesting results by Thompson et al., suggest that a screw configuration formed by KE60° and DFS greatly increases the amount of fines together with a very low amount of coarse granules, in comparison to configurations formed by various KE blocks. However, it is still not conclusive which specific mechanism leads to the production of fines. The breakage of coarse granules or a possible failure during growth stage of coalescence between the powder bed and liquid droplets could both have an impact (Iveson, 2001). Our results show that DFS impact is driven by screw speed and/or mass flow to screw speed ratio and can be very different depending on operating point. Moreover, breakage mechanism is more likely to cause the production of fines.

5.4.2.3. Liquid distribution studies

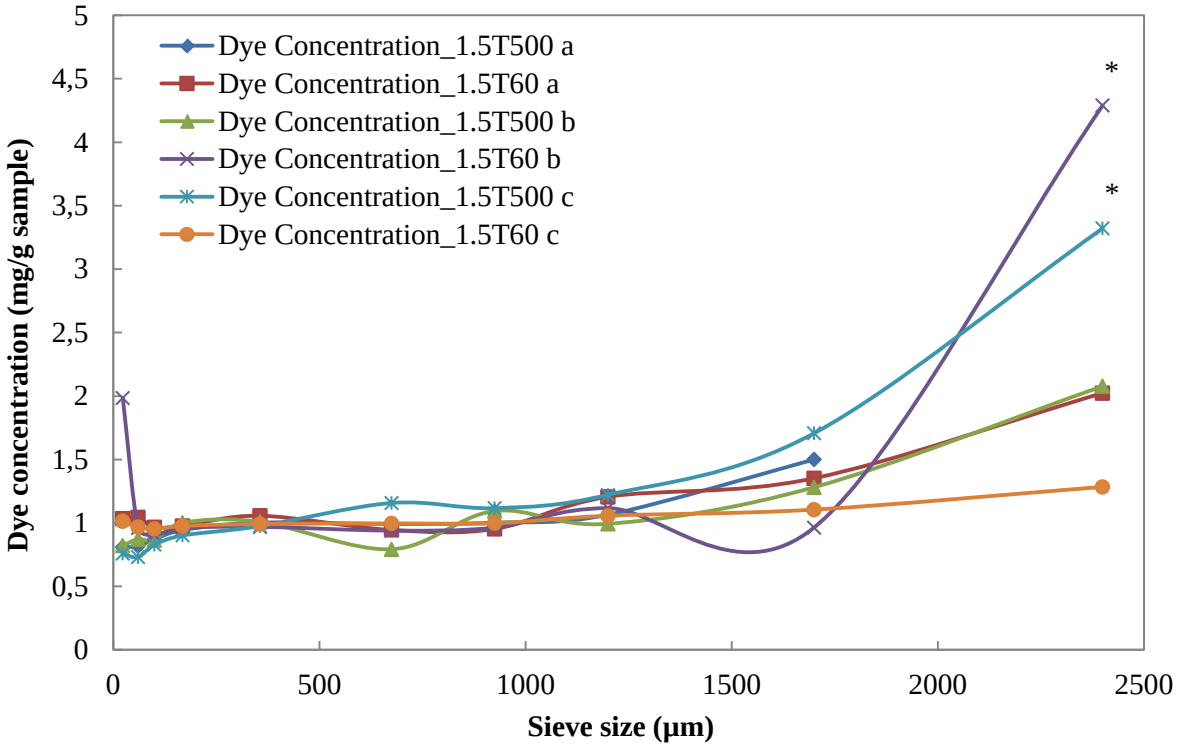

Figure 5.13. Liquid distribution of screw configurations a, b, c at 500 and 60 rpm. Target dye concentration of 0.875 mg/g sample. * symbol represents statistically significant differences obtained from a non-parametric Kruskal-Wallis test with 0.05 significance level (n = 1).

Liquid distribution obtained in this study shows a constant trend of dye concentration for granules samples of particle size between 0 and 1500 µm, indicating a good liquid distribution (Figure 5.13). It is also important to highlight that all samples show an increase in dye concentration corresponding to granules above 1500 µm particle size that suggests the homogeneity in liquid distribution decreases in the case of bigger size granules. Statistical analysis using a non-parametric test (Kruskal-Wallis) suggests that dye concentration values are significantly different between them (indicated by * symbol) ($P<0.05$). As observed in previous results, PSD of screw configuration *a* (DFS) produced high number of fines due to a breakage

mechanism. This mechanism does not affect liquid distribution results which indicate there is a good liquid distribution achieved by configurations with KE (Figure 5.13). It can also be observed that granules from configuration *a* performed at 1.5 kg/h powder feed rate and 60 rpm, had a population with a maximum size <2000 µm as there were no granules collected above this sieve fraction. The trend observed for granules of particle size below 1500 µm with a dye concentration around 1.0 mg/g of sample suggests good homogeneity and liquid distribution properties compared to study 1, when conveying elements were applied (see Figure 5.14 below). It was already described by El Hagrasy et al., that the enhanced liquid distribution obtained when using KE is due to the high-shear applied by KE providing mixing efficiency and growth mechanisms (El Hagrasy and Litster, 2013b). An improvement in liquid distribution as the number of kneading elements increased was also reported. Similar observations were shown by Sayin et al., when looking at liquid distribution properties of different screw configurations comprised of DFS and one block of KE. These results also indicated a better homogeneity and a linear liquid distribution when using KE alone with dye concentrations around 0.15 mg/g of sample (Sayin et al., 2015b).

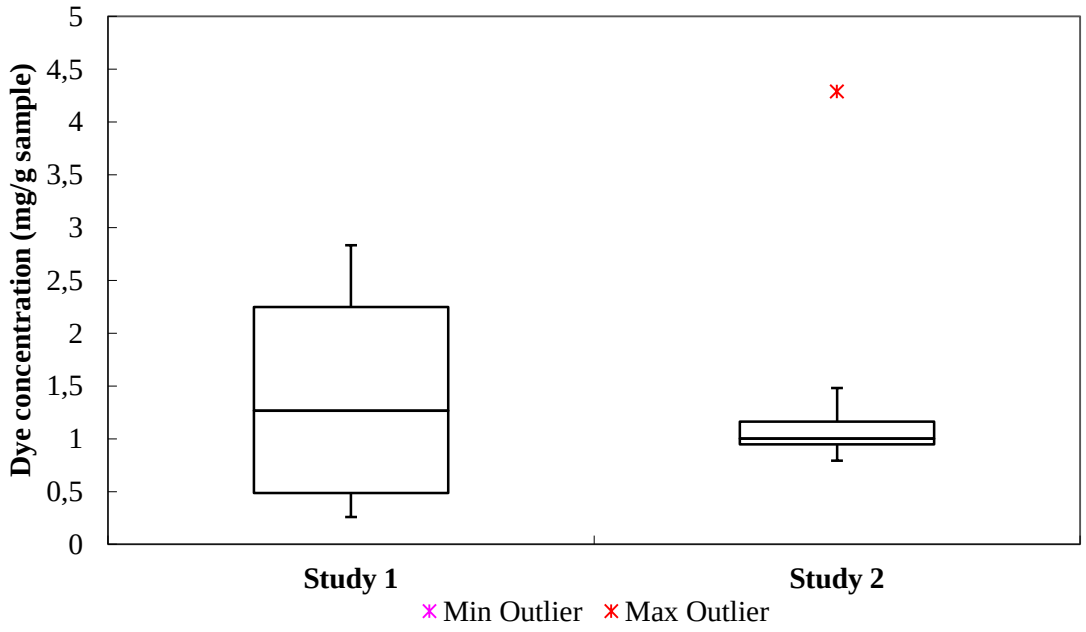

Figure 5.14. Boxplot comparison of dye concentration (mg/g sample) between studies 1 and 2

Statistical analysis on the spread of data between screw configurations based on CE (Study 1) and configurations based on KE and other mixing elements (Study 2) is depicted in Figure 5.14. It can be observed that dye concentrations (mg/g sample) of granules from study 1 are widely spread (0.5-2.5 mg/g sample) compared to granules from study 2 (0.9-1.2 mg/g sample). Therefore, liquid distribution is much less variable when using a screw configuration based on mixing elements.

5.5. Conclusions

In this study, the influence of processing conditions and screw element performance was determined by the characterisation of main particle attributes such as particle size and liquid distribution. In our first study, the performance of conveying elements (CE) towards homogeneity and mixing efficiency was assessed by applying different filling degrees of powder material within the barrel. Poor liquid distributions were obtained and there were no evident changes between full and starved conditions. The attempt to stretch the design of space by applying equivalent processing parameters appears to be non-conclusive regarding granules particle size and liquid distribution. The mixing degree applied by CE is proven to be not as efficient as the shear provided by mixing elements such as KE. The second study helped to determine the screw element involved in under-granulation phenomena generated by a combined screw element configuration. We can conclude that the DFS element causes a high population of fine granules to appear when compared to the other two configurations where this element is absent, due to a breakage mechanism whose rate is dependent on barrel fill (mass flow to screw speed ratio) rather than shear (screw speed). Also, coarse granules are reduced when using DFS element. Distribution properties between the granulation liquid containing a dye or tracer and the powder bed were also characterised by liquid distribution studies. These suggest that liquid distribution is improved when a screw configuration formed by mixing elements such as KE, DME, DFS is used. Moreover, the observed breakage behaviour of DFS element does not seem to impact granules liquid distribution.

6. Conclusions and future work

6.1. Conclusions

The work presented in this thesis was focused on the study of two applications, HME and TSG, by utilising the same processing equipment with different set-ups. Both processing techniques have the potential to be used as part of a continuous manufacturing platform and are generating great interest due to its reduced processing time and cost required for the manufacturing of solid dosage forms (Baronsky-Probst et al., 2016; Teżyk et al., 2016). A twin-screw extruder or granulator can be fit into a continuous manufacturing platform by connecting the inlet to blending and feeding equipment and attaching downstream processing equipment such as a pelletiser or a tablet press at the outlet (Vercruysse et al., 2015).

The first application was focused on the pharmaceutical development and characterisation of HME formulations with the aim to improve the dissolution properties and consequently, the oral bioavailability of the poorly soluble drug ABZ. Two different polymeric carriers with hydrophilic properties were applied. The use of a low viscosity grade polymer such as PVP K12 resulted in easily extrudable formulations. An intermeshing co-rotating twin-screw extruder with 3 mixing zones and conveying elements was used. Processing conditions comprised barrel temperatures in the range of 70 – 145 °C and 70 – 135 °C, screw speed of 100 rpm and a throughput of 0.10 – 0.23 kg/h. Barrel temperatures required to be optimised in order to obtain less porous extruded materials. Successful and stable amorphous solid dispersions of ABZ in a PVP K12 matrix were obtained, with no recrystallisation events occurring after 6 months storage as shown by XRPD and DSC results. Previous literature research and knowledge of the melting temperature, glass transition temperature and degradation temperature were crucial to ensure the

stability of the formulations based on reduced mobility properties provided by the polymer. The characterisation of solid state and dissolution properties provided a better understanding of the impact that processing conditions and material attributes can have on final product. For example, differences in dissolution profiles that do not achieve 100 % drug release despite complete tablet dissolution, suggest the presence of molecular interactions such as cross-linking effects between ABZ and PVP K12 that would need to be further studied (see section 6.2). These might be possibly caused by the hydrophobic properties of ABZ together with the formation of possible covalent bonds. It is then concluded that despite successful amorphous solid dispersions of ABZ were obtained by HME process, the presence of molecular interactions play a key role on formulation in-vitro performance. It was also evidenced that, although amorphous dispersions of ABZ were obtained, there seems to be a limit of detection for low crystalline content (physical mixtures) when using DSC. Further analysis of the extruded materials by Micro-CT and SEM evidenced that PVP K12 materials presented high porosity properties that increase as drug content also increases. The application of a sophisticated technique such as Micro-CT was useful to understand the impact of HME processing parameters such as barrel temperature in the formation of well-shaped extruded materials as well as overall porosity properties. A reduction in processing temperature from 145 $^{\circ}$C to 135 $^{\circ}$C improved physical and porosity properties of PVP K12 extruded materials although porosity was not completely removed. Micro-CT analysis evidenced density differences throughout the matrices which could be due to the effect of processing/cooling temperature or correspond to drug and polymer densities. In the last case, a lack of homogeneous drug distribution would need to be confirmed, as it

can affect drug content uniformity of the final dosage form. Other amorphous solid dispersions of ABZ were developed by HME using PEG 6000. Extrusion experiments in this case were performed at relatively low processing temperatures, 30 – 58 °C, screw speed of 50 rpm and a throughput of 0.09 – 0.20 kg/h. Micro-CT analysis of these formulations showed the formation of more compact and uniform polymer matrices and also a decrease of internal porosity when compared to PVP K12 materials. Amorphous solid dispersions produced in this case achieved a great increase in ABZ dissolution rate. However, the amorphous form was only stable in solution for a total period of 30 minutes, after which ABZ precipitation occurred due to conversion to the crystalline form. This could be possibly explained by a pH change from 2 to 3 and also by the high hydrophilic properties of PEG 6000 (Gullapalli and Mazzitelli, 2015). In addition, XRPD diffractograms evidenced recrystallisation events after 6 months storage. The low T_g and the partial crystalline properties of PEG 6000 can have influenced the stability properties due to an increased mobility of the drug molecules within the matrix (Baghel et al., 2016).

Further studies comprised the understanding of TSG performance by applying an engineering perspective to define the processing parameters of the design of space. The use of twin-screw granulators at industrial scale can provide many benefits associated to twin-screw equipment to produce intermediate granules that can be processed into tablets. Many TSG studies are carried out to elucidate the growth mechanisms underlying particle formation into agglomerates or granules provided by co-rotating twin-screws. In this research, the influence of different processing parameters on twin-screw performance and final granule attributes was evaluated. Previous research (Thompson and Sun, 2010) associated final product attributes to

screw element design. However, there were still challenges regarding the elucidation of the actual mechanisms behind liquid distribution and fines production (under-granulation phenomena). The studies performed in chapter 5 have contributed to a better understanding of the relation between screw element design and granulation performance which is reflected on particle size and liquid distribution properties. It was concluded that breakage mechanism causes fines production when a screw configuration with DFS element is used.

6.2. Future work

It was observed that PVP K12 may have generated cross-linking interactions with our drug molecule ABZ, leading to non-consistent drug release profiles. In order to determine these interactions, further experimental analysis would be required. For example, the use of isothermal titration calorimetry (ITC) has previously been successful in the determination of polymer-polymer molecular interactions comprising PVP. A possible covalent interaction between PVP K12 and ABZ would also need to be studied. Another useful technique that could be used is turbidimetric titration where different ratios drug-polymer are studied to determine their relative molecular weight distributions. Alternatively, spectroscopic techniques could be used such as near-infrared (NIR) spectroscopy which is highly sensitive to the appearance of chemical shifts between functional groups and has previously been used to assess PVP K12 molecular interactions with other drug molecules. In-line NIR could be applied as a novel PAT tool to perform real-time measurements of the process. The set-up of the twin-screw extruder would be slightly modified by attaching a NIR probe at the end part of the die.

Further studies would also be required to assess the potential enhancement of the oral bioavailability of the HME formulations developed. In-vitro and in-vivo studies of solid dosage forms (e.g. tablets, pellets) obtained from ABZ amorphous solid dispersions could provide useful information. The tablets used during T3 analysis to evaluate the dissolution behaviour of ABZ solid dispersions can be considered as initial dosage forms. Examples of in-vitro and in-vivo studies comprise dissolution profile and pharmacokinetic studies which are focused to know the bioavailability properties of ABZ formulations. It would also be recommended to test other suitable polymeric carriers for HME processing such as Soluplus®, hypromellose (HPMC) and hypromellose phthalate (HPMC-P). The main advantage of Soluplus® is given by its physicochemical properties like high water solubility, low viscosity and low T_g and T_m values that provide ease of processability by HME. In the case of HPMC and HPMC-P, high T_g values provide high stability properties of the amorphous form. Also, a mathematical model for HME process could be implemented to optimise the process and also the properties of the extruded materials. For instance, powder feed rate can be adjusted based on recorded pressure and temperature values by the application of a mathematical model.

7. References

Airaksinen, S., Karjalainen, M., Shevchenko, A., Westermarck, S., Leppanen, E., Rantanen, J., Yliruusi, J., 2005. Role of water in the physical stability of solid dosage formulations. Journal of pharmaceutical sciences 94, 2147-2165.

Albers, J., Alles, R., Matthee, K., Knop, K., Nahrup, J.S., Kleinebudde, P., 2009. Mechanism of drug release from polymethacrylate-based extrudates and milled strands prepared by hot-melt extrusion. European journal of pharmaceutics and biopharmaceutics 71, 387-394.

Alhijjaj, M., Yassin, S., Reading, M., Zeitler, J.A., Belton, P., Qi, S., 2016. Characterization of Heterogeneity and Spatial Distribution of Phases in Complex Solid Dispersions by Thermal Analysis by Structural Characterization and X-ray Micro Computed Tomography. Pharmaceutical research.

Allen, T., 2003. Powder Sampling and Particle Size Determination. Elsevier Science.

Allison, G., Cain, Y.T., Cooney, C., Garcia, T., Bizjak, T.G., Holte, O., Jagota, N., Komas, B., Korakianiti, E., Kourti, D., Madurawe, R., Morefield, E., Montgomery, F., Nasr, M., Randolph, W., Robert, J.-L., Rudd, D., Zezza, D., 2015. Regulatory and Quality Considerations for Continuous Manufacturing May 20–21, 2014 Continuous Manufacturing Symposium. Journal of pharmaceutical sciences 104, 803-812.

Almeida, A., Possemiers, S., Boone, M.N., De Beer, T., Quinten, T., Van Hoorebeke, L., Remon, J.P., Vervaet, C., 2011. Ethylene vinyl acetate as matrix for oral sustained release dosage forms produced via hot-melt extrusion. European journal of pharmaceutics and biopharmaceutics 77, 297-305.

Almeida, A., Saerens, L., De Beer, T., Remon, J.P., Vervaet, C., 2012. Upscaling and in-line process monitoring via spectroscopic techniques of ethylene vinyl acetate hot-melt extruded formulations. International journal of pharmaceutics 439, 223-229.

Alshehri, S.M., Park, J.B., Alsulays, B.B., Tiwari, R.V., Almutairy, B., Alshetaili, A.S., Morott, J., Shah, S., Kulkarni, V., Majumdar, S., Martin, S.T., Mishra, S., Wang, L., Repka, M.A., 2015. Mefenamic acid taste-masked oral disintegrating tablets with enhanced solubility via molecular interaction produced by hot melt extrusion technology. Journal of drug delivery science and technology 27, 18-27.

Alshehri, S.M., Tiwari, R.V., Alsulays, B.B., Ashour, E.A., Alshetaili, A.S., Almutairy, B., Park, J.B., Morott, J., Sandhu, B., Majumdar, S., Repka, M.A., 2016. Investigation of the combined effect of MgO and PEG on the release profile of mefenamic acid prepared via hot-melt extrusion techniques. Pharmaceutical development and technology, 1-14.

Alsulays, B.B., Park, J.B., Alshehri, S.M., Morott, J.T., Alshahrani, S.M., Tiwari, R.V., Alshetaili, A.S., Majumdar, S., Langley, N., Kolter, K., Gryczke, A., Repka, M.A., 2015. Influence of Molecular Weight of Carriers and Processing Parameters on the Extrudability, Drug Release, and Stability of Fenofibrate Formulations Processed by Hot-Melt Extrusion. Journal of drug delivery science and technology 29, 189-198.

Alvarez-Murga, M., Bleuet, P., Hodeau, J.-L., 2012. Diffraction/scattering computed tomography for three-dimensional characterization of multi-phase crystalline and amorphous materials. Journal of Applied Crystallography 45, 1109-1124.

Amidon, G.L.L., H. Shah, V.P. Crison, J.R., 1995. A theoretical basis for a biopharmaceutical drug classification. Pharmaceutical research 12, 413-420.

Anderberg, E.K., Bisrat, M., and Nyström, C. , 1988. Physicochemical aspects of drug release. VII. The effect of surfactant concentration and drug particle size on solubility and dissolution rate of felodipine, a sparingly soluble drug. International journal of pharmaceutics 47, 67-77.

Andrews, G.P., AbuDiak, O.A., Jones, D.S., 2010. Physicochemical characterization of hot melt extruded bicalutamide-polyvinylpyrrolidone solid dispersions. Journal of pharmaceutical sciences 99, 1322-1335.

Andrews, G.P., Margetson, D.N., Jones, D.S., McAllister, M.S., Diak, O.A., 2009. Hot-melt extrusion: An emerging drug delivery technology. Pharmaceutical Technology Europe 21, 18-23.

Andrews, G.P.M., D.N. Jones, D.S. McAllister, S.M. Diak, O.A., 2008. A basic guide: Hot-melt extrusion. UKICRS 13.

Baghel, S., Cathcart, H., O'Reilly, N.J., 2016. Polymeric Amorphous Solid Dispersions: A Review of Amorphization, Crystallization, Stabilization, Solid-State Characterization, and Aqueous Solubilization of Biopharmaceutical Classification System Class II Drugs. Journal of pharmaceutical sciences 105, 2527-2544.

Baird, J.A., Olayo-Valles, R., Rinaldi, C., Taylor, L.S., 2010. Effect of Molecular Weight, Temperature, and Additives on the Moisture Sorption Properties of Polyethylene Glycol. Journal of pharmaceutical sciences 99, 154-168.

Baird, J.A., Taylor, L.S., 2012. Evaluation of amorphous solid dispersion properties using thermal analysis techniques. Advanced drug delivery reviews 64, 396-421.

Baronsky-Probst, J., Moltgen, C.V., Kessler, W., Kessler, R.W., 2016. Process design and control of a twin screw hot melt extrusion for continuous pharmaceutical tamper-resistant tablet production. European journal of pharmaceutical sciences: Official journal of the European Federation for Pharmaceutical Sciences 87, 14-21.

Beer, P., Wilson, D., Huang, Z., De Matas, M., 2014. Transfer from high-shear batch to continuous twin screw wet granulation: a case study in understanding the relationship between process parameters and product quality attributes. Journal of pharmaceutical sciences 103, 3075-3082.

Bhagurkar, A.M., Angamuthu, M., Patil, H., Tiwari, R.V., Maurya, A., Hashemnejad, S.M., Kundu, S., Murthy, S.N., Repka, M.A., 2016. Development of an Ointment Formulation Using Hot-Melt Extrusion Technology. AAPS PharmSciTech 17, 158-166.

Bianco, S., Tewes, F., Tajber, L., Caron, V., Corrigan, O.I., Healy, A.M., 2013. Bulk, surface properties and water uptake mechanisms of salt/acid amorphous composite systems. International journal of pharmaceutics 456, 143-152.

Bikiaris, D., Papageorgiou, G.Z., Stergiou, A., Pavlidou, E., Karavas, E., Kanaze, F., Georgarakis, M., 2005. Physicochemical studies on solid dispersions of poorly water-soluble drugs. Thermochimica Acta 439, 58-67.

Bochmann, E.S., Neumann, D., Gryczke, A., Wagner, K.G., 2016. Micro-scale prediction method for API-solubility in polymeric matrices and process model for

forming amorphous solid dispersion by hot-melt extrusion. European journal of pharmaceutics and biopharmaceutics 107, 40-48.

Börner, M., Michaelis, M., Siegmann, E., Radeke, C., Schmidt, U., 2016. Impact of impeller design on high-shear wet granulation. Powder Technology 295, 261-271.

Brouwers, J., Brewster, M.E., Augustijns, P., 2009. Supersaturating drug delivery systems: the answer to solubility-limited oral bioavailability? Journal of pharmaceutical sciences 98, 2549-2572.

Bruce, C., Fegely, K.A., Rajabi-Siahboomi, A.R., McGinity, J.W., 2007. Crystal growth formation in melt extrudates. International journal of pharmaceutics 341, 162-172.

Bruker, 2014. Bruker Micro-CT academy. 1.

Bühler, V., 2005. Polyvinylpyrrolidone Excipients for Pharmaceuticals: Povidone, Crospovidone and Copovidone. Springer.

Busignies, V., Leclerc, B., Porion, P., Evesque, P., Couarraze, G., Tchoreloff, P., 2006. Quantitative measurements of localized density variations in cylindrical tablets using X-ray microtomography. European journal of pharmaceutics and biopharmaceutics 64, 38-50.

Butler, J.M.D., J.B., 2010. The developability classification system: Application of biopharmaceutics concepts to formulation development. Journal of pharmaceutical sciences 99, 4940-4954.

Chan, E.L., Reynolds, G.K., Gururajan, B., Hounslow, M.J., Salman, A.D., 2013. Blade–granule bed stress in a cylindrical high shear granulator: I—Online measurement and characterisation. Chemical Engineering Science 86, 38-49.

Chan, S.Y., Qi, S., Craig, D.Q., 2015. An investigation into the influence of drug-polymer interactions on the miscibility, processability and structure of polyvinylpyrrolidone-based hot melt extrusion formulations. International journal of pharmaceutics 496, 95-106.

Chan Seem, T., Rowson, N.A., Gabbott, I., de Matas, M., Reynolds, G.K., Ingram, A., 2016. Asymmetric distribution in twin screw granulation. European journal of pharmaceutics and biopharmaceutics 106, 50-58.

Cheng, H., Friis, A., 2010. Modelling extrudate expansion in a twin-screw food extrusion cooking process through dimensional analysis methodology. Food and Bioproducts Processing 88, 188-194.

Chirkot, T.H., S. Swanborough, A. , 2009. Monitoring the output of pharmaceutical hot melt extruders with near-infrared spectroscopy. Thermo Fisher Scientific Application note: 51836.

Chu, K.R., Lee, E., Jeong, S.H., Park, E.-S., 2012. Effect of particle size on the dissolution behaviors of poorly water-soluble drugs. Archives of Pharmacal Research 35, 1187-1195.

Corrigan, O.I., Murphy, C.A., Timoney, R.F., 1979. Dissolution properties of polyethylene glycols and polyethylene glycol-drug systems. International journal of pharmaceutics 4, 67-74.

Crean, B., Parker, A., Roux, D.L., Perkins, M., Luk, S.Y., Banks, S.R., Melia, C.D., Roberts, C.J., 2010. Elucidation of the internal physical and chemical microstructure of pharmaceutical granules using X-ray micro-computed tomography, Raman microscopy and infrared spectroscopy. European journal of pharmaceutics and biopharmaceutics 76, 498-506.

Crowley, M.M., Zhang, F., Repka, M.A., Thumma, S., Upadhye, S.B., Battu, S.K., McGinity, J.W., Martin, C., 2007. Pharmaceutical applications of hot-melt extrusion: part I. Drug development and industrial pharmacy 33, 909-926.

Dahan, A., Wolk, O., Agbaria, R., 2014. Provisional in-silico biopharmaceutics classification (BCS) to guide oral drug product development. Drug design, development and therapy, 1563.

Damian, F., Blaton, N., Naesens, L., Balzarini, J., Kinget, R., Augustijns, P., Van den Mooter, G., 2000. Physicochemical characterisation of solid dispersions of the antiviral agent UC-781 with polyethylene glycol 6000 and Gelucire 44/14. European Journal of Pharmaceutical Sciences 10, 311-322.

De Beer, T., Burggraeve, A., Fonteyne, M., Saerens, L., Remon, J.P., Vervaet, C., 2011. Near infrared and Raman spectroscopy for the in-process monitoring of pharmaceutical production processes. International journal of pharmaceutics 417, 32-47.

De Jaeghere, W., De Beer, T., Van Bocxlaer, J., Remon, J.P., Vervaet, C., 2015. Hot-melt extrusion of polyvinyl alcohol for oral immediate release applications. International journal of pharmaceutics 492, 1-9.

Dhenge, R.M., Cartwright, J.J., Hounslow, M.J., Salman, A.D., 2012. Twin screw granulation: steps in granule growth. International journal of pharmaceutics 438, 20-32.

Dhenge, R.M., Fyles, R.S., Cartwright, J.J., Doughty, D.G., Hounslow, M.J., Salman, A.D., 2010. Twin screw wet granulation: Granule properties. Chemical Engineering Journal 164, 322-329.

Dhenge, R.M., Washino, K., Cartwright, J.J., Hounslow, M.J., Salman, A.D., 2013. Twin screw granulation using conveying screws: Effects of viscosity of granulation liquids and flow of powders. Powder Technology 238, 77-90.

Dhirendra, K.L., S. Udupa, N. Atin, K., 2009. Solid dispersions: A review. Pakistan journal of pharmaceutical sciences 22, 234-246.

Dierickx, L., Saerens, L., Almeida, A., De Beer, T., Remon, J.P., Vervaet, C., 2012. Co-extrusion as manufacturing technique for fixed-dose combination mini-matrices. European journal of pharmaceutics and biopharmaceutics 81, 683-689.

Dierickx, L., Van Snick, B., Monteyne, T., De Beer, T., Remon, J.P., Vervaet, C., 2014. Co-extruded solid solutions as immediate release fixed-dose combinations. European journal of pharmaceutics and biopharmaceutics 88, 502-509.

Djuric, D., Kleinebudde, P., 2008. Impact of screw elements on continuous granulation with a twin-screw extruder. Journal of pharmaceutical sciences 97, 4934-4942.

Djuric, D., Van Melkebeke, B., Kleinebudde, P., Remon, J.P., Vervaet, C., 2009. Comparison of two twin-screw extruders for continuous granulation. European journal of pharmaceutics and biopharmaceutics 71, 155-160.

Dong, Z., Chatterji, A., Sandhu, H., Choi, D.S., Chokshi, H., Shah, N., 2008. Evaluation of solid state properties of solid dispersions prepared by hot-melt extrusion and solvent co-precipitation. International journal of pharmaceutics 355, 141-149.

Douglas, P., Albadarin, A.B., Sajjia, M., Mangwandi, C., Kuhs, M., Collins, M.N., Walker, G.M., 2016. Effect of poly ethylene glycol on the mechanical and thermal properties of bioactive poly(epsilon-caprolactone) melt extrudates for pharmaceutical applications. International journal of pharmaceutics 500, 179-186.

Dubois, J.L., Ford, J.L., , 1985. Similarities in the release rates of different drugs from polyethylene glycol 6000 solid dispersions. The Journal of pharmacy and pharmacology 37, 494-496.

El Hagrasy, A.S., Hennenkamp, J.R., Burke, M.D., Cartwright, J.J., Litster, J.D., 2013a. Twin screw wet granulation: Influence of formulation parameters on granule properties and growth behavior. Powder Technology 238, 108-115.

El Hagrasy, A.S., Litster, J.D., 2013b. Granulation rate processes in the kneading elements of a twin screw granulator. AIChE Journal 59, 4100-4115.

Farber, L., Tardos, G., Michaels, J.N., 2003. Use of X-ray tomography to study the porosity and morphology of granules. Powder Technology 132, 57-63.

Feng, X., Vo, A., Patil, H., Tiwari, R.V., Alshetaili, A.S., Pimparade, M.B., Repka, M.A., 2016. The effects of polymer carrier, hot melt extrusion process and downstream processing parameters on the moisture sorption properties of amorphous solid dispersions. The Journal of pharmacy and pharmacology 68, 692-704.

Feng, Y., Wang, K., Yao, J., Webley, P.A., Smart, S., Wang, H., 2013. Effect of the addition of polyvinylpyrrolidone as a pore-former on microstructure and mechanical strength of porous alumina ceramics. Ceramics International 39, 7551-7556.

Forster, A.H., J. Tucker, I. Rades, T., 2001. Selection of excipients for melt extrusion with two poorly water-soluble drugs by solubility parameter calculation and thermal analysis. International journal of pharmaceutics 226, 147-161.

Franco, M., Trapani, G., Latrofa, A., Tullio, C., Provenzano, M.R., Serra, M., Muggironi, M., Biggio, G., Liso, G., 2001. Dissolution properties and anticonvulsant activity of phenytoin-polyethylene glycol 6000 and -polyvinylpyrrolidone K-30 solid dispersions. International journal of pharmaceutics 225, 63-73.

Frizon, F., Eloy, J.d.O., Donaduzzi, C.M., Mitsui, M.L., Marchetti, J.M., 2013. Dissolution rate enhancement of loratadine in polyvinylpyrrolidone K-30 solid dispersions by solvent methods. Powder Technology 235, 532-539.

Fu, Q., Fang, M., Hou, Y., Yang, W., Shao, J., Guo, M., Li, M., Li, J., Wang, Y., He, Z., Sun, J., 2016. A physically stabilized amorphous solid dispersion of nisoldipine obtained by hot melt extrusion. Powder Technology 301, 342-348.

Fukuda, M., Miller, D.A., Peppas, N.A., McGinity, J.W., 2008. Influence of sulfobutyl ether beta-cyclodextrin (Captisol) on the dissolution properties of a poorly

soluble drug from extrudates prepared by hot-melt extrusion. International journal of pharmaceutics 350, 188-196.

Fukuda, M., Peppas, N.A., McGinity, J.W., 2006. Properties of sustained release hot-melt extruded tablets containing chitosan and xanthan gum. International journal of pharmaceutics 310, 90-100.

Fule, R., Amin, P., 2014. Development and evaluation of lafutidine solid dispersion via hot melt extrusion: Investigating drug-polymer miscibility with advanced characterisation. Asian Journal of Pharmaceutical Sciences 9, 92-106.

Fule, R., Dhamecha, D., Maniruzzaman, M., Khale, A., Amin, P., 2015. Development of hot melt co-formulated antimalarial solid dispersion system in fixed dose form (ARLUMELT): Evaluating amorphous state and in vivo performance. International journal of pharmaceutics 496, 137-156.

Gerhardt, A., 2009. Moisture effects on solid dosage forms - Formulation, processing and stability. Journal of GXP compliance 13, 58-66.

Ghebremeskel, A.N., Vemavarapu, C., Lodaya, M., 2007. Use of surfactants as plasticizers in preparing solid dispersions of poorly soluble API: selection of polymer-surfactant combinations using solubility parameters and testing the processability. International journal of pharmaceutics 328, 119-129.

Gryczke, A.S., S. Maniruzzaman, M. Beck, J. Douroumis, D., 2011. Orally disintegrating tablets (ODTs) containing Ibuprofen granules prepared by HME. Colloids and Surfaces B: Biointerfaces 86, 275-284.

Gullapalli, R.P., Mazzitelli, C.L., 2015. Polyethylene glycols in oral and parenteral formulations--A critical review. International journal of pharmaceutics 496, 219-239.

Guns, S., Mathot, V., Martens, J.A., Van den Mooter, G., 2012. Upscaling of the hot-melt extrusion process: comparison between laboratory scale and pilot scale production of solid dispersions with miconazole and Kollicoat IR. European journal of pharmaceutics and biopharmaceutics 81, 674-682.

Haaf, F., Sanner, A., and Straub, F., 1985. Polymers of N-vinylpyrrolidone: Synthesis, characterisation and uses. Polymer Journal 17, 143-152.

Hancock, B.C., Mullarney, M.P. , 2005. X-ray microtomography of solid dosage forms. Pharm Tech, 92-100.

Hansen, C.M., 2000. Hansen Solubility Parameters Handbook.

Hoffmann, T., Rieck, C., Bück, A., Peglow, M., Tsotsas, E., 2015. Influence of Granule Porosity during Fluidized Bed Spray Granulation. Procedia Engineering 102, 458-467.

ICH, 2009. ICH Harmonised Tripartite Guideline Pharmaceutical Development Q8(R2).

Islam, M.T., Maniruzzaman, M., Halsey, S.A., Chowdhry, B.Z., Douroumis, D., 2014. Development of sustained-release formulations processed by hot-melt extrusion by using a quality-by-design approach. Drug delivery and translational research 4, 377-387.

Ito, A., Watanabe, T., Yada, S., Hamaura, T., Nakagami, H., Higashi, K., Moribe, K., Yamamoto, K., 2010. Prediction of recrystallization behavior of troglitazone/polyvinylpyrrolidone solid dispersion by solid-state NMR. International journal of pharmaceutics 383, 18-23.

Iveson, S.M., Litster, J.D., Hapgood, K., Ennis, B.J., 2001. Nucleation, growth and breakage phenomena in agitated wet granulation processes: a review. Powder Technology 117, 3-39.

Jenkins, R., Snyder, R.L., 1996. Introduction to X-ray powder diffractometry. Wiley, New York.

Jones, D.S., Margetson, D.N., McAllister, M.S., Yu, T., Shu, L., McCoy, C.P., Andrews, G.P., 2014. Thermodynamically stable amorphous drug dispersions in amorphous hydrophilic polymers engineered by hot melt extrusion. Chemical Engineering Research and Design 92, 3046-3054.

Jung, H., Medina, L., GarcÍA, L., Fuentes, I., Moreno-Esparza, R., 1998. Biopharmaceutics: Absorption Studies of Albendazole and Some Physicochemical Properties of the Drug and Its Metabolite Albendazole Sulphoxide. Journal of Pharmacy and Pharmacology 50, 43-48.

Kalivoda, A., Fischbach, M., Kleinebudde, P., 2012. Application of mixtures of polymeric carriers for dissolution enhancement of fenofibrate using hot-melt extrusion. International journal of pharmaceutics 429, 58-68.

Karande, A.D., Heng, P.W., Liew, C.V., 2010. In-line quantification of micronized drug and excipients in tablets by near infrared (NIR) spectroscopy: Real time monitoring of tabletting process. International journal of pharmaceutics 396, 63-74.

Karashima, M., Kimoto, K., Yamamoto, K., Kojima, T., Ikeda, Y., 2016. A novel solubilization technique for poorly soluble drugs through the integration of nanocrystal and cocrystal technologies. European journal of pharmaceutics and biopharmaceutics 107, 142-150.

Kasim, N.A., Whitehouse, M., Ramachandran, C., Bermejo, M., Lennernäs, H., Hussain, A.S., Junginger, H.E., Stavchansky, S.A., Midha, K.K., Shah, V.P., Amidon, G.L., 2004. Molecular properties of WHO essential drugs and provisional biopharmaceutical classification. Molecular Pharmaceutics 1, 85-96.

Kašpar, O., Tokárová, V., Oka, S., Sowrirajan, K., Ramachandran, R., Štěpánek, F., 2013. Combined UV/Vis and micro-tomography investigation of acetaminophen dissolution from granules. International journal of pharmaceutics 458, 272-281.

Kate, L., Gokarna, V., Borhade, V., Prabhu, P., Deshpande, V., Pathak, S., Sharma, S., Patravale, V., 2016. Bioavailability enhancement of atovaquone using hot melt extrusion technology. European journal of pharmaceutical sciences: Official journal of the European Federation for Pharmaceutical Sciences 86, 103-114.

Kawabata, Y., Wada, K., Nakatani, M., Yamada, S., Onoue, S., 2011. Formulation design for poorly water-soluble drugs based on biopharmaceutics classification system: basic approaches and practical applications. International journal of pharmaceutics 420, 1-10.

Kawakami, K., 2012. Modification of physicochemical characteristics of active pharmaceutical ingredients and application of supersaturatable dosage forms for improving bioavailability of poorly absorbed drugs. Advanced drug delivery reviews 64, 480-495.

Keleb, E.I., Vermeire, A., Vervaet, C., Remon, J.P., 2004. Twin screw granulation as a simple and efficient tool for continuous wet granulation. International journal of pharmaceutics 273, 183-194.

Kelly, A.L., Halsey, S.A., Bottom, R.A., Korde, S., Gough, T., Paradkar, A., 2015. A novel transflectance near infrared spectroscopy technique for monitoring hot melt extrusion. International journal of pharmaceutics 496, 117-123.

Kerč, J., Srčič, S., 1995. Thermal analysis of glassy pharmaceuticals. Thermochimica Acta 248, 81-95.

Khan, S., Batchelor, H., Hanson, P., Perrie, Y., Mohammed, A.R., 2011. Physicochemical characterisation, drug polymer dissolution and in vitro evaluation of phenacetin and phenylbutazone solid dispersions with polyethylene glycol 8000. Journal of pharmaceutical sciences 100, 4281-4294.

Kipping, T., Rein, H., 2016. Continuous production of controlled release dosage forms based on hot-melt extruded gum arabic: Formulation development, in vitro characterization and evaluation of potential application fields. International journal of pharmaceutics 497, 36-53.

Kitak, T., Dumicic, A., Planinsek, O., Sibanc, R., Srcic, S., 2015. Determination of Solubility Parameters of Ibuprofen and Ibuprofen Lysinate. Molecules 20, 21549-21568.

Kothari, K., Ragoonanan, V., Suryanarayanan, R., 2015. The Role of Drug–Polymer Hydrogen Bonding Interactions on the Molecular Mobility and Physical Stability of Nifedipine Solid Dispersions. Molecular Pharmaceutics 12, 162-170.

Kumar, A., Alakarjula, M., Vanhoorne, V., Toiviainen, M., De Leersnyder, F., Vercruysse, J., Juuti, M., Ketolainen, J., Vervaet, C., Remon, J.P., Gernaey, K.V., De Beer, T., Nopens, I., 2016. Linking granulation performance with residence time and granulation liquid distributions in twin-screw granulation: An experimental investigation. European journal of pharmaceutical sciences: Official journal of the European Federation for Pharmaceutical Sciences 90, 25-37.

Kumar, A., Vercruysse, J., Toiviainen, M., Panouillot, P.E., Juuti, M., Vanhoorne, V., Vervaet, C., Remon, J.P., Gernaey, K.V., De Beer, T., Nopens, I., 2014. Mixing and transport during pharmaceutical twin-screw wet granulation: experimental analysis via chemical imaging. European journal of pharmaceutics and biopharmaceutics 87, 279-289.

Kyerematen, S.O., Pudlas, M., Woehrle, G.H., 2014. A fast and reliable empirical approach for estimating solubility of crystalline drugs in polymers for hot melt extrusion formulations. Journal of pharmaceutical sciences 103, 2847-2858.

LaFountaine, J.S., Prasad, L.K., Brough, C., Miller, D.A., McGinity, J.W., Williams, R.O., 3rd, 2016. Thermal Processing of PVP- and HPMC-Based Amorphous Solid Dispersions. AAPS PharmSciTech 17, 120-132.

Lakshman, J.P.C., Yu. Kowalski, J. Serajuddin, A., 2008. Application of melt extrusion in the development of a physically and chemically stable high-energy amorphous solid dispersion of a poorly water-soluble drug. Molecular Pharmaceutics 5, 994-1002.

Laukamp, E.J., Vynckier, A.K., Voorspoels, J., Thommes, M., Breitkreutz, J., 2015. Development of sustained and dual drug release co-extrusion formulations for individual dosing. European journal of pharmaceutics and biopharmaceutics 89, 357-364.

Lawal, A., Kalyon, D.M., 1995. Mechanisms of mixing in single and co-rotating twin screw extruders. Polymer Engineering and Science 35, 1325-1338.

Lee, J.Y., Kang, W.S., Piao, J., Yoon, I.S., Kim, D.D., Cho, H.J., 2015. Soluplus(R)/TPGS-based solid dispersions prepared by hot-melt extrusion equipped with twin-screw systems for enhancing oral bioavailability of valsartan. Drug design, development and therapy 9, 2745-2756.

Lee, K.T., Ingram, A., Rowson, N.A., 2013. Comparison of granule properties produced using Twin Screw Extruder and High Shear Mixer: A step towards understanding the mechanism of twin screw wet granulation. Powder Technology 238, 91-98.

Leonardi, D., Barrera, M.G., Lamas, M.C., Salomón, C.J., 2007. Development of Prednisone: Polyethylene glycol 6000 fast-release tablets from solid dispersions: solid-state characterisation, dissolution behavior and formulation parameters. AAPS PharmSciTech 8, Article 108.

Leonardi, D., Echenique, C., Lamas, M.C., Salomón, C.J., 2009. High efficacy of albendazole-PEG 6000 in the treatment of Toxocara canis larva migrans infection. The Journal of antimicrobial chemotherapy 64, 375-378.

Leuenberger, H., 2001. New trends in the production of pharmaceutical granules: batch versus continuous processing. European Journal of Pharmaceutics and Biopharmaceutics 52, 289-296.

Li, H., Thompson, M.R., O'Donnell, K.P., 2015. Examining drug hydrophobicity in continuous wet granulation within a twin screw extruder. International journal of pharmaceutics 496, 3-11.

Li, J., Tao, L., Buckley, D., Tao, J., Gao, J., Hubert, M., 2013. The effect of the physical state of binders on high-shear wet granulation and granule properties: a mechanistic approach to understand the high-shear wet granulation process. part IV. the impact of rheological state and tip-speeds. Journal of pharmaceutical sciences 102, 4384-4394.

Lin, C.W., Cham, T.M., 1996. Effect of particle size on the available surface area of nifedipine from nifedipine - polyethylene glycol 6000 solid dispersions. International journal of pharmaceutics 127, 261-272.

Litster, J.D.H., K.P. Michaels, J.N. Sims, A. Roberts, M. Kameneni, S.K. Hsu, T., 2001. Liquid distribution in wet granulation: dimensionless spray flux. Powder Technology 114, 32-39.

Liu, J., Cao, F., Zhang, C., Ping, Q., 2013. Use of polymer combinations in the preparation of solid dispersions of a thermally unstable drug by hot-melt extrusion. Acta Pharmaceutica Sinica B 3, 263-272.

Liu, Y., Thompson, M.R., O'Donnell, K.P., 2015. Function of upstream and downstream conveying elements in wet granulation processes within a twin screw extruder. Powder Technology 284, 551-559.

Lute, S.V., Dhenge, R.M., Hounslow, M.J., Salman, A.D., 2016. Twin screw granulation: Understanding the mechanism of granule formation along the barrel length. Chemical Engineering Research and Design 110, 43-53.

Lyons, J.G., Devine, D.M., Kennedy, J.E., Geever, L.M., O'Sullivan, P., Higginbotham, C.L., 2006. The use of agar as a novel filler for monolithic matrices produced using hot melt extrusion. European journal of pharmaceutics and biopharmaceutics 64, 75-81.

Lyons, J.G., Hallinan, M., Kennedy, J.E., Devine, D.M., Geever, L.M., Blackie, P., Higginbotham, C.L., 2007. Preparation of monolithic matrices for oral drug delivery using a supercritical fluid assisted hot melt extrusion process. International journal of pharmaceutics 329, 62-71.

Ma, Q., Wang, C., Li, X., Guo, H., Meng, J., Liu, J., Xu, H., 2016. Fabrication of water-soluble polymer-encapsulated As4S4 to increase oral bioavailability and chemotherapeutic efficacy in AML mice. Scientific reports 6, 29348.

Madan, S.M., S., 2012. Hot melt extrusion and its pharmaceutical applications. Asian Journal of Pharmaceutical Sciences 7, 123-133.

Mahlin, D., Bergstrom, C.A., 2013. Early drug development predictions of glass-forming ability and physical stability of drugs. European journal of pharmaceutical sciences: official journal of the European Federation for Pharmaceutical Sciences 49, 323-332.

Mangwandi, C., JiangTao, L., Albadarin, A.B., Dhenge, R.M., Walker, G.M., 2015. High shear granulation of binary mixtures: Effect of powder composition on granule properties. Powder Technology 270, 424-434.

Maniruzzaman, M., Boateng, J.S., Bonnefille, M., Aranyos, A., Mitchell, J.C., Douroumis, D., 2012. Taste masking of paracetamol by hot-melt extrusion: an in vitro and in vivo evaluation. European journal of pharmaceutics and biopharmaceutics 80, 433-442.

Maniruzzaman, M., Boateng, J.S., Snowden, M.J., Douroumis, D., 2012. A review of hot-melt extrusion: process technology to pharmaceutical products. ISRN pharmaceutics, Article ID 436763.

Maniruzzaman, M., Islam, M.T., Halsey, S., Amin, D., Douroumis, D., 2016. Novel Controlled Release Polymer-Lipid Formulations Processed by Hot Melt Extrusion. AAPS PharmSciTech 17, 191-199.

Maniruzzaman, M., Nair, A., Scoutaris, N., Bradley, M.S., Snowden, M.J., Douroumis, D., 2015. One-step continuous extrusion process for the manufacturing of solid dispersions. International journal of pharmaceutics 496, 42-51.

Marriner, S.E.M., D.L. Dickson, B. Bogan, J.A., 1986. Pharmacokinetics of albendazole in man. European Journal of Clinical Pharmacology 30, 705-708.

Martinez-Marcos, L., Lamprou, D.A., McBurney, R.T., Halbert, G.W., 2016. A novel hot-melt extrusion formulation of albendazole for increasing dissolution properties. International journal of pharmaceutics 499, 175-185.

Martins de Oliveira Jr., J., and Germano Martins, A.C., 2010. Non-conventional applications of computerized tomography: Analysis of solid dosage forms produced by pharmaceutical industry. American Institute of Physics 153-159.

Maru, S.M., de Matas, M., Kelly, A., Paradkar, A., 2011. Characterization of thermal and rheological properties of zidovudine, lamivudine and plasticizer blends with ethyl cellulose to assess their suitability for hot melt extrusion. European journal of pharmaceutical sciences: Official journal of the European Federation for Pharmaceutical Sciences 44, 471-478.

Mehuys, E., Vervaet, C., Remon, J.P., 2004. Hot-melt extruded ethylcellulose cylinders containing a HPMC–Gelucire® core for sustained drug delivery. Journal of Controlled Release 94, 273-280.

Meier, R., Thommes, M., Rasenack, N., Moll, K.P., Krumme, M., Kleinebudde, P., 2016. Granule size distributions after twin-screw granulation - Do not forget the feeding systems. European journal of pharmaceutics and biopharmaceutics 106, 59-69.

Mezhericher, M., 2014. Development of drying-induced stresses in pharmaceutical granules prepared in continuous production line. European journal of pharmaceutics and biopharmaceutics 88, 866-878.

Michaeli, W., Frings, W., Höcker, H., Berghaus, U., 1993. Reactive Extrusion of Styrene Polymers. International Polymer Processing 8, 308-318.

Miller, L.A., Carrier, R.L., Ahmed, I., 2007. Practical considerations in development of solid dosage forms that contain cyclodextrin. Journal of pharmaceutical sciences 96, 1691-1707.

Mirza, Z., Liu, J., Glocheux, Y., Albadarin, A.B., Walker, G.M., Mangwandi, C., 2015. Effect of impeller design on homogeneity, size and strength of pharmaceutical granules produced by high-shear wet granulation. Particuology 23, 31-39.

Mitra, A., Li, L., Marsac, P., Marks, B., Liu, Z., Brown, C., 2016. Impact of polymer type on bioperformance and physical stability of hot melt extruded formulations of a poorly water soluble drug. International journal of pharmaceutics 505, 107-114.

Morott, J.T., Pimparade, M., Park, J.B., Worley, C.P., Majumdar, S., Lian, Z., Pinto, E., Bi, Y., Durig, T., Repka, M.A., 2015. The effects of screw configuration and polymeric carriers on hot-melt extruded taste-masked formulations incorporated into orally disintegrating tablets. Journal of pharmaceutical sciences 104, 124-134.

Moyano, J.R.L., J. Pérez, J.I. Arias, M.J. Sánchez-Soto, P.J., 2014. Thermal analysis of albendazole investigated by HSM, DSC and FTIR. Microscopy: Advances in scientific research and education (A. Méndez-Vilas, Ed.), 1043-1050.

Mu, B., Thompson, M.R., 2012. Examining the mechanics of granulation with a hot melt binder in a twin-screw extruder. Chemical Engineering Science 81, 46-56.

Nakayama, Y., Takeda, E., Shigeishi, T., Tomiyama, H., Kajiwara, T., 2011. Melt-mixing by novel pitched-tip kneading disks in a co-rotating twin-screw extruder. Chemical Engineering Science 66, 103-110.

Netchacovitch, L., Thiry, J., De Bleye, C., Dumont, E., Dispas, A., Hubert, C., Krier, F., Sacre, P.Y., Evrard, B., Hubert, P., Ziemons, E., 2016. A simple calibration approach based on film-casting for confocal Raman microscopy to support the development of a hot-melt extrusion process. Talanta 154, 392-399.

Newman, A., 2015. Pharmaceutical Amorphous Solid Dispersions. John Wiley & Sons.

Newman, A., Knipp, G., Zografi, G., 2012. Assessing the performance of amorphous solid dispersions. Journal of pharmaceutical sciences 101, 1355-1377.

O'Donnell, K.P.W., R.O., 2012. Formulating poorly water soluble drugs. Springer.

Oka, S., Emady, H., Kašpar, O., Tokárová, V., Muzzio, F., Štěpánek, F., Ramachandran, R., 2015. The effects of improper mixing and preferential wetting of active and excipient ingredients on content uniformity in high shear wet granulation. Powder Technology 278, 266-277.

Okwuosa, T.C., Stefaniak, D., Arafat, B., Isreb, A., Wan, K., and Alhnan, A., 2016. A lower temperature FDM 3D printing for the manufacture of patient-specific immediate release tablets. Pharmaceutical research 33, 2704-2712.

Otsuka, M., Ibe, K., Tokudome, Y., Ohshima, H., 2009. Nano- and macro-geometrical structural change of caffeine and theophylline anhydrate tablets during

hydration process by using X-ray computed tomography. Colloids and surfaces. B, Biointerfaces 73, 351-359.

Ozeki, Y., 2003. Comparison of the compression characteristics between new one-step dry-coated tablets (OSDRC) and dry-coated tablets (DC). International journal of pharmaceutics 259, 69-77.

Özgüney, I., Shuwisitkul, D., Bodmeier, R., 2009. Development and characterization of extended release Kollidon SR mini-matrices prepared by hot-melt extrusion. European journal of pharmaceutics and biopharmaceutics 73, 140-145.

Özkan, Y., Doğanay, N., Dikmen, N., Işimer, A., 2000. Enhanced release of solid dispersions of etodolac in polyethylene glycol. Il Farmaco 55, 433-438.

Padmanabhan, B., 2008. Understanding the Extruder Processing Zone: the heart of a twin screw extruder. Plastics, Additives and Compounding 10, 30-35.

Palem, C.R., Dudhipala, N., Battu, S.K., Goda, S., Repka, M.A., Yamsani, M.R., 2015. Combined dosage form of pioglitazone and felodipine as mucoadhesive pellets via hot melt extrusion for improved buccal delivery with application of quality by design approach. Journal of drug delivery science and technology 30, 209-219.

Parikh, D.M., 2005. Handbook of pharmaceutical granulation technology Taylor & Francis.

Park, J.B., Kang, C.Y., Kang, W.S., Choi, H.G., Han, H.K., Lee, B.J., 2013. New investigation of distribution imaging and content uniformity of very low dose drugs using hot-melt extrusion method. International journal of pharmaceutics 458, 245-253.

Pawar, J., Tayade, A., Gangurde, A., Moravkar, K., Amin, P., 2016. Solubility and dissolution enhancement of efavirenz hot melt extruded amorphous solid dispersions using combination of polymeric blends: A QbD approach. European journal of pharmaceutical sciences: Official journal of the European Federation for Pharmaceutical Sciences 88, 37-49.

Perfetti, G., Casteele, E.V.d., Rieger, B., Wildeboer, W.J., Meesters, G.M.H., 2010. X-ray micro tomography and image analysis as complementary methods for morphological characterization and coating thickness measurement of coated particles. Advanced Powder Technology 21, 663-675.

Perissutti, B., Newton, J.M., Podczeck, F., and Rubessa, F. , 2002. Preparation of extruded carbamazepine and PEG 4000 as a potential rapid release dosage form. European journal of pharmaceutics and biopharmaceutics 53, 125-132.

PerkinElmer, 2011. Tg and melting point of a series of Polyethylene glycols using the material pocket. Application Note. PerkinElmer.

Pharmacopeia, U.S., 2012. <616> Bulk density and tapped density of powders.

Pharmacopeia, U.S., 2011. Uniformity of dosage units, United States Pharmacopeia.

Pina, M.F., Zhao, M., Pinto, J.F., Sousa, J.J., Craig, D.Q.M., 2014. The Influence of Drug Physical State on the Dissolution Enhancement of Solid Dispersions Prepared Via Hot-Melt Extrusion: A Case Study Using Olanzapine. Journal of pharmaceutical sciences 103, 1214-1223.

Poutiainen, S., Pajander, J., Savolainen, A., Ketolainen, J., Jarvinen, K., 2011. Evolution of granule structure and drug content during fluidized bed granulation by

X-ray microtomography and confocal Raman spectroscopy. Journal of pharmaceutical sciences 100, 5254-5269.

Pranzo, M.B., Cruickshank, D., Coruzzi, M., Caira, M.R., Bettini, R., 2010. Enantiotropically related albendazole polymorphs. Journal of pharmaceutical sciences 99, 3731-3742.

Qi, S., Belton, P., Nollenberger, K., Clayden, N., Reading, M., Craig, D.Q., 2010. Characterisation and prediction of phase separation in hot-melt extruded solid dispersions: a thermal, microscopic and NMR relaxometry study. Pharmaceutical research 27, 1869-1883.

Qi, S., Gryczke, A., Belton, P., Craig, D.Q., 2008. Characterisation of solid dispersions of paracetamol and EUDRAGIT E prepared by hot-melt extrusion using thermal, microthermal and spectroscopic analysis. International journal of pharmaceutics 354, 158-167.

Quinn, K., Gullapalli, R.P., Merisko-Liversidge, E., Goldbach, E., Wong, A., Liversidge, G.G., Hoffman, W., Sauer, J.M., Bullock, J., Tonn, G., 2012. A formulation strategy for gamma secretase inhibitor ELND006, a BCS class II compound: development of a nanosuspension formulation with improved oral bioavailability and reduced food effects in dogs. Journal of pharmaceutical sciences 101, 1462-1474.

Quintavalle, U., Voinovich, D., Perissutti, B., Serdoz, F., Grassi, G., Dal Col, A., Grassi, M., 2008. Preparation of sustained release co-extrudates by hot-melt extrusion and mathematical modelling of in vitro/in vivo drug release profiles.

European journal of pharmaceutical sciences: Official journal of the European Federation for Pharmaceutical Sciences 33, 282-293.

Rauwendaal, C., 2005. Recent advances in barrier screw design. Plastics, Additives and Compounding 7, 36-39.

Rauwendaal, C., 2008. New developments in mixing and screw design. Plastics Additives & Compounding November/December, 32-36.

Reintjes, T., 2011. Solubility enhancement with BASF pharma polymers; Solubilizer Compendium. BASF SE.

Repka, M.A., Battu, S.K., Upadhye, S.B., Thumma, S., Crowley, M.M., Zhang, F., Martin, C., McGinity, J.W., 2007. Pharmaceutical applications of hot-melt extrusion: Part II. Drug development and industrial pharmacy 33, 1043-1057.

Rowe, R.C.S., P.J. Quinn, M.E., 2009. Handbook of pharmaceutical excipients, Sixth Edition ed. Pharmaceutical Press and American Pharmacists Association.

Rumondor, A.C.F., Taylor, L.S., 2009. Effect of Polymer Hygroscopicity on the Phase Behavior of Amorphous Solid Dispersions in the Presence of Moisture. Molecular Pharmaceutics 7, 477-490.

Russe, I.S., Brock, D., Knop, K., Kleinebudde, P., Zeitler, J.A., 2012. Validation of Terahertz coating thickness measurements using X-ray microtomography. Molecular Pharmaceutics 9, 3551-3559.

Saerens, L., Dierickx, L., Quinten, T., Adriaensens, P., Carleer, R., Vervaet, C., Remon, J.P., De Beer, T., 2012. In-line NIR spectroscopy for the understanding of

polymer-drug interaction during pharmaceutical hot-melt extrusion. European journal of pharmaceutics and biopharmaceutics 81, 230-237.

Saleh, M.F., Dhenge, R.M., Cartwright, J.J., Hounslow, M.J., Salman, A.D., 2015. Twin screw wet granulation: Binder delivery. International journal of pharmaceutics 487, 124-134.

Sarhangi Fard, A., Anderson, P.D., 2013. Simulation of distributive mixing inside mixing elements of co-rotating twin-screw extruders. Computers & Fluids 87, 79-91.

Sarode, A.V., Kumbharkhane, A.C., 2012. Dielectric relaxation and thermodynamic properties of polyvinylpyrrolidone using time domain reflectometry. Polymer International 61, 609-615.

Sathigari, S.K., Radhakrishnan, V.K., Davis, V.A., Parsons, D.L., Babu, R.J., 2012. Amorphous-state characterization of efavirenz--polymer hot-melt extrusion systems for dissolution enhancement. Journal of pharmaceutical sciences 101, 3456-3464.

Sauceau, M., Fages, J., Common, A., Nikitine, C., Rodier, E., 2011. New challenges in polymer foaming: A review of extrusion processes assisted by supercritical carbon dioxide. Progress in Polymer Science 36, 749-766.

Sayin, R., El Hagrasy, A.S., Litster, J.D., 2015a. Distributive mixing elements: Towards improved granule attributes from a twin screw granulation process. Chemical Engineering Science 125, 165-175.

Sayin, R., Martinez-Marcos, L., Osorio, J.G., Cruise, P., Jones, I., Halbert, G.W., Lamprou, D.A., Litster, J.D., 2015b. Investigation of an 11mm diameter twin screw

granulator: Screw element performance and in-line monitoring via image analysis. International journal of pharmaceutics 496, 24-32.

Schilling, S.U., McGinity, J.W., 2010. Novel application of hot-melt extrusion for the preparation of monolithic matrices containing enteric-coated particles. International journal of pharmaceutics 400, 24-31.

Shah, S., Maddineni, S., Lu, J., Repka, M.A., 2013. Melt extrusion with poorly soluble drugs. International journal of pharmaceutics 453, 233-252.

Sharma, K.V., Bascal, Z., Kilpatrick, H., Ashrafi, K., Willis, S.L., Dreher, M.R., Lewis, A.L., 2016. Long-term biocompatibility, imaging appearance and tissue effects associated with delivery of a novel radiopaque embolization bead for image-guided therapy. Biomaterials 103, 293-304.

Sherry Ku, M., 2008. Use of the biopharmaceutical classification system in early drug development. The AAPS Journal 10.

Singhal, S.L., V.K. Arora, V., 2011. Hot Melt Extrusion Technique. WebmedCentral Pharmaceutical Sciences 2, WMC001459.

Sinka, I.C., Burch, S.F., Tweed, J.H., Cunningham, J.C., 2004. Measurement of density variations in tablets using X-ray computed tomography. International journal of pharmaceutics 271, 215-224.

Sondej, F., Bück, A., Koslowsky, K., Bachmann, P., Jacob, M., Tsotsas, E., 2015. Investigation of coating layer morphology by micro-computed X-ray tomography. Powder Technology 273, 165-175.

Stegemann, S.L., F. Franchi, D. de Jong, H. Lindén, H., 2007. When poor solubility becomes an issue: From early stage to proof of concept. Euroopean Journal of Pharmaceutical Sciences 31, 249-261.

Sun, N., Wei, X., Wu, B., Chen, J., Lu, Y., Wu, W., 2008. Enhanced dissolution of silymarin/polyvinylpyrrolidone solid dispersion pellets prepared by a one-step fluid-bed coating technique. Powder Technology 182, 72-80.

Szakonyi, G., Zelkó, R., 2012. The effect of water on the solid state characteristics of pharmaceutical excipients: Molecular mechanisms, measurement techniques, and quality aspects of final dosage form. International journal of pharmaceutical investigation 2, 18-25.

Tan, B.M., Loh, Z.H., Soh, J.L., Liew, C.V., Heng, P.W., 2014. Distribution of a viscous binder during high shear granulation--sensitivity to the method of delivery and its impact on product properties. International journal of pharmaceutics 460, 255-263.

Taupitz, T., Dressman, J.B., Buchanan, C.M., Klein, S., 2013. Cyclodextrin-water soluble polymer ternary complexes enhance the solubility and dissolution behaviour of poorly soluble drugs. Case example: itraconazole. European journal of pharmaceutics and biopharmaceutics 83, 378-387.

Teżyk, M., Milanowski, B., Ernst, A., Lulek, J., 2016. Recent progress in continuous and semi-continuous processing of solid oral dosage forms: a review. Drug development and industrial pharmacy 42, 1195-1214.

Tho, I., Liepold, B., Rosenberg, J., Maegerlein, M., Brandl, M., Fricker, G., 2010. Formation of nano/micro-dispersions with improved dissolution properties upon dispersion of ritonavir melt extrudate in aqueous media. European journal of pharmaceutical sciences: Official journal of the European Federation for Pharmaceutical Sciences 40, 25-32.

Thompson, M.R., Sun, J., 2010. Wet granulation in a twin-screw extruder: implications of screw design. Journal of pharmaceutical sciences 99, 2090-2103.

Tokudome, Y., Ohshima, H., Otsuka, M., 2009. Non-invasive and rapid analysis for observation of internal structure of press-coated tablet using X-ray computed tomography. Drug development and industrial pharmacy 35, 678-682.

Torrado, S.L., M.L. Torrado, G. Bolas, F. Torrado, S. Cadorniga, R., 1997. A novel formulation of albendazole solution: oral bioavailability and efficacy evaluation. International journal of pharmaceutics 156, 181-187.

Torrado, S., Torrado, S., Cadorniga, R., and Torrado, J.J., 1996a. Formulation parameters of albendazole solution. International journal of pharmaceutics 140, 45-50.

Torrado, S.T., S. Torrado, J.J. Cadorniga, R., 1996b. Preparation, dissolution and characterization of albendazole solid dispersions. International journal of pharmaceutics 140, 247-250.

Traini, D., Loreti, G., Jones, A.S., Young, P.M., 2008. X-ray computed microtomography for the study of modified release systems. Microscopy and Analysis 22, 13-15.

Trapani, G., Franco, M., Latrofa, A., Pantaleo, M.R., Provenzano, M.R., Sanna, E., Maciocco, E., Liso, G., 1999. Physicochemical characterization and in vivo properties of Zolpidem in solid dispersions with PEG 4000 and 6000. International journal of pharmaceutics 184, 121-130.

Urbanetz, N.A., Lippold, B.C., 2005. Solid dispersions of nimodipine and polyethylene glycol 2000: dissolution properties and physico-chemical characterisation. European journal of pharmaceutics and biopharmaceutics 59, 107-118.

Van Melkebeke, B., Vervaet, C., Remon, J.P., 2008. Validation of a continuous granulation process using a twin-screw extruder. International journal of pharmaceutics 356, 224-230.

Van Zuilichem, D.L., Kuiper, E., Stolp, W., Jager, T., 1999. Mixing effects of constituing elements of mixing screws in single and twin screw extruders. Powder Technology 106, 147-159.

Vasa, D.M., Dalal, N., Katz, J.M., Roopwani, R., Nevrekar, A., Patel, H., Buckner, I.S., Wildfong, P.L., 2014. Physical characterization of drug:polymer dispersion behavior in polyethylene glycol 4000 solid dispersions using a suite of complementary analytical techniques. Journal of pharmaceutical sciences 103, 2911-2923.

Vercruysse, J., Burggraeve, A., Fonteyne, M., Cappuyns, P., Delaet, U., Van Assche, I., De Beer, T., Remon, J.P., Vervaet, C., 2015a. Impact of screw configuration on the particle size distribution of granules produced by twin screw granulation. International journal of pharmaceutics 479, 171-180.

Vercruysse, J., Cordoba Diaz, D., Peeters, E., Fonteyne, M., Delaet, U., Van Assche, I., De Beer, T., Remon, J.P., Vervaet, C., 2012. Continuous twin screw granulation: influence of process variables on granule and tablet quality. European journal of pharmaceutics and biopharmaceutics 82, 205-211.

Vercruysse, J., Delaet, U., Van Assche, I., Cappuyns, P., Arata, F., Caporicci, G., De Beer, T., Remon, J.P., Vervaet, C., 2013. Stability and repeatability of a continuous twin screw granulation and drying system. European Journal of Pharmaceutics and Biopharmaceutics 85, 1031-1038.

Vercruysse, J., Peeters, E., Fonteyne, M., Cappuyns, P., Delaet, U., Van Assche, I., De Beer, T., Remon, J.P., Vervaet, C., 2015b. Use of a continuous twin screw granulation and drying system during formulation development and process optimization. European journal of pharmaceutics and biopharmaceutics 89, 239-247.

Vercruysse, J., Toiviainen, M., Fonteyne, M., Helkimo, N., Ketolainen, J., Juuti, M., Delaet, U., Van Assche, I., Remon, J.P., Vervaet, C., De Beer, T., 2014. Visualization and understanding of the granulation liquid mixing and distribution during continuous twin screw granulation using NIR chemical imaging. European journal of pharmaceutics and biopharmaceutics 86, 383-392.

Verheyen, S., Blaton, N., Kinget, R., Van den Mooter, G. , 2002. Mechanism of increased dissolution of diazepam and temazepam from polyethylene glycol 6000 solid dispersions. International journal of pharmaceutics 249, 45-58.

Verhoeven, E., De Beer, T.R., Van den Mooter, G., Remon, J.P., Vervaet, C., 2008. Influence of formulation and process parameters on the release characteristics of

ethylcellulose sustained-release mini-matrices produced by hot-melt extrusion. European journal of pharmaceutics and biopharmaceutics 69, 312-319.

Verhoeven, E., Siepmann, F., De Beer, T.R., Van Loo, D., Van den Mooter, G., Remon, J.P., Siepmann, J., Vervaet, C., 2009. Modeling drug release from hot-melt extruded mini-matrices with constant and non-constant diffusivities. European journal of pharmaceutics and biopharmaceutics 73, 292-301.

Verreck, G., Decorte, A., Heymans, K., Adriaensen, J., Liu, D., Tomasko, D., Arien, A., Peeters, J., Van den Mooter, G., Brewster, M.E., 2006a. Hot stage extrusion of p-amino salicylic acid with EC using CO2 as a temporary plasticizer. International journal of pharmaceutics 327, 45-50.

Verreck, G., Decorte, A., Li, H., Tomasko, D., Arien, A., Peeters, J., Rombaut, P., Van den Mooter, G., Brewster, M.E., 2006b. The effect of pressurized carbon dioxide as a plasticizer and foaming agent on the hot melt extrusion process and extrudate properties of pharmaceutical polymers. The Journal of Supercritical Fluids 38, 383-391.

Verstraete, G., Van Renterghem, J., Van Bockstal, P.J., Kasmi, S., De Geest, B.G., De Beer, T., Remon, J.P., Vervaet, C., 2016. Hydrophilic thermoplastic polyurethanes for the manufacturing of highly dosed oral sustained release matrices via hot melt extrusion and injection molding. International journal of pharmaceutics 506, 214-221.

Vo, A.Q., Feng, X., Morott, J.T., Pimparade, M.B., Tiwari, R.V., Zhang, F., Repka, M.A., 2016. A novel floating controlled release drug delivery system prepared by

hot-melt extrusion. European journal of pharmaceutics and biopharmaceutics 98, 108-121.

Vynckier, A.K., De Beer, M., Monteyne, T., Voorspoels, J., De Beer, T., Remon, J.P., Vervaet, C., 2015a. Enteric protection of naproxen in a fixed-dose combination product produced by hot-melt co-extrusion. International journal of pharmaceutics 491, 243-249.

Vynckier, A.K., Lin, H., Zeitler, J.A., Willart, J.F., Bongaers, E., Voorspoels, J., Remon, J.P., Vervaet, C., 2015b. Calendering as a direct shaping tool for the continuous production of fixed-dose combination products via co-extrusion. European Journal of Pharmaceutics and Biopharmaceutics 96, 125-131.

Wang, A., Liu, Y., Liang, R., Zhang, X., Sun, K., Wu, Z., Liu, W., 2016. Preparation and evaluation of rotigotine-loaded implant for the treatment of Parkinson's disease and its evolution study. Saudi pharmaceutical journal: SPJ: The official publication of the Saudi Pharmaceutical Society 24, 363-370.

Wiederhold, N.P., 2016. Pharmacokinetics and safety of posaconazole delayed-release tablets for invasive fungal infections. Clinical pharmacology: Advances and applications 8, 1-8.

Williams, M.T., Y. Jones, D.S. Andrews, G.P., 2010. Hot-melt extrusion technology: Optimizing drug delivery. European Industrial Pharmacy.

Windbergs, M., Strachan, C.J., Kleinebudde, P., 2009. Tailor-made dissolution profiles by extruded matrices based on lipid polyethylene glycol mixtures. Journal of controlled release: Official journal of the Controlled Release Society 137, 211-216.

Yang, F., Su, Y., Zhu, L., Brown, C.D., Rosen, L.A., Rosenberg, K.J., 2016. Rheological and solid-state NMR assessments of copovidone/clotrimazole model solid dispersions. International journal of pharmaceutics 500, 20-31.

Young, C.R.D., C. Cerea, M. Farrel, T. Fegely, K.A. Rajabi-Siahboomi, A. McGinity, J.W., 2005. Physicochemical characterization and mechanisms of release of Theophylline from melt-extruded dosage forms. International journal of pharmaceutics 301, 112-120.

Yu, S., Reynolds, G.K., Huang, Z., de Matas, M., Salman, A.D., 2014. Granulation of increasingly hydrophobic formulations using a twin screw granulator. International journal of pharmaceutics 475, 82-96.

Yun, F., Kang, A., Shan, J., Zhao, X., Bi, X., Li, J., Di, L., 2014. Preparation of osthole-polymer solid dispersions by hot-melt extrusion for dissolution and bioavailability enhancement. International journal of pharmaceutics 465, 436-443.

Zaid, A.N., Al-Ramahi, R.J., Ghoush, A.A., Qaddumi, A., Zaaror, Y.A., 2013. Weight and content uniformity of lorazepam half-tablets: A study of correlation of a low drug content product. Saudi pharmaceutical journal: SPJ: The official publication of the Saudi Pharmaceutical Society 21, 71-75.

Zeitler, J.A., Gladden, L.F., 2009. In-vitro tomography and non-destructive imaging at depth of pharmaceutical solid dosage forms. European journal of pharmaceutics and biopharmaceutics 71, 2-22.

Zhang, G.G., Law, D., Schmitt, E.A., Qiu, Y., 2004. Phase transformation considerations during process development and manufacture of solid oral dosage forms. Advanced drug delivery reviews 56, 371-390.

Appendix 1: Dissolution profile studies – Data normalisation

Chapters 2 and 3

All data points (weights in µg) collected from the T3 measurement system were normalised. The tablet weight (mg) in each case and the formulation drug content (% w/w) were used to calculate the specific drug amount (µg) per tablet. The normalised values of amount of drug released (µg) were transformed to % of drug released. Data point collection time was also transformed from minutes to hours for plotting purposes. An example of data normalisation is shown below.

Formulation F2 of ABZ – PVP K12

Extrudate theoretical ABZ content of 5 % (w/w)

Extrudate measured ABZ content of 4.53 % (w/w)

Tablet weight = 10.30 mg

4.53 % of 10.30 mg = 466.59 µg of ABZ

Normalised value (µg) = Measured amount released (µg) / 466.59 µg

Appendix 2: Publications

The work carried out in this thesis and the work performed in collaboration with the C-SOPS group (Purdue University) were published as journal articles. The details of the published articles are shown below.

Martinez-Marcos, L., Lamprou, D.A., McBurney, R.T., Halbert, G.W., 2016. A novel hot-melt extrusion formulation of albendazole for increasing dissolution properties. International journal of pharmaceutics 499, 175-185.

Sayin, R., Martinez-Marcos, L., Osorio, J.G., Cruise, P., Jones, I., Halbert, G.W., Lamprou, D.A., Litster, J.D., 2015. Investigation of an 11mm diameter twin screw granulator: Screw element performance and in-line monitoring via image analysis. International journal of pharmaceutics 496, 24-32.

Osorio, J.G., Sayin, R., Kalbag, A.V., Litster, J.D., Martinez-Marcos, L., Lamprou, D.A., Halbert, G.W., 2016. Scaling of continuous twin screw wet granulation. AIChE Journal.